UNIVERSITY OF
BIRMINGHAM

CONFINED IMPINGING JETs: AN ALTERNATIVE APPROACH TO TRADITIONAL FOOD EMULSIFICATION TECHNIQUES

By

ERNESTO TRIPODI

A thesis submitted to
The University of Birmingham
For the degree of
DOCTOR OF PHILOSOPHY

School of Chemical Engineering
College of Engineering and Physical Science
University of Birmingham
2019

Abstract

In the food sector, the development of innovative manufacturing technologies represents an exciting area of research. Within this context, Confined Impinging Jets (CIJs) offer potential for the large throughput production of tailored emulsion-based microstructures at lower energy inputs than conventional emulsification routes. Overall, this thesis aims to demonstrate that CIJs can be considered as a reliable alternative to existing emulsification methods by assessing its processing capacity and performance in delivering emulsion-based microstructures from a wide range of different formulations.

The use of CIJs was initially explored for the production of emulsions with dispersed phase contents of up to 80 wt.%, in both a surfactant-poor and surfactant-rich regime, under varying mass jet flow rates, W_{jet}, and residence times. From both a computational and experimental study, it was observed that the CIJs emulsification capacity was strictly dependent on the mass jet flow rate ($W_{jet} > 176$ g/min) and the pre-emulsion droplet size (>10μm). CIJs emulsification performance remained (almost) unaffected by variations in the oil mass fraction. All systems showed the lowest droplet size (~8μm) and similar droplet size distributions under the highest W_{jet}. Conditionally onto the Tween20 availability, the emulsion $d_{3,2}$ was primarily determined by formulation characteristics in the surfactant poor-regime and by the CIJs energy dissipation rate in the surfactant-rich regime.

CIJs emulsification performance was further assessed at varying energy dissipation rates ($\bar{\varepsilon}_{th}$) and residence times for the production of 10 and 40 wt.% oil-in-water emulsions stabilised by an array of particles (Silica) and mixed emulsifier (Tween20-Silica) concentrations. Overall, it was demonstrated that droplet size reduction was promoted as higher energy levels of $\bar{\varepsilon}_{th}$ were approached, regardless of the formulation. Following emulsion recirculation under a fixed jet mass flow rate, the residence time associated with two passes was sufficient to ensure no further

changes in terms of both average droplet size ($d_{3,2}$) and span of the droplet size distribution. Only when Tween20 and Silica were mixed at low concentrations (0.01 and 0.1 wt.%, respectively), this emulsifier system could not promote any droplet size reduction even during multipassing. All systems showed excellent stability over 40 days of storage and it was possible to demonstrate that the combination of the emulsifiers aided in prolonging emulsion integrity.

Finally, a comparison of the emulsification performance of CIJs with that of both high- (high pressure homogeniser, HPH; high-shear mixer, HSM) and low-energy (rotating membrane, RM) emulsification techniques was studied and compared based on a wide range of processing (average energy dissipation rate, $\bar{\varepsilon}_{th}$; flow regime; energy density, Ev; and energy efficiency, EF) as well as formulation (dispersed phase content, and type of emulsifier) parameters. It was observed that during HPH, HSM and CIJs processing, emulsions were produced under a turbulent flow regime, contrarily to RM where the flow was laminar. The performance of the HPH was very much dependent on the type of emulsifier used, while all other techniques were practically unaffected by both emulsifier and oil phase content. Overall, the HPH treatment generated the highest $\bar{\varepsilon}_{th}$ and comparable Ev to the HSM. The CIJs operated at intermediate $\bar{\varepsilon}_{th}$ and Ev conditions, while RM exhibited the lowest values for both these parameters. CIJs and the RM were the most energy efficient processes. For all techniques (with the exception of RM where recirculation was not performed), emulsion recirculation (under fixed hydrodynamic conditions) significantly affected droplet size distribution but only marginally reduced $d_{3,2}$. However, increasing the residence time within the emulsification apparatus (via recirculation), strongly decreased the EF of all processing techniques. The CIJs still remained the most energy-efficient method while HPH and HSM processing resulted in lower EFs with their relative values dependent on the type of emulsifier used.

Acknowledgments

Undertaking this PhD has been a life changing experience both personally and professionally. I am indebted to a number of people who made this four year long journey so special and unforgettable.

I would like to thank Prof. Norton for providing me with his support and guidance every time it was needed. A special thank also goes to Abigail, Ioanna, Tom and all the members of the microstructure group for your help and our (professional and ludic) discussions. I would also like to express my gratitude to Eddie. Although only for a short time, I have truly appreciated your advices and our long chats during my final period in Birmingham.

My enormous gratitude also goes to John Hooper for your help during the challenging times at the beginning of the PhD and to Lynn Draper for your kindness and being a pillar of strength for all the postgraduates in Chemical Engineering. I would like to thank all the group of 'internationals' in Chemical Engineering for all the good times.

I am grateful to Felice, Peggy and Sylvain for welcoming me in the 'fantastic, unpredictable' world of FEI at P&G and your continuous support during the past five months of double duty. A special thanks goes to Alberto, Mauro, Francesco, Raffaele and all the people in BIC for the fun times, your encouragement and lightening this last period.

I would like to thank Francesca, you have made this period better.

A gigantic thank you goes to Aris, Dorin and Mattia. Your true and genuine friendship is invaluable to me, and I am more than aware that only a 'thank you' is not enough to express how grateful I am to have had you with me during this time.

I would like to thank my brother, Giacomo. You are the better part of me and I will always look up to you. A big thank to my family, aunt Franca, my grandparents (Grazia and Ernesto) for your love. Thank to Frank and Mico, for a series of reasons that are too difficult (and perhaps better not) to write down.

Finally, I wish to thank Fotis. I do not think I will ever have a vocabulary wide enough to express how much I admire you. You made me a better person and a better scientist. You have been an endless source of motivation, inspiration, support and patience during the past four years. None of this, none of the smaller and greater achievements would have ever been possible without you, so thank you.

Table of contents

List of figures

Chapter 1

Chapter 2

Chapter 3

Chapter 4

Chapter 5

List of tables

Chapter 4

Chapter 5

Nomenclature

Symbols

b	Process function exponent	/
$d_{3,2}$	Sauter diameter	m
D	Diameter	m
ΔA	Interfacial area difference	m^2/m^3
ΔKE	Difference in Kinetic energy flow rate	W
ΔP	Pressure difference	Kg/m s^2
E_v	Energy density	J/m^3
E_{th}	Theoretical energy	J/m^3
ε	Energy dissipation rate	W/kg
$\bar{\varepsilon}_{th}$	Average energy dissipation rate	W/kg
η	Viscosity	Pa.s
$[\eta]$	Intrinsic viscosity	/
γ	Interfacial tension	N/m
$\dot{\gamma}$	Shear rate	1/s
K	Consistency index	$Pa.s^m$
K_p	Power number	/
λ_K	Kolmogorov eddy size	m
m	Power law index	/
m_{em}	Total mass of emulsified ingredients	kg
n	Recirculation step	/
N	Revolutions per second	1/s
ω	Frequency	1/s
P_h	Homogenisation pressure	Pa
ϕ	Volume fraction	/
ϕ_c	Maximum packing concentration	
Q	Volumetric flow rate	m^3/s
R_M	Membrane radius	m
R_V	Vessel radius	m
RPM	Revolutions per minute	1/min

ρ	Density	kg/ m^3
t_{dp}	Time to reach the desired amount of dispersed phase	s
t_{res}	Residence time	s
T	Temperature	˚C
θ	Contact angle	rad
V	Volume	m^3
w	CIJs jet-to-jet distance	m
W	CIJs chamber width	m
W_{jet}	Mass jet flow rate	kg/s
ζ	Zeta potential	mV

Abbreviations

AFM	Atomic force microscopy
CFD	Computational fluid dynamics
CIJs	Confined Impinging Jets
CMC	Critical micelle concentration
DLS	Dynamic light scattering
DQMOM	Direct-Quadrature-Method-Of-Moments
DSC	Differential Scanning calorimetry
DSD	Droplet size distribution
EF	Energy efficiency
EM	Electron microscopy
HLB	Hydrophilic-lipophilic-balance
HPH	High-pressure homogeniser
HSD	High speed disperser
HSM	High-shear mixer
IEM	Interaction-by-Exchange-with-the-Mean
LES	Large eddy simulation
LIF	Laser induced fluorescence
LM	Light microscopy
NMR	Neutron magnetic resonance

NS	Neutron scattering
PIT	Phase inversion temperature
PIV	Particle image velocimetry
PLIF	Planar laser induced fluorescence
PRE	Pre-emulsion
RANS	Reynolds-averaged-Navier-Stokes
Re	Reynolds number
RM	Rotating membrane
Si	Silica
SLS	Static light scattering
T20	Tween20
Ta	Taylor number
TI	Turbulent-inertial
TV	Turbulent-viscous
US	Ultrasound

Chapter 1

Introduction

1.1. Background

A large number of food products (e.g. mayonnaise, milk, soup, cake batter, spread, margarine, among others) consist of an emulsion microstructure or have been emulsified at some stage during their manufacture (1). In their simplest configuration, emulsions represent a mixture of two immiscible liquids (typically oil and water), where droplets of one liquid (i.e. dispersed phase) are dispersed in the other (i.e. continuous phase). One can distinguish between oil-in-water (o/w) emulsions, where an aqueous phase surrounds oil droplets or vice versa water-in-oil (w/o) emulsions, where water droplets are encompassed within an oily continuous phase. Due to the immiscibility of the two phases, emulsions are thermodynamically unstable (2). In fact, once droplets are formed they tend to merge together in order to minimise the contact area between the two immiscible phases. However, it is possible to form emulsions which have extended stability through the addition of emulsifiers (2). Typical emulsifiers included in food formulations are surfactants, proteins, nanoparticles (or often a mixture of these). Emulsifiers contribute to the droplet stabilisation during both processing and storage (3). During processing, emulsifiers bind at the drop interface thus preventing drop-drop contact under the usually intense mixing conditions imposed and subsequently coalescence. Furthermore, surfactants and proteins, which are surface-active, reduce the interfacial tension upon adsorption at the interface and facilitate droplet breakage. During storage, emulsifiers additionally prevent droplets from coming into contact and possibly coalescing over time. Besides coalescence, other mechanisms of emulsion instability can also take place, with creaming, flocculation and Ostwald ripening representing some common examples (4). One must note that instability phenomena are often interrelated and the occurrence of one type of instability may trigger others (4).

What is more, the complexity of emulsion-based systems also stems from the fact that emulsions often contain a complex mixture of other ingredients (e.g. water, oil, emulsifiers,

polysaccharides, proteins, colorants, minerals, acid, bases, vitamins, preservatives) which solely and through their mutual interactions contribute to the overall properties of the product (e.g. texture, appearance, shelf-life, nutritional values etc) (5-7). In fact, the inherent complexity of such systems becomes apparent at different levels and ultimately entails that emulsion properties depend on a large span of factors (8). At a molecular level, each of the molecular species presents different physical and chemical properties. These species interact with each other to form the different phases. All of these formulation related aspects, together with the choice of the right processing methods as well as storage conditions, contribute to the properties of the final emulsion-based product (8).

Within this context, the tailored control and understanding of the emulsion microstructural characteristics represents a possible strategical approach for the development of more functional foodstuff as well as for the improvement of existing ones (9, 10). If on one side, microstructural features (i.e. emulsion average droplet size and droplet size distribution) are mainly influenced by the choice of both formulation and processing parameters, on the other, these primarily determine the emulsion bulk properties (e.g. texture, appearance, shelf-life among some examples), Figure 1 (9, 10).

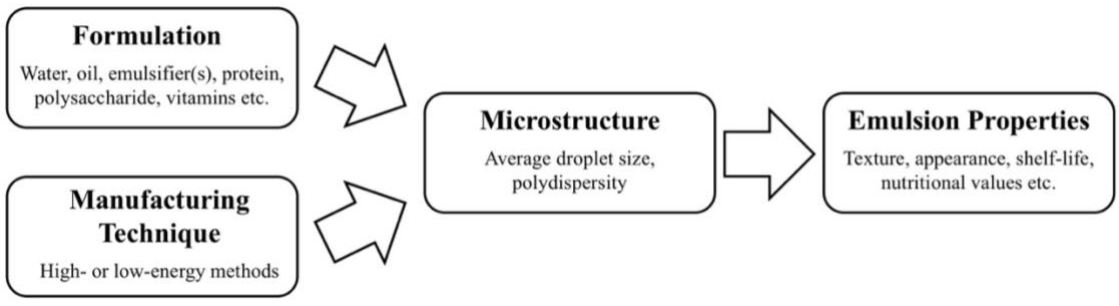

Figure 1.1 Schematic representation of the microstructure as a key, central parameter to tailor and control the influence of both formulation and manufacturing parameters on the final emulsion properties.

A detailed description of the basic emulsion constituents, of their influence on the microstructure and stability of conventional as well as of more complex systems, of the available spectrum of processing techniques and the relationship between microstructure design and product properties is provided in Chapter 2.

The remaining of this introduction will only focus on providing the literature background that relates to the main topic of this thesis, i.e. the Confined Impinging Jets.

1.2. Confined Impinging Jets

This section aims to provide a comprehensive literature review on previous studies reported on the use of Confined Impinging Jets (CIJs) for different applications. In CIJs, two fluids continuously collide at high velocities within a confined environment (e.g. mixing chamber), thus generating high-levels of turbulence over rather short residence times. A schematic representation of a typical CIJs geometrical configuration is represented in Fig. 1.2. One of the strengths of such processing method lays in the fact that it exploits the impact of the two jets to generate large energy dissipation rates rather than the application of pressure, shear or cavitation.

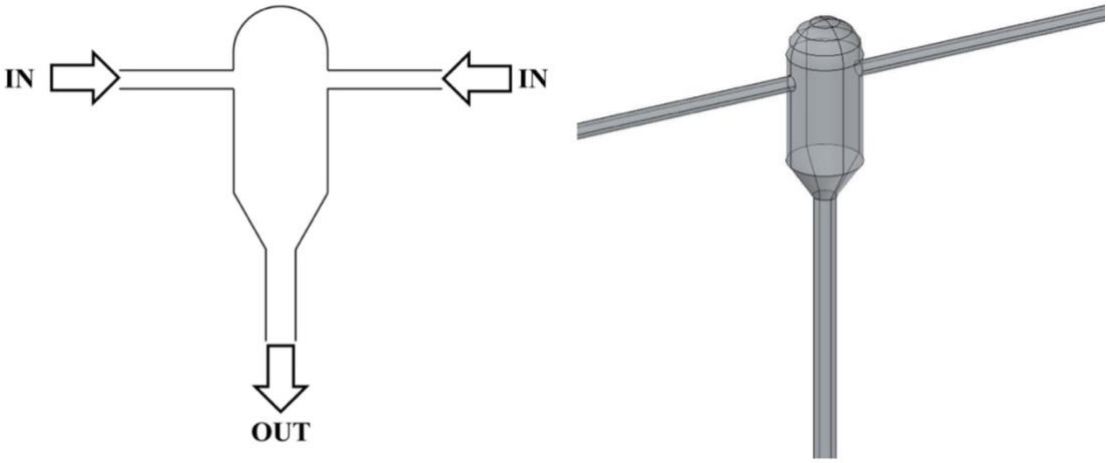

Figure 1.2. Schematic and 3D representation of a typical CIJs geometrical configuration.

Despite the simplicity and flexibility of the technique, the majority of reports on CIJs extensively describe the use of this method for mixing purposes (whether for the formation of nanoparticles or to enhance the mixing between miscible liquids) from both an experimental and computational standpoint. A significantly smaller number of reports concerns the investigation of the CIJs processing performance for emulsion production.

Consequently, the first part of this section focuses on the review of previous works conducted on the adoption of CIJs for mixing purposes, while the second part emphasises on the investigations exploring the potential of CIJs as a novel methodology for the continuous, turbulent production of emulsion based systems.

1.2.1. CIJs performance in mixing applications

The pioneering work of Johnson and Prud'homme (11) was one of the first reports exploiting the processing features of CIJs for the flash precipitation of nanoparticles. In this investigation, it was recognised that CIJs represented an attractive method due to the possibility of delivering mixing times shorter than those for precipitation. The CIJs flow regime and characteristic mixing time were studied by using a highly sensitive and robust parallel reaction. The onset of the turbulent regime was detected at jet Reynolds numbers as low as 90, while the characteristic mixing time assumed values as small as 95 ms. These results clearly highlighted that even at relatively low jet velocities, the mixing within the CIJs chamber was of turbulent nature and allowed the formation of a reduced amount of by-products. It was also observed that the processing performance (i.e. the reaction conversion) was improved as the Reynolds numbers were increased due to the higher levels of turbulence achieved during operation. The work also determined a scale-up rule for CIJs at varying jet velocity, fluids' viscosity and chamber dimensions, and showed that the experiments were also easy to duplicate at a production scale.

Further studies from the same authors focused on the production of block-copolymer covered nano-particles made out of hydrophobic, organic compounds at high-solid loads (12). CIJs was chosen for this application as it guaranteed mixing times comparable or shorter (depending on the processing conditions) than the nucleation and growth time of the nanoparticles as well as the induction time for deposition of the copolymer portion on their surface. The former two characteristic times could be adjusted by finely choosing the type and concentration of both copolymer and nanoparticles. On the other side, the characteristic CIJs mixing time and flow regime could be influenced by varying the jet velocities as well as the geometrical characteristics of the mixing chamber. It was found that this processing method allowed mixing times in the range of milliseconds, which resulted overall much shorter than either characteristic times related to nanoparticles and copolymer, thus permitting the design of particle dispersions with a very narrow size distribution, well within the nano-size range.

Although these studies effectively demonstrated the suitability of CIJs to rapidly produce nanoparticles under an easy-to-achieve turbulent-flow regime, their main limitations consisted in that the provided scale-up rules required new experiments for any change in either the CIJs geometrical or processing conditions. This is the reason why subsequently the Computational Fluid Dynamics (CFD) characterisation of the CIJs received particular attention. In particular, an investigation aimed to predict the experimental data (i.e. reaction conversion and residence time) showed by Johnson and Prud'homme (11), through the development of a CFD model (13). The CFD model solved the k-ε turbulence model, integrated with the Direct-Quadrature-Method-Of-Moments (DQMOM) model and coupled to the Interaction-by-Exchange-with-the-Mean (IEM) model, to describe mixing at the molecular level. It was found that the developed strategy could accurately predict the experimental data from Johnson and Prud'homme, thus opening for the first time a novel path for the 'experiment-free' design and scale up of the CIJs technology.

A similar model implemented with a Reynolds-Averaged Navier-Stokes (RANS) approach (rather than the k-ε turbulence model) coupled to population balance equations, was also used to predict the actual nanoparticle formation upon reaction of the two streams in the CIJs (14). The experimental set of data used to probe the suitability of the model was previously published in another work (15), which studied the formation of barium sulphate nano-particles for different turbulence levels, CIJs geometries and degree of initial supersaturation. The model successfully predicted the average nanoparticle size found in the previous experimental work. In a following study, the same authors expanded the prediction capability of this model and additionally established a scale-up criterion based on two different CIJs geometries having different dimensions but overall similar geometrical characteristics (16). It was found that the Reynolds number alone could not be used as an appropriate scaling variable, since data relative to different geometries could not be correlated. However, all data collapsed in a single curve by taking as the scale-up parameter the ratio between the characteristic mixing and reaction times. Therefore it was suggested that this simple yet effective correlation could also be extended to other chemical systems in the presence of two competitive processes (e.g. particle nucleation and molecular growth).

A succeeding experimental work investigated the processing performance of CIJs for the production of a range of water-soluble (Salbutamol sulfate and mannitol) and poorly water-soluble (ibuprofen and cyclosporine) nanodrugs (17). Flash nanoprecipitation was obtained when either Salbutamol sulfate or cyclosporine were processed, whereas the CIJs was not suitable for the production of nanodrugs containing either of the other two compounds. It was proposed that the CIJs aptness to produce nanodrugs strongly depended on the compound formation time in relation to the processing environment. For this reason, it was suggested that in order to broaden the range of compounds which could be processed through the CIJs as well as achieve narrower

particle size distributions, the mixing chamber could be optimised to generate compound formation times longer than the mixing time but smaller than the total residence time.

A further study on the use of CIJs for the production of nanoparticles was conducted to measure the mean nanoparticle size resulting from a heterogenous reaction and its yield for a wide range of jet flow rates (18), Figure 1.3.

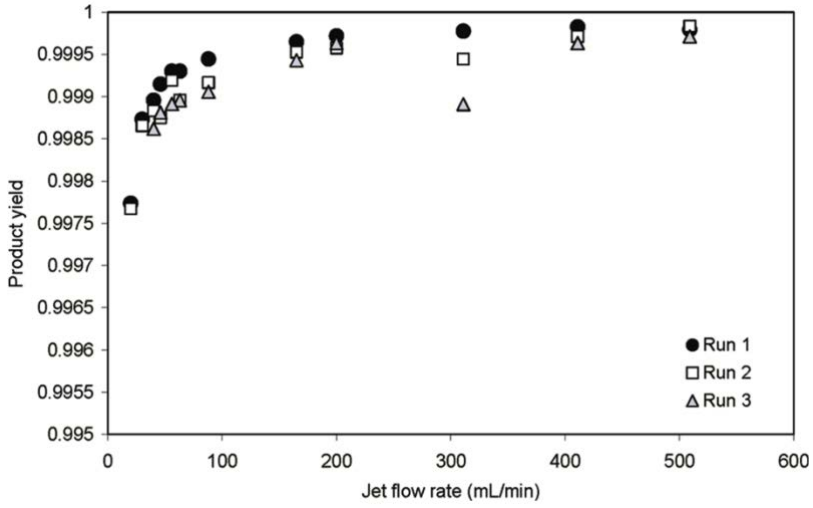

Figure 1.3. Effect of the jet flow rate on the reproducibility of the product yield of a precipitation reaction (18).

Furthermore for each jet flow rate, the study assessed through CFD the energy dissipation rate profiles and their mean values, with the latter then compared with both the theoretical and experimental estimates of the average turbulent energy dissipation rate. It was found that the product yield increased with the jet flow rate while the particle size decreased as both the jet flow rate and the concentration of the input reactants were higher, in agreement with observations in other studies (11, 12, 14, 15). .

It was proposed that as higher jet flow rates were approached, the flow became progressively more turbulent and boosted the mixing of reactants, in turn causing the generation of smaller

particles. This effect became even more evident as more reactants where injected into the systems. From the CFD simulations, the establishment of an impingement plane in the middle of the chamber (i.e. the area where jet collision takes place) was observed, which corresponded to a peak in energy dissipation rate. Away from the impingement point, the energy dissipation rate rapidly decayed in both the radial and axial directions. Despite the fact that the generated turbulence was found to be rather inhomogeneous, the small dimensions of the mixing chamber allowed for the incoming fluids to pass through the maximum energy dissipation rate region, thus resulting in products with rather homogeneous properties (i.e. highly narrow particle size distribution). It must also be noted that CFD results were obtained from a k-ε turbulence model, which resulted more practical than the more powerful yet too time intensive Large Eddy Simulations (LES) or RANS models (more suitable to describe transient phenomena, such as those taking place within the CIJs geometry) employed by other studies (13, 14, 16). Despite this simplification, the data of the average energy dissipation rates derived from CFD with those obtained both experimentally and theoretically showed excellent agreement over the entire range of jet flow rates. The work concluded that the CIJs displayed increasing promise for applications requiring controlled mixing conditions to ensure elevated quality of the product. In a following report, the same authors investigated the production of submicron iron oxide particles through CIJs coupled with a sonication probe (acting on the area of jet collision) at varying feed flow rates, feed type and concentration, as well as at different stabiliser addition points (whether in situ or after the reaction) and sonication strategy (whether in situ or after the reaction) (19). The size of the formed particles decreased as both the jet flow rate and the feed concentration were increased. Higher jet velocities caused more dissipation energies which drove the formation of smaller particles, while higher feed concentrations resulted in smaller particles since more reactants were present in the CIJs mixing volume. It was observed that, upon collision, the jet

impingement also induced the formation of large agglomerates. However, the agglomerate size could be easily reduced by sonication after the reaction, thus obtaining nanoparticle dispersions having smaller mean particle sizes and narrower particle size distributions. In situ sonication did not limit the formation of agglomerates at high flow rates, where the turbulence generated in the CIJs was indicated as sufficient to give high product yield even in the absence of the sonication probe.

After the set of studies presented above, the majority of works found in subsequent literature assessed (both computationally and experimentally) the CIJs mixing performance as well as the flow regime established during operation.

The flow field in a linear version of the CIJs was experimentally evaluated for a series of different geometrical configurations (i.e. ratio of the widths of chamber to the jet, W/w, and ratio of the chamber width to the chamber depth, W/d) and hydrodynamic conditions, by using Planar Laser Induced Fluorescence (PLIF) (20). The main goal of this investigation was to find the optimal geometrical and operational conditions allowing self-sustainable turbulent flow regime (i.e. oscillation of the impingement plane, formation of vortices downstream the impingement point and generation of a vortex street throughout the CIJs mixing chamber). It was observed that the sustainable chaotic flow was enabled when $W/w = 6$, $W/d \geq 2$ and Re_{jet} was above 300. Therefore it was proved that both CIJs geometrical features and processing conditions were key parameters in influencing the type of flow regime established during CIJs operation.

Another study focused on assessing the flow characteristics and mixing performance of a T- and Y-CIJs jet configurations by using both experimental, i.e. Laser Induced Fluorescence (LIF) and Particle Image Velocimetry (PIV), and computational, i.e. CFD, tools (21). Experimental data were compared with the results obtained from CFD simulations based on a Detached Eddy-SST-k-ω turbulence model, which was described as a cost-efficient and highly accurate method

to probe the transient turbulent conditions in CIJs. A laminar regime was detected for $Re_{jet} \leq 200$, while a transition region was observed up to a $Re_{jet} \approx 1000$. Above this value, the flow regime was dominated by the presence of vortices as demonstrated from both LIF and PIV images. No major differences were found among the two geometries, with the only exception being the presence of an elongated mixing region in the Y-geometry due to the presence of the angled inlets. Interestingly, the authors demonstrated the unsuitability of the RANS turbulence model to represent the rather complex CIJs phenomena. On the other hand, the use of the Detached Eddy-SST-k-ω turbulence model could generate results which excellently compared with experimental data.

The CIJs mixing performance was assessed in a subsequent study by using PLIF at $100 \leq Re_{jet} \leq 500$ (22). Although this study evaluated a lower range of Reynolds numbers compared to the work described earlier, in this case mixing was aided by means of a vibration technique. Vibration-aided processes represent a practice usually employed in mixing applications to cause the onset of convective mixing at lower hydrodynamic conditions (23-25). The effect of different fluid viscosities through the addition of glycerol to an aqueous solution was also evaluated. Data suggested that the increase in the viscosity of the incoming jets did not hinder the observed mixing characteristics. On the other hand, higher excitation frequencies caused turbulent mixing at lower Reynolds numbers according to the expectations. Under equal excitation frequency, higher Reynolds numbers were responsible for generating an oscillating impingement plane, which in turn reduced the scale of segregation thus ultimately improving the CIJs mixing performance.

CIJs mixing characteristics were also investigated for the purpose of mixing fluids with dissimilar viscosities again by means of PLIF. The balancing of the flow of two inlet streams with different viscosities was determined as the key variable to create an optimal environment

for the establishment of the desired mixing conditions. Once this was controlled, the onset of turbulent mixing was observed in the region of $120 \leq Re_{jet} \leq 150$, above which the presence of vortices boosted CIJs mixing performance.

The study of the CIJs flow field characteristics under highly turbulent conditions was further investigated in an additional report both experimentally, by means of Particle Image Velocimetry (PIV), and computationally, by means of CFD simulations based on LES as the turbulence model. Interestingly, it was observed from PIV visualisation that the stagnation point in the mixing chamber fluctuated within ± 2.5mm. The findings were in agreement with the data obtained from CFD simulations. It was proposed that in order to mitigate this fluctuation, a smaller mixing chamber would ensure the impact of the two streams at its centre and as a consequence result in maximum turbulent energy dissipation. The 3D turbulent environment detected from PIV could be replicated and confirmed by the CFD results through the LES model. The work also demonstrated the unsuitability of the k-ε model to describe the turbulent energy distribution within the CIJs cavity, which lead to an error (if compared to both PIV and LES) in its estimation of up to 30%.

In order to further enhance the capacity to deliver optimal mixing conditions, CIJs was also combined with a High Speed Disperser, HSD (26). This strategy was adopted to eliminate any possible restriction in the CIJs mixing performance arising from the presence of two pumps with limited power. The study investigated the micromixing performance of the CIJs-HSD system for an iodate-iodate chemical reaction for a range of processing (i.e. jet flow rate, HSD rotational speed) as well as structural (i.e. HSD coupling distance) parameters (26). Firstly the solutions were forced to collide and mix within the CIJs. Subsequently the outcoming stream flowed and impacted into the surfaces of the HSD, which induced further shearing to reduce the scale of segregation (i.e. to enhance the micromixing) between the two starting fluids. The results showed

that the micromixing time decreased at higher HSD rotation speeds whereas remained mostly unaffected by variation in the jet flow rate as well as in the HSD coupling distance. A micromixing time in the range of 0.1-0.3 ms for the CIJs-HSD was measured, compared to that of the CIJs alone, 0.35-0.5 ms. Based on the observed results, it was proposed that the CIJs-HSD system resulted an affective intensification strategy to deliver enhanced mixing performance.

1.2.2. The adoption of CIJs for emulsification

The expansion of the CIJs capability to applications focusing on the production of emulsions has only received particular attention over the last decade. One of the first report focusing on the CIJs potential to deliver emulsion-based microstructures compared the CIJs emulsification performance with that of more established homogenisation techniques, such as the high-pressure homogeniser, HPH, high-shear mixer, HSM, and ultrasound treatment, US (27). Dilute (dispersed phase volume fraction below 10 v/v %) o/w emulsions stabilised by either Tween20 or Lecithin were manufactured in the different emulsification methods under varying processing conditions, and emulsion quality was assessed in terms of average droplet size. The average energy dissipation rate was chosen as the parameter to cross-compare the performance of each of the techniques employed in the study, Figure 1.4. The data showed that the CIJs treatment generated mean energy dissipation rates comparable to those of both HSM and US. The emulsion droplet size resulting from the HSM was smaller than the CIJs, but only in the region of high energy dissipation rates. Compared to both methods, the US produced smaller droplet sizes. The droplet size achieved following the high-pressure treatment showed similar values to the US but at significantly higher mean energy dissipation rates (1000 times larger) than those evaluated in the other three methods.

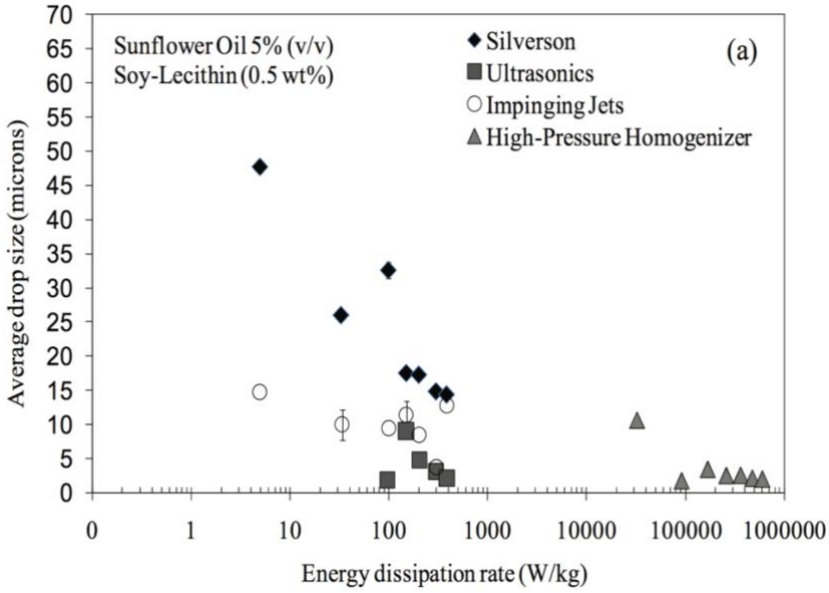

Figure 1.4. Emulsion droplet sizes produced under various energy dissipation rates in different emulsification techniques (27).

The change in the emulsifier type and the oil load did not cause major variations in the observed trends. Although submicron droplet sizes could not be generated within the CIJs, for the first time it showed potential for the turbulent continuous production of macro-emulsions through the generation of levels of turbulence comparable to those of already-established emulsification techniques.

The production of dilute (dispersed phase volume fraction below 10 v/v %) o/w emulsions via the CIJs (starting from roughly mixed pre-emulsions) was further explored under a wide range of turbulent processing conditions and various emulsifier types (1 wt.% of Tween20, Sodium Dodecyl sulphate, SDS, Whey Protein, Lecithin, Span80) (28). The smallest emulsion average droplet size (~ 5 μm) was observed under fully turbulent conditions, i.e. by approaching the highest jet flow rate, regardless on both the type of emulsifier and the dispersed phase content, Figure 1.5. At Reynolds numbers below 10^4, the presence of different emulsifiers caused variations in the droplet size. Surfactants (SDS or Lecithin) having the smallest molecular weight

and inducing the lowest o/w interfacial tensions resulted in the smallest droplet sizes (~ 10 µm). On the other hand, the presence of larger emulsifiers (Tween20, Span80 and Whey protein) provided bigger droplets (~ 30 - 40 µm). The turbulent conditions established during CIJs operation at Reynolds numbers above 10^4 were able to mitigate the observed differences in droplet size observed at lower jet flow rates, with all the systems showing a similar average droplet size independently from the type of emulsifier.

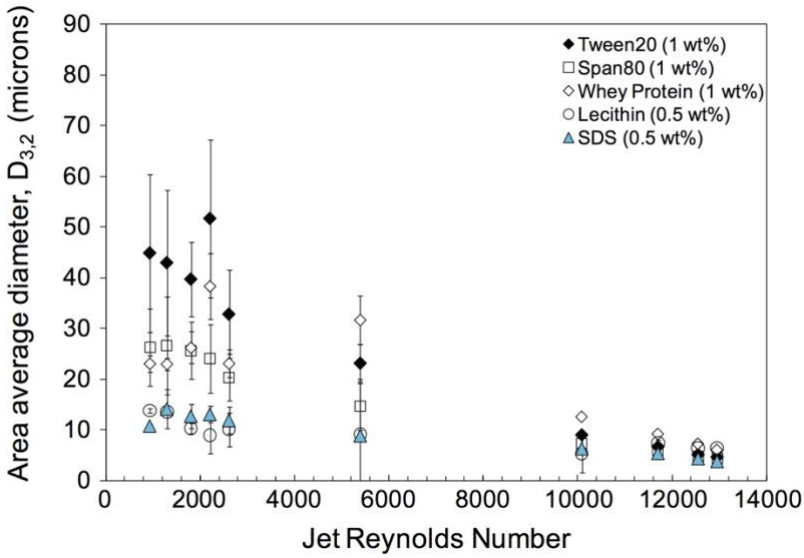

Figure 1.5. Emulsion droplet sizes produced under various jet Reynolds numbers via the CIJs (28).

The increase in the dispersed phase mass fraction only caused larger droplet sizes (if compared to the more diluted systems) at low Reynolds numbers but no differences were again observed for Re_{jet} above 10^4. Emulsions were also recirculated up to 10 times under fixed hydrodynamic conditions (i.e. the highest jet flow rate) to assess the effect of prolonging the exposure of the formed emulsions to the CIJs turbulent conditions. No major changes in the average droplet size were observed after passing four times the emulsions through the CIJs cavity, while the width of the droplet size distribution remained practically unvaried upon recirculation.

The emulsification capacity of CIJs was also evaluated for the production of 10 wt.% o/w emulsion containing as the dispersed phase oils with different viscosities (sunflower oil, 50 cP, silicon oils, 5 and 50 cP, heptane, 0.56 cP and dodecane, 1.34 cP) in the presence of 1 wt.% of either SDS or Tween20. Starting from a rough pre-emulsion, emulsification was carried out in the turbulent regime under varying jet flow rates and the mean droplet size as well as the droplet size distribution upon both processing and recirculation were assessed. Under fixed CIJs hydrodynamic conditions and emulsifier type, emulsification of oils with higher viscosity (sunflower and a silicon oil) generated larger droplet sizes. Contrarily the processing of less viscous oils (a silicon oil, heptane and dodecane) resulted in smaller droplet sizes over the whole range of hydrodynamic conditions. Upon recirculation, the average droplet size was reduced up to either the fourth pass (for higher viscosity oils) or further up to the fifth pass (for lower viscosity oils) with no additional reductions after that, in agreement with a previous study (28). What is more, the increase in the number of passes under a fixed jet flow rate did not produce variations in the width of the droplet side distribution of higher viscosity dispersed phases (both sunflower and silicone oils with a value of viscosity equal to 50 cP) yet caused considerably narrower distributions for the case of oils with lower viscosity (all the other oils examined in the study). Overall, it was proposed that oil droplets with lower viscosities could be more easily affected by the turbulent conditions established during the CIJs operation.

In another study, the emulsion droplets formed following the jet collision were visualised by means of a high speed camera. The mean droplet size and the size distributions were then extracted from the captured images by means of an image analysis software. Differently from the studies previously described, the two distinct phases (water and Exxol D80) were separately injected into the CIJs cavity and either o/w or w/o emulsions were formed depending on the ratio of the two jet flow rates. No surfactant was present in either phases probably because the report

only focused on the evaluation of the emulsion droplet size and distribution immediately after the jet collision. Another reason may be that by using a surface active component, i.e. by reducing the o/w interfacial tension, the formed droplets could result too small to be visualised. The droplet size was found to decrease at higher jet velocities, i.e. at higher energy dissipation rates. At low jet velocity, the resulting mean drop size depended on the ratio of the two jet flow rates. This effect was minimised once higher jet velocities were approached. When the water stream was injected at higher flow rate the oil one (i.e. oil was dispersed as droplets), the formed droplets resulted larger and with a lower polydispersity than the opposite situation. The authors proposed that, when water was the continuous phase, the inertial stresses experienced by the droplets were higher than the other scenario, i.e. when Exxol D80 was instead used as the continuous phase.

The use of CIJs was also recently exploited for the production of both micro- and nano-sized emulsion droplets when used in conjunction with a sonication probe acting in the area where the jet collision took place (29). In this study, two equally formulated (5 and 10 v/v %) sunflower or silicon o/w pre-emulsions were pumped into the CIJs mixing chamber at various jet flow rates and under different levels of sonication amplitude, in the presence of 0.5 wt.% of SDS, Polyglycerol polyricinoleate (PGPR) or a mixture of the two (at equal ratio). The study confirmed that the smallest droplet size was observed as the highest jet flow rate was approached independently on the dispersed phase volume fraction, the type of oil and the type of surfactant systems. In conjunction with the sonication probe, the emulsion droplet size resulting from the processing presented a droplet size < 700 nm, compared to the treatment of emulsions via the CIJs alone, which had a mean diameter above 1 μm even after 10 passes, Figure 1.6.

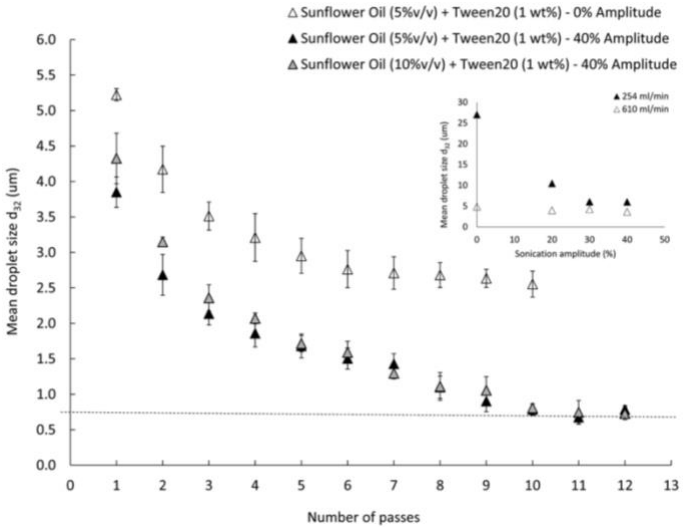

Figure 1.6. Effect of the oil content and of the in situ sonication on the recirculation under fixed CIJs jet flow rate, 610 g/min, on the emulsion average droplet size (29).

The last study (to the best of the author's knowledge) available in the literature reporting on the use of CIJs for emulsification purposes is represented by our work and focused on the investigation of the CIJs performance and capacity for the production of highly concentrated emulsions (30). This will be discussed in more details in the third chapter of this thesis.

1.3. Research scope

Innovation is a key and essential part of the food industry. The development of innovative processes and products is however a rather complex practice. It involves rapid translation of scientific results into high-value application(s), the utilisation of technical advances from other disciplines as well as quick response to the rapidly changing society and business needs.

An exciting area of research currently focuses on the development of manufacturing approaches using Confined Impinging Jets (CIJs) for the production of emulsions. CIJs offer the ability to create emulsion-based microstructures with lower energy inputs than conventional emulsification routes. Since the application of CIJs for emulsification purposes is still a relatively new area of investigation, the central purpose of this thesis is to demonstrate the applicability of

CIJs as a reliable alternative to existing emulsification methods. This is conducted by assessing the CIJs processing capacity and performance in delivering emulsion-based systems starting from a wide span of different formulations. Ultimately, in providing a solid understanding of the CIJs processing characteristics and its limitations, this work aims to represent a strong starting platform for eventual future works scoping the application of CIJs in this field.

1.4. Thesis layout

The thesis follows the alternative format of the University of Birmingham where both literature review and results are presented in separate chapters (Chapters 2-5) which corresponded to different publication style papers that are either published, submitted for publication or can be potentially submitted in the future.

Chapter 2. This section contains a literature background on simple as well as more complex emulsion systems keeping at its central core the influence of the choice of both formulation and processing aspects on the emulsion microstructure, and its relationship with the properties of emulsion based products. The content of this chapter is published under the title " Food Structure Development in Emulsion Systems" as part of the "Handbook of Food Structure Development".

Chapter 3. This section explores the CIJs performance in the production of dilute as well as highly concentrated emulsions under a wide range of hydrodynamic conditions as well as in both the surfactant-poor and -rich regime. The content of this chapter is published under the title "Production of oil-in-water emulsions with varying dispersed-phase content using Confined Impinging Jet Mixers" in the Journal of Industrial and Engineering Chemistry Research.

Chapter 4. This section reports on the CIJs performance for the production of dilute as well as semi-concentrated emulsions stabilised by either nanoparticles (Pickering emulsions) or surfactant-particle mixed systems. The content of this chapter is under review in the Journal of Food and Bioproducts Processing under the title "Pickering and mixed emulsifier stabilised emulsions formed via Confined Impinging Jets processing".

Chapter 5. This section aims to offer a comprehensive comparison of the CIJs performance with that of already-established both low- and high-energy emulsification techniques.

Chapter 6. In this final section the conclusions of this work are summarised along with the suggestions for future work.

1.5. Dissemination of research findings

1.5.1. Publications

- Tripodi E., Lazidis A., Norton I.T., Spyropoulos F. Food structure development. In: Handbook of food structure development. The Royal Society of Chemistry; 2019.

- Tripodi E., Lazidis A., Norton I.T., Spyropoulos F. On the production of oil-in-water emulsions with varying dispersed phase content using Confined Impinging Jet Mixers. Industrial & Engineering Chemistry Research. 2019;58(32):14859-72

- Tripodi E., Norton I.T., Spyropoulos F. Pickering and mixed emulsifier stabilised emulsions formed via Confined Impinging Jets processing. Under review in the Journal of Food and Bioproducts processing.

1.5.2. Conference oral presentations

- "Low-energy emulsification using Confined Impinging Jets". *Food Factory*, Laval (France), 18-20 October 2016.

- "Low-energy manufacture of food emulsions using Confined Impinging Jet Reactors". *10th European PhD Workshop on Food Engineering and Technology*, Nestlé Product Technology Centre, Singen (Germany), 28-29 April 2017.

- "Confined Impinging Jets: a low-energy approach for food emulsification manufacturing". *The KTN Early Careers Researcher in Food Conference*, Birmingham (UK), 17 October 2017. (1st prize for oral presentation)

- "Confined Impinging Jets: a low-energy approach for food emulsification manufacturing". *Mars – Waltham Centre for Petcare Nutrition*, Waltham (UK), 31 January 2018.

- "Confined Impinging Jets: a low-energy approach for food emulsification manufacturing". *Centre for Innovative Manufacturing Conference*, Nottingham (UK), 25-26 March 2018.

- "Confined Impinging Jets: a low-energy approach for food emulsification manufacturing". *IchemE Mixing Special Interest Group Conference*, Manchester (UK), 13 April 2018.

- "Confined Impinging Jets: a novel approach to food emulsification". *16th European Conference on Mixing – Mixing 16*, Tolouse (France), 9-12 September 2018.

- "Confined Impinging Jets: a low-energy perspective over the turbulent food emulsification". *Future of Food and Drink: Product, Process and Beyond*, Cambridge (UK), 26 September 2018.

- "Confined Impinging Jets: a novel approach to food emulsification". Nestlé Product Technology Centre, York (UK), 2 November 2018.

List of references

(1) Dalgleish D.G. *Food emulsions-their structures and structure-forming properties*. Food Hydrocolloids 2006; 20 (4): 415-22.

(2) Li Y., Xiang D. *Stability of oil-in-water emulsions performed by ultrasound power or high-pressure homogenization*. Plos one 2019; 14 (3): e0213189.

(3) Wei Z., Cheng J., Huang Q. *Food-grade Pickering emulsions stabilized by ovotransferrin fibrils*. Food Hydrocolloids 2019; 94: 592-602.

(4) Bibette J., Morse D.C., Witten T.A., Weitz D.A. *Stability criteria for emulsions*. Physical Review Letters. 1992; 69 (16): 2439-42.

(5) Bai L., Huan S., Li Z., McClements D.J. *Comparison of emulsifying properties of food-grade polysaccharides in oil-in-water emulsions: Gum arabic, beet pectin, and corn fiber gum*. Food Hydrocolloids. 2017; 66: 144-53.

(6) Kavitake D., Balyan S., Devi P.B., Shetty P.H. *Interface between food grade flavour and water soluble galactan biopolymer to form a stable water-in-oil-in-water emulsion*. International Journal of Biological Macromolecules. 2019; 135: 445-52.

(7) Mason T.G., Wilking J.N., Meleson K., Chang C.B., Graves S.M. *Nanoemulsions: formation, structure, and physical properties*. Journal of Physics: Condensed Matter. 2006; 18(41): R635-R66.

(8) Hu Y.-T., Ting Y., Hu J.-Y., Hsieh S.-C. *Techniques and methods to study functional characteristics of emulsion systems*. Journal of Food and Drug Analysis. 2017; 25(1): 16-26.

(9) Wu B.-c., McClements D.J. *Design of reduced-fat food emulsions: Manipulating microstructure and rheology through controlled aggregation of colloidal particles and biopolymers*. Food Research International. 2015; 76: 777-86.

(10) Kargar M., Spyropoulos F., Norton I.T. *Microstructural design to reduce lipid oxidation in oil-inwater emulsions*. Procedia Food Science. 2011; 1: 104-8.

(11) Johnson B.K., Prud'homme R.K. *Chemical processing and micromixing in confined impinging jets*. AIChE Journal. 2003; 49(9): 2264-82.

(12) Johnson B.K., Prud'homme R.K. *Flash nano-precipitation of organic actives and block copolymers using a Confined Impinging Jets Mixer*. Australian Journal of Chemistry. 2003; 56(10): 1021-4.

(13) Liu Y., Fox R.O. *CFD predictions for chemical processing in a confined impinging-jets reactor*. AIChE Journal. 2006; 52(2): 731-44.

(14) Gavi E., Rivautella L., Marchisio D.L., Vanni M., Barresi A.A., Baldi G. *CFD Modelling of nano-particle precipitation in Confined Impinging Jet Reactors. Chemical Engineering Research and Design*. 2007; 85(5): 735-44.

(15) Marchisio D.L., Vigil R.D., Fox R.O. *Quadrature method of moments for aggregation–breakage processes*. Journal of Colloid and Interface Science. 2003; 258(2): 322-34.

(16) Gavi E., Marchisio D.L., Barresi A.A. *CFD modelling and scale-up of Confined Impinging Jet Reactors*. Chemical Engineering Science. 2007; 62(8): 2228-41.

(17) Chiou H., Chan H.-K., Prud'homme R.K., Raper J.A. *Evaluation on the use of Confined Liquid Impinging Jets for the synthesis of nanodrug particles*. Drug Development and Industrial Pharmacy. 2008; 34(1): 59-64.

(18) Siddiqui S.W., Zhao Y., Kukukova A., Kresta S.M. *Characteristics of a Confined Impinging Jet Reactor: energy dissipation, homogeneous and heterogeneous reaction products, and effect of unequal flow*. Industrial & Engineering Chemistry Research. 2009; 48(17): 7945-58.

(19) Siddiqui S.W., Unwin P.J., Xu Z., Kresta S.M. *The effect of stabilizer addition and sonication on nanoparticle agglomeration in a confined impinging jet reactor*. Colloids and Surfaces A: Physicochemical and Engineering Aspects. 2009; 350(1): 38-50.

(20) Ashar Sultan M., Fonte C.P., Dias M.M., Lopes J.C.B., Santos R.J. *Experimental study of flow regime and mixing in T-jets mixers*. Chemical Engineering Science. 2012; 73: 388-99.

(21) Metzger L., Kind M. *On the transient flow characteristics in Confined Impinging Jet Mixers - CFD simulation and experimental validation*. Chemical engineering science. 2015; 133: 91-105.

(22) Shi Z.-h., Li w.-f., Du K.-j., Liu H.-f., Wang F.-c. *Experimental study of mixing enhancement of viscous liquids in confined impinging jets reactor at low jet Reynolds numbers*. Chemical Engineering Science. 2015; 138: 216-26.

(23) Ito Y., Komori S. *A vibration technique for promoting liquid mixing and reaction in a microchannel*. AIChE Journal. 2006; 52(9): 3011-7.

(24) Brito M.S.C.A., Esteves L.P., Fonte C.P., Dias M.M., Lopes J.C.B., Santos R.J. Mixing of fluids with dissimilar viscosities in Confined Impinging Jets. Chemical Engineering Research and Design. 2018; 134: 392-404.

(25) Niu X., Liu L., Wen W., Sheng P. *Hybrid Approach to High-Frequency Microfluidic Mixing*. Physical Review Letters. 2006; 97(4): 044501.

(26) Nie A., Gao Z., Xue L., Cai Z., Evans G.M., Eaglesham A. *Micromixing performance and the modeling of a confined impinging jet reactor/high speed disperser*. Chemical Engineering Science. 2018;184:14-24.

(27) Siddiqui S.W. *Mixing performance of various geometries - Emulsification perspective*. Procedia Food Science. 2011; 1: 131-7.

(28) Siddiqui S.W., Norton I.T. *Oil-in-water emulsification using Confined Impinging Jets*. Journal of Colloid and Interface Science. 2012; 377(1): 213-21.

(29) Siddiqui S.W., Wan Mohamad W.A.F., Mohd. Rozi M.F., Norton I.T. *Continuous, high-throughput flash-synthesis of submicron food emulsions using a Confined Impinging Jet Mixer: effect of in situ turbulence, sonication, and small surfactants*. Industrial & Engineering Chemistry Research. 2017; 56(44): 12833-47.

(30) Tripodi E., Lazidis A., Norton I.T., Spyropoulos F. *On the production of oil-in-water emulsions with varying dispersed phase content using Confined Impinging Jet Mixers*. Industrial & Engineering Chemistry Research. 2019; 58(32): 14859-72.

Chapter 2

Literature Review

The content of this chapter is published as follows:

E. Tripodi, A. Lazidis, I.T. Norton, F. Spyropoulos. "*Food Structure Development in Emulsion Systems*". In A. Lazidis, I.T. Norton, F. Spyropoulos (eds.). "*Handbook for Food Structure Development*". 1st ed. Cambridge: Royal Society of Chemistry, 2019.

2.1. Introduction

Food emulsions represent structurally complex systems containing a multitude of constituents. These molecular species (e.g. water, fat, emulsifiers, carbohydrates, proteins, salt, sugar, etc.) contribute through their micro- and macroscale characteristics and interactions to the emulsion microstructure, which ultimately determines many of the physical properties and functionalities of the food they are part of. For this reason, the development of emulsion architectures with tailored features represents a critical step in optimizing or enhancing the features of existing products as well as designing novel, tastier, and healthier foods.

Controlling the performance of emulsions can be conducted by carefully choosing both the formulation and the processing characteristics. The cautious selection of the emulsion constituents and the understanding of their contribution to the product microstructure offer the opportunity to shape the properties of conventional emulsions and design structurally complex systems with enhanced bulk properties, as well as to ensure their stability. The selection of the most suitable manufacturing method represents an additional critical step, during which ingredients are brought together to create the desired microstructural features. Both micro- as well as macrocharacteristics of the product can be probed, measured, and quantified through the use of an ever expanding array of analysis techniques. The discussion that follows ultimately demonstrates that the formulation and processing aspects involved in the development of emulsion structure can be controlled to optimize or design systems with specific functionality and performance.

2.2. The emulsion microstructure

Whilst emulsions define, to a great extent, the rheology and texture of many food systems, controlling the development of their microstructure, its behaviour, and stability can sometimes

be challenging. In an effort to systematically address these challenges, one can design emulsion-based products by the careful choice of (*i*) the formulation and (1) the processing route. This section focuses on the former and aims to describe the basic constituents (and their contribution to the microstructure) of conventional emulsions but also to that of more complex systems.

2.2.1. Conventional emulsion microstructure

In its simplest definition, an oil-in-water (o/w) emulsion (Figure 2.1.A) consists of oil droplets (dispersed phase) surrounded by water (continuous phase) and the interfacial region (interface) that separates the two (2); water-in-oil (w/o) emulsions (Figure 2.1.B) are similarly defined (2). Each of these three emulsion structural features has a different contribution to the final architecture and thus to its bulk properties (3).

2.2.1.1. The continuous phase

The bulk properties of the continuous phase influence a wide range of emulsion characteristics but most importantly its stability and texture. Texture is related to mouth perception and to attributes such as creaminess, thickness and mouthfeel. Texture in relation to emulsions can typically be instrumentally characterised through the study of their rheological and tribological properties (4-7). Dynamic viscosity, an important rheological parameter of the continuous phase of emulsions can be tuned in order to enhance mouthfeel perception as well as to extend product shelf-life (8). In o/w emulsions, increasing the viscosity of the continuous phase is usually achieved by the inclusion of thickening or bulking agents into the formulation (9, 10). Typical thickeners that are found in foods are polysaccharides (e.g. gums, starch, pectin, cellulose or its derivatives), as well as proteins or blends of any of the above (11). In w/o emulsions, the continuous phase rheology is usually determined by the presence (or not) of a

fat crystal network and its physical characteristics such as fat composition, solid fat content, crystal size/shape and the strength of the network that entraps the water droplets (12). Controlling and altering the fat composition and the processing conditions (such as thermal history, applied mechanical forces etc.) offer a direct way to modify the network properties and thus the emulsion microstructure in this case (13).

Whether the continuous phase is predominantly water (o/w) or oil (w/o) also significantly impacts on the emulsion's electrical conductivity. The monitoring of the electrical conductivity can be used to evaluate emulsion stability (creaming or phase inversion or in a more extreme case phase separation), as well as to assess both the droplet size and the distribution polydispersity (14-16). The emulsion's capacity to be diluted is another important feature that is primarily controlled by the continuous phase and that can have a major impact in oral processing, when the emulsion is diluted with saliva and maximum flavour release is required, or during processing in order to improve emulsification efficiency (17).

The relative solubility of the dispersed into the continuous phase has a major influence on emulsion stability. The onset and progression of Ostwald ripening, increases at higher dispersed phase solubility (18). The control of this phenomenon is of vital importance for beverages and drinks containing flavour oils (high-water solubility), whereas it has negligible impact in dairy-like emulsions usually containing triglyceride oils (low-water solubility) (19).

2.2.1.2. The dispersed phase

The dispersed phase has a dramatic impact on the final properties of emulsion products (texture, stability, appearance, delivery, and encapsulation of functional components, etc.) through features such as the droplet size and distribution, volume fraction, charge, type, and physical state of the droplet constituents. The contribution of the dispersed phase to the overall product

rheology is predominately linked to the droplet size, its polydispersity and concentration/volume fraction (20, 21). For volume fractions (ϕ) below the maximum packing concentration ($\phi < 0.75$, for spheres), smaller droplets can result in pronounced variations in product viscosity and mechanical properties, such as viscoelasticity, that in turn can affect mouthfeel (22). At values close to the maximum packing concentration ($0.50 < \phi < 0.75$), emulsion polydispersity plays a major role in final properties. When two monodisperse systems of different sizes are mixed together, they exhibit a minimum in viscosity at a specific combination; a minimum not observed for tri-modal (or more) dispersions (23). For even more concentrated emulsions ($\phi > 0.75$), droplets deform by coming into contact, with the final system exhibiting solid-like properties, such as a yield stress; mayonnaise is a classic example of such an effect (23).

The charge of the disperse phase plays a significant role in the physicochemical stability and in the organoleptic and nutritional properties of emulsions, mostly due to the large variety of components that may interact with the droplet interface. Emulsion stability's prevention of creaming and flocculation can dramatically decrease as a consequence of the presence of salts that act as charge screeners for ionic emulsifiers (24). Due to their charge, droplets may attract metal ions present in solution, thus accelerating oxidative damage or drops may also bind oppositely-charged flavour molecules and affect their release performance; both effects can alter product taste (25, 26).

The dispersed phase of some emulsion-based food products may undergo partial crystallisation; milk, margarine, butter and ice cream being a few examples. Depending on shear and temperature, the presence of crystals in droplets can cause partial coalescence, which influences the physical stability, texture and rheological features of the product (27). Although, partial coalescence is undesirable for applications requiring high stability against creaming and

flocculation, it also represents an essential step in the production of foods, such as margarine, butter and ice-cream, improving product stiffness and stability (28-30).

Finally, features such as droplet concentration, size and refractive index have a large influence on the appearance of emulsion-based products (e.g. lightness, colour etc.), which in turn can influence consumer perception (31). Lightness and colour can be enhanced by increasing the difference in the refractive indices of the two phases (32). Alternatively, transparent products can be obtained by matching the refractive indexes of both the continuous and dispersed phase or by significantly reducing droplet size below a certain threshold value (e.g. nanoemulsions) (33, 34).

2.2.1.3. The interface

The interfacial region of a food emulsion is mainly characterised by the presence of water, oil and surface active molecules, with the latter, generally called emulsifiers, being used to extend emulsion longevity against thermodynamic instability (35). During processing, emulsifiers are expected to quickly adsorb at the interface, reducing interfacial tension and thus favouring droplet break-up while at the same time limiting droplet contacts and coalescence; the latter performance is also required during storage in order to extend final product stability (36, 37). Typically, emulsifiers are divided into three broad categories (38, 39): low-molecular weight surfactants; high-molecular weight surfactants or most commonly proteins; and nanoparticles.

2.2.1.3.1. Low-molecular weight surfactants

Low-molecular weight surfactants represent surface-active molecules consisting of a hydrophilic head group and a hydrophobic tail that, once at the oil/water interface, orientate their structure so that these two domains are largely present in the water and oil phase,

respectively (40). Depending on the relative size of the hydrophilic and hydrophobic parts, surfactants may be more suitable to stabilise o/w or w/o emulsions. The Hydrophilic Lipophilic Balance (HLB) value represents an empirical method to evaluate this tendency (41); surfactants with low HLB values (3-8) tend to form w/o emulsions, while those with high HLB values (8-20) tend to stabilise o/w emulsions. Surfactants are also categorised based on the charge of their head group (42, 43). *Nonionic surfactants* possess no charge and find extensive use as stabilisers in food emulsions due to their low toxicity and irritability; examples are ethoxylated sorbitan esters (Tweens and Spans), polyoxyethylene ethers (POE) and sugar esters (sorbital monooleate, sucrose palmitate). *Ionic surfactants* can carry either a positive or a negative charge but their application is restricted to products requiring low surfactant concentration, since they can cause irritation and have varying levels of toxicity; examples of negatively charged surfactants are citric acid ester of monoglycerides (CITREM), diacetyl tartaric acid monoglycerides (DATEM), and Sodium Lauryl Sulfate (SLS), while lauric arginate is an example of a positively charged surfactant that also exhibits high antimicrobial activity (44). Finally, *zwitteronic surfactants* show both a positive and a negative charge, and so their net behaviour depends on solution conditions (e.g. pH, ionic strength, etc.); common examples are represented by phospholipids, such as lecithins, which show improved stabilisation performance when used in combination with other emulsifiers.

Surfactants are often used in mixtures where their synergistic behaviour can enhance formulation performance (e.g. improved shelf-life and product stability against temperature variations) (45). Surfactants quickly and reversibly adsorb at an emulsion interface by generating low-interfacial tensions, thus favouring the formation of small droplets, although they do not usually form strong interfaces (compared to proteins or particles that form viscoelastic interfacial layers instead) and therefore droplet collisions in such systems may be

prone to coalesce (46). An important feature of low-molecular weight surfactants is that they exist as monomers (with high surface activity) below a certain concentration, but form aggregates (i.e. micelles) above this Critical Micelle Concentration (CMC) (47). When CMC is exceeded, emulsion properties such as interfacial tension do not drastically change; for instance, o/w interfacial tension decreases by increasing the surfactant concentration while still below the CMC, but remains relatively constant above it (48).

In practice, food products rarely contain only surfactants, as these are used in combination with proteins, polysaccharides and in many cases particles. Under these scenarios, emulsions may exhibit a completely different behaviour than when the surfactant(s), protein(s), polysaccharide(s) or particles species are used alone (49).

2.2.1.3.2. High-molecular weight emulsifiers - Proteins

Proteins are an important class of emulsifiers that determine the properties (texture, stability and mouthfeel) of a wide range of products such as milk, whipped cream and salad dressing, among others (50). Compared to low molecular weight surfactants, proteins are also surface active but adsorb at the interface at a slower rate due to their larger hydrodynamic volume. Furthermore, upon adsorption, proteins lower the interfacial tension to a lesser extent due to the physical challenges in orienting their hydrophilic and lipophilic domains (which are spread across their more complex molecular structure) to be positioned within the water or oil phases, respectively (51). Proteins reversibly adsorb at the interface, forming a viscoelastic layer of gel-like properties that greatly enhances droplet resistance to coalescence (52, 53). Features of the formed interfacial layer depend on protein configuration, which in turn is mainly determined by protein concentration and its structure (e.g. distribution of the hydrophobic and hydrophilic parts on the protein chain), and can be susceptible to solution conditions such as pH, ionic

strength and temperature (54). Emulsion droplets tend to flocculate at pH values close to the isoelectric point of the protein or when the ionic strength in the system exceeds a critical value; in both cases droplet repulsion via an adsorbed protein-driven electrostatic mechanism is not sufficient to prevent droplet attraction (55). Furthermore, as a consequence of thermal variations, proteins may unfold at the interface exposing reactive groups (e.g. sulfhydryl or non-polar groups) which cause attraction between droplets and in turn promote their flocculation or coalescence (56). Nevertheless, establishing a general protein functionality against these parameters is not trivial, since in food products, proteins are often present as mixtures (51).

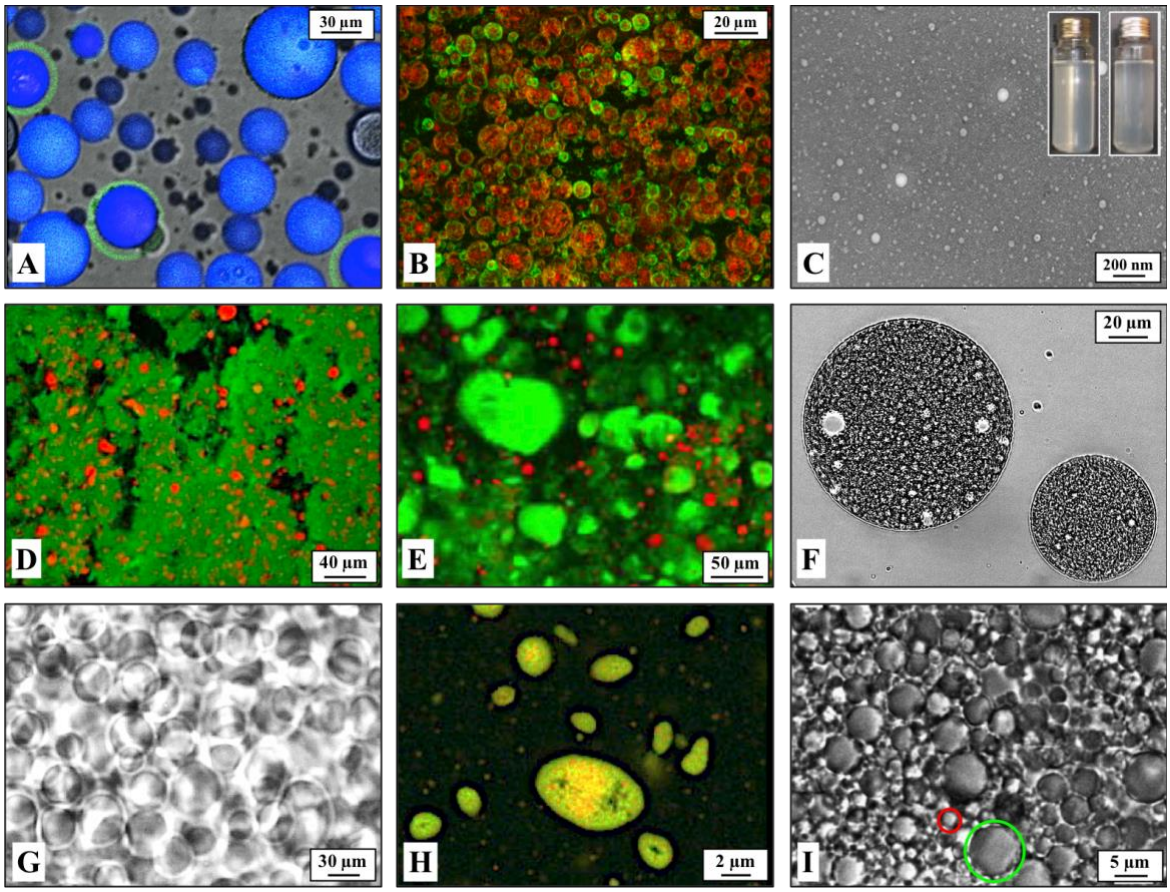

Figure 2.1. Simple and complex emulsion microstructures. **(A)** o/w emulsion stabilised by sodium caseinate/chitosan (NaCAS/CS) complexes; fluorescent emissions from the NaCAS/CS complexes (green) and the oil droplets (blue) – *adapted from* (72); **(B).** w/o emulsion stabilised by tripalmitin crystal nanoparticles; fluorescent emissions from the water droplets (red) and tripalmitin (green) – *image courtesy of Ms Lucie Villedieu, University of Birmingham*; **(C).** o/w nanoemulsion stabilised by Tween 80; insets are images of near transparent nanoemulsion samples, taken immediately (left) and 56 days (right) after formation – *adapted from* (73); **(D).**

o/w emulsion gel of whey protein isolate (thermally-set); fluorescent emissions from the oil droplets (red) embedded within the WPI gel network (green) – *adapted from* (74); **(E).** o/w emulsion gel of Pea Protein (pH-set); fluorescent emissions from the oil droplets (red) embedded within the PP gel network (green) – *adapted from* (75); **(F).** $w_1/o/w_2$ double emulsion stabilized by PGPR (internal w_1/o interface) and Tween 20 (external o/w_2 interface) – *image courtesy of Mr Mehul Shingadia, University of Birmingham*; **(G).** Gelatin/Dextran w/w emulsion under mild shear – *adapted from* (76); **(H).** Sodium caseinate/pectin hydrogel particles containing an o/w emulsion; fluorescent emissions from the oil droplets (red) and the protein (green) part of their hydrogel particle carriers – *adapted from* (77); **(I).** a/o/w emulsions showing air cells (e.g. green circle) and oil droplets (e.g. red circle); air cells (~7 μm) are co-dispersed with oil droplets (~0.6 μm) within an aqueous medium, to give the final tri-phasic emulsion microstructure – *adapted from* (78).

2.2.1.3.3. Nanoparticles

Emulsions stabilised by solid nanoparticles (Pickering emulsions; see Figure 2.1.A & 2.1.B) have received great attention due to their enhanced stability against coalescence and capacity to provide surfactant-free formulations. These characteristics are particularly attractive for applications where high concentrations of surfactants are associated with toxicity or irritancy, and/or the used surfactants originate from or are associated with unsustainable sources (57). Particles can achieve effective stabilisation if their size is at least one order of magnitude smaller than that of emulsion droplets. If successfully adsorbed at an interface, they can form a mechanical barrier against droplet coalescence (39). Particles are generally not surface-active; therefore their adsorption at the interface does not (significantly) lower interfacial tension (58). Instead, the thermodynamic advantage associated with their interfacial adsorption resides with their capacity to reduce the effective surface area of oil/water contact (59). Similarly, to surfactant HLB, particle wettability is the criterion used to establish the suitability of these species to stabilise o/w or a w/o emulsions. Wettability is expressed in terms of the contact angle (θ) which provides a measure of the degree of particle hydrophilicity/hydrophobicity (49). For efficient stabilisation, particles should be predominantly wetted by the continuous

phase; $\theta < 90°$ for particles preferentially wetted by water (o/w emulsions) or $\theta > 90°$ for the opposite case, Figure 2.2.

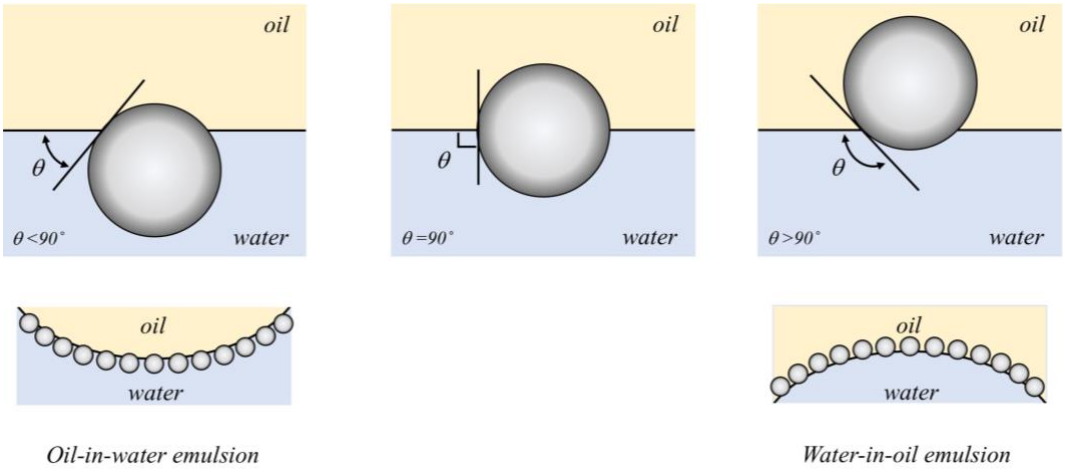

Figure 2.2. Relation between the particle contact angle and the resulting emulsion microstructure.

However at the same time, θ should not be too close to either 0 or 180°, in which case the energy of particle desorption from the interface becomes much lower; the energy of desorption for particles of $\theta \sim 90°$ is found to be (depending also on their actual dimensions) in the order of 10_6 kT, compared to that for low-molecular weight emulsifiers which is in the region of 10 kT (60). Due to the large energy needed for desorption, it is hypothesised that interfacial adsorption of particles is almost irreversible (61).

Although superior in terms of stability, Pickering emulsions usually possess droplets with larger diameters compared to those delivered via an equivalent processing environment but in the presence of surfactants. This is a direct consequence of the inability of particles to (significantly) lower interfacial-tension (i.e. promote droplet break-up) and of their much reduced interfacial adsorption rate (62). These issues can be to an extent addressed by carefully controlling the processing environment used to generate these structures, in terms of both

energy input and residence time (63). However attractive, the use of particles for the stabilisation of food emulsions is challenging. One of the main issues hindering the industrial application of these systems is the difficulty of sourcing suitable food-grade colloidal species to be used in commercial products; or, similarly, constructing (from food-grade material) particulate structures within the appropriate size regime for Pickering functionality. In the last years, investigation on the stabilisation performance of food-grade particles such as starch and quinoa granules, cellulose and chitin nanocrystals as well as flavonoid particles, has opened new pathways for the successful introduction of Pickering emulsions in the food sector (64-68).

2.2.2. Complex emulsion microstructures

As the consumer demand for healthier and more functional products has increased during the last years, this has generated further academic and industrial interest in creating more complex emulsion microstructures capable of facilitating the development of such emulsion-based formulated foods (69, 70). As a consequence, a number of complex emulsion architectures (see Figure 2.1.C-I), such as nano-, double, water-in-water, hydrogel particle stabilised and air-filled emulsions, have received a great deal of attention (71) and the present section aims to briefly introduce these systems and highlight their major advantages and drawbacks over conventional emulsions.

2.2.2.1. Nanoemulsions and microemulsions

Nanoemulsions (Figure 2.1.C) are similar to conventional emulsions from a structural point of view, but with droplet dimensions spanning from 10 to 200 nm (34). In the food industry, nanoemulsions have been receiving particular attention due to opportunities they offer over traditional emulsions such as optical transparency, improved encapsulation, delivery and

bioavailability of functional components, enhanced texture at lower dispersed phase concentration, as well as increased stability against creaming and flocculation (79, 80). Several challenges still limit the use of nanoemulsions in food products: (*i*) poor stability against Ostwald ripening and chemical degradation; (ii) the requirement for a larger emulsifier concentration; and (iii) the enhanced bioavailability of components whose (now higher) consumption may result in an increased risk of toxicity (81). Microemulsions show certain similarities to nanoemulsions (e.g. transparency, large interfacial area) yet they are different in nature (79). In fact, microemulsions are thermodynamically stable (differently from nanoemulsions which can only be kinetically stabilised) thus the form spontaneously, that is their properties do not depend on the method of preparation.

2.2.2.2. Gelled emulsions

Emulsion gels refer to a class of complex systems where it is possible to convert a biopolymer (either protein or polysaccharide) stabilised oil-in-water emulsion to a soft/solid-like material by controlling the mechanism of biopolymer gelation via common processing operations such as heating (Figure 2.1.D), addition of ionic species (e.g. Ca^{2+}), acidification (Figure 2.1.E) or enzymatic treatment) (11). In this case, emulsions droplets can be classified as active or inactive fillers to the external network. Active fillers are bound to the gel matrix and can either increase or decrease the gel stiffness depending on the ratio of the droplet/gel moduli, while inactive fillers do not interact with the gel network and always tend to decrease the matrix stiffness (82). Besides constituting the bases of a wide variety of food products (e.g. creams, mayonnaise, yoghurt etc.), emulsion gels have shown promising applications in the controlled release of lipophilic components, extended resistance against lipid oxidation and potential in the development of reduced oil/calorie emulsion-based products (83-85).

2.2.2.3. Duplex emulsions

Duplex or double emulsions (Figure 2.1.F), such as water-in-oil-in-water ($w_1/o/w_2$) or oil-in-water-in-oil ($o_1/w/o_2$) emulsions, have been termed as emulsions of emulsions; a primary (simple) emulsion (e.g. w/o) further emulsified into another aqueous phase to ultimately give water droplets (w_1) that are within oil droplets (o) that are in turn suspended in a water continuous phase (w_2) (86). Of particular interest to the food industry are $w_1/o/w_2$ emulsions due to their potential to be used for the design of low-fat products, for encapsulating and protecting water-soluble bioactive compounds (within their inner aqueous compartments), as well as to controlling aroma and flavour release (87). The major challenges that hinder the successful industrial application of double emulsions are mainly associated with (*i*) the challenges in finding scalable and reliable manufacturing methods for their manufacture and (1) the stability issues that arise as a consequence of the osmotic pressure difference between the two water phases (88).

2.2.2.4. Water-in-Water emulsions

Water-in-Water (w/w) emulsions (Figure 2.1.G) represent dispersions of water droplets within another immiscible water continuous phase, in the presence of a charged biopolymer, or a mixture of two biopolymers , or even a mixture of a biopolymer with a micelle-forming surfactant (89). The w/w systems form due to phase separation phenomena taking place as a result of the thermodynamic incompatibility (or compatibility) of the water-soluble biopolymers (proteins or polysaccharides) included into the formulation; a typical example is the gelatin/dextran aqueous mixtures (76). As a result, an emulsion-like microstructure can be produced at water contents approaching 99% but with dispersed phase fractions of even 50%

(90). The phase behaviour and thus w/w microstructure are influenced by biopolymer physicochemical properties (e.g. molecular weight, charge etc.) and solution conditions (pH, ionic strength, temperature and applied shear) (91). These emulsions are characterised by extremely low values of interfacial tension (in the order of μN/m rather than the mN/m values measured for a typical oil/water interface) and have shown relevance in applications involving (*i*) texture modification through rheology, (1) encapsulation and delivery of (mainly) hydrophilic bioactive substances (1) and the production of fat-reduced products (92-94).

2.2.2.5. Filled-hydrogel particle emulsions

Filled hydrogel particle emulsions (Figure 2.1.H) can be thought as a type of oil-in-water1-in-water2 (o/w_1/w_2) emulsions, in which oil droplets (o) are trapped within biopolymer particles (w_1) which in turn are suspended in a continuous phase (w_2). Again in this case, the two aqueous phases are immiscible as a result of phase separation phenomena (thermodynamic incompatibility) as with w/w emulsions (95). The resulting particle properties (e.g. shape, structure, dimensions, appearance etc.) can be controlled by varying operating conditions; such as heating, cooling etc. (96). Filled-hydrogel particle emulsions have shown promise for applications aiming to extend product physical stability, the encapsulation and release of lipophilic bioactives and the production of reduced-fat products (97). With reference to the last two functionalities, the oil content present in these systems (in comparison to the absence of any oil in w/w emulsions) can be used to enclose lipophilic species and produce reduced-fat products of superior organoleptic properties. However, the additional processing steps and material required for their production still pose a serious challenge to their widespread application in food products (97).

2.2.2.6. Air-filled emulsions

Air-filled emulsions (Figure 2.1.I) represent a three-phasic system where two dispersed phases, oil droplets and air bubbles (of comparable size), are embedded within an aqueous continuous phase (98). The inclusion of microbubbles together with oil droplets allows the production of reduced-calories emulsions with sensory and textural behaviour that closely resembles that of their full-fat counterparts (99). However, the stability of such three-phase systems is seriously jeopardised by instability phenomena encountered in both emulsions and foams (e.g. gravitational drainage, coalescence and disproportionation). Speciality proteins (hydrophobins) have been shown to mitigate such instabilities but their excessive cost together with the challenges associated with the very production of the air-filled emulsions, have hindered the industrial application of these systems (100, 101).

2.3. Thermodynamic aspects

Emulsions are inherently unstable systems and the thermodynamic aspects of emulsion stability/instability phenomena have been extensively reviewed elsewhere (e.g. (3)). This section briefly outlines the main mechanisms by which emulsion instability can develop and progress to, if given enough time, complete phase separation. These include: ***creaming*** (or ***sedimentation***), the upwards (or downwards) movement of droplets under the influence of gravity because of a density difference between the continuous and dispersed phases (102); ***flocculation***, referring to the aggregation of two or more droplets into so-called flocs without loss to their individual integrity (51); ***coalescence***, the merger of two or more droplets into a single larger entity (103), or ***partial coalescence***, occurring in o/w emulsions containing an oil phase (often triglycerides) that undergoes partial crystallisation (104); ***Ostwald ripening***, the diffusional mass transfer of dispersed phase from smaller to larger droplets due to the Laplace

pressure difference that exists between such disparate in size entities (105); and ***phase inversion***, referring to the reversal between the dispersed and continuous phases in an emulsion; (e.g. an oil-in-water emulsion inverting to a water-in-oil emulsion) (106). These types of instabilities are not limited to simple emulsions alone, with more complex microstructures also prone to the same or related destabilisation phenomena. For example, double emulsions suffer from poor stability due to Laplace and/or osmotic pressure differences between their two aqueous phases (107); a phenomenon that is in many ways similar to Ostwald ripening. In addition to physical instability phenomena, chemical destabilisation processes, such as lipid oxidation, could also potentially lead to microstructural damage to emulsions (27). Overall, it is important to note that emulsion instability is a rather complex process taking place via a number of well understood but almost always interrelated and inter-promoting mechanisms.

2.4. Processing routes for emulsion structure development

In order to tailor the desired emulsion microstructure a very important parameter is the choice of the most suitable manufacturing method (108). Homogenisation is the technique responsible for bringing together the two immiscible phases, along with surfactants and other stabilisers, to create the desired microstructure (i.e. average droplet size and size distribution) that ultimately determines the final properties of the product such as texture, appearance and shelf-life (108). This section deals with the processing aspects of creating an emulsion: from the theoretical concepts of emulsification to the description of conventional and unconventional processing techniques used nowadays for emulsion manufacturing at both the industrial and laboratory scales.

Emulsion microstructure, in terms of processing, strongly depends on the type of homogenisation device employed and its operational principles (109). Homogenisation

techniques can be either mechanical or non-mechanical (110); in the former category, emulsion formation occurs under the application of highly disruptive forces (high or intermediate-energy methods) or spontaneously as a consequence of droplet detachment from a pore or microchannel edge (low-energy methods). On the other hand, non-mechanical methods exploit physical principles to generate emulsion microstructure.

2.4.1. Mechanical methods

2.4.1.1. Droplet break-up versus droplet coalescence

In mechanical methods, the emulsion microstructure is formed by a balance between droplet disruption (break-up) and droplet coalescence (110). ***Droplet break-up*** largely depends on the choice of the technique since the geometrical characteristics of the device, the flow regime and the energy input determine the mode of droplet formation. Droplet disruption can take place only if (*i*) the external disruptive forces are able to overcome Laplace pressure and (1) these forces are applied for a period longer than the time required for droplet deformation (111). Laplace pressure is the force responsible for maintaining the droplets' spherical shape and it counteracts any external stresses. It is proportional to interfacial tension and inversely proportional to the Sauter mean diameter of the droplets. This means that the force resisting droplet break-up increases as the dimension of the droplet reduces; i.e. larger external stresses must be applied to break smaller droplets.

External stresses acting on emulsion droplets arise from the flow regime generated within the homogenisation device. It is possible to distinguish between laminar viscous (LV), interfacial driven (ID), turbulent and cavitation flow regimes (17, 111). In the *laminar flow regime*, droplets are subjected to forces generated by simple shear, pure elongational stresses as well as a combination of both (36). Elongational stresses are more effective than shear forces

since these cause the rotation of the liquid inside a drop, thus dissipating part of the energy applied for droplet disruption (1). During pure elongation, drop recirculation is inhibited and a larger portion of the total energy input is actually used to cause droplet break-up (1). In the laminar regime, the viscosity ratio (defined as the ratio of the viscosity of the dispersed phase over the viscosity of the continuous phase) has a fundamental importance because pure shear droplet disruption cannot occur for a viscosity ratio above 4, whereas in the case of pure elongation, droplet disruption is always possible for any value of viscosity ratio (40). The *interfacial driven* flow regime differs from conventional methods (i.e. where the interfacial tension counteracts disruptive forces through the Laplace pressure) because in this case the interfacial tension is the driving force causing the spontaneous droplet snap-off in correspondence to the edge of a pore (or micro junction) (111). In fact, when droplets approach the edge of a microchannel or pore, they have a non-circular shape usually with a higher interfacial energy than the corresponding spherical droplet of the same volume. After detachment from the edge, the droplet will spontaneously adopt the lowest interfacial-energy configuration (112, 113). *Turbulent flow* is the regime most commonly encountered in traditional emulsification methods. In the turbulent regime, fluid flow is chaotic and is characterised by the presence of a spectrum of eddies within the fluid (36). In this case, the smallest eddies are responsible for generating the energy dissipation responsible for droplet break-up (111). From the Kolmogorov theory, it is possible to estimate the dimension of the smallest eddy within the turbulent environment based on the value of the energy dissipation rate imposed by the homogenisation techniques as well as the continuous phase flow and physicochemical properties (i.e. the viscosity and density, respectively) (114). Based on the comparison between the average emulsion droplet size and the smallest Kolmogorov eddy size, it is possible to distinguish between the Turbulent Inertial (TI) and Turbulent Viscous (TV)

flow regimes (115). In the TI-flow regime the resulting droplet size is larger than the smallest eddy size predicted by the Kolmogorov theory. In this regime, the resulting droplet size does not depend on the viscosity of the continuous phase and it is independent on the dispersed phase mass fraction (116). In the TV-flow regime, the resulting droplet size is smaller than that predicted by Kolmogorov, which makes this regime more effective in producing smaller droplet sizes (in comparison to the TI one) (116). Finally, the *cavitation flow regime* is characterised by the presence of shock-waves that propagate through the fluid causing droplets to be disrupted, providing efficient mixing and resulting in the formation of very fine and highly stable emulsions (117). This flow regime is of fundamental importance in high-pressure and ultrasonic homogenisation processes (118, 119).

During each of these flow regimes it is also possible to define the concept of maximum stable droplet diameter, which provides an estimation of the largest droplet diameter that can resist disruption under specific energy dissipation conditions (120). Several studies have proposed a direct proportionality relationship between this maximum stable diameter and the mean emulsion droplet size (121-123). If the constant of proportionality is known, the Sauter diameter can replace the maximum droplet size in these relationship, thus providing further ways to predict and optimise the process performance (110). Nonetheless, it must be noted that to establish this relationship is not always possible and may change depending on the formulation and processing technique investigated (124, 125).

Emulsion droplet size reduction is clearly affected by the employed mechanical method as well as specific formulation elements such as viscosities of the two phases, dispersed phase volume fraction and interfacial tension. However, droplet size decrease is also heavily hindered by ***droplet coalescence*** throughout the duration of an emulsification process. Droplet coalescence is mainly caused by droplet collisions during homogenisation (126). Emulsifiers

are commonly associated with a decrease in interfacial tension (certainly in the case of surfactants) and thus can facilitate droplet break-up. Yet, emulsifiers are also included into emulsion formulations in order to prevent droplets from coalescing (127). An ideal emulsifier must adsorb at the interface as quickly as possible and create a strong boundary that is robust enough not to rupture upon droplet contacts/collisions (127). The resistance of an interfacial layer to coalescence depends on the type as well as on the concentration of the emulsifier; surfactants quickly adsorb and form a fluid interface when compared to the more slowly-adsorbing proteins or particles that instead form a viscoelastic interfacial layer (128). Depending on the amount of emulsifier used during homogenisation one can distinguish between the surfactant poor- and rich-regimes (128, 129). Within the surfactant-poor regime, final droplet size is strictly dependent on the amount of surfactant used. In this case, the presence of surfactant at the interface is inadequate (partial interfacial coverage) and contacts between droplets will tend to result in coalescence with emulsion droplet size increasing (or similarly total interfacial area is decreasing) until surfactant concentration is sufficient to allow full interfacial coverage (128, 129). In the surfactant-rich regime, final droplet size is primarily dependent on the type of homogenisation process chosen and the flow regime induced, since the ample emulsifier content in the system can ensure full interfacial coverage of droplets and thus limited coalescence events (128, 129).

2.4.1.2. Energy density and energy efficiency

Mechanical emulsification methods can be compared based on the concepts of energy density and energy efficiency (3). Energy density, defined as the energy input per unit volume of emulsion, has been shown to be a suitable measure for evaluating the extent of droplet disruption during continuous mechanical emulsification (110, 130). In fact, data of Sauter mean

droplet diameters as a function of corresponding energy density values have been shown (when plotted on a logarithmic scale for both axes) to give a linear relationship, with a slope that remains constant for the same type of mechanical process; e.g. a slope of 0.4 for High-Shear Mixing, or a slope of 0.6 for High-Pressure Homogenisation (110, 130). This relationship, also known as process function, provides a strong basis for product design of emulsion-based products, as it relates an emulsion microstructure element (mean droplet size) to the processing conditions utilised for its production (energy density), thus essentially allowing for the control of emulsion structure via the selection of appropriate process conditions (110, 130).

Emulsification techniques can also be compared based on the concept of energy efficiency, defined as the ratio of the theoretical energy required to form an emulsion (proportional to the interfacial tension and the difference in interfacial area) over the energy density (i.e. the actual amount of energy expended by the homogenisation technique) (111). In order to form small droplets, homogenisation techniques must create conditions where the actual energy expenditure is much larger than the theoretical one in order to overcome the significant pressure gradient present within droplets (3, 111). This is the reason why normally emulsification processes are methods of relatively low energy efficiency; with typical energy efficiency values ranging from 10^{-3} % (high-energy methods) to 1% (intermediate-energy methods) (3, 111).

2.4.1.3. High-energy versus intermediate-energy mechanical methods

Mechanical methods can be divided in high- and intermediate-energy approaches (109). High-energy methods include well-established techniques such as high-shear mixing, high-pressure homogenisation and sonication. Intermediate-energy methods, such as confined impinging jets, microfluidic devices and membrane emulsification, have been developed much more recently. Although these approaches show promise in terms of emulsion structure formation at a much-

reduced energy density and with a significantly higher energy efficiency (in comparison to typical high-energy processing routes), their industrial adoption is currently hindered mainly due to manufacturing challenges associated with the relatively modest product throughputs that they can be presently achieved.

2.4.1.3.1. High-energy mechanical methods

High-shear mixers are the most common devices used in food industry for emulsion manufacturing (131). Within this unit operation, ingredients are blended together inside a mixing head that creates high energy dissipation rates as a consequence of the movement of the rotor head and its proximity to the shear stator (132, 133). The intensity of the mixing can be adjusted by controlling the revolution of the rotating head and the distance (from the rotor) that the stator is placed together with its geometry (131). They can operate both in batch or in continuous mode, process fluids of viscosity within the low- to medium-range and produce emulsion droplets smaller than 1μm (17). Essentially a variant of high-shear mixers, *colloid mills* also work on the rotor-stator principle (134). The intensity of the shear stresses achieved in this case can be higher than those in simple high shear mixing, and colloid mills can relatively easily handle high-viscosity material producing emulsions with droplet sizes smaller than 1μm (3, 17). In *high-pressure homogenisers*, usually a coarse pre-emulsion is forced through a narrow gap where it is subjected to highly-disruptive forces (a combination of turbulence and cavitation or laminar and elongational, depending on the geometry of the nozzle) caused by flow under large pressures (typical values of 50 up to 2000 bar) (135, 136). High-pressure homogenisers can handle fluids of low to medium viscosity and can produce droplets as small as 0.1 μm (3, 17). In *ultrasonic homogenisation*, ultrasonic waves cause the generation of cavitation effects that propagate and disrupt droplets (118, 137). Although most commonly used

at a bench-scale, variants operating in a continuous mode and at a large scale do exist (137). Depending on the configuration, nanoemulsions (droplet diameter < 200 nm) can be produced using ultrasonic homogenisation, which can process fluids of low to medium viscosity (3, 17).

2.4.1.3.2. Intermediate- and low-energy mechanical methods

High-energy approaches to emulsification have been traditionally used due to their capability of delivering large product throughputs, to handle a large variety of raw material and produce considerably small droplets (109). Nonetheless, these techniques suffer from (*i*) low energy efficiencies (a large part of energy input is wasted without being utilised for droplet size reduction purposes); (1) increases to product temperature during processing (as a result of energy being dissipated as heat) which can be detrimental to the quality of heat-sensitive species; (1) relatively low batch-to-batch reproducibility (in terms of droplet size and size distribution control) due to the large volumes of processed material (138, 139). In recent years, more sustainable, lower-energy alternatives have been proposed to overcome the limitations of high-energy manufacturing techniques. Confined Impinging Jets (Figure 2.3), microfluidic and membrane emulsification (Figure 2.3) represent some examples of such intermediate-energy methods.

In *Confined Impinging Jets* (CIJs) the collision of two fluids within a mixing-chamber causes large levels of turbulence (Figure 2.3) over a confined volume of product, in turn causing droplet break-up and size reduction (140). In this case, the process conditions can be tuned by adapting the flow rate of the two jets. At a lab-scale, this technique has shown potential in delivering continuous operation, coupled with high product throughputs at intermediate energy input, processing low viscosity emulsions and obtaining droplet sizes of a few micrometres (141, 142). *Membrane and microchannel emulsification* represent low-energy techniques

where emulsion formation occurs spontaneously as a consequence of droplet detachment from a membrane pore or at a microchannel junction (139, 143). Both methods rely on a bottom-up approach to emulsion formation (droplets are produced one-at-a-time to give the required dispersed phase fraction) rather than the top-down approach of turbulent processing (comminution of one phase within another immiscible one). The performance of both processes can be controlled by adjusting the geometrical characteristics (e.g. pore/microchannel dimensions/shape and material of construction) or by changing their configuration (rotating and cross flow membrane, or flow-focusing and edge microchannel emulsification) (143, 144). Although both techniques offer the major advantage of producing emulsions with highly controlled droplet sizes in a highly-energy efficient manner, they do suffer from (*i*) low product throughput that currently limits their use at bench-scale operation and (1) only being able to handle fluids of low viscosity (3, 17). Approaches currently explored in terms of increasing the throughput of membrane and microchannel emulsification methods include the use of membrane modules of much higher porosity and straight through pore geometry (145) (e.g. laser drilled steel membranes) and surfactant delivery through the dispersed phase (as oppose to its conventional positioning within the continuous phase; see Figure 2.4) (146) and the development of microfluidic parallelization arrangements (147).

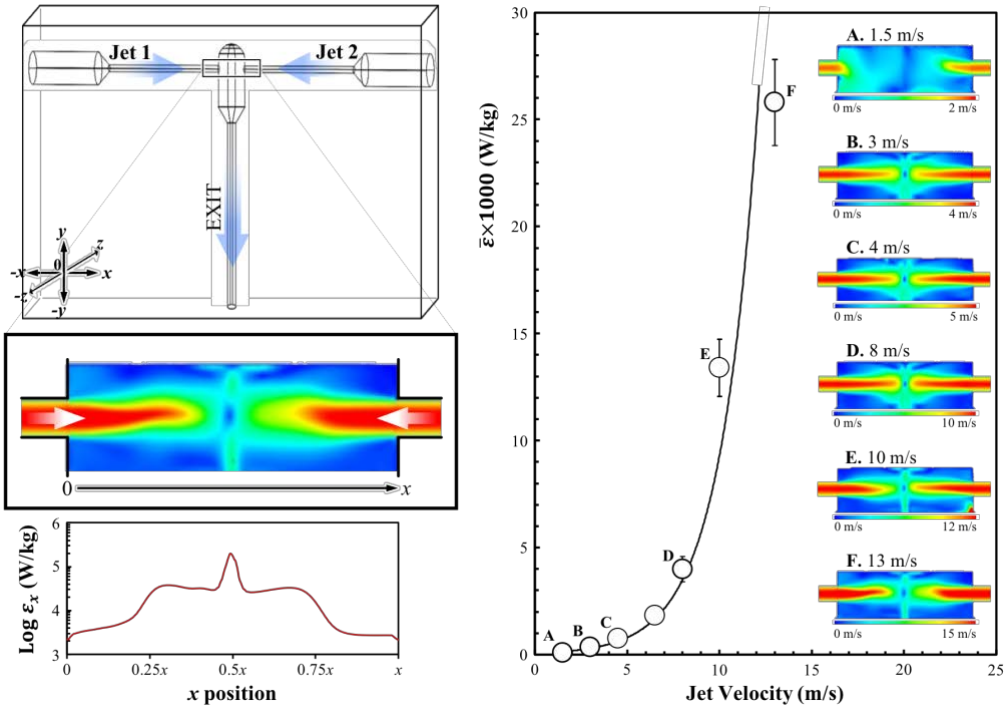

Figure 2.3. An example of a Confined Impinging Jet (CIJ) geometry (*top left*) showing the two channels of jet entry. A typical CFD velocity profile showing jet collision (*middle left*) and associated energy dissipation values (ε_x) calculated along the jet collision path (x position; 0 $\rightarrow$ x) by the model (*bottom left*). CFD derived mean energy dissipation values ($\bar{\varepsilon}$) generated within the CIJ chamber as a function of jet velocity (*right*). Inset: CFD profiles are also provided for selected jet velocities.

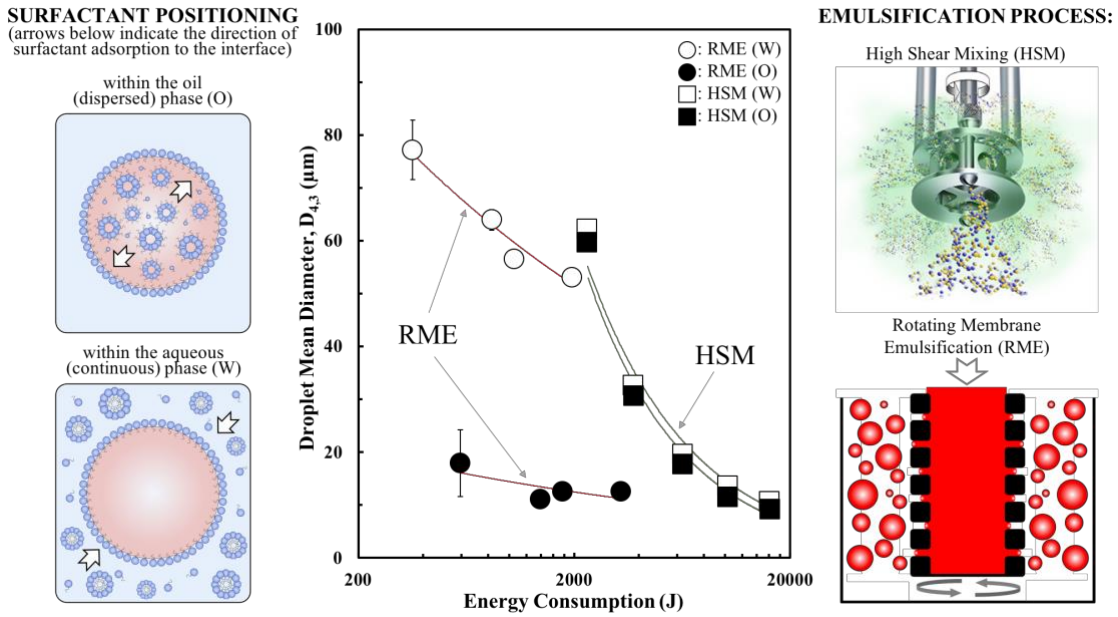

Figure 2.4. Effect of surfactant (Tween 20) positioning (dispersed *vs* continuous phase; see left hand side) on the droplet size (μm) of o/w emulsions produced either by high shear mixing (HSM) or rotating membrane emulsification (RME) and associated energy consumption (J). *Data shown adapted from* (146). *HSM image courtesy of Silverson (http://www.silverson.co.uk/images/uploads/products/lab-how-it-works-stage-4.jpg).*

2.4.2. Non-mechanical methods

Non-mechanical emulsification methods exploit specific physical principles in order to drive emulsion formation, with the *phase inversion temperature* (PIT) method being amongst the most heavily used techniques (148). The PIT method takes advantage of the change in the optimal curvature and solubility of non-ionic surfactants, as a consequence of variations in temperature, to induce a transition from an o/w emulsion (below the surfactant PIT) to a w/o emulsion (above the surfactant PIT) (149, 150). Through this triggered phase inversion phenomenon, the PIT method allows the formation of nanoemulsions with controlled microstructures by using a non-mechanical and low-cost approach to emulsification (compared to traditional emulsification techniques based on turbulence) (151, 152). On the other hand, the higher surfactant-to-oil ratio required coupled with the limited applicability of the technique to only a relatively small combination of water/oil/surfactant systems and experimental conditions, has hindered its industrial adoption (153).

2.5. Emulsion microstructure characterisation

The emulsion microstructure as well as its individual structural constituents can significantly affect, amongst other things, the processability, texture, sensory perception and overall functionality as well as the shelf-life of the final food system. It is therefore critical for formulators to have the appropriate experimental tools to be able to characterise, evaluate and measure a range of emulsion structural and bulk properties. Part C (Food Structure Analysis, Characterisation & Modelling) of the handbook where this chapter is published presents an

extensive discussion on the currently available toolbox for the interrogation of food structure, which quite often is indeed relevant also to emulsion microstructure. As such, and in order not to replicate the discussion carried out elsewhere, the aim of the present section is to provide only a brief overview of the most important experimental techniques used to probe the emulsion microstructure and allow the extraction of information on the overall emulsion architecture (e.g. droplet size) or its individual features (e.g. the interfacial layer) as well as on product bulk properties (e.g. flow behaviour) (154).

2.5.1. Visualisation of the emulsion microstructure

Light Microscopy (LM) is suitable for the visualisation of microstructural features with dimensions of ~1μm and can provide information regarding droplet size distribution and the presence of flocculated or coalesced droplets (3). *Electron Microscopy (EM)* has a higher resolution that allows for microstructural elements smaller than 1μm to be visualised; such as nano-sized droplets, nanoparticles, micelles or vesicles (155). It is worth noting that sample preparation in both LM and EM could impact on the to-be-characterised microstructure, thus generating artefacts (156, 157). *Atomic Force Microscopy* (*AFM*) offers the advantage of significantly high resolution, allowing the visualisation of structures and aggregates at the molecular level (e.g. biopolymers, surfactants), coupled with minimal specimen preparation (157-159). One of the main disadvantages of AFM is that imaging soft structures can be challenging (158).

2.5.2. Characterisation of the emulsion microstructure and its components

Static Light Scattering (SLS) is commonly used to measure emulsion droplet sizes and droplet size distributions (160, 161). Droplets with diameters within the range of 100 nm – 1000 μm

can be in theory detected but, in order to avoid multiscattering, excessive dilution is needed (<0.01%), which can affect the emulsion microstructure (160). *Dynamic Light Scattering (DLS)* overcomes some of the limitations of the static configuration and allows for measurement of colloidal matter down to 1 nm. DLS exploits the continuous rearrangement of droplets due to Brownian motion that causes intensity fluctuations over time, which are converted to information regarding droplet size and droplet size distribution data (162).

In *Neutron Magnetic Resonance (NMR)* the emulsion is subjected to a static magnetic field gradient and the hydrogen atoms are excited to higher energy levels causing a signal that (*i*) is detectable from the NMR and (1) has an amplitude dependent on the movement of the nuclei in the sample (163). Thus, by measuring the attenuation of the signal generated by the molecule movement in an emulsion it is possible to derive information regarding the droplet size and droplet size distribution (154). NMR is an useful tool in terms of non-intrusively determining the droplet size distribution of dilute as well as concentrated emulsions, emulsion stability and fat content, with minimal sample preparation (163). Nevertheless, despite its great potential, the wide application of NMR in industrial settings is somewhat limited by its cost (3).

Several methods are available for the measurement of the oil-water *interfacial tension* in the presence of an emulsifier species, with direct measurement techniques using a microbalance (the Du Noüy Ring and the Wilhelmy Plate) and methods based on gravity-distorted drops (*Pendant drop*) among the most important (102, 164) . The *Pendant Drop* technique also offers the possibility of varying the drop volume in a controlled manner. The monitoring of droplet interfacial changes as a consequence of volume deformation can result in the determination of the interfacial tension and interfacial dilatational rheology (3). Further characterization methods of interfacial layer properties are currently available, e.g. *spinning drop*, *maximum bubble pressure*, *capillary rise* amongst others (102, 164).

Neutron Scattering (NS) has been used for the determination of emulsion properties such as droplet shape, dimension and distribution as well as to probe the structure of the interface (e.g. thickness and distribution of components as a function of the distance from the surface) (165).

2.5.3. Assessing emulsion flow and thermal behaviour

Rheological methods study how a material deforms/flows once subjected to a certain force or deformation and (bulk) rheology can represent a useful tool to extract information on food systems relative to their processing, shelf-life, and sensory perception (166). Several experimental tests exist that can be categorised depending on the mode of deformation (transient or dynamic) (22). Transient tests evaluate time-dependent properties such as viscosity, relaxation stress and compliance whereas dynamic tests study properties in the frequency-domain and information regarding the sample viscoelasticity can be extracted (22). *Interfacial rheology* techniques are available to characterise the relationship between the interfacial stress and the resulting interfacial layer deformation (167, 168). Depending on emulsifier type, the interface may show different viscoelastic properties in response to shear, dilation or oscillation; equivalent to shear, elongation and oscillation in bulk rheology (167, 168). *Tribology* (thin film rheology) provides information on texture and mouthfeel through the characterisation of friction and lubrication properties of a thin film of product (169). The understanding of the influence of factors such as the emulsion droplet size, stability to coalescence, fat content, amongst others, on the emulsion tribological properties can potentially allow for the design of reduced-fat products that provide a full-fat oral response (170).

In food emulsions, *Differential Scanning Calorimetry* (*DSC*) represents a useful tool to determine a wide range of properties (e.g. water and fat crystallisation, emulsion stability and partial coalescence, lipid emulsifier crystallisation, emulsion type and droplet size distribution)

as a consequence of thermal transitions mimicking processing and storage conditions (e.g. crystallisation, melting, etc.) (171).

2.6. Emulsion microstructure and performance

The demand from consumers for healthier options across different processed food categories, following increased public awareness of the impact of diet on health, has presented formulators and industry with the need to design convenient and tasty but healthy foods with enhanced functionalities (172). In Part B (Food Structure Development for Performance & Functionality) of the handbook where this chapter is published the relationship between food structure design and food system performance is explored in great detail, including where appropriate in-depth discussion relating to emulsion microstructures. The current section aims to provide a much more concise outline of recent applications where emulsion systems have been applied in foods in order to provide specific functionality/performance. The relationship between the design of an emulsion microstructure and the performance that this provides is a common thread in the segments that follow.

2.6.1. Emulsion microstructure and rheology

The understanding of the rheology of dispersions has been shown to be a useful tool in the prediction and control of processability (i.e. flowability) and sensory features of emulsion-based products such as creaminess, thickness, pourability, spreadability etc. (22). All of these properties can be associated to the measured shear viscosity, which is ultimately influenced by a variety of structural factors (e.g. dispersed phase volume fraction, droplet size and size distribution, dispersed and continuous phase rheology, etc.) (173).

One of the major factors that drastically changes emulsion rheology is the *dispersed phase volume fraction*, (ϕ). In dilute systems (ϕ < 10%) where colloidal forces and hydrodynamic inter-particle interactions may be considered as negligible, emulsion viscosity (η) depends only on the continuous phase viscosity (η_o) and linearly increases with ϕ. for spherical droplets this relationship can be described following the Einstein's equation:

$$\eta = \eta_0 (1 + 2.5\,\phi) \qquad (2.1)$$

As the concentration of dispersed phase increases further, and in the absence of colloidal interactions, emulsion viscosity (in addition to ϕ) is also influenced by the intrinsic viscosity, [η], which takes into account the shape of the droplets ([η] = 2.5 for hard spheres) and the maximum packing concentration (ϕ_c), which is the fraction of closely packed particles (in the range of 0.6 - 0.7 for spherical and non-interacting spheres). One of the most used equations was derived by Dougherty and Krieger and is applicable over the whole range of volume fractions:

$$\eta = \eta_0 \left(1 - \frac{\phi}{\phi_c}\right)^{-[\eta]\phi} \qquad (2.2)$$

When colloidal interactions cannot be neglected, emulsion viscosity is more appropriately linked to the effective volume fraction; resulting from the presence of a steric or electrostatic layer around the droplets (174). Above the maximum packing concentration, droplets are in such close proximity that they start deforming, and the emulsion exhibits a solid-like behaviour characterised by an elastic modulus and a yield stress (166).

Besides the concentration of the dispersed phase, the droplet size also plays a major role in determining the final emulsion rheology. For dispersed phase volume fractions below ϕ_c,

smaller droplet sizes give rise to a larger viscosity increase (with increasing ϕ) and exhibit a more pronounced non-Newtonian behaviour compared to emulsions with the same overall dispersed phase volume but of greater average droplet sizes (21, 166, 175). For moderately concentrated dispersions ($\phi < \phi_c$), the emulsion polydispersity has a higher degree of importance over the average droplet size. Droplets with a bimodal size distribution can pack more efficiently and the resulting emulsion viscosity is lower than either of the viscosities of the two size populations if present as monodisperse emulsions (21, 166, 175). However, when emulsions with three or more different average droplet sizes are mixed together, this effect is lost and the viscosity of the blend increases with the degree of emulsion polydispersity (20). Above ϕ_c, emulsions exhibit a variegated rheological behaviour, having a mechanical response both solid- and liquid-like depending on the applied load (176).

2.6.2. Emulsion microstructure and oral processing

Emulsion oral processing tends to be evaluated through a combination of rheological and tribological techniques (172). Rheology best describes the initial stages of oral manipulation while tribology corresponds to the squeezing and swallowing steps that follow (177). Several studies have shown a good correlation between initial thickness perception, sliminess and stickiness and shear viscosity measured at 50 s^{-1}(178). On the other hand, thin-film tribological properties demonstrated a more sensible relation to texture. For instance, comparisons between low- and full-fat emulsion samples (of matching rheological properties), revealed that tribology measurements were able to capture the distinct microstructural differences among the two systems that bulk rheology failed to recognise (179).

Although rheological and tribological tests can correlate well with overall oral perception, changes to emulsion composition and microstructure in response to the “environmental”

conditions within the oral cavity (e.g. pH, temperature etc.) and under the dynamic forces applied during oral manipulation, must also be considered (172). During oral processing, emulsions are prone to droplet coalescence as well as flocculation, with both phenomena linked to a creamy perception (180-182). In gelled emulsions, with oil droplets trapped within the gel network, fat release is dependent on whether the globules act as active or inactive fillers and sensory perception is related to the melting of the gel structure (183).

2.6.3. Emulsion microstructure for encapsulation and release

Emulsions represent an efficient medium where functional components can be encapsulated and then released at specific locations within the gastrointestinal (GI) tract in a controlled and gradual manner or in response to an environmental cue (e.g. change in pH, ionic strength, temperature etc.) (184). *Conventional* as well as *nano*-emulsions have been extensively studied for the encapsulation of lipophilic species (e.g. fatty acids, carotenoids and antioxidants) (185). Their release performance can be tuned through manipulation of microstructural parameters such as droplet size, composition of the interfacial layer and physical state of the lipid phase. In general, smaller droplet sizes allow for greater release rates (71, 97). Coating the interface of emulsion droplets with surface-active agents (e.g. phospholipids, proteins) has been shown to delay chemical degradation of the enclosed bioactives and slow down their release as a result of interfacial displacement of the original emulsifiers by the surface-active moieties secreted by the human body (185, 186). Finally, the presence of crystals within oil droplets has been shown to delay the release of lipophilic components (187). Although, both conventional and nano-emulsion microstructures have shown great promise for the encapsulation and release of lipophilic components, it is worth noting that a large proportion of bioactives with relevance to

the food industry are primarily water-soluble (e.g. minerals, vitamins, enzymes, proteins etc.) (188).

More complex emulsion microstructures have also shown potential in terms of acting as suitable carrier systems. *Gelled emulsions* can be utilised for the controlled and/or triggered release of lipophilic components at specific locations in the GI tract by tuning changes to the gel structure in response to variations in temperature, pH, salt concentration or the application of mechanical forces (189). Droplets that are bound to the matrix (inactive fillers) are usually released more quickly than unbound droplets (active fillers) (189). *Double emulsions* have attracted attention as effective media for the encapsulation of both hydrophilic and lipophilic components, with $w_1/o/w_2$ microstructures being the main focus (190). Hydrophilic components can be incorporated in the inner w_1 phase, whereas lipophilic bioactives are enclosed within the oil compartment of the double emulsion architecture. Oil droplets can also act as a barrier to the discharge of w_1-enclosed hydrophilic actives by increasing the diffusion timescales for their release (190, 191). Similarly to this, *hydrogel filled particle emulsions* (97) can operate as carriers of lipophilic components within their oil droplets, with the biopolymer particle network surrounding these further regulating release performance.

Although currently more relevant to pharmaceutics, the capacity of emulsion microstructures to facilitate the release of multiple actives (co-release) is an extremely attractive proposition that can be easily envisaged to apply within the foods arena in the future. Microemulsions and double emulsions have been studied for the co-release of at least two actives. However, co-delivery in both cases is practically limited to either simultaneous or sequential, rather than independent, release profiles (192-194). A simple o/w emulsion microstructure has also been shown to act in this capacity but to additionally offer the co-

encapsulation of two model actives in a segregated manner and to deliver these independently in response to disparate stimuli/triggers (72).

2.6.4. Fat, salt and sugar reduction

Despite their significant contribution to the taste, aroma and texture of food products, fat, salt and sugar have been shown to influence long-term health status. Formulators, regulatory bodies and more recently consumers are now increasingly aware of the diet-related health implications arising from the consumption of foods containing high amounts of these components and the public in particular has become more conscious of their eating habits. In emulsion-based products, engineering the emulsion microstructure has been proposed as a possible vehicle to lower fat, salt and sugar content without affecting significantly the organoleptic properties of products developed for a healthier lifestyle.

Fat reduction in emulsion systems is not a trivial operation since fats play a determining role in the overall texture and mouthfeel of these systems, which in turn make the product, from a customer perspective, acceptable and enjoyable from a consumer perspective (195). Some strategies (e.g. interfacial engineering, addition of thickening agents, controlling the manifestation of instability phenomena) have been proposed in addition to the use of complex types of emulsions to achieve this target. In the effort to reduce lipid adsorption within the GI tract, interfacial properties of the oil droplets can be modified either by using an emulsifier able to create a viscoelastic interfacial layer (e.g. proteins), adopting Pickering stabilisation or by coating droplets with non-digestible fibres (e.g. inulin-type fructans) (196-198). Textural and rheological features of full-fat products can be duplicated by controlling the network formation caused by thickening agents (e.g. agar, alginate, xanthan) or using fat substitutes such as protein micro-particles or starch granules as fat replacers (199-202). The general drawback of these

approaches is that their adoption may not be able to compensate for the loss of other emulsion food properties such as appearance, mouthfeel (associated with thin-film rather than bulk flow behaviour) or flavour profile, due to the reduced fat content (203, 204). During oral processing the occurrence of emulsion instability phenomena such as flocculation or partial coalescence can be induced to increase the viscosity of the product and thus mimic fat-related sensory attributes such as creaminess and mouth coating (205, 206). On the other hand, if not-well controlled, coalescence or phase inversion instability phenomena can negatively impact product perception (203, 204). In *double emulsions* (for instance $w_1/o/w_2$), fat reduction can be in theory achieved whilst still preserving both rheological and sensorial properties of the full fat, because: (*i*) the incorporation of w_1 droplets within the oil ones allows for less fat being used, while at the same time (1) the overall volume fraction of perceived oil globules in the system remains practically unchanged (195, 207). Similarly to double emulsions, the inclusion of air bubbles as replacers of fat globules in *air-bubble filled emulsions* has shown the prospect of creating tri-phasic systems of reduced calorific content and similar rheological features as the corresponding simple o/w emulsions (99, 208). Finally, *hydrogel particle filled emulsions* have also shown potential in replicating the sensorial performance of traditional full-fat products. This can be achieved by manipulating the responsiveness of the gel particle to the oral stresses involved during oral processing, as well as by controlling how particle deformation would regulate the release/expulsion of the fat droplets it contains (77).

For the food industry, *salt* and *sugar* reduction also represent a challenging task (93). At the moment, the only successful applied approaches consist in the use of salt or sugar substitutes such as mineral salts in the former case or either natural (e.g. Steviol glycosides, stevioside) or artificial (e.g. aspartame, acelsufame-K) sweeteners in the latter case (209, 210). Both however can have major drawbacks in terms to off-tastes (for both salt replacers and natural sweeteners)

or perceived/actual health hazards (for artificial sweeteners) (209, 210). Attempts for salt and sugar reduction have also been conducted through the manipulation of the emulsion microstructure, with double emulsions and gels filled with emulsion droplets amongst the main strategies. For instance, through the encapsulation of salt or sugars within the inner (w_1) droplets of a double emulsion ($w_1/o/w_2$), it is possible to regulate the release of both components and effectively optimise their detection by the taste receptors in the mouth. As a result, this approach can be employed to enhance the saltiness/sweetness perception of emulsions with reduced salt/sugar content to ideally match that of their full salt/sugar predecessors (99, 211). Another proposed strategy involves trapping sugar (or equivalently salt) molecules within a gel network filled with emulsion droplets (212-214). By modulating the interaction between the droplets and the gel network, it is possible to tune the fracture behaviour of these systems. The formation of more brittle gels, i.e. with a lower Young's modulus, allows (upon mastication) the rupture of the network into smaller fragments, in turn enhances sweetness (or saltiness) perception (212, 214).

2.7. Conclusions and future perspective

The relationship between emulsion microstructure development, through the control of both formulation and processing aspects, and product performance has been the common theme throughout this chapter. Nonetheless the design and development of emulsion structures is a rather complex operation and one that is practically impossible to cover in full detail within the confines of a single book chapter. If nothing else, the discussion presented here serves to clearly demonstrate the significant formulation/processing challenges facing both industry and academia for the development of new, enjoyable, nutritious and inexpensive emulsion-based

food microstructures that meet growing consumer needs. It is these very challenges that also present food formulators and engineers with exciting opportunities for further innovation.

The continuously increasing public awareness of the impact of diet on health, has increased the demand for healthy foods and thus the necessity to develop and design novel products having superior properties. Despite the great deal of interest that has been dedicated towards this, the combination of food engineering and sensory sciences and human physiology, in order to correlate biological response (e.g. digestion, absorption) and organoleptic properties (e.g. mouthfeel, taste, aroma) to the emulsion microstructural features, remains a fascinating and still expanding research area. In addition, the production of convenient and tasty foods should strive to improve current manufacturing efficiencies and production costs either through the development of new emulsification methods or through the further optimisation of existing ones. Successful scale-up and scale-down approaches are equally important in order to develop processing techniques that possess the flexibility to be adapted to large scale industrial manufacturing as well as to late customisation/home finishing of food products.

List of references

(1) Tucker III C.L., Moldenaers P. *Microstructural evolution in polymer blends*. Annual Review of Fluid Mechanics. 2002; 34(1): 177-210.

(2) Robins M.M., Wilde P.J. *Colloids and Emulsions*. In: Caballero B. (ed.). *Encyclopedia of Food Sciences and Nutrition*. 2nd ed. Oxford: Academic Press; 2003. p. 1517-24.

(3) McClements D.J. *Food Emulsions: Principles, Practices and Techniques*. 3rd ed. Boca Raton: CRC press; 2016.

(4) Ma Z., Boye J.I. *Advances in the design and production of reduced-fat and reduced-Cholesterol salad dressing and mayonnaise: A review*. Food and Bioprocess Technology. 2013; 6(3): 648-70.

(5) Akhtar M., Stenzel J., Murray B.S., Dickinson E. *Factors affecting the perception of creaminess of oil-in-water emulsions*. Food Hydrocolloids. 2005; 19(3): 521-6.

(6) Aben S., Holtze C., Tadros T., Schurtenberger P. *Rheological investigations on the creaming of depletion-flocculated emulsions*. Langmuir. 2012; 28(21): 7967-75.

(7) McClements D.J. *Comments on viscosity enhancement and depletion flocculation by polysaccharides*. Food Hydrocolloids. 2000; 14(2): 173-7.

(8) Saha D., Bhattacharya S. *Hydrocolloids as thickening and gelling agents in food: a critical review*. Journal of Food Science and Technology. 2010; 47(6): 587-97.

(9) Sworn G. *Hydrocolloid thickeners and their applications*. In: Williams P.A., Phillips G.O. (eds.). *Gums and Stabilisers for the Food Industry 12*: 1st ed. Cambridge: The Royal Society of Chemistry; 2004. p. 13-22.

(10) de Vries J. *Hydrocolloid gelling agents and their applications*. In: Williams P.A., Phillips G.O., (eds.). *Gums and Stabilisers for the Food Industry 12*: 1st ed. Cambridge: The Royal Society of Chemistry; 2004. p. 23-31.

(11) Dickinson E. *Emulsion gels: The structuring of soft solids with protein-stabilized oil droplets*. Food Hydrocolloids. 2012; 28(1): 224-41.

(12) Lupi F.R., Gabriele D., de Cindio B., Sánchez M.C., Gallegos C. *A rheological analysis of structured water-in-olive oil emulsions*. Journal of Food Engineering. 2011; 107(3): 296-303.

(13) Narine S.S., Marangoni A.G. *Relating structure of fat crystal networks to mechanical properties: a review*. Food Research International. 1999; 32(4): 227-48.

(14) Tyrode E., Allouche J., Choplin L., Salager J.-L. *Emulsion catastrophic inversion from abnormal to normal morphology. 4. Following the emulsion viscosity during three inversion protocols and extending the critical dispersed-phase concept*. Industrial & Engineering Chemistry Research. 2005; 44(1): 67-74.

(15) Feitosa K., Marze S., Saint-Jalmes A., Durian D.J. *Electrical conductivity of dispersions: from dry foams to dilute suspensions*. Journal of Physics: Condensed Matter. 2005; 17(41): 6301-5.

(16) Varka E.M., Ampatzidis C., Kostoglou M., Karapantsios T., Dutschk V. *On the use of electrical conductance measurements for the stability of oil-in-water Pickering emulsions.* Colloids and Surfaces A: Physicochemical and Engineering Aspects. 2010; 365(1): 181-8.

(17) Walstra P., Smulders P.E.A. *Emulsion Formation*. In: Bink B.P. (ed.). *Modern Aspects of Emulsion Science*: Cambridge: The Royal Society of Chemistry; 1998. p. 56-99.

(18) McClements D.J., Henson L., Popplewell L.M., Decker E.A., Jun Choi S. *Inhibition of ostwald ripening in model beverage emulsions by addition of poorly water soluble triglyceride oils*. Journal of Food Science. 2012; 77(1): C33-C8.

(19) Piorkowski D.T., McClements D.J. *Beverage emulsions: Recent developments in formulation, production, and applications*. Food Hydrocolloids. 2014; 42: 5-41.

(20) Pal R. *Effect of droplet size on the rheology of emulsions*. AIChE Journal. 1996; 42(11): 3181-90.

(21) Pal R. *Rheology of simple and multiple emulsions*. Current Opinion in Colloid & Interface Science. 2011; 16(1): 41-60.

(22) Tabilo-Munizaga G., Barbosa-Cánovas G.V. *Rheology for the food industry*. Journal of Food Engineering. 2005; 67(1): 147-56.

(23) Pal R. *Rheology of high internal phase ratio emulsions*. Food Hydrocolloids. 2006; 20(7): 997-1005.

(24) Ogawa S., Decker E.A., McClements D.J. *Production and characterization of o/w emulsions containing cationic droplets stabilized by lecithin−chitosan membranes*. Journal of Agricultural and Food Chemistry. 2003; 51(9): 2806-12.

(25) Singh H., Ye A., Horne D. *Structuring food emulsions in the gastrointestinal tract to modify lipid digestion*. Progress in Lipid Research. 2009; 48(2): 92-100.

(26) Mei L., Decker E.A., McClements D.J. *Evidence of iron association with emulsion droplets and its impact on lipid oxidation*. Journal of Agricultural and Food Chemistry. 1998; 46(12): 5072-7.

(27) Coupland J.N., McClements D.J. *Lipid oxidation in food emulsions*. Trends in Food Science & Technology. 1996; 7(3): 83-91.

(28) Boode K., Walstra P., de Groot-Mostert A.E.A. *Partial coalescence in oil-in-water emulsions 2. Influence of the properties of the fat*. Colloids and Surfaces A: Physicochemical and Engineering Aspects. 1993; 81: 139-51.

(29) Goff H.D. *Formation and stabilisation of structure in ice-cream and related products*. Current Opinion in Colloid & Interface Science. 2002; 7(5): 432-7.

(30) Buldo P., Andersen U., Wiking L. *Microstructure and material properties of milk fat systems during temperature fluctuations*. Food Biophysics. 2013; 8(4): 262-72.

(31) McClements D.J. *Colloidal basis of emulsion color*. Current Opinion in Colloid & Interface Science. 2002; 7(5): 451-5.

(32) Chantrapornchai W., Clydesdale F.M., McClements D.J. *Understanding Colors in Emulsions*. In: Culver, C.A., Wrolstad R.E. (eds.). *Color Quality of Fresh and Processed Foods*: Washington, DC: American Chemical Society; 2008. p. 364-87.

(33) Ziming Sun J., Erickson M.C.E., Parr J.W. *Refractive index matching and clear emulsions*. International Journal of Cosmetic Science. 2005; 27(6): 355-6.

(34) Silva H.D., Cerqueira M.Â., Vicente A.A. *Nanoemulsions for food applications: development and characterization*. Food and Bioprocess Technology. 2012; 5(3): 854-67.

(35) Wilde P.J. *Interfaces: their role in foam and emulsion behaviour*. Current Opinion in Colloid & Interface Science. 2000; 5(3): 176-81.

(36) Walstra P. *Principles of emulsion formation*. Chemical Engineering Science. 1993; 48(2): 333-49.

(37) Palanuwech J., Coupland J.N. *Effect of surfactant type on the stability of oil-in-water emulsions to dispersed phase crystallization*. Colloids and Surfaces A: Physicochemical and Engineering Aspects. 2003; 223(1): 251-62.

(38) Das K.P., Kinsella J.E. *Stability Of Food Emulsions: Physicochemical Role Of Protein And Nonprotein Emulsifiers*. In: Kinsella J.E. (ed.). *Advances in Food and Nutrition Research*. Oxford: Academic Press; 1990. p. 81-201.

(39) Dickinson E. *Food emulsions and foams: Stabilization by particles*. Current Opinion in Colloid & Interface Science. 2010; 15(1): 40-9.

(40) Walstra P. *Physical Chemistry of Foods*. New York: Dekker M; 2003.

(41) Pasquali R.C., Taurozzi M.P., Bregni C. *Some considerations about the hydrophilic-lipophilic balance system*. International Journal of Pharmaceutics. 2008; 356(1): 44-51.

(42) Butt H.J., Graf K., Kappl M. *Physics and Chemistry of Interfaces*. 3rd ed. Weinheim: Wiley-VCH; 2003.

(43) McClements D.J., Rao J. *Food-grade nanoemulsions: Formulation, fabrication, properties, performance, biological fate, and potential toxicity*. Critical Reviews in Food Science and Nutrition. 2011; 51(4): 285-330.

(44) Chang Y., McLandsborough L., McClements D.J. *Fabrication, stability and efficacy of dual-component antimicrobial nanoemulsions: Essential oil (thyme oil) and cationic surfactant (lauric arginate)*. Food Chemistry. 2015; 172: 298-304.

(45) Kronberg B. *Surfactant mixtures*. Current Opinion in Colloid & Interface Science. 1997; 2(5): 456-63.

(46) Dalgleish D.G. *Food emulsions-their structures and structure-forming properties*. Food Hydrocolloids. 2006; 20(4): 415-22.

(47) Zana R. *Dynamics of Surfactant Self-Assemblies*. 1st ed. Boca Raton: CRC Press; 2005.

(48) Stang M., Karbstein H., Schubert H. *Adsorption kinetics of emulsifiers at oil—water interfaces and their effect on mechanical emulsification*. Chemical Engineering and Processing: Process Intensification. 1994; 33(5): 307-11.

(49) Pichot R., Spyropoulos F., Norton I.T. *Mixed-emulsifier stabilised emulsions: Investigation of the effect of monoolein and hydrophilic silica particle mixtures on the stability against coalescence*. Journal of Colloid and Interface Science. 2009; 329(2): 284-91.

(50) Dickinson E. *Flocculation of protein-stabilized oil-in-water emulsions*. Colloids and Surfaces B: Biointerfaces. 2010; 81(1): 130-40.

(51) Damodaran S. *Protein stabilization of emulsions and foams*. Journal of Food Science. 2005; 70(3): R54-R66.

(52) Wilde P., Mackie A., Husband F., Gunning P., Morris V. *Proteins and emulsifiers at liquid interfaces*. Advances in Colloid and Interface Science. 2004; 108-109: 63-71.

(53) Dan A., Gochev G., Krägel J., Aksenenko E.V., Fainerman V.B., Miller R. *Interfacial rheology of mixed layers of food proteins and surfactants*. Current Opinion in Colloid & Interface Science. 2013; 18(4): 302-10.

(54) Dickinson E. *Milk protein interfacial layers and the relationship to emulsion stability and rheology*. Colloids and Surfaces B: Biointerfaces. 2001; 20(3): 197-210.

(55) Sagis L.M.C., Scholten E. *Complex interfaces in food: Structure and mechanical properties*. Trends in Food Science & Technology. 2014; 37(1): 59-71.

(56) Singh H., Sarkar A. *Behaviour of protein-stabilised emulsions under various physiological conditions*. Advances in Colloid and Interface Science. 2011; 165(1): 47-57.

(57) Chevalier Y., Bolzinger M.-A. *Emulsions stabilized with solid nanoparticles: Pickering emulsions*. Colloids and Surfaces A: Physicochemical and Engineering Aspects. 2013; 439: 23-34.

(58) Xiao J., Li Y., Huang Q. *Recent advances on food-grade particles stabilized Pickering emulsions: Fabrication, characterization and research trends*. Trends in Food Science & Technology. 2016; 55: 48-60.

(59) Aveyard R., Binks B.P., Clint J.H. *Emulsions stabilised solely by colloidal particles*. Advances in Colloid and Interface Science. 2003; 100-102: 503-46.

(60) Dickinson E. *Use of nanoparticles and microparticles in the formation and stabilization of food emulsions*. Trends in Food Science & Technology. 2012; 24(1): 4-12.

(61) Hunter T.N., Pugh R.J., Franks G.V., Jameson G.J. *The role of particles in stabilising foams and emulsions*. Advances in Colloid and Interface Science. 2008; 137(2): 57-81.

(62) Dickinson E. *Stabilising emulsion-based colloidal structures with mixed food ingredients*. Journal of the Science of Food and Agriculture. 2013; 93(4): 710-21.

(63) Zhang N., Zhang L., Sun D. *Influence of emulsification process on the properties of Pickering emulsions stabilized by layered double hydroxide particles*. Langmuir. 2015; 31(16): 4619-26.

(64) Kalashnikova I., Bizot H., Cathala B., Capron I. *New Pickering emulsions stabilized by bacterial cellulose nanocrystals*. Langmuir. 2011; 27(12): 7471-9.

(65) Luo Z., Murray B.S., Yusoff A., Morgan M.R.A., Povey M.J.W., Day A.J. *Particle-stabilizing effects of flavonoids at the oil-water interface*. Journal of Agricultural and Food Chemistry. 2011; 59(6): 2636-45.

(66) Yusoff A., Murray B.S. *Modified starch granules as particle-stabilizers of oil-in-water emulsions*. Food Hydrocolloids. 2011; 25(1): 42-55.

(67) Tzoumaki M.V., Moschakis T., Kiosseoglou V., Biliaderis C.G. *Oil-in-water emulsions stabilized by chitin nanocrystal particles*. Food Hydrocolloids. 2011; 25(6): 1521-9.

(68) Duffus L.J., Norton J.E., Smith P., Norton I.T., Spyropoulos F. *A comparative study on the capacity of a range of food-grade particles to form stable o/w and w/o Pickering emulsions*. Journal of Colloid and Interface Science. 2016; 473: 9-21.

(69) Norton I., Moore S., Fryer P. *Understanding food structuring and breakdown: engineering approaches to obesity*. Obesity Reviews. 2007; 8(s1): 83-8.

(70) Aguilera J.M. *Why food microstructure?* Journal of Food Engineering. 2005; 67(1): 3-11.

(71) McClements D.J. *Encapsulation, protection, and release of hydrophilic active components: Potential and limitations of colloidal delivery systems*. Advances in Colloid and Interface Science. 2015; 219: 27-53.

(72) Spyropoulos F., Kurukji D., Taylor P., Norton I.T. *Fabrication and utilization of bifunctional protein/polysaccharide coprecipitates for the independent codelivery of two model actives from simple oil-in-water emulsions*. Langmuir. 2018; 34(13): 3934-48.

(73) Guerra-Rosas M.I., Morales-Castro J., Ochoa-Martínez L.A., Salvia-Trujillo L., Martín-Belloso O. *Long-term stability of food-grade nanoemulsions from high methoxyl pectin containing essential oils*. Food Hydrocolloids. 2016; 52: 438-46.

(74) Luo N., Ye A., Wolber F.M., Singh H. *Structure of whey protein emulsion gels containing capsaicinoids: Impact on in-mouth breakdown behaviour and sensory perception*. Food Hydrocolloids. 2019; 92: 19-29.

(75) Ben-Harb S., Panouillé M., Huc-Mathis D., Moulin G., Saint-Eve A., Irlinger F., et al. *The rheological and microstructural properties of pea, milk, mixed pea/milk gels and gelled emulsions designed by thermal, acid, and enzyme treatments*. Food Hydrocolloids. 2018; 77: 75-84.

(76) Wolf B., Frith W.J. *String phase formation in biopolymer aqueous solution blends*. Journal of Rheology. 2003; 47(5): 1151-70.

(77) Chung C., Degner B., Decker E.A., McClements D.J. *Oil-filled hydrogel particles for reduced-fat food applications: Fabrication, characterization, and properties*. Innovative Food Science & Emerging Technologies. 2013; 20: 324-34.

(78) Tchuenbou-Magaia F.L., Norton I.T., Cox P.W. *Hydrophobins stabilised air-filled emulsions for the food industry*. Food Hydrocolloids. 2009; 23(7): 1877-85.

(79) Goindi S., Kaur A., Kaur R., Kalra A., Chauhan P. *19 - Nanoemulsions: an emerging technology in the food industry*. In: Grumezescu A.M., (ed.). *Emulsions*. 1st ed. Oxford: Academic Press; 2016. p. 651-88.

(80) Tadros T., Izquierdo P., Esquena J., Solans C. *Formation and stability of nano-emulsions*. Advances in Colloid and Interface Science. 2004; 108-109: 303-18.

(81) Donsì F. *Chapter 11 - Applications of Nanoemulsions in Foods*. In: Jafari S.M., McClements D.J., (eds.). *Nanoemulsions*. 1st ed. Oxford: Academic Press; 2018. p. 349-77.

(82) Sala G., van de Velde F., Cohen Stuart M.A., van Aken G.A. *Oil droplet release from emulsion-filled gels in relation to sensory perception*. Food Hydrocolloids. 2007; 21(5): 977-85.

(83) Sato A.C.K., Moraes K.E.F.P., Cunha R.L. *Development of gelled emulsions with improved oxidative and pH stability*. Food Hydrocolloids. 2014; 34: 184-92.

(84) Oliver L., Berndsen L., van Aken G.A., Scholten E. *Influence of droplet clustering on the rheological properties of emulsion-filled gels*. Food Hydrocolloids. 2015; 50: 74-83.

(85) Malone M.E., Appelqvist I.A.M. *Gelled emulsion particles for the controlled release of lipophilic volatiles during eating*. Journal of Controlled Release. 2003; 90(2): 227-41.

(86) Garti N., Bisperink C. *Double emulsions: progress and applications*. Current Opinion in Colloid & Interface Science. 1998; 3(6): 657-67.

(87) Muschiolik G. *Multiple emulsions for food use*. Current Opinion in Colloid & Interface Science. 2007; 12(4): 213-20.

(88) Garti N., Benichou A. *Recent Developments in Double Emulsions in Food Applications*. In: Friberg S., K. L., Sjöblom J., (eds.). 1st ed. *Food Emulsions*. New York: Marcel Dekker; 2003. p. 362-422.

(89) Capron I., Costeux S., Djabourov M. *Water in water emulsions: phase separation and rheology of biopolymer solutions*. Rheologica Acta. 2001; 40(5): 441-56.

(90) Buzza D.M.A., Fletcher P.D.I., Georgiou T.K., Ghasdian N. *Water-in-Water Emulsions Based on Incompatible Polymers and Stabilized by Triblock Copolymers-Templated Polymersomes*. Langmuir. 2013; 29(48): 14804-14.

(91) Frith W.J. *Mixed biopolymer aqueous solutions-phase behaviour and rheology*. Advances in Colloid and Interface Science. 2010; 161(1): 48-60.

(92) Pawlik A., Fryer P., Norton I.T. *Formulation Engineering of Food Emulsions*. In: Norton J.E., Fryer P.J., Norton I.T., (eds.). *Formulation Engineering of Foods*. 1st ed. Oxford: Wiley-Blackwell; 2013.

(93) Norton J.E., Gonzalez Espinosa Y., Watson R.L., Spyropoulos F., Norton I.T. *Functional food microstructures for macronutrient release and delivery*. Food & Function. 2015; 6(3): 663-78.

(94) Dickinson E. *Exploring the frontiers of colloidal behaviour where polymers and particles meet*. Food Hydrocolloids. 2016; 52: 497-509.

(95) Matalanis A., Lesmes U., Decker E.A., McClements D.J. *Fabrication and characterization of filled hydrogel particles based on sequential segregative and aggregative biopolymer phase separation*. Food Hydrocolloids. 2010; 24(8): 689-701.

(96) McClements D.J. *Designing biopolymer microgels to encapsulate, protect and deliver bioactive components: Physicochemical aspects*. Advances in Colloid and Interface Science. 2017; 240: 31-59.

(97) McClements D.J. *Advances in fabrication of emulsions with enhanced functionality using structural design principles*. Current Opinion in Colloid & Interface Science. 2012; 17(5): 235-45.

(98) Tchuenbou-Magaia F.L. *Hydrophobins and Air Filled Emulsions*. PhD [dissertation]. Birmingham: University of Birmigham; 2012.

(99) Norton J.E., Wallis G.A., Spyropoulos F., Lillford P.J., Norton I.T. *Designing food structures for nutrition and health benefits*. Annual Review of Food Science and Technology. 2014; 5(1): 177-95.

(100) Tchuenbou-Magaia F.L., Al-Rifai N., Ishak N.E.M., Norton I.T., Cox P.W. *Suspensions of air cells with cysteine-rich protein coats: Air-filled emulsions*. Journal of Cellular Plastics. 2011; 47(3): 217-32.

(101) Le Révérend B.J.D., Norton I.T., Cox P.W., Spyropoulos F. *Colloidal aspects of eating*. Current Opinion in Colloid & Interface Science. 2010; 15(1): 84-9.

(102) Tadros T. *Interface, Liquid-liquid*. In: Tadros T. (ed.). *Encyclopedia of Colloid and Interface Science*. Berlin, Heidelberg: Springer Berlin Heidelberg; 2013. p. 635-6.

(103) Ivanov I.B., Danov K.D., Kralchevsky P.A. *Flocculation and coalescence of micron-size emulsion droplets*. Colloids and Surfaces A: Physicochemical and Engineering Aspects. 1999; 152(1): 161-82.

(104) Boode K., Walstra P. *Partial coalescence in oil-in-water emulsions 1. Nature of the aggregation*. Colloids and Surfaces A: Physicochemical and Engineering Aspects. 1993; 81: 121-37.

(105) Kabalnov A. *Coalescence in Emulsions*. In: Binks B.P. (ed.). *Modern Aspects of Emulsion Science*. Cambridge: Royal Society of Chemistry; 1998. p. 205-60.

(106) Brooks B.W., Richmond H.N., Zerfa M. *Phase Inversions and Drop Formation in Agitated Liquid-Liquid Dispersions in the Presence of Nonionic Surfactants*. In: Binks B.P. (ed.). *Modern Aspects of Emulsion Science*. Cambridge: Royal Society of Chemistry; 1998. p. 175-204.

(107) Muschiolik G., Dickinson E. *Double emulsions relevant to food systems: preparation, stability, and applications*. Comprehensive Reviews in Food Science and Food Safety. 2017; 16(3): 532-55.

(108) Windhab E.J., Dressler M., Feigl K., Fischer P., Megias-Alguacil D. *Emulsion processing-from single-drop deformation to design of complex processes and products*. Chemical Engineering Science. 2005; 60(8): 2101-13.

(109) Jafari S.M., Assadpoor E., He Y., Bhandari B. *Re-coalescence of emulsion droplets during high-energy emulsification*. Food Hydrocolloids. 2008; 22(7): 1191-202.

(110) Schubert H., Engel R. *Product and Formulation Engineering of Emulsions*. Chemical Engineering Research and Design. 2004; 82(9): 1137-43.

(111) Rayner M. *Scales and Forces in Emulsification*. In: Rayner M., Dejmek P., (eds.). *Engineering Aspects of Food Emulsification and Homogenisation*. 1st ed. Boca Raton: CRC press; 2015. p. 3-32.

(112) Yasuno M., Nakajima M., Iwamoto S., Maruyama T., Sugiura S., Kobayashi I., et al. *Visualization and characterization of SPG membrane emulsification*. Journal of Membrane Science. 2002; 210(1): 29-37.

(113) Kobayashi I., Mukataka S., Nakajima M. *Effect of slot aspect ratio on droplet formation from silicon straight-through microchannels*. Journal of Colloid and Interface Science. 2004; 279(1): 277-80.

(114) Vankova N., Tcholakova S., Denkov N.D., Ivanov I.B., Vulchev V.D., Danner T. *Emulsification in turbulent flow: 1. Mean and maximum drop diameters in inertial and viscous regimes*. Journal of Colloid and Interface Science. 2007; 312(2): 363-80.

(115) Vankova N., Tcholakova S., Denkov N.D., Vulchev V.D., Danner T. *Emulsification in turbulent flow: 2. Breakage rate constants*. Journal of Colloid and Interface Science. 2007; 313(2): 612-29.

(116) Tcholakova S., Lesov I., Golemanov K., Denkov N.D., Judat S., Engel R., et al. *Efficient emulsification of viscous oils at high drop volume fraction*. Langmuir. 2011; 27(24): 14783-96.

(117) Patist A., Bates D. *Ultrasonic innovations in the food industry: From the laboratory to commercial production*. Innovative Food Science & Emerging Technologies. 2008; 9(2): 147-54.

(118) Canselier J.P., Delmas H., Wilhelm A.M., Abismaïl B. *Ultrasound emulsification-an overview*. Journal of Dispersion Science and Technology. 2002; 23(1-3): 333-49.

(119) Håkansson A., Fuchs L., Innings F., Revstedt J., Bergenståhl B., Trägårdh C. *Visual observations and acoustic measurements of cavitation in an experimental model of a high-pressure homogenizer*. Journal of Food Engineering. 2010; 100(3): 504-13.

(120) Boxall J.A., Koh C.A., Sloan E.D., Sum A.K., Wu D.T. *Droplet size scaling of water-in-oil emulsions under turbulent flow*. Langmuir. 2012; 28(1): 104-10.

(121) Sprow F.B. *Distribution of drop sizes produced in turbulent liquid-liquid dispersion*. Chemical Engineering Science. 1967; 22(3): 435-42.

(122) Calabrese R.V., Wang C.Y., Bryner N.P. *Drop breakup in turbulent stirred-tank contactors. Part III: Correlations for mean size and drop size distribution*. AIChE Journal. 1986; 32(4): 677-81.

(123) Baldyga J., Podgórska W. *Drop break-up in intermittent turbulence: Maximum stable and transient sizes of drops*. The Canadian Journal of Chemical Engineering. 1998; 76(3): 456-70.

(124) Zhou G., Kresta S.M. *Correlation of mean drop size and minimum drop size with the turbulence energy dissipation and the flow in an agitated tank*. Chemical Engineering Science. 1998; 53(11): 2063-79.

(125) Pacek A.W., Man C.C., Nienow A.W. *On the Sauter mean diameter and size distributions in turbulent liquid/liquid dispersions in a stirred vessel*. Chemical Engineering Science. 1998; 53(11): 2005-11.

(126) Tesch S., Schubert H. *Influence of increasing viscosity of the aqueous phase on the short-term stability of protein stabilized emulsions*. Journal of Food Engineering. 2002; 52(3): 305-12.

(127) Tesch S., Gerhards C., Schubert H. *Stabilization of emulsions by OSA starches*. Journal of Food Engineering. 2002; 54(2): 167-74.

(128) Tcholakova S., Denkov N.D., Sidzhakova D., Ivanov I.B., Campbell B. *Interrelation between drop size and protein adsorption at various emulsification conditions*. Langmuir. 2003; 19(14): 5640-9.

(129) Tcholakova S., Denkov N.D., Danner T. *Role of surfactant type and concentration for the mean drop size during emulsification in turbulent flow*. Langmuir. 2004; 20(18): 7444-58.

(130) Schubert H., Ax K., Behrend O. *Product engineering of dispersed systems*. Trends in Food Science & Technology. 2003; 14(1): 9-16.

(131) Zhang J., Xu S., Li W. *High shear mixers: A review of typical applications and studies on power draw, flow pattern, energy dissipation and transfer properties*. Chemical Engineering and Processing: Process Intensification. 2012; 57-58: 25-41.

(132) Calabrese R.V., Chang T.P.K., Dang P.T. *Drop breakup in turbulent stirred-tank contactors. Part I: Effect of dispersed-phase viscosity*. AIChE Journal. 1986; 32(4): 657-66.

(133) Hall S., Cooke M., El-Hamouz A., Kowalski A.J. *Droplet break-up by in-line Silverson rotor–stator mixer*. Chemical Engineering Science. 2011; 66(10): 2068-79.

(134) Urban K., Wagner G., Schaffner D., Röglin D., Ulrich J. *Rotor-Stator and disc systems for emulsification processes*. Chemical Engineering & Technology. 2006; 29(1): 24-31.

(135) Lee L., Norton I.T. *Comparing droplet breakup for a high-pressure valve homogeniser and a Microfluidizer for the potential production of food-grade nanoemulsions*. Journal of Food Engineering. 2013; 114(2): 158-63.

(136) Qian C., McClements D.J. *Formation of nanoemulsions stabilized by model food-grade emulsifiers using high-pressure homogenization: Factors affecting particle size*. Food Hydrocolloids. 2011; 25(5): 1000-8.

(137) Behrend O., Ax K., Schubert H. *Influence of continuous phase viscosity on emulsification by ultrasound*. Ultrasonics Sonochemistry. 2000; 7(2): 77-85.

(138) van der Graaf S., Schroën C.G.P.H., Boom R.M. *Preparation of double emulsions by membrane emulsification-a review*. Journal of Membrane Science. 2005; 251(1): 7-15.

(139) Vladisavljević G.T., Kobayashi I., Nakajima M. *Production of uniform droplets using membrane, microchannel and microfluidic emulsification devices*. Microfluidics and Nanofluidics. 2012; 13(1): 151-78.

(140) Johnson B.K., Prud'homme R.K. *Chemical processing and micromixing in confined impinging jets*. AIChE Journal. 2003; 49(9): 2264-82.

(141) Siddiqui S.W., Wan Mohamad W.A.F., Mohd. Rozi M.F., Norton I.T. *Continuous, high-throughput flash-synthesis of submicron food emulsions using a Confined Impinging Jet Mixer: effect of in situ turbulence, sonication, and small surfactants*. Industrial & Engineering Chemistry Research. 2017; 56(44): 12833-47.

(142) Siddiqui S.W., Norton I.T. *Oil-in-water emulsification using Confined Impinging Jets*. Journal of Colloid and Interface Science. 2012; 377(1): 213-21.

(143) Joscelyne S.M., Trägårdh G. *Membrane emulsification-a literature review*. Journal of Membrane Science. 2000; 169(1): 107-17.

(144) Ushikubo F.Y., Oliveira D.R.B., Michelon M., Cunha R.L. *Designing food structure using microfluidics*. Food Engineering Reviews. 2015; 7(4): 393-416.

(145) Hancocks R.D., Spyropoulos F., Norton I.T. *The effects of membrane composition and morphology on the rotating membrane emulsification technique for food grade emulsions*. Journal of Membrane Science. 2016; 497: 29-35.

(146) Lloyd D.M., Norton I.T., Spyropoulos F. *Process optimisation of rotating membrane emulsification through the study of surfactant dispersions*. Journal of Food Engineering. 2015; 166: 316-24.

(147) Nisisako T., Ando T., Hatsuzawa T. *High-volume production of single and compound emulsions in a microfluidic parallelization arrangement coupled with coaxial annular world-to-chip interfaces*. Lab on a Chip. 2012; 12(18): 3426-35.

(148) Tadros T.F. *Emulsion Science and Technology: A General Introduction*. In: Tadros T.F. (ed.). *Emulsion Science and Technology*. 1st ed. Weinheim: Wiley-VCH; 2009. p. 1-56.

(149) Ee S.L., Duan X., Liew J., Nguyen Q.D. *Droplet size and stability of nano-emulsions produced by the temperature phase inversion method*. Chemical Engineering Journal. 2008; 140(1): 626-31.

(150) Fernandez P., André V., Rieger J., Kühnle A. *Nano-emulsion formation by emulsion phase inversion*. Colloids and Surfaces A: Physicochemical and Engineering Aspects. 2004; 251(1): 53-8.

(151) Izquierdo P., Esquena J., Tadros T.F., Dederen C., Garcia M.J., Azemar N., et al. *Formation and stability of nano-emulsions prepared using the Phase Inversion Temperature method*. Langmuir. 2002; 18(1): 26-30.

(152) Izquierdo P., Esquena J., Tadros T.F., Dederen J.C., Feng J., Garcia-Celma M.J., et al. *Phase behavior and nano-emulsion formation by the phase inversion temperature method.* Langmuir. 2004; 20(16): 6594-8.

(153) Perazzo A., Preziosi V., Guido S. *Phase inversion emulsification: Current understanding and applications*. Advances in Colloid and Interface Science. 2015; 222: 581-99.

(154) McClements D.J. *Critical review of techniques and methodologies for characterization of emulsion stability*. Critical Reviews in Food Science and Nutrition. 2007; 47(7): 611-49.

(155) Klang V., Valenta C. *Lecithin-based nanoemulsions*. Journal of Drug Delivery Science and Technology. 2011; 21(1): 55-76.

(156) Caillet A., Cogné C., Andrieu J., Laurent P., Rivoire A. *Characterization of ice cream structure by direct optical microscopy. Influence of freezing parameters*. LWT - Food Science and Technology. 2003; 36(8): 743-9.

(157) Yang H., Wang Y., Lai S., An H., Li Y., Chen F. *Application of atomic force microscopy as a nanotechnology tool in food science*. Journal of Food Science. 2007; 72(4): R65-R75.

(158) Ricci D., Braga P.C. *How the Atomic Force Microscope Works*. In: Braga P.C., Davide R., (eds.). *Atomic Force Microscopy*. 1st ed. Totowa: Humana Press; 2004. p. 3-12.

(159) Gunning A.P., Mackie A.R., Wilde P.J., Morris V.J. *Atomic force microscopy of emulsion droplets: Probing droplet-droplet interactions*. Langmuir. 2004;20(1):116-22.

(160) Lehner D., Kellner G., Schnablegger H., Glatter O. *Static light scattering on dense colloidal systems: New instrumentation and experimental results*. Journal of Colloid and Interface Science. 1998; 201(1): 34-47.

(161) Lindner H., Fritz G., Glatter O. *Measurements on concentrated oil in water emulsions using static light scattering*. Journal of Colloid and Interface Science. 2001; 242(1): 239-46.

(162) Brar S.K., Verma M. *Measurement of nanoparticles by light-scattering techniques*. TrAC Trends in Analytical Chemistry. 2011; 30(1): 4-17.

(163) Balinov b., Mariette F., Söderman O. *NMR Studies of Emulsions with Particular Emphasis on Food Emulsions*. In: Friberg S., K. L., Sjöblom J., (eds.). 1st ed. *Food Emulsions*. New York: Marcel Dekker; 2003. p. 601-40.

(164) Korenko M., Šimko F. *Measurement of interfacial tension in liquid−liquid high-temperature systems*. Journal of Chemical & Engineering Data. 2010; 55(11): 4561-73.

(165) Hone J.H.E., Cosgrove T., Saphiannikova M., Obey T.M., Marshall J.C., Crowley T.L. *Structure of physically adsorbed polymer layers measured by small-angle neutron scattering using contrast variation methods*. Langmuir. 2002; 18(3): 855-64.

(166) Derkach S.R. *Rheology of emulsions*. Advances in Colloid and Interface Science. 2009; 151(1): 1-23.

(167) Murray B.S. *Interfacial rheology of food emulsifiers and proteins*. Current Opinion in Colloid & Interface Science. 2002; 7(5): 426-31.

(168) Miller R., Fainerman V.B., Krägel J., Loglio G. *Surface rheology of adsorbed surfactants and proteins.* Current Opinion in Colloid & Interface Science. 1997; 2(6): 578-83.

(169) Goh S.M. *Tribology of Foods*. In: Wang Q.J., Chung Y.-W. (eds.). Encyclopedia of Tribology. Boston, MA: Springer; 2013. p. 3871-3.

(170) Dresselhuis D.M., Klok H.J., Stuart M.A.C., de Vries R.J., van Aken G.A., de Hoog E.H.A. *Tribology of o/w emulsions under mouth-like conditions: Determinants of friction*. Food Biophysics. 2007; 2(4): 158-71.

(171) Miao S., Mao L. *DSC Applications to Characterizing Food Emulsions* In: Chiavaro E. (ed.). *Differential Scanning Calorimetry*. 1st ed. Boca Raton: CRC Press; 2015. p. 243-72.

(172) Dickinson E. *On the road to understanding and control of creaminess perception in food colloids*. Food Hydrocolloids. 2018; 77: 372-85.

(173) Mitchell J.R., Wolf B. *Relationship between Food Rheology and Perception*. In: Norton I.T., Spyropoulos F., Cox P.W. (eds.). *Practical Food Rheology*. 1st ed. Oxford: Blackwell Publishing Ltd.; 2010. p. 173-92.

(174) Tadros T.F. *Fundamental principles of emulsion rheology and their applications*. Colloids and Surfaces A: Physicochemical and Engineering Aspects. 1994; 91: 39-55.

(175) Fischer P., Windhab E.J. *Rheology of food materials*. Current Opinion in Colloid & Interface Science. 2011; 16(1): 36-40.

(176) Cohen-Addad S., Höhler R. *Rheology of foams and highly concentrated emulsions*. Current Opinion in Colloid & Interface Science. 2014; 19(6): 536-48.

(177) Stokes J.R., Boehm M.W., Baier S.K. *Oral processing, texture and mouthfeel: From rheology to tribology and beyond*. Current Opinion in Colloid & Interface Science. 2013; 18(4): 349-59.

(178) Malone M.E., Appelqvist I.A.M., Norton I.T. *Oral behaviour of food hydrocolloids and emulsions. Part 1. Lubrication and deposition considerations*. Food Hydrocolloids. 2003; 17(6): 763-73.

(179) Stokes J.R. *'Oral' Tribology*. In: Chen J., Engelen L. (eds.). *Food Oral Processing*. 1st ed. Oxford: Blackwell Publishing Ltd.; 2012. p. 265-87.

(180) Sarkar A., Goh K.K.T., Singh H. *Colloidal stability and interactions of milk-protein-stabilized emulsions in an artificial saliva*. Food Hydrocolloids. 2009; 23(5): 1270-8.

(181) Zhang R., Zhang Z., Zhang H., Decker E.A., McClements D.J. *Influence of emulsifier type on gastrointestinal fate of oil-in-water emulsions containing anionic dietary fiber (pectin)*. Food Hydrocolloids. 2015; 45: 175-85.

(182) Dresselhuis D.M., de Hoog E.H.A., Cohen Stuart M.A., Vingerhoeds M.H., van Aken G.A. *The occurrence of in-mouth coalescence of emulsion droplets in relation to perception of fat*. Food Hydrocolloids. 2008; 22(6): 1170-83.

(183) van Aken G.A., de Hoog E.H.A., Vingerhoeds M.H. *19-Oral processing and perception of food emulsions: the relevance for fat reduction in food*. In: McClements D.J., Decker E.A. (eds.). *Designing Functional Foods*. 1st ed. Boca Raton: CRC Press; 2009. p. 481-501.

(184) Noshad M., Mohebbi M., Koocheki A., Shahidi F. *Influence of interfacial engineering on stability of emulsions stabilized with soy protein isolate*. Journal of Dispersion Science and Technology. 2016; 37(1): 56-65.

(185) McClements D.J., Li Y. *Structured emulsion-based delivery systems: Controlling the digestion and release of lipophilic food components*. Advances in Colloid and Interface Science. 2010; 159(2): 213-28.

(186) Sagalowicz L., Leser M.E. *Delivery systems for liquid food products*. Current Opinion in Colloid & Interface Science. 2010; 15(1): 61-72.

(187) Abramov S., Ruppik P., Schuchmann H.P. *Crystallization in emulsions: A thermo-optical method to determine single crystallization events in droplet clusters*. Processes. 2016; 4(3): 25.

(188) McClements D.J., Decker E.A., Park Y., Weiss J. *Structural design principles for delivery of bioactive components in nutraceuticals and functional foods*. Critical Reviews in Food Science and Nutrition. 2009; 49(6): 577-606.

(189) Mao L., Roos Y.H., Biliaderis C.G., Miao S. *Food emulsions as delivery systems for flavor compounds: A review*. Critical Reviews in Food Science and Nutrition. 2017; 57(15): 3173-87.

(190) Jiménez-Colmenero F. *Potential applications of multiple emulsions in the development of healthy and functional foods*. Food Research International. 2013; 52(1): 64-74.

(191) Mao L., Wang D., Liu F., Gao Y. *Emulsion design for the delivery of β-carotene in complex food systems*. Critical Reviews in Food Science and Nutrition. 2018; 58(5): 770-84.

(192) Aditya N.P., Aditya S., Yang H., Kim H.W., Park S.O., Ko S. *Co-delivery of hydrophobic curcumin and hydrophilic catechin by a water-in-oil-in-water double emulsion*. Food Chemistry. 2015; 173: 7-13.

(193) Chong D., Liu X., Ma H., Huang G., Han Y.L., Cui X., et al. *Advances in fabricating double-emulsion droplets and their biomedical applications*. Microfluidics and Nanofluidics. 2015; 19(5): 1071-90.

(194) Callender S.P., Mathews J.A., Kobernyk K., Wettig S.D. *Microemulsion utility in pharmaceuticals: Implications for multi-drug delivery*. International Journal of Pharmaceutics. 2017; 526(1): 425-42.

(195) Lobato-Calleros C., Reyes-Hernández J., Beristain C.I., Hornelas-Uribe Y., Sánchez-García J.E., Vernon-Carter E.J. *Microstructure and texture of white fresh cheese made with canola oil and whey protein concentrate in partial or total replacement of milk fat*. Food Research International. 2007; 40(4): 529-37.

(196) Wilde P.J., Chu B.S. *Interfacial & colloidal aspects of lipid digestion*. Advances in Colloid and Interface Science. 2011; 165(1): 14-22.

(197) Wu X., Zhang L., Zhang X., Zhu Y., Wu Y., Li Y., et al. *Ethyl cellulose nanodispersions as stabilizers for oil in water Pickering emulsions*. Scientific Reports. 2017; 7(1): 12079.

(198) Buttriss J.L., Stokes C.S. *Dietary fibre and health: an overview*. Nutrition Bulletin. 2008; 33(3): 186-200.

(199) Rayner M., Timgren A., Sjöö M., Dejmek P. *Quinoa starch granules: a candidate for stabilising food-grade Pickering emulsions*. Journal of the Science of Food and Agriculture. 2012; 92(9): 1841-7.

(200) Tharanathan R.N. Starch-Value addition by modification. *Critical Reviews in Food Science and Nutrition*. 2005; 45(5): 371-84.

(201) Aykan V., Sezgin E., Guzel-Seydim Z.B. *Use of fat replacers in the production of reduced-calorie vanilla ice cream*. European Journal of Lipid Science and Technology. 2008; 110(6): 516-20.

(202) Rolls E.T., Norton A.B., Lazidis A., Norton I.T., Mills T. *The neuronal encoding of oral fat by the coefficient of sliding friction in the cerebral cortex and amygdala*. Cerebral Cortex. 2018; 28(11): 4080-9.

(203) McClements D.J. *Reduced-fat foods: The complex science of developing diet-based strategies for tackling overweight and obesity*. Advances in Nutrition. 2015; 6(3): 338S-52S.

(204) Chung C., Smith G., Degner B., McClements D.J. *Reduced fat food emulsions: Physicochemical, sensory, and biological aspects*. Critical Reviews in Food Science and Nutrition. 2016; 56(4): 650-85.

(205) Mao Y., Julian McClements D. *Fabrication of reduced fat products by controlled heteroaggregation of oppositely charged lipid droplets*. Journal of Food Science. 2012; 77(5): E144-E52.

(206) Benjamins J., Vingerhoeds M.H., Zoet F.D., de Hoog E.H.A., van Aken G.A. *Partial coalescence as a tool to control sensory perception of emulsions*. Food Hydrocolloids. 2009; 23(1): 102-15.

(207) Lobato-Calleros C., Recillas-Mota M.T., Espinosa-solares T., Alvarez-Ramirez J., Vernon-Carter E.J. *Microstructural and rheological properties of low-fat stirred yoghurts made with skim milk and multiple emulsions*. Journal of Texture Studies. 2009; 40(6): 657-75.

(208) Norton I.T., Cox P.W., Tchuenbou-Magaia F.L., inventors; University of Birmingham, assignee. Low fat food containing gas bubbles (Patent no. WO 2010/067059 Al); 2010.

(209) Chiu N., Hewson L., Yang N., Linforth R., Fisk I. *Controlling salt and aroma perception through the inclusion of air fillers*. LWT - Food Science and Technology. 2015; 63(1): 65-70.

(210) Belloir C., Neiers F., Briand L. *Sweeteners and sweetness enhancers*. Current Opinion in Clinical Nutrition & Metabolic Care. 2017; 20(4): 279-85.

(211) Chiu N., Tarrega A., Parmenter C., Hewson L., Wolf B., Fisk I.D. *Optimisation of octinyl succinic anhydride starch stablised w1/o/w2 emulsions for oral destablisation of encapsulated salt and enhanced saltiness*. Food Hydrocolloids. 2017; 69: 450-8.

(212) Sala G., Stieger M. *Time to first fracture affects sweetness of gels*. Food Hydrocolloids. 2013; 30(1): 73-81.

(213) Mills T., Spyropoulos F., Norton I.T., Bakalis S. *Development of an in-vitro mouth model to quantify salt release from gels*. Food Hydrocolloids. 2011; 25(1): 107-13.

(214) Koliandris A., Lee A., Ferry A.-L., Hill S., Mitchell J. *Relationship between structure of hydrocolloid gels and solutions and flavour release*. Food Hydrocolloids. 2008; 22(4): 623-30.

Chapter 3

On the production of oil-in-water emulsions with varying dispersed phase content using Confined Impinging Jets

The content of this chapter is published as follows:

Tripodi E., Lazidis A., Norton I.T., Spyropoulos F. *On the production of oil-in-water emulsions with varying dispersed phase content using Confined Impinging Jet Mixers*. Industrial & Engineering Chemistry Research. 2019; 58(32): 14859-72.

Abstract

This work reports for the first time on the use of Confined Impinging Jet Mixers (CIJs) for the production of emulsions with dispersed phase content up to 80 wt.%, in both the surfactant-poor and -rich regime, following the exposure to varying CIJs hydrodynamic conditions. It was observed computationally and experimentally that the CIJs capacity resulted strictly dependent on the mass jet flow rate (W_{jet}>176 g/min) and the pre-emulsion droplet size (>10μm). CIJs emulsification performance remained (almost) unaffected by the variation in the oil mass fraction. All systems showed the lowest droplet size (~8μm) and similar droplet size distributions under the highest W_{jet}. Conditionally onto the Tween20 availability, the emulsion $d_{3,2}$ was primarily determined by formulation characteristics in the surfactant poor-regime and by the CIJs energy dissipation rate in the surfactant-rich regime. In conclusion, this study offers further insights into the CIJs suitability as a realistic alternative to already-established emulsification methods.

Keywords

Emulsification

Confined Impinging Jets

High-dispersed phase

Surfactant poor and rich regime

3.1. Introduction

In industrial practice, emulsification processing is commonly conducted within the turbulent regime caused by mixing (high-shear mixing, colloidal milling), pressure (high-pressure homogenisation, microfluidisation) or ultrasound (sonication). The industrial appeal of these methods mainly stems from their capacity to allow continuous and large-throughput processing as well as their flexibility in terms of handling a wide range of materials (1).

It is presently well accepted that eddy formation plays a key part in droplet break-up under turbulence, with the smallest size eddies determining the size of the smallest droplets achievable during emulsification (2). According to the Kolmogorov-Hinze theory (3, 4), the size of these eddies is given by:

$$\lambda_k = \bar{\varepsilon}^{-1/4} \rho_c^{-3/4} \eta_c^{3/4} \qquad (3.1)$$

where λ_k is the Kolmogorov eddy size, $\bar{\varepsilon}$ is the mean energy dissipation rate, and ρ_c and η_c the density and viscosity of the continuous phase, respectively. Eq. 3.1 holds for relatively oil volume fractions up to 40%, while for more concentrated systems (40% < ϕ < 75%), where viscosity may significantly deviate from that of the continuous phase, the η_c term is replaced by the emulsion viscosity (η_{em}) (5). Turbulent emulsification can normally occur in the turbulent inertial (TI) or turbulent viscous (TV) regimes. (5) In the TI regime, droplets deform under the action of hydrodynamic velocity and pressure fluctuations, resulting in droplets that tend to be larger than λ_k. In the TV regime, droplets deform under the action of viscous stresses both inside and between eddies, hence their final size can be smaller than λ_k. Depending on the flow regime, the maximum stable droplet diameter (d_{max}) (6), which is defined as the largest droplet diameter that can resist droplet break-up, can be estimated from:

$$d_{max}^{TI} = \bar{\varepsilon}^{-2/5} \rho_c^{-1/5} \gamma^{3/5} \qquad (3.2)$$

$$d_{max}^{TV} = \bar{\varepsilon}^{-1/2} \eta_c^{-1/2} \gamma \qquad (3.3)$$

$$d_{max}^{TV} = \bar{\varepsilon}^{-1/2} \eta_c^{-1/2} \gamma \qquad (3.3)$$

where γ is the equilibrium interfacial tension.

Besides the hydrodynamic conditions established during emulsification, the final emulsion microstructure (in terms of the average droplet diameter and size distribution) will be also strongly influenced by the presence of surfactants (7). Such surface-active species will tend to quickly adsorb at the oil/water interface, thus lowering the interfacial tension and facilitating droplet break-up, while at the same time (post-adsorption) can assist in hindering coalescence phenomena associated with droplet contacts/collisions. Depending on the extremities of surfactant availability in the system, emulsification can take place under a surfactant-poor or a surfactant-rich regime (8). In the surfactant-poor regime, although turbulence will promote droplet break-up, the resulting, more often partially covered, droplets will tend to merge. On the other hand, the surplus of surface active species in the surfactant-rich regime ensures high adsorption rates and rapid interfacial stabilisation, and thus final droplet size is heavily dependent on droplet disruption due to turbulence.

Despite their widespread industrial utilisation and large product throughput capability, turbulent emulsification methods are still based on high-energy processing, and, as such, they are characterized by inherently low-energy efficiencies (9). In addition, the energy dissipation distribution can be highly non-uniform, very often resulting in larger droplet sizes and/or broader droplet size distributions (10). Such microstructural inconsistences can be partially addressed by repeatedly exposing the system to the original or similar turbulent processing conditions (multi-passing). However, this also results in significant increases in the total energy input and further unavoidable reductions to the overall energy efficiency.

In order to mitigate these limitations, a number of studies have proposed alternative emulsification approaches, such as membrane or microchannel emulsification, where droplet

formation occurs spontaneously rather than as a consequence of turbulence effects (11, 12). Though promising in terms of their much lower energy input and enhanced energy efficiency, these techniques are, at present, limited to bench-scale operation and are faced with a number of challenges to their industrial adoption, including their current incapacity to deliver high product throughputs (13).

Emulsification using Confined Impinging Jet (CIJs) has more recently attracted some attention due to its potential to deliver both large throughputs combined to superior energy efficiencies, if compared to high-energy approaches (14). Under CIJs operation, two jets (either of the two immiscible phases or of the same coarse pre-emulsion) collide at high velocities within a mixing cavity resulting in large energy dissipation rates. Due to the small volume of the mixing chamber, the vast majority of the droplets are exposed to the high-energy dissipation zone, which allows great control over the final emulsion microstructure. On the other hand, the short residence time (~10^{-3} s) within the mixing environment limits droplet collisions and thus coalescence phenomena. The mean energy dissipation rate ($\bar{\varepsilon}_{th}$) created following the jet collision can be theoretically estimated(15) according to:

$$\bar{\varepsilon}_{th} = \frac{\Delta KE + 2\, Q_{jet}\, \Delta P}{\rho V_{CIJs}} \qquad (3.4)$$

where ΔKE is the difference in kinetic energy between the two inlets and the outlet, Q_{jet} is the jet flow rate, ΔP is the pressure at which the jets collide, ρ represents the density of either the pure phase in each jet or of the pre-emulsion, and V_{CIJs} is the volume within the CIJs geometry where impingement takes place.

Originally, CIJs has been extensively studied from both an experimental and computational perspective for the production of nanoparticles due to the fast processing mixing times (14). Transient CFD simulations on the CIJs have been used to find reliable scale-up criteria and describe mixing processes at the microscale (16, 17).

On the other hand, emulsification by using CIJs represents a relatively new topic thus the published literature in this area is somewhat limited. The emulsification performance of CIJs has been compared against that of established emulsification techniques, such as high-shear mixing, high-pressure homogenisation and sonication (18). This work reported that, for significantly low energy inputs and at low oil volume fractions (5-10 vol.%), CIJs produced smaller emulsion droplet sizes than both ultrasound treatment and high-shear mixing. Nevertheless, at energy inputs much higher than those achievable under CIJs operation, sonication and homogenisation both generated emulsions of considerably smaller droplet sizes. In another study (19), the production of dilute emulsions (5 and 10 vol.%) as a function of jet flow rate (up to 610 g/min) and emulsifier type (Tween20, Span80, Whey Protein, Lecithin or Sodium Dodecyl Sulphate, all at a fixed concentration of 1 wt.%) was investigated. Within this range of hydrodynamic conditions, the smallest droplet sizes (~ 2μm) were obtained at the highest jet flow rate (610 g/min) regardless of the type of emulsifier employed. Dilute emulsions of average droplet diameters below 700 nm were reported elsewhere (20), but these could only be produced by coupling CIJs operation with sonication.

It is clear that although the appeal of the CIJs operation has indeed generated some knowledge regarding its processing performance in the field of emulsification, the level of understanding necessary to fully appreciate the method's true potential and possible industrial applicability is far from being achieved.

The aim of the present study is to extend current emulsification understanding associated with CIJs operation. This is obtained by investigating both computationally and experimentally the CIJs emulsification capacity followed by an experimental evaluation of the CIJs performance for the production of emulsions with a wide range of oil mass fractions,

under either a surfactant-poor or a surfactant-rich regime, and as a result of exposure to varying CIJs hydrodynamic conditions and residence times. In all cases emulsions are produced by the CIJs treatment of coarse pre-emulsions, rather than the impingement of jets consisting of the two immiscible pure phases, and product microstructure is assessed in terms of final droplet size, droplet size distribution and long-term stability (over a 40 days storage period).

The current work reports for the first time on the use of CIJs for the production of emulsions with dispersed phase contents above 10 wt.% (and up to 80 wt.%) and relates the achieved microstructures to the hydrodynamic conditions (mean energy dissipation rate and jet mass flow rate) within the geometry; as characterised by both theoretical and computational models.

3.2. Materials and methods

3.2.1. Materials

All oil-in-water (o/w) emulsions were prepared by using as the continuous phase de-ionised water obtained from a reverse osmosis filtration system. Commercial sunflower oil (viscosity= 50 mPa.s) purchased by a local retailer was used as the dispersed phase. Polysorbate20, i.e. Tween20, (Hydrophilic-Lipophilic-Balance, HLB, =16.7, molecular weight =1227.54 g/mol) was supplied by Sigma-Aldrich Company (UK) and used as the emulsifier.

3.2.2. Methods

3.2.2.1. Emulsification procedure

Emulsions were produced following a two-step procedure, which included: *(i)* high-shear mixing to form the initial coarse pre-emulsion followed by *(ii)* emulsification within the CIJs.

3.2.2.1.1. Pre-emulsion preparation

For the preparation of the pre-emulsions, the required concentration of Tween20 was dissolved in water and mixed by using a magnetic stirrer for 10 min, before the addition of the desired amount of sunflower oil. Water, surfactant and vegetable oil (together forming a dispersion of 500 mL) were then pre-emulsified by means of a Silverson L5 Series Laboratory High-Shear Mixer, equipped with an emulsor screen of 33 mm in diameter, for 3 min at defined rotational speeds. Details of the rotational speeds used for the preparation of the pre-emulsions are elucidated within the discussion of the results section.

3.2.2.1.2 Rheological measurements

The flow behaviour of all pre-emulsions was measured using a Kinexus Pro, stress-controlled rheometer (Malvern Instruments, UK). Flow curves for the 10 and 40 wt.% oil content pre-emulsions were obtained using a double gap geometry (with 2 mm gap thickness), while those for the 60 and 80 wt.% systems were obtained using a cone and plate geometry (diameter: 40 mm; and angle: 4º). Each measurement was repeated three times. The average shear viscosity (η) values for the pre-emulsions of varying dispersed (oil) phase content are shown in Figure 3.1 as a function of the applied shear rate ($\dot{\gamma}$). All flow curves were fitted to a simple power-law model (21):

$$\eta = K \cdot \dot{\gamma}^{\,m-1} \qquad (5)$$

where K is the consistency constant and m the power-law index; the values of both are reported in the inset table of Figure 3.1.

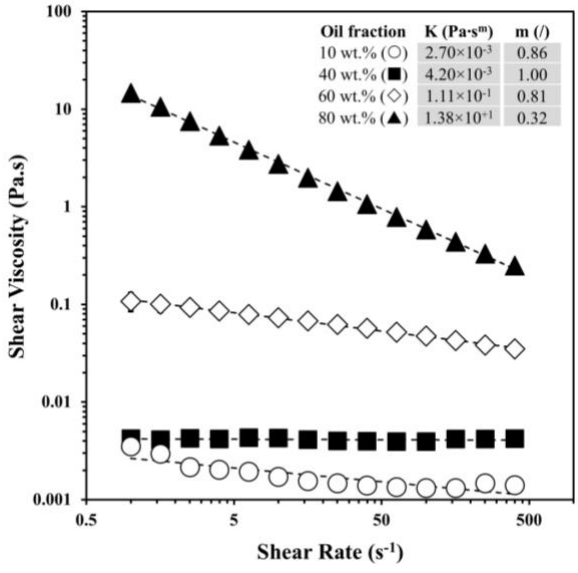

Figure 3.1. Flow curves for the 10 (○), 40 (■), 60 (◇) and 80 wt.% (▲) oil content o/w pre-emulsions formed in the presence of 1 wt.% Tween20. All shear viscosity data points are mean values (n=3) and error bars represent one standard deviation of the mean; where not visible, error bars are smaller than the used symbols. Solid curves represent the best fit to a power-law model (see main text for detail). Inset table: consistency constant K and power-law index m parameters from the power-law model.

3.2.2.1.3. Emulsion preparation

In the second step, the pre-emulsions were processed through the CIJs geometry (Figure 3.2) by means of a single pulse-less micro-pump (external gear pump) with jet mass flow rates varying from 85.2 to 702 g/min. Prior impingement the flow was split into two equal streams by using a Y-junction, whereas after leaving the CIJs chamber emulsions samples were collected and stored in sample pots.

To study the effect of multipassing, emulsions were processed through the CIJs under fixed inlet mass jet flow rate (359 g/min) and were collected in a beaker. This was then transferred back to the feed and the formed emulsion re-processed up to 4 times. Each experiment was repeated twice.

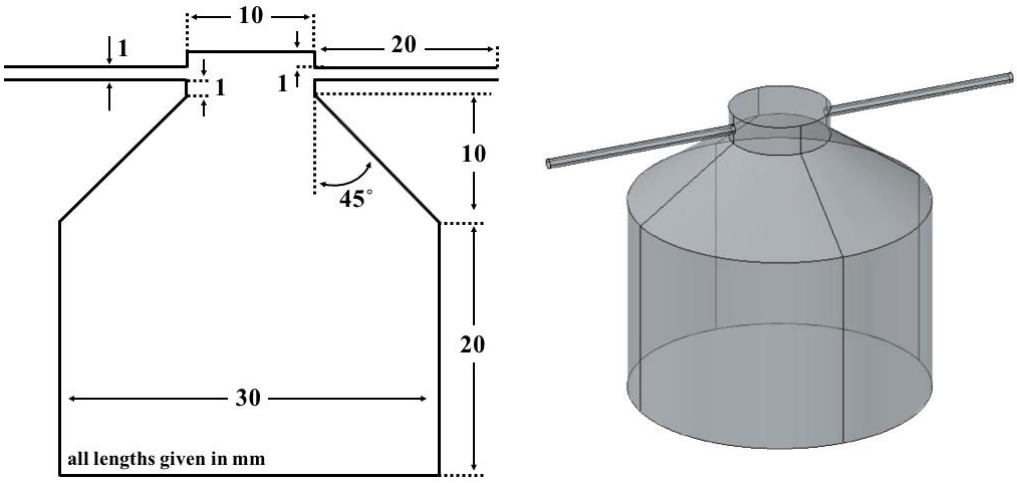

Figure 3.2. Schematic and 3D representation of the CIJs geometry used in this study; all dimensions are given in mm.

3.2.2.2. Droplet size and droplet size measurements

The measurement of droplet size and droplet size distribution were carried out by using a Mastersizer 2000 (Malvern Instruments). Samples were diluted to 3 vol.% in order to avoid multiple-light scattering. Each sample was prepared and tested twice at room temperature (22˚C).

3.2.2.3. Interfacial tension measurements

The equilibrium interfacial tensions were measured using a K11-Force Tensiometer (Krüss, GmbH) equipped with a Wilhelmy plate for *(i)* the plain oil-water interface and *(ii)* at varying concentration of the surfactant. The equilibrium interfacial tension of the plain oil-water interface resulted equal to 24.95 ± 0.02 mN/m whereas by increasing the Tween20 concentration from 0.01 to 2 wt.% the equilibrium interfacial tension decreased from 6.04 ± 0.01 to 5.29 ± 0.02 mN/m, respectively.

3.2.2.4. Stability

In order to evaluate the stability of the processed emulsions, samples were stored in the laboratory at room temperature (22˚C) over a period of 40 days. Since creaming occurred in most of the sample analysed in this study, the samples were gently re-disperse before re-measuring the droplet size.

3.2.2.5. CFD simulations

Commercial Ansys 18 Fluent 18.0 was used to simulate the fluid flow into CIJs. The geometry was modelled using the Design Modeler in the Ansys Workbench and was divided in multiple connected volumes. The grid was generated using a curvature size function; the inlet tubes and the impingement zone were meshed using a Multizone method whereas the rest of the geometry by a sweep method resulting in 2,400,000 hexahedral cells (grid element quality = 0.723 ± 0.159). Information about the velocity and energy dissipation rate profiles at varying jet flow rate was obtained for water (density 998 Kg/m^3 and viscosity 1 mPa.s). CFD simulations of the flow of two pure aqueous streams clearly model a simplified system and thus obviously do not offer insights into many of the key physical phenomena taking place

during emulsification within the CIJs device; e.g. droplet break-up or coalescence mechanisms. However, as the shear viscosity of (at least) the 10 wt.% oil pre-emulsion is relatively close to that of pure water (Figure 3.1), the model does hold some value.

The Large-Eddy-Simulation (LES) model would represent a more suitable method to describe the transient phenomena taking place during mixing but it is also acknowledged to be a highly time intensive solving model (15). Thus, for the purpose of this study the standard k-ε model was used to model the fluid flow. As boundary conditions *(i)* constant inlet velocities for both inlet tubes *(ii)* zero-gauge pressure for the outlet and *(iii)* no wall slip for the walls were specified. The SIMPLE pressure-velocity coupling, the Least Squares Cell Based gradient and second order methods were used. Since the flow inside the geometry is unsteady, a steady-state simulation was initially run to initialise the transient calculation. Three time steps of size varying between 6 to 0.6×10^{-6} s were used. Following this procedure all the residuals fell below 10^{-4}.

The benefit to this study is that both the velocity contours of the simulated flow and the energy dissipation rates achieved within the CIJs geometry can be calculated by the model and then used to (at least qualitatively) firstly assess whether jet impingement does take place and secondly obtain a measure of the magnitude of the turbulence realised in relation to the inlet jet mass flow rate. Figure 3.3 provides an example (for W_{jet} = 702 g/min) of the approach used for the calculation of mean energy dissipation rates ($\bar{\varepsilon}_{CFD}$) along the impingement path of the jets (*x*-axis) from the CFD data. The energy dissipation rate (ε_{CFD}) along the *x*-axis, from the left entry channel to the CIJs chamber (*x* = 0 mm) to the channel on the right (*x* =10 mm), is firstly calculated at three different *y*-positions (*y* = -0.25 mm, *y* = 0 mm and *y* = 0.25 mm) (see Figure 3.3.B). All three energy dissipation rate curves obtained by the simulation (see Figure 3.3.C) exhibit a peak (at an ε_{CFD} value of ~1.8×10^{5} W/Kg)

corresponding to a position on the *x*-axis of 5 mm, thus confirming that the jet impingement point is observed at the centre of the CIJs chamber. $\bar{\varepsilon}_{CFD}$ is then calculated as the average of these three ε_{CFD} curves, corresponding, in this case (W_{jet} = 702 g/min), to be 2.58×10^4 W/Kg.

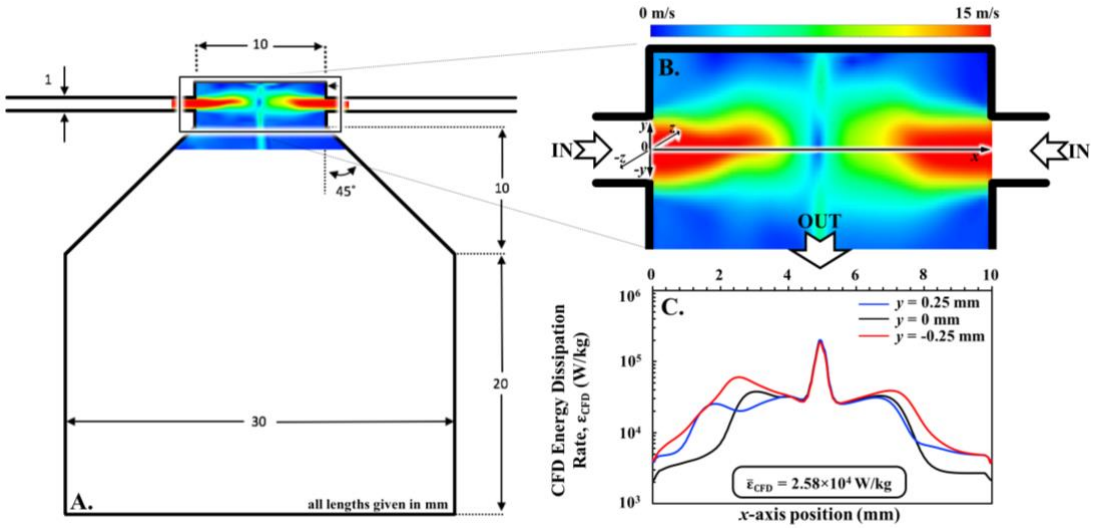

Figure 3.3. A. CFD-obtained velocity contours of the simulated flow and impingement of two aqueous jets (of equal mass flow rates of 702 g/min) within the mixing chamber of the CIJs geometry used in this study. **B.** Enlarged view of velocity contours within the mixing chamber of the CIJs geometry together with the *x*, *y* and *z* axes; the *x*-axis extends from 0 → 10 mm, the *y*-axis from -0.5 mm → 0.5 mm, and the *z*-axis from -0.5 mm → 0.5 mm (*x*, *y*, *z* = 0 as shown in the schematic). **C.** Energy dissipation rate (ε_{CFD}) as a function of position along the *x*-axis and at three different positions on the *y*-axis; *y* = -0.25 mm, *y* = 0 mm and *y* = 0.25 mm. $\bar{\varepsilon}_{CFD}$ (2.58×10^4 W/kg) is calculated as the average of the three ε_{CFD} curves (see main text for further detail).

3.3. Results and discussion

3.3.1. Assessment of CIJs emulsification capacity

In the present study, CIJs emulsification capacity is firstly assessed using a CFD computational approach in order to understand the effect of the inlet jet mass flow rate (W_{jet}) on the hydrodynamic conditions (i.e. energy dissipation rate and velocity profiles) realised within the CIJs geometry (Figure 3.2). The CIJs processing capacity is then further interrogated by investigating the effect of pre-emulsion droplet size and dispersed phase content on the final emulsion microstructure.

3.3.1.1. Modelling of CIJs operation

The resulting relationship between $\bar{\varepsilon}_{CFD}$ and W_{jet} (the latter corresponding to the range of jet mass flow rates investigated experimentally here) is presented in Figure 3.4; velocity contours for selected W_{jet} values are also shown. The velocity profiles clearly suggest that at W_{jet} < 176 g/min, the two jets do not optimally impinge and therefore poor mixing conditions prevail. In addition to this, the CFD data shows that at low W_{jet} values (< 266 g/min) the mean energy dissipation rate is relatively low and only marginally rises with increasing jet mass flow rates (Figure 3.4). However, for W_{jet} values above 266 g/min, $\bar{\varepsilon}_{CFD}$ increases rapidly, reaching a value of 2.58×10^4 W/Kg at the highest jet mass flow rate (702 g/min). The inset plot in Figure 3.4 compares the calculated $\bar{\varepsilon}_{CFD}$ values to the theoretical mean energy dissipation rates ($\bar{\varepsilon}_{th}$) as predicted by eq. 3.4 for a pure aqueous phase. The two mean energy dissipation rates show excellent agreement, with the only exception being the $\bar{\varepsilon}_{CFD}$ values at the lowest jet mass flow rate. Despite this, it is clear that, within the range of W_{jet} values where efficient mixing within the CIJs cavity is to be expected, the CFD simulation can sufficiently estimate the CIJs flow dynamics as predicted by theory.

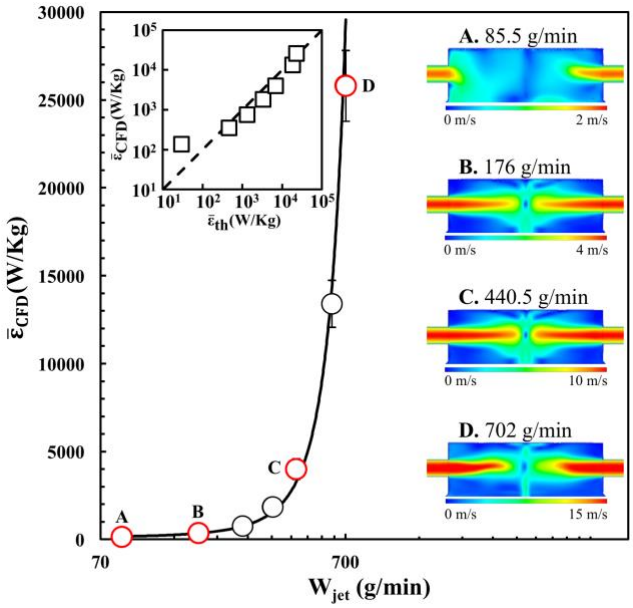

Figure 3.4. Mean energy dissipation rate from the CFD simulations ($\bar{\varepsilon}_{CFD}$) as a function of jet mass flow rate (W_{jet}). $\bar{\varepsilon}_{CFD}$ values are calculated as described in the main text and error bars represent one standard deviation; where not visible, error bars are smaller than the used symbol. Velocity profiles derived from the CFD simulations are also provided as insets for selected W_{jet} values; **A.** 85.5 g/min, **B.** 176 g/min, **C.** 440.5 g/min, and **D.** 702 g/min. Inset graph shows $\bar{\varepsilon}_{CFD}$ against theoretical mean energy dissipation rates ($\bar{\varepsilon}_{th}$; eq. 3.4), across the range of W_{jet} values used in the present study.

The reason for the compromised CIJs operation at low W_{jet} values is suggested to relate to the geometry of the device used here. Compared to CIJs configurations used elsewhere in either experimental or computational studies on CIJs (15-17, 19), the geometry employed here presents a different geometrical design. For the purpose of this investigation, the CIJs cavity was devised with a longer jet-to-jet distance and a larger outlet diameter in an attempt to overcome the backpressure developed during the emulsification of more concentrated emulsions. These differences in the geometry of the devices are potentially responsible for the failure of the jets to collide at the lowest W_{jet} values. Differently, the reduced jet-to-jet distance and narrower outlet of the configurations used elsewhere (15-17, 19) resulted in jet collisions taking place over the entire range of tested jet mass flow rates. Although one must

note that, at higher W_{jet} (≥ 176 g/min), the mixing capacity of the CIJs configuration employed here appears to align with that of the previously used geometry; a peak in the ε_{CFD} profiles at the point of jet impingement as well as a similar exponential rise in $\bar{\varepsilon}_{CFD}$ with increasing W_{jet}, have both been reported in these past studies (15-17, 19).

3.3.1.2. The effect of the pre-emulsion droplet size on the CIJs emulsification capacity

The effect of varying the initial droplet size of the o/w pre-emulsions (possessing either 10 wt.% or 40 wt.% oil mass fractions, respectively) processed through the CIJs configuration on the emulsification capacity of the device (in terms of the average droplet size ($d_{3,2}$) of the corresponding final emulsion produced) is shown in Figure 3.5. The pre-mixing conditions in the used high-shear mixer were chosen in order to obtain pre-emulsions with significantly different initial average droplet sizes, which were then passed through the CIJs device using a range of W_{jet} values (85.5 - 702 g/min). The data presented in Figure 3.5 clearly show that pre-emulsions prepared at 2000 RPM underwent the greatest change in droplet diameter upon CIJs processing. For both the 10 and 40 wt.% oil content pre-emulsions prepared at 2000 RPM ($d_{3,2}$ ~73μm), the original droplet size is initially reduced (at the lowest mass flow rate). As W_{jet} values increase, this droplet size reduction becomes less pronounced only to again sharply increase at higher CIJs mass flow rates. Pre-emulsions prepared at 4000 RPM ($d_{3,2}$~14μm) deviated from this behaviour and changes to the original droplet size were only observed at the highest mass flow rates for both oil contents. In contrast to the last two systems, pre-emulsions prepared at 6000 ($d_{3,2}$~9μm) and 9000 RPM ($d_{3,2}$~6μm) did not undergo any size change throughout the range of W_{jet} values and regardless of the oil mass fraction in the system.

Droplet size distribution (DSD) data confirmed these observations, Figure 3.6 (A-B). The DSD of both the 10 wt.% pre-emulsions prepared at 2000 and 4000 RPM decreased appreciably when processed at the highest W_{jet} (702 g/min), Figure 3.6 (A). On the other hand, insignificant changes in terms of DSD were observed when pre-emulsions prepared at both 6000 and 9000 RPM were processed through the CIJs, Figure 3.6 (B). Analogous trends were also observed for the DSD of 40 wt.% (pre-) emulsions (not shown).

The erratic behaviour observed while processing the pre-emulsions with the largest droplet size (2000 RPM) through the CIJs geometry is hypothesised to relate to the poor mixing conditions and deficient jet impingement that take place at lower W_{jet} and as revealed by the CFD model (Section 3.3.1.1). However, the processing capacity of the CIJs device is not only determined by W_{jet}. The data in Figure 3.5 suggests that the CIJs emulsification potential is also very much dependent on the original droplet size of the to-be-processed pre-emulsion. It appears that a clear threshold value in terms of the pre-emulsion original size ($d_{3,2}$) exists in order for CIJs intervention to be successful; in this case, a $d_{3,2}$ value of ~10 μm. Above this threshold it is possible for CIJs processing to impact and therefore reduce the original pre-emulsion droplet size; providing of course that the used W_{jet} is high enough. Conversely, processing pre-emulsions with droplet sizes lower than this threshold does not lead to any change in the original droplet size regardless of the hydrodynamic conditions (i.e. W_{jet}).

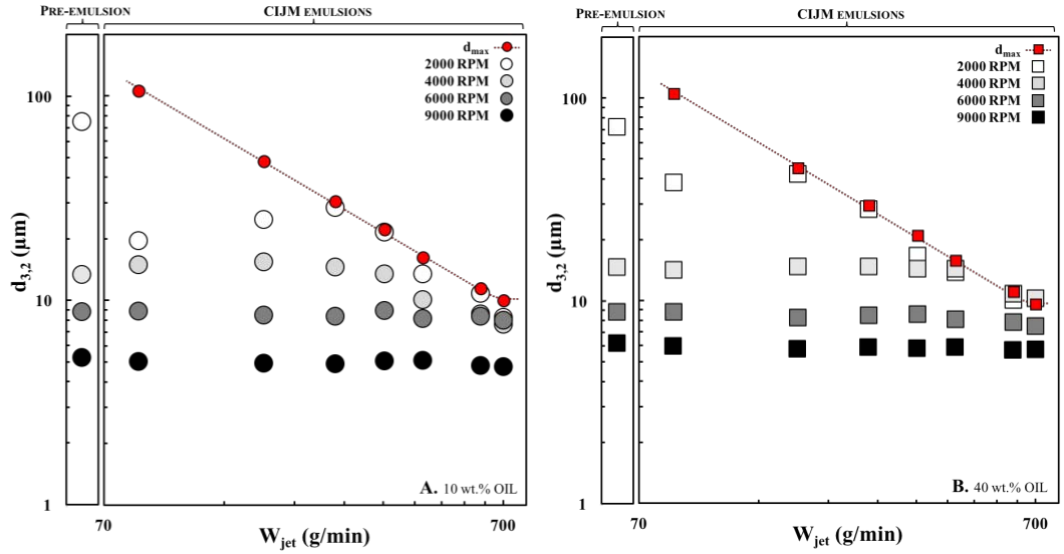

Figure 3.5. Final emulsion Sauter mean diameter ($d_{3,2}$) as a function of jet mass flow rate (W_{jet}), following CIJs processing of pre-emulsions (original droplet sizes for these are also given) in the presence of 1 wt.% Tween20. (**A**) CIJs treatment of 10 wt.% oil mass fraction pre-emulsions prepared using a high shear mixer at 2000 (○), 4000 (●), 6000 (●) and 9000 (●) RPM. (**B**) CIJs treatment of 40 wt.% oil mass fraction pre-emulsions prepared using a high shear mixer at 2000 (□), 4000 (■), 6000 (■) and 9000 (■) RPM. Red full circles (●) and red full squares (■) represent the maximum stable droplet diameter d_{max} (µm) calculated at each corresponding W_{jet} using eq. 3.2 for pre-emulsions of 10 wt.% and 40 wt.% oil mass fractions, respectively; in both cases dotted curves are only shown to guide the reader's eye. All data points are mean values (n=2) and error bars represent one standard deviation of the mean; where not visible, error bars are smaller than the used symbol.

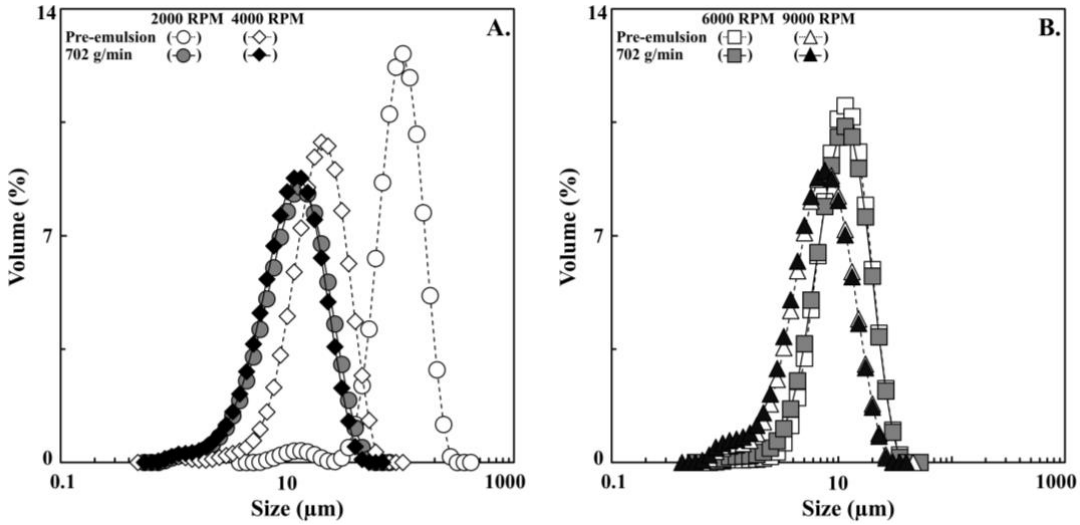

Figure 3.6. Droplet size distributions of 10 wt.% o/w pre-emulsions (empty symbols) prepared using a high shear mixer at 2000 (circles), 4000 (diamonds), 6000 (squares) and 9000 (triangles) RPM and of emulsions (filled symbols) processed through the CIJs at the highest mass jet flow rate, i.e. 702 g/min, in the presence of 1 wt.% of Tween20.

The dependency of both the pre-emulsion droplet size and jet mass flow rate on the CIJs emulsification capacity can also be explained using the concept of maximum stable droplet diameter (d_{max}). Extensively utilised in literature to describe the balance between deforming and restoring forces acting on droplets subjected to turbulent flow, d_{max} is essentially the (mean) maximum droplet diameter that is able to retain a stable size under the imposed hydrodynamic conditions (22). A previous study (23) reports that, during the processing of relatively low viscosity systems, CIJs is expected to operate under Turbulent Inertial (TI) flow regime conditions; this is indeed confirmed in the latter parts of the present work for both the 10 and 40 wt.% oil content systems studied here. d_{max} can be therefore estimated for each jet mass flow rate W_{jet} using eq. 3.2; the calculated d_{max} values are also provided in Figure 3.5.

For both oil content pre-emulsions prepared at 2000 RPM, final emulsion mean droplet sizes ($d_{3,2}$) produced at low jet mass flow rates (W_{jet} < 266 g/min for the 10 wt.% and W_{jet} < 176 g/min for the 40 wt.% oil content systems, respectively) initially assume values smaller than the corresponding d_{max}. However, as W_{jet} is increased further and CIJs is expected to operate under optimal emulsifying conditions, final emulsion $d_{3,2}$ begins to decrease and closely follows the theoretically calculated d_{max}. The onset of the alignment between $d_{3,2}$ and d_{max} for pre-emulsions prepared at 4000 RPM is suppressed and only occurs at high jet mass flow rates ($W_{jet} \geq 352.75$ g/min), regardless of oil content in the system.

Finally, pre-emulsions prepared at 6000 and 9000 RPM pass through the CIJs geometry to give final emulsions of practically unchanged droplet sizes. Thus, these systems, as previously discussed due to their much smaller pre-emulsion droplet sizes, are seemingly unaffected by the induced turbulent conditions and understandably do not exhibit any alignment with any of the corresponding d_{max} values; one could argue that a negligible size reduction can be observed for pre-emulsions produced at 6000 RPM when subjected to the

highest jet mass flow rate (702 g/min), but it is probably more realistic to treat this decrease as both experimentally and statistically insignificant.

Overall, the relation between final emulsion $d_{3,2}$ and theoretical d_{max} appears to support the impact on the CIJs emulsification capacity of both the original pre-emulsion droplet size and jet mass flow rate that was proposed earlier. It is suggested that the close agreement between final emulsion $d_{3,2}$ and theoretical d_{max} is in itself a good indicator of successful CIJs emulsification capacity. In keeping with the preceding discussion on the CIJs emulsification potential, $d_{3,2}$ / d_{max} alignment is only realised for pre-emulsions with droplet sizes similar or greater than the theoretical d_{max} value corresponding to the hydrodynamic conditions produced by the used W_{jet}; providing also that the employed jet mass flow rate is high enough to encourage successful jet impingement that is also associated with an increased energy dissipation rate. The interplay between $d_{3,2}$ and d_{max} is probably better demonstrated in Figure 3.7; where these two droplet dimensions are plotted against one another for systems of varying oil content and pre-emulsion droplet sizes processed through the CIJs device over a range of W_{jet}. The data suggests that when the characteristics of the pre-emulsions (i.e. in terms of oil content and droplet size) and the processing conditions that these are subjected to (i.e. in terms of W_{jet}) are both controlled to allow for the successful emulsification performance of the CIJs geometry, then final emulsion $d_{3,2}$ and d_{max} exhibit a liner dependency ($d_{3,2} = c\ d_{max}$). Since the pioneering study by Sprow (24), the linear relationship between the Sauter and the maximum stable droplet diameters has been extensively reported for a number of conventional emulsification techniques (e.g. high-shear and static mixers, simple agitated tanks, etc.) and the value of parameter *c* has been found to vary between 0.38 and 0.70 (25, 26). In the present study, the slope of the linear dependency between $d_{3,2}$ and d_{max} is found to be 0.86 (± 0.10); this is shown in Figure 3.7 as a solid straight line, with the

shaded area denoting the minimum (c - σ) and maximum (c + σ) slopes, where σ is the standard deviation. It is not clear at this stage why the c value for the CIJs device is higher than in other emulsification techniques or even whether this difference infers to variations in some tangible processing characteristics associated with the operation of the device (compared to that in conventional methods). Nonetheless, it must also be noted that establishing a clear correlation between $d_{3,2}$ and d_{max} may not always be possible, as the dependency may vary randomly and more importantly not always be linear (26).

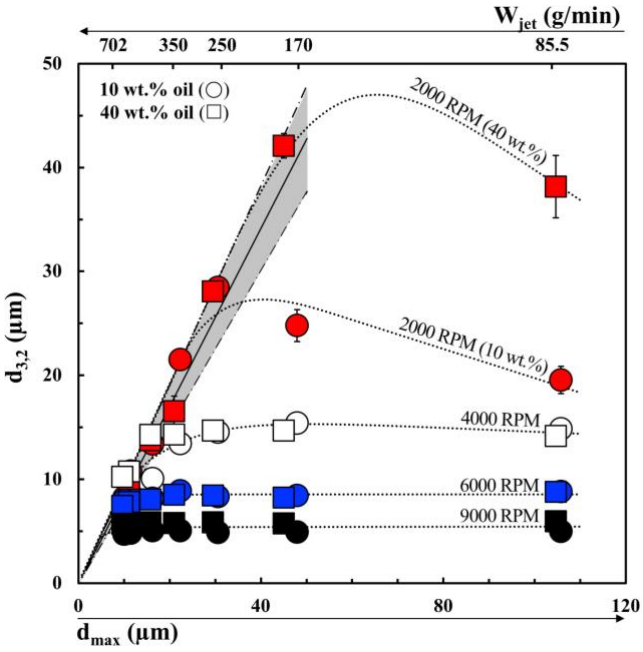

Figure 3.7. Final emulsion Sauter mean diameter ($d_{3,2}$) following CIJs processing of pre-emulsions (initially prepared using the high-shear mixer at RPM values as indicated on the graph) with 10 wt.% (circles) and 40 wt.% (squares) oil mass fractions, respectively, and in the presence of 1 wt.% Tween20, as a function of the maximum stable diameter (d_{max}) and jet flow rate (W_{jet}). Dotted curves are only shown to guide the reader's eye. Solid straight line (and shaded area) denotes a liner dependency between $d_{3,2}$ and dmax (see main text for further detail). All data points are mean values (n=2) and error bars represent one standard deviation of the mean; where not visible, error bars are smaller than the used symbol.

3.3.2. CIJs emulsification performance

Based on the findings of the previous section, in order to evaluate the CIJs emulsification performance for a range of processing and formulation parameters (e.g. hydrodynamic

conditions, dispersed phase mass fractions and concentration of the emulsifier), all pre-emulsions to-be-processed through the CIJs geometry were produced using as mild high-shear mixing conditions as possible. This in order to ensure CIJs performance is not jeopardised by the pre-emulsion droplet size. The 10 and 40 wt.% oil pre-emulsions were prepared (as previously) in the high-shear mixer at 2000 RPM (for 3 minutes), whereas for the more concentrated systems, both 60 and 80 wt.%, slightly more intense mixing was required (3500 RPM for 3 minutes) to obtain a well-dispersed system; processing the latter more concentrated systems at 2000 RPM resulted in rapid phase separation which took place prior to commencing CIJs processing. As a result, the 10 and 40 wt.% pre-emulsions had a similar average droplet size (75 µm and 72 µm, respectively), while the 60 and 80 wt.% systems possessed initial droplet sizes of 52 µm and 28 µm, respectively, Figure 3.5; in all cases pre-emulsion droplet size was maintained above the threshold of ~10 µm (see previous section).

3.3.2.1 Effect of oil mass fraction

The Sauter diameters, $d_{3,2}$, of the final emulsions produced by processing pre-emulsions containing a wide range of dispersed phase mass fractions (10-80 wt.%) through the CIJs device at varying jet mass flow rates, W_{jet}, are presented in Figure 3.8. Overall, the behaviour of systems with varying dispersed phase mass fractions upon CIJs processing was very similar. At low W_{jet}, final emulsion droplet size was initially decreased, with this reduction becoming less evident at slightly higher mass flow rates (176 g/min), but eventually increasing to give a more abrupt reduction in $d_{3,2}$ once W_{jet} became high enough (W_{jet} > 266 g/min). The latter range of jet mass flow rates was previously identified to correspond to optimal CIJs operation, and under the hydrodynamic conditions imposed in this case the progressive increase in the dispersed phase mass fraction from 10 to 60 wt.% content did not

result in significant variations in the Sauter diameters of the final emulsions. The 80 wt.% oil content emulsion exhibited lower final droplet sizes than the other systems, with these differences becoming less pronounced at higher W_{jet} (≥ 615 g/min), where all systems exhibited similar droplet sizes (~7-9 µm) regardless of dispersed phase fraction.

The pre-emulsion DSDs maintained their monodisperse characteristics when processed through the CIJs for all the dispersed phase mass fractions, Figure 3.9 (A-B). Regardless on both the monodispersity of the pre-emulsions and the oil content, all systems showed a similar DSD when processed under the highest CIJs hydrodynamic conditions.

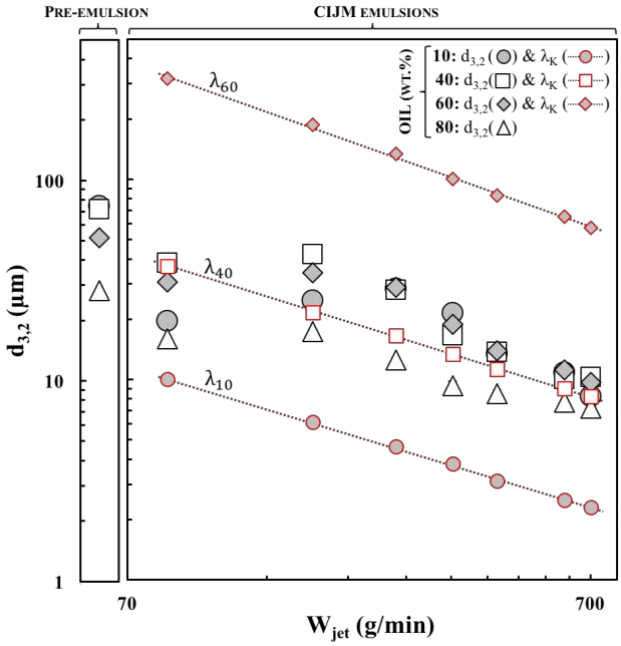

Figure 3.8. Final emulsion Sauter mean diameter ($d_{3,2}$) as a function of jet mass flow rate (W_{jet}), following CIJs processing of pre-emulsions (original droplet sizes for these are also given) with 10 (●), 40 (□), 60 (◆) and 80 (Δ) wt.% oil content and in the presence of 1 wt.% Tween20. Red outline symbols represent the theoretical Kolmogorov eddy sizes (λ_k; eq. 3.1) corresponding to the characteristics of the 10, 40 and 60 wt.% dispersed phase mass fraction systems. Dotted lines are only shown to guide the reader's eye. All data points are mean values (n=2) and error bars represent one standard deviation of the mean; where not visible, error bars are smaller than the used symbols.

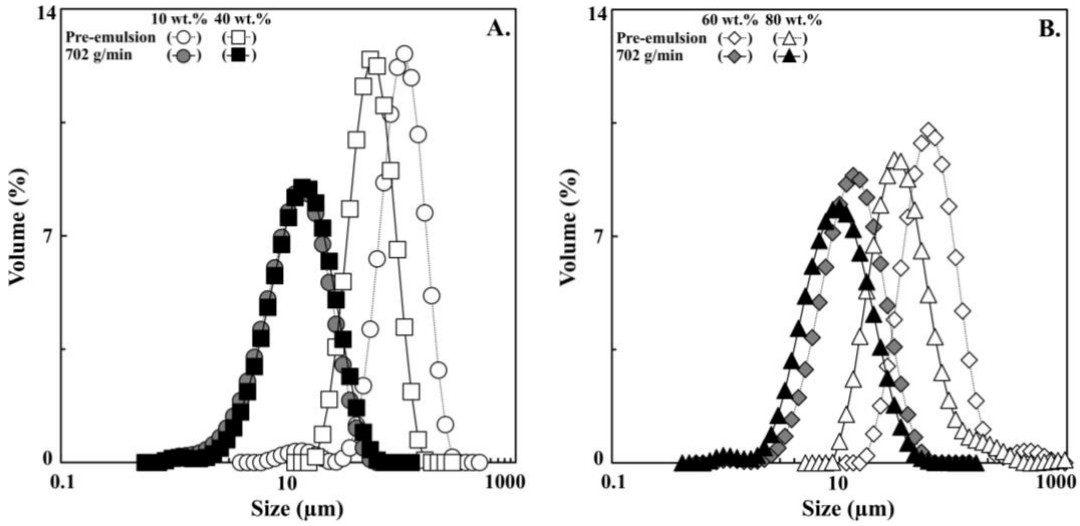

Figure 3.9. Droplet size distributions of o/w pre-emulsions (empty symbols) and emulsions (filled symbols) processed through the CIJs at the highest mass jet flow rate, i.e. 702 g/min, with 10 (circles), 40 (squares), 60 (diamonds) and 80 (triangles) wt.% as the oil content in the presence of 1 wt.% of Tween20.

At constant energy input and emulsifier content, emulsion droplet size should be expected to increase with higher dispersed phase mass fractions due to (amongst others): a potential increase in the frequency of droplets collisions and thus higher rates of coalescence; the increased viscosity, which hinders droplet break-up; the increase in total interfacial area and the subsequently increased likelihood of a reduction in emulsifier interfacial adsorption rates (27, 28). This dependency has been indeed observed in conventional emulsification processes; for example, high-pressure homogenisation was reported (29) to produce emulsions (at a constant surfactant concentration) with consistently larger droplet sizes as the dispersed phase mass fraction was increased from 10 to 50 wt.% and throughout the range of homogenisation pressures used. However, previous studies on CIJs reported (19) that, under fully turbulent conditions, the hydrodynamic environment established within the CIJs geometry was able to produce emulsions of similar droplet sizes independently from either the type of surfactant or dispersed phase volume fraction used; albeit the latter was not greatly varied (5 and 10 vv.%).

Although this aligns with the minimal effect of oil content observed here for systems of up to 60 wt.% oil, it does not support the behaviour exhibited by the 80 wt.% dispersed phase emulsions. One could argue that the lower final emulsion $d_{3,2}$ value of the 80 wt.% oil content system is due to the fact that the pre-emulsion droplet size for these systems was lower as well. It is proposed that this is not the case and that the observed droplet size reduction is instead due to a change in the turbulent flow regime, which has been previously reported to take place as a result of increasing the dispersed phase mass fraction (6). In highly-concentrated systems (ϕ > 75%), droplet disruption does not take place due to turbulence, which is mostly suppressed because of the large number of droplets; this has also been observed for lower fraction systems (up to 15 wt.%), which however possess much smaller droplet sizes (~200 nm), to again give a large overall number of droplets (30). Alternatively droplet break-up in this case tends to be driven by hydrodynamic interactions between neighbouring droplets (5).

In order to determine whether a transition from a TI regime to a TV regime takes place for the systems studied here, the $d_{3,2}$ values of all emulsions up to an oil content of 60 wt.% were compared with theoretically calculated Kolmogorov eddy size, λ_k, (estimated by eq. 3.1) (Figure 3.8); the λ_k value corresponding to the 80 wt.% oil systems cannot be calculated by eq. 3.1 since at such high dispersed phase contents, turbulence is mostly suppressed by the presence of a high population of droplets (5, 31). The data presented in Figure 3.8 confirms that such a flow transition occurs; in fact proposing that it takes place as the oil content of the emulsions is increased from 40 to 60 wt.%. In a previous study utilising two conventional rotor-stator emulsification methods, a transition from TI to TV regime was also detected at dispersed phase mass fractions between 40 and 60 wt.% (5). However, literature also suggests that emulsion droplets generated under TV conditions would be typically expected to have

smaller droplet sizes compared to those produced in a TI regime (32), a hypothesis that is not supported here. A possible explanation for this lays in the dual contribution that an increase in emulsion viscosity (or in our case an increase in dispersed phase mass fraction) has on both d_{max} and λ_k. As emulsion viscosity is raised, d_{max} (as established during emulsification within a TV-regime; eq. 3.3) is reduced, thus favouring droplet fragmentation. On the other hand, the same viscosity increase will also suppress the formation of small eddies (eq. 3.1) and as a consequence the minimum (lower limit) droplet size that can be formed is elevated. Either of these two scenarios will prevail when flow conditions (TI or TV regime) are fully established. However, for the systems studied here, these two opposite effects appear to offset one another, thus leading to similar droplet sizes between the systems of low to moderate (10 and 40 wt.%; TI regime) and high (60 wt.%; TV regime) dispersed phase contents. This potentially also denotes that although a transition from a TI to TV regime does take place within the dispersed phase mass fraction range from 40 to 60 wt.%, the latter (TV) turbulent flow is probably not yet fully established at the 60 wt.% oil content.

The interplay between emulsion dispersed phase content and the CIJs hydrodynamic conditions was explored further by recirculating all systems (formed after one pass) through the device for a total of 4 passes. As such, the time that each system experiences the hydrodynamic conditions imposed within the CIJs geometry is extended without changes to the jet mass flow rate, which in this case was fixed at 352.75 g/min; this W_{jet} value is within the previously determined optimum CIJs emulsification performance range, but at the same time not too high to overshadow any effects arising as a result of dispersed phase content. The Sauter diameters of the final emulsions produced following multiple passes through the CIJs geometry are presented in Figure 3.10.

The obtained data show that both the 10 and 40 wt.% dispersed phase emulsions reach a minimum droplet size after the second pass through the geometry and, despite their different oil content, they both maintain similar $d_{3,2}$ values. However, the average droplet sizes for the 60 and 80 wt.% oil content emulsions still decrease up to the third pass; both systems also display smaller $d_{3,2}$ values in comparison to the less concentrated systems (10 and 40 wt.% dispersed phase). These results confirm that emulsions formed under a TV regime (60 wt.% oil content) or in the presence of a significantly high population of droplets (80 wt.% oil content), will possess smaller droplets than those generated under TI conditions (10 and 40 wt.% oil content) even though the processing conditions used in either case are indeed similar (6). Therefore, it is also suggested that although the transition from a TI to a TV-regime (between 40 and 60 wt.% dispersed phase) is perhaps not fully realised after a single pass through the CIJs geometry (see earlier discussion), increasing the residence time of the 60 wt.% oil content within the high energy dissipation zone of the device assists in fully establishing the Turbulent-Viscous flow regime conditions.

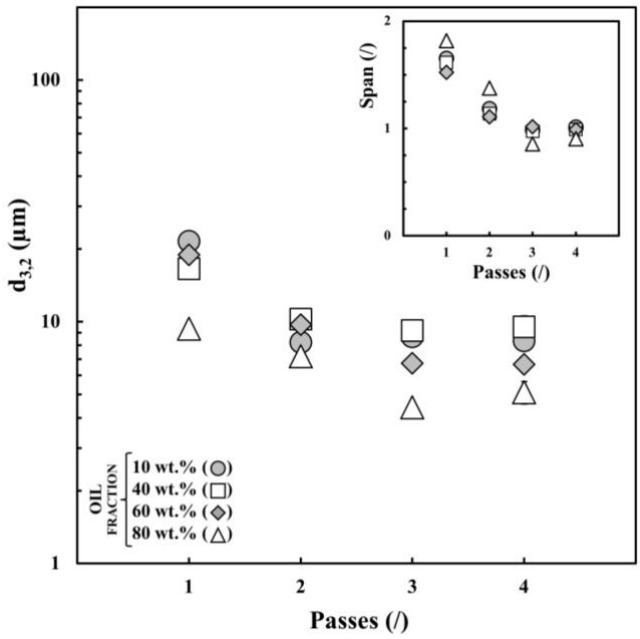

Figure 3.10. Sauter diameter ($d_{3,2}$) and span values (inset graph) of emulsions (in the presence of 1 wt.% Tween20) with varying oil content as a function of the number of passes through the CIJs geometry at a fixed jet flow rate of 352.75 g/min. All data points are mean values (n=2) and error bars represent one standard deviation of the mean; where not visible, error bars are smaller than the used symbols.

CIJs recirculation was also found to impact on the droplet size distribution of the emulsions, Figure 3.11 (A-B); perhaps to a more significant extent than the effect that multi-passing had on emulsion average droplet size.

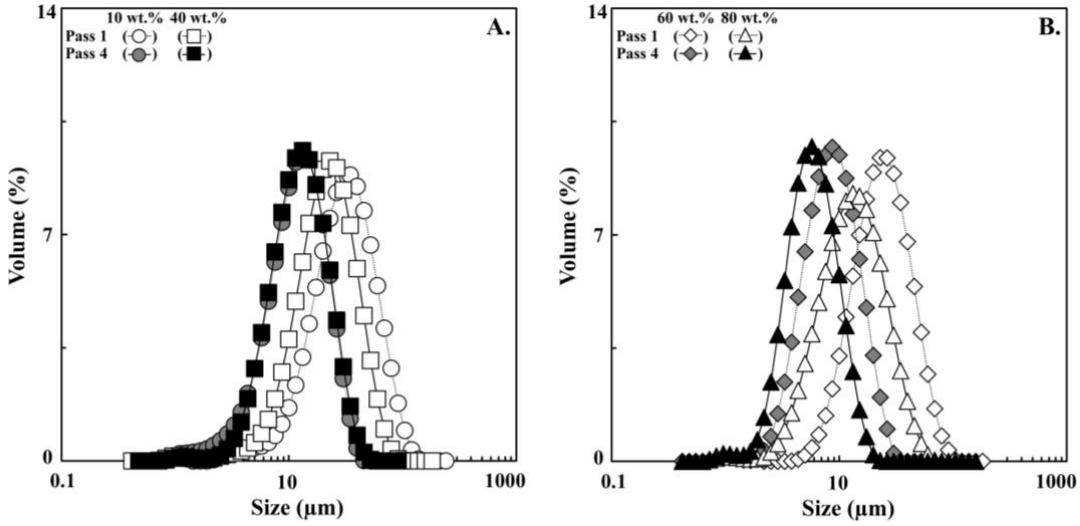

Figure 3.11. Droplet size distributions of o/w emulsions in the presence of 1 wt.% of Tween20 at varying oil content as a function of the number of passes through the CIJs geometry at a fixed flow rate of 352 g/min.

Regardless of dispersed phase mass fraction and number of passes, the droplet size distributions for all systems remained monomodal; the span values for these as a function of the number of passes through the CIJs geometry are presented in Figure 3.10. Independent from the oil mass fraction, all size distributions became narrower, exhibiting a reduction in the initial span of 1.4 – 1.6 (first pass) to values in the range of 0.8 – 1 (after the third pass); negligible or no changes were observed after the fourth pass. The effect of extending the residence time within the CIJs processing environment has been previously studied for emulsions of much lower dispersed phase contents (up to a volume fraction of 0.1) (19). Similarly to the findings reported here, the past study concluded that the major emulsion microstructure change occurring during multipassing is the narrowing of the droplet size distribution and that the average droplet size is only mildly influenced by the number of passes. This behaviour has also been reported by studies evaluating the emulsification performance during high-pressure homogenisation and microfluidisation, where in both cases the droplet size distribution (rather than droplet size) was primarily affected by recirculation (33, 34).

3.3.2.2 Effect of surfactant concentration

The effect of surfactant (Tween20) concentration on the Sauter diameter, $d_{3,2}$, of emulsions possessing a range of oil mass fractions (10 - 80 wt.%) and produced within the CIJs device under varying hydrodynamic conditions (in this case represented by the theoretical mean energy dissipation rate, $\bar{\varepsilon}_{th}$) is shown in Figure 3.12. Surfactant concentrations of 0.01, 0.1, 1, and 2 wt.%, were used for the preparation of all systems, however emulsions with a higher dispersed phase content (60 and 80 wt.%) at the lower Tween20 concentrations (0.01 and 0.1 wt.%) phase separated almost immediately following pre-mixing (pre-emulsion formation)

and CIJs processing in this case was not possible. All other pre-emulsions were stable enough to pass through the CIJs geometry and final emulsion $d_{3,2}$ values, regardless of oil content or surfactant concentration, exhibited overall the same dependency (see Figure 3.12) on hydrodynamic conditions as discussed earlier (e.g. Figure 3.8); i.e. emulsification performance is shown to be jeopardised at low jet mass flow rates (or similarly here at low $\bar{\varepsilon}_{th}$) and the onset of optimum CIJs operation is only achieved once this is appropriately increased. The range where successful CIJs emulsification performance is expected to be realised corresponds to the shaded area(s) also shown in Figure 3.12. The discussion in this section will only focus on emulsions produced within this optimal CIJs processing window.

Emulsion $d_{3,2}$ dependency on Tween20 concentration within the CIJs optimal processing region is firstly evaluated at two fixed but dissimilar $\bar{\varepsilon}_{th}$ values representing the low energy dissipation rate at the onset of the CIJs optimal operating conditions ($\bar{\varepsilon}_{th}^{L}$) and the highest energy dissipation rate ($\bar{\varepsilon}_{th}^{H}$) employed. Due to the stability issues exhibited by the 60 and 80 wt.% oil content systems at the lower Tween20 concentrations, the aforementioned analysis is only meaningful for the 10 and 40 wt.% dispersed phase emulsions; the behaviour of the latter systems is shown in the inset graphs of Figure 3.12 (A) and (B), respectively.

The droplet size of the 10 wt.% o/w emulsions is reduced from approximately 30μm to a minimum value of ~10μm, independently from the amount of surfactant in the system (Figure 3.12.A). As also shown by the data in the inset graph, varying the surfactant concentration in systems produced under fixed, either mild ($\bar{\varepsilon}_{th}^{L}$) or fully ($\bar{\varepsilon}_{th}^{H}$) turbulent, hydrodynamic conditions does not result in emulsions with considerably different droplet sizes. For the 40 wt.% systems, differences in emulsion droplet size for varying surfactant contents were more evident (Figure 3.12.B). The lowest Tween20 concentration (0.01 wt.%) was clearly shown to result in the highest droplet sizes, while all other formulations (0.1 to 2 wt.%) all culminated

in similar $d_{3,2}$ values independently from $\bar{\varepsilon}_{th}$. The extent of the difference in the droplet sizes between these two sub-groups became progressively more marked as the energy dissipation rate was increased (Figure 3.12.B). While at $\bar{\varepsilon}_{th}^{L}$ emulsion droplet sizes remain practically unaffected by variations in the amount of Tween20, at $\bar{\varepsilon}_{th}^{H}$ the Sauter diameter of the systems decreases from ~20μm (at a Tween20 concentration of 0.01 wt.%) to a plateau value of ~10 μm (for a surfactant content greater or equal to 0.1 wt.% of Tween20). Finally, the dependency of $d_{3,2}$ on $\bar{\varepsilon}_{th}$ for both the 60 and 80 wt.% systems containing either a 1 or 2 wt.% surfactant concentration, is shown in Figure 3.12.C. Whereas this Tween20 concentration variation results in negligible changes to the droplet sizes of the 60 wt.% o/w emulsions, the same surfactant increase in the 80 wt.% oil content systems produced droplets of consistently smaller $d_{3,2}$ values over the entire range of $\bar{\varepsilon}_{th}$.

Overall, it appears that the capacity of the CIJs device to reduce the size of emulsion droplets is heavily affected by surfactant availability; which, within the context of the present discussion, is essentially the surfactant concentration relative to the dispersed phase content. CIJs processing of formulations where surfactant availability is low, will produce emulsions with a final droplet size that, although affected by the mixing conditions imposed, is primarily driven by surfactant concentration and dispersed phase content; i.e. formulation rather than processing characteristics. Conversely, CIJs treatment of formulations of high surfactant availability, will produce emulsions with droplet sizes that are predominantly governed by the hydrodynamic conditions established during processing and only marginally depend on formulation attributes.

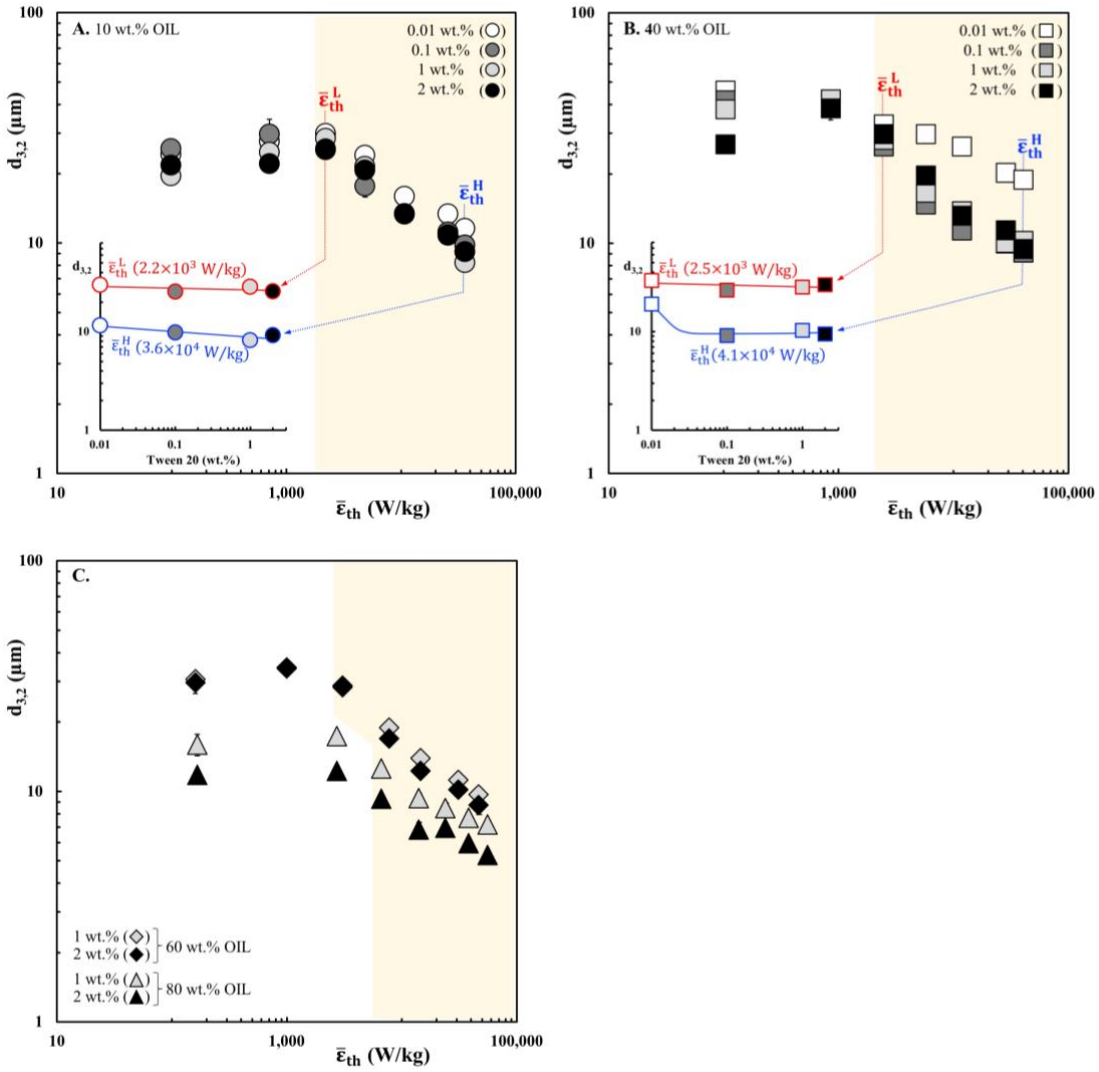

Figure 3.12. Final emulsion Sauter mean diameter ($d_{3,2}$) as a function of the theoretical mean energy dissipation rate ($\bar{\varepsilon}_{th}$; eq. 3.4) following a single pass during CIJs processing of pre-emulsions with of 10 wt.% (A), 40 wt.% (B), 60 wt.% or 80 wt.% (C) oil mass fractions in the presence of Tween20 concentrations ranging from 0.01 to 2 wt.%. Inset graphs in (A) and (B) show the dependency of final $d_{3,2}$ on Tween20 concentration at fixed low ($\bar{\varepsilon}_{th}^{L}$) and high ($\bar{\varepsilon}_{th}^{H}$) mean energy dissipation rates (see main text for further detail). In the three charts, the highlighted area represents the region of optimal CIJs processing conditions, determined as explained in Section 3.3.1. All data points are mean values (n=2) and error bars represent one standard deviation of the mean; where not visible, error bars are smaller than the used symbols.

The existence of these surfactant-poor and surfactant-rich regimes has been previously reported for conventional emulsification turbulent processing (high shear mixing, homogenisation, microfluidisation), both when either the two oil and aqueous immiscible

phases or a pre-emulsion are treated, and for a range of species offering interfacial stabilisation (surfactants, proteins and particles) (35-38). In all cases two well-defined regimes have been observed in terms of the dependence of $d_{3,2}$ on surfactant/emulsifier concentration; at low concentrations, emulsion droplet size is highly sensitive to the amount of surfactant/emulsifier present in the system and it relates to the extent of droplet coalescence events, while at high concentrations $d_{3,2}$ is practically independent of surfactant/emulsifier content and is mostly determined by the degree of drop breakup as imposed by processing conditions (35, 36, 38). Increasing the dispersed (oil) phase fraction in the system is suggested to affect droplet size behaviour in both the surfactant-poor and surfactant-rich regimes in two ways. Increasing oil content will accelerate coalescence events, because of the subsequent increase in the frequency of droplet collisions, and thus droplet size is expected to also increase (30, 34). However, at higher dispersed phase fractions, the effective viscosity of the emulsion is also increased and consequently, as turbulent intensity is reduced, coalescence efficiency and therefore the rate of coalescence events would tend to decrease (30).

In an attempt to further explore the dependency of dispersed phase content on emulsion droplet size, the $d_{3,2}$ values achieved within the optimal CIJs processing window (shaded region in the main plots of Figure 3.12) are presented in Figure 3.13 in terms of fractional droplet size reduction ($d_{3,2}/d_o$). The $d_{3,2}/d_o$ quantity is the ratio of the droplet size achieved for a given system produced under a specific $\bar{\varepsilon}_{th}$ value ($d_{3,2}$) over the droplet size of the same system but as realised following processing at the low energy dissipation rate ($\bar{\varepsilon}_{th}^{L}$) at the onset of the CIJs optimal operating conditions (d_o). $d_{3,2}/d_o$ is a useful measure of the CIJs emulsification performance as, rather than assessing emulsion formation in terms of achieved droplet size, it evaluates the droplet reduction capacity of the device with reference to the droplet size initially obtained upon processing under the mildest operating conditions that still

fall within the pre-determined optimal operation of the CIJs geometry. Droplet size data for all emulsions are in this way effectively 'normalised' and thus can be cross-compared regardless of their dispersed phase or surfactant content. Assessing the interplay between $d_{3,2}/d_o$ and $\bar{\varepsilon}_{th}$ confirms the occurrence of the surfactant-poor and surfactant-rich regimes discussed earlier (Figure 3.13). The data forms two clusters of behaviour that correspond to either a surfactant-poor or surfactant-rich regime, with both groups exhibiting a power law dependency with $\bar{\varepsilon}_{th}$; data within the two clusters where fitted to a simple power law model ($\frac{d_{3,2}}{d_o} = K \cdot \bar{\varepsilon}_{th}^{b}$), with values for the exponents b and for R^2 also given (Figure 3.13). Analysis of the data in Figure 3.13 further reveals that, in terms of emulsion droplet size reduction capacity, CIJs processing is practically independent from the dispersed phase content in the systems. This suggests that, although these systems do possess droplet sizes that are determined by both processing attributes and formulation-specific characteristics, the rate of droplet size reduction achieved within the CIJs device as a function of the generated energy dissipation rate $\bar{\varepsilon}_{th}$ is unaffected by either of the dispersed phase or surfactant content alone, but instead is primarily driven by surfactant availability, as jointly determined by both these quantities.

.

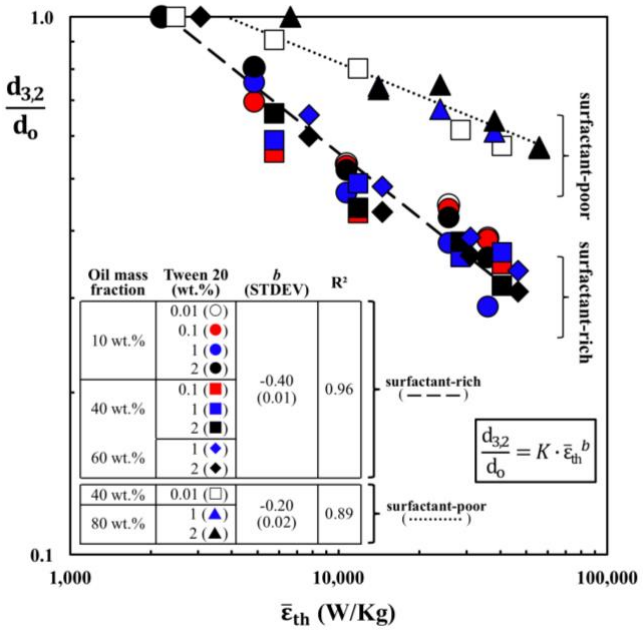

Figure 3.13. Fractional droplet size reduction ($d_{3,2}/d_o$) as a function of the mean energy dissipation rate ($\bar{\varepsilon}_{th}$) realised during CIJs processing of pre-emulsions with varying dispersed phase and surfactant (Tween20) content (detail on both these is given on the graph). Lines shown are the best fit of the two data clusters to a simple power law model (see main text for further detail). The inset table provides detail about the quality of the fit to the power law model.

3.3.2.3. Long-term emulsion stability

The long-term stability of emulsions with a range of surfactant concentrations (0.01 – 2 wt.%) and dispersed phase mass fractions (10 – 80 wt.%) produced using the CIJs device was evaluated over a period of 40 days. All systems were produced at a fixed jet mass flow rate of 352.75 g/min, which is within the previously determined optimum CIJs emulsification performance range, and were stored at room temperature (22˚C) over a period of 40 days. The Sauter mean diameters for systems of increasing dispersed phase content both immediately after CIJs processing and following the 40 days storage period are presented in Figure 3.14 as a function of surfactant concentration. Selected droplet size distribution curves at both time

intervals for emulsions stabilised by 2 wt.% of Tween20 and for each of the oil mass fractions studied here are also provided as insets to the main graphs.

The $d_{3,2}$ data for the 10 wt.% oil content emulsions (Figure 3.14.A) clearly demonstrates that the droplet size of these systems remained (within experimental error) unchanged during storage regardless of the surfactant concentration used. The inset graph in Figure 3.14.A further confirms the high stability of these systems over the 40 days storage period. As the dispersed phase content is increased to 40 wt.% (Figure 3.14.B), emulsion stability becomes dependent on surfactant content. Emulsions with the lowest surfactant content (0.01 wt.% Tween20) phase separated during storage, while systems with 0.1 wt.% Tween20 exhibited an increase in droplet size (from 14.7 μm to 29.1 μm) during storage. Therefore, although the latter systems retained an emulsion microstructure, the occurrence of coalescence during storage was not avoided and their stability was jeopardised. However, formulations with higher surfactant concentrations (1 – 2wt.%) were stable throughout the storage period (Figure 3.14.B). Finally, emulsions of either 60 or 80 wt.% oil mass fractions exhibited the same stability behaviour during storage (Figure 3.14.C-D). Although as previously mentioned, CIJs processing of emulsions at these dispersed phase fractions was not achievable at the lower surfactant concentrations (0.01 wt.% and 0.1 wt.% Tween20), increasing the surfactant content (≥1 wt.%) resulted in practically unchanged mean droplet sizes and droplet size distribution curves during storage.

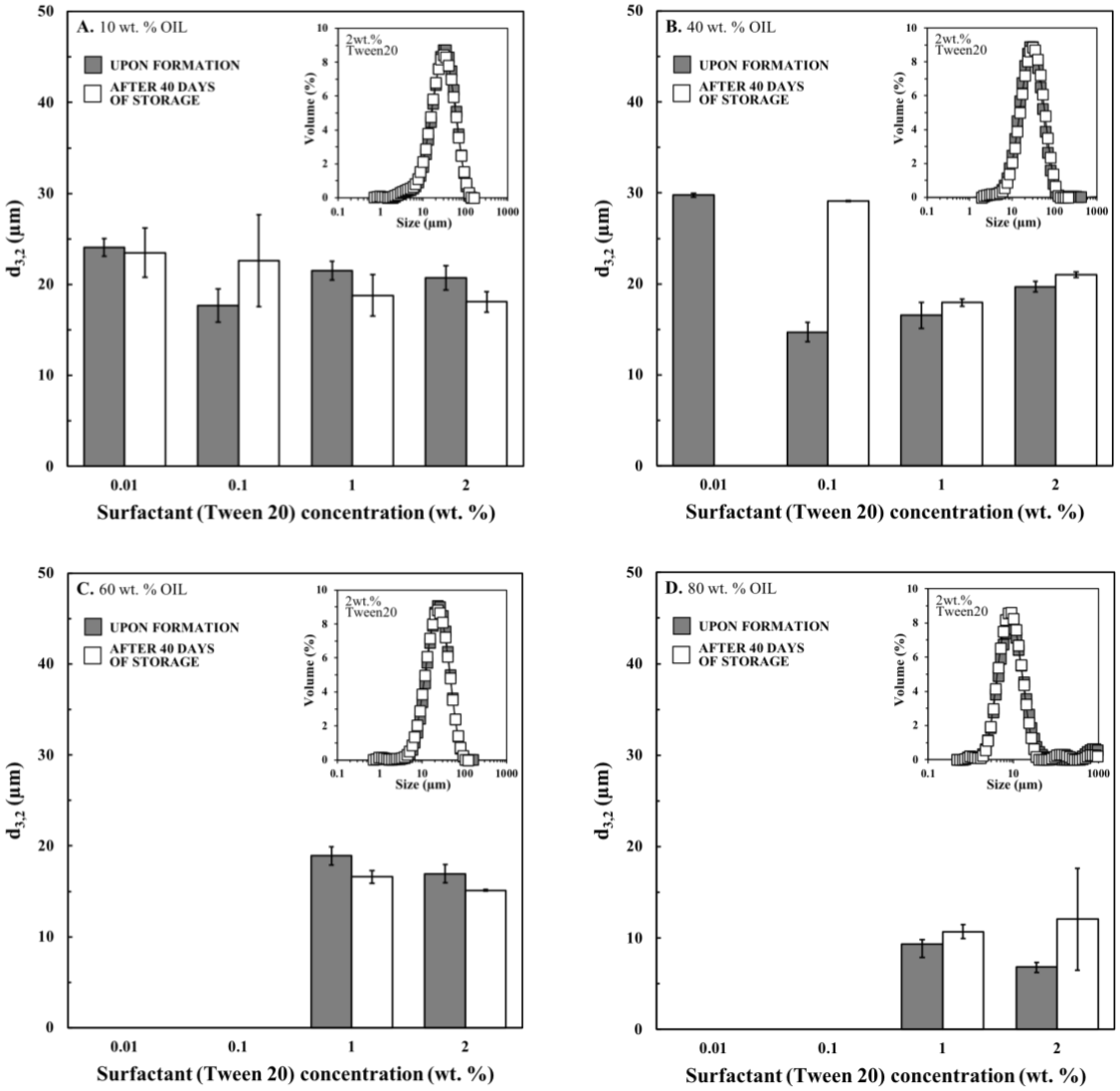

Figure 3.14. Long-term stability of emulsions with 10 (A), 40 (B), 60 (C) and 80 wt.% (D) produced in the CIJs geometry (at a fixed jet mass flow rate of 352.75 g/min) as a function of surfactant (Tween20) concentration; solid (grey) and open bars represent Sauter mean diameters ($d_{3,2}$) immediately after CIJs processing and following a storage period of 40 days at room temperature (22˚C), respectively. All data points are mean values (n=2) and error bars represent one standard deviation of the mean. Inset graphs present the droplet size distribution of each system (for a corresponding dispersed phase fraction) stabilised by 2 wt.% of Tween20, immediately after CIJs processing (solid grey symbols) and following a storage period of 40 days at room temperature, i.e. 22˚C, (open symbols).

It is worth noting that the behaviour discussed earlier in terms of surfactant availability and droplet size reduction capacity does not fully coincide with observations made with regards to

stability under storage. It might have been expected that systems generated within the surfactant-poor regime would also exhibit poor emulsion stability, while those formed under a surfactant-rich environment would display long-term stability. Although this is indeed the case for the majority of the systems, there are outliers to this behaviour. The 40 wt.% oil mass content emulsion with a 0.1 wt.% Tween20 concentration was previously suggested to arise from CIJs processing within the surfactant-rich regime, however the long-term stability of this system is shown here to be compromised. Conversely, even though the 80 wt.% oil mass fraction emulsions with either 1 or 2 wt.% Tween20 concentrations were proposed to be formed within a surfactant-poor regime, both systems remained stable over the tested storage period. The link between surfactant availability during emulsion formation and consequent long-term stability is therefore much more complex. This equally implies that the surfactant-rich and surfactant-poor regimes are not always able to be clearly defined as well as that emulsion stability (even when the microstructure was originally formed under conditions of high availability of the interface stabilising species) can be compromised by other factors; e.g. changes to the conformation of the stabilising species following their adsorption at an interface (39).

3.4. Conclusions

This study firstly aims to assess the Confined Impinging Jet Mixer (CIJs) capacity to realise optimal processing environment under the hydrodynamic/formulation conditions investigated here, from both a computational and experimental perspective. It is suggested that optimal CIJs operation is realised when (i) the inlet jet mass flow rate, W_{jet}, > 176 g/min and at the same time (ii) the pre-emulsion $d_{3,2}$ is higher than the d_{max} evaluated under fixed W_{jet}.

Following the findings of the first result section, the second part of this study focuses on the experimental assessment of the CIJs emulsification performance for the processing of o/w emulsions with a wide range of oil contents, in the surfactant-poor and surfactant-rich regime, at different operational conditions and residence times. Overall, the emulsion $d_{3,2}$ decrease as W_{jet} increases (within the optimal range of operation) independently on the dispersed phase mass fraction. Under the strongest hydrodynamic conditions, all systems showed a similar droplet size distribution and polydispersity. It was also observed, based on a comparison with the theoretically calculated Kolmogorov eddy size, a transition from a turbulent inertial (TI) to turbulent viscous (TV) regime of emulsification taking place by increasing the oil mass fraction from 40 to 60 wt.%. It is suggested as the emulsion droplet size reduction for highly concentrated systems (80 wt.%) is instead due to the predominant hydrodynamic interactions between neighbouring droplets rather than to turbulence effects. The increase of the residence time (e.g. multipassing) under fixed hydrodynamic conditions primarily causes a reduction of the span of the droplet size distribution of the processed emulsions.

It is also proposed that the ability of CIJs processing to reduce the emulsion $d_{3,2}$ is strongly dependent on the surfactant availability (e.g. surfactant concentration to the oil content). The $d_{3,2}$ of formulations with low surfactant availability (e.g. surfactant-poor regime) is majorly driven by surfactant concentration and oil content (e.g. formulation aspects) rather than the

energy dissipation rate generated by jet collisions (e.g. processing aspects) as in the case of formulations with high surfactant availability (e.g. surfactant-rich regime).

Although, most of the systems overall show a good stability upon storage regardless of their formulation, to establish a clear correlation between the surfactant availability and the long-term storage stability results a rather complex operation.

In conclusion, this study offers novel insights into the emulsification by using CIJs, thus further extending the potential of its application for the (continuous, high-throughput and low-energy) processing of more concentrated systems under a wide range of hydrodynamic conditions and formulation parameters.

List of References

(1) Donsì F. *Chapter 11 - Applications of Nanoemulsions in Foods*. In: Jafari S.M., McClements D.J., (eds.). *Nanoemulsions*. 1st ed. Oxford: Academic Press; 2018. p. 349-77

(2) Rayner M. *Scales and Forces in Emulsification*. In: Rayner M., Dejmek P., (eds.). *Engineering Aspects of Food Emulsification and Homogenisation*. 1st ed. Boca Raton: CRC press; 2015. p. 3-32.

(3) Kolmogorov A.N. *Drop breakage in turbulent flow*. Comptes rendus de l'Académie des Sciences. 1949; 66: 825-30.

(4) Hinze J.O. *Fundamentals of the hydrodynamic mechanism of splitting in dispersion processes*. AIChE Journal. 1955; 1(3): 289-95.

(5) Tcholakova S., Lesov I., Golemanov K., Denkov N.D., Judat S., Engel R., et al. *Efficient emulsification of viscous oils at high drop volume fraction*. Langmuir. 2011;2 7(24): 14783-96.

(6) Vankova N., Tcholakova S., Denkov N.D., Ivanov I.B., Vulchev V.D., Danner T. *Emulsification in turbulent flow: 1. Mean and maximum drop diameters in inertial and viscous regimes*. Journal of Colloid and Interface Science. 2007; 312(2): 363-80.

(7) Li Z., Dai L., Wang D., Mao L., Gao Y. *Stabilization and rheology of concentrated emulsions using the natural emulsifiers quillaja saponins and rhamnolipids*. Journal of Agricultural and Food Chemistry. 2018;66 (15): 3922-9.

(8) Håkansson A. Droplet breakup in high-pressure homogenizers. In: Rayner M., Dejmek P., (eds.). *Engineering Aspects of Food Emulsification and Homogenisation*. 1st ed. Boca Raton: CRC press; 2015. p. 125-48.

(9) Seekkuarachchi I.N., Tanaka K., Kumazawa H. *Formation and charaterization of submicrometer Oil-in-Water (O/W) emulsions, using high-energy emulsification*. Industrial & Engineering Chemistry Research. 2006; 45(1): 372-90.

(10) Joscelyne S.M., Trägårdh G. *Membrane emulsification-a literature review*. Journal of Membrane Science. 2000; 169(1): 107-17.

(11) Lloyd D.M., Norton I.T., Spyropoulos F. *Processing effects during rotating membrane emulsification*. Journal of Membrane Science. 2014; 466: 8-17.

(12) Neethirajan S., Kobayashi I., Nakajima M., Wu D., Nandagopal S., Lin F. *Microfluidics for food, agriculture and biosystems industries*. Lab on a Chip. 2011; 11(9): 1574-86.

(13) McClements D.J. *Food Emulsions: Principles, Practices and Techniques*. 3rd ed. Boca Raton: CRC press; 2016.

(14) Johnson B.K., Prud'homme R.K. *Chemical processing and micromixing in confined impinging jets*. AIChE Journal. 2003; 49(9): 2264-82.

(15) Siddiqui S.W., Zhao Y., Kukukova A., Kresta S.M. *Characteristics of a Confined Impinging Jet Reactor: energy dissipation, homogeneous and heterogeneous reaction products, and effect of unequal flow*. Industrial & Engineering Chemistry Research. 2009; 48(17): 7945-58.

(16) Liu Y., Fox R.O. *CFD predictions for chemical processing in a confined impinging-jets reactor*. AIChE Journal. 2006; 52(2): 731-44.

(17) Gavi E., Marchisio D.L., Barresi A.A. *CFD modelling and scale-up of Confined Impinging Jet Reactors*. Chemical Engineering Science. 2007; 62(8): 2228-41.

(18) Siddiqui S.W. *Mixing performance of various geometries-Emulsification perspective*. Procedia Food Science. 2011; 1: 131-7.

(19) Siddiqui S.W., Norton I.T. *Oil-in-water emulsification using Confined Impinging Jets*. Journal of Colloid and Interface Science. 2012; 377(1): 213-21.

(20) Siddiqui S.W., Wan Mohamad W.A.F., Mohd. Rozi M.F., Norton I.T. *Continuous, high-throughput flash-synthesis of submicron food emulsions using a Confined Impinging Jet Mixer: effect of in situ turbulence, sonication, and small surfactants.* Industrial & Engineering Chemistry Research. 2017; 56(44): 12833-47.

(21) Barnes H., Hutton J.F., Walers K. *An introduction to Rheology*. Amsterdam: Elsevier; 1989.

(22) Calabrese R.V., Wang C.Y., Bryner N.P. *Drop breakup in turbulent stirred-tank contactors. Part III: Correlations for mean size and drop size distribution*. AIChE Journal. 1986; 32(4): 677-81.

(23) Siddiqui S.W. *The effect of oils, low molecular weight emulsifiers and hydrodynamics on oil-in-water emulsification in Confined Impinging Jet Mixer*. Colloids and Surfaces A: Physicochemical and Engineering Aspects. 2014; 443: 8-18.

(24) Sprow F.B. *Distribution of drop sizes produced in turbulent liquid-liquid dispersion*. Chemical Engineering Science. 1967; 22(3): 435-42.

(25) Zhou G., Kresta S.M. *Correlation of mean drop size and minimum drop size with the turbulence energy dissipation and the flow in an agitated tank*. Chemical Engineering Science. 1998; 53(11): 2063-79.

(26) Pacek A.W., Man C.C., Nienow A.W. *On the Sauter mean diameter and size distributions in turbulent liquid/liquid dispersions in a stirred vessel*. Chemical Engineering Science. 1998; 53(11): 2005-11.

(27) Jafari S.M., Assadpoor E., He Y., Bhandari B. *Re-coalescence of emulsion droplets during high-energy emulsification*. Food Hydrocolloids. 2008; 22(7): 1191-202.

(28) Tesch S., Gerhards C., Schubert H. *Stabilization of emulsions by OSA starches*. Journal of Food Engineering. 2002; 54(2): 167-74.

(29) Floury J., Desrumaux A., Lardières J. *Effect of high-pressure homogenization on droplet size distributions and rheological properties of model oil-in-water emulsions*. Innovative Food Science & Emerging Technologies. 2000; 1(2): 127-34.

(30) Narsimhan G., Goel P. *Drop coalescence during emulsion formation in a High-Pressure Homogenizer for tetradecane-in-water emulsion stabilized by sodium dodecyl sulfate*. Journal of Colloid and Interface Science. 2001; 238(2): 420-32.

(31) Golemanov K., Tcholakova S., Denkov N.D., Ananthapadmanabhan K.P., Lips A. *Breakup of bubbles and drops in steadily sheared foams and concentrated emulsions*. Physical Review E. 2008; 78(5): 051405.

(32) Walstra P. *Emulsions*. In: Lyklema J., (ed.). *Fundamentals of Interface and Colloid Science*. 5th ed. Oxford: Academic Press; 2005. p. 8.1-8.94.

(33) Lee L., Norton I.T. *Comparing droplet breakup for a high-pressure valve homogeniser and a Microfluidizer for the potential production of food-grade nanoemulsions*. Journal of Food Engineering. 2013; 114(2): 158-63.

(34) Qian C., McClements D.J. *Formation of nanoemulsions stabilized by model food-grade emulsifiers using high-pressure homogenization: Factors affecting particle size*. Food Hydrocolloids. 2011; 25(5): 1000-8.

(35) Tcholakova S., Denkov N.D., Danner T. *Role of surfactant type and concentration for the mean drop size during emulsification in turbulent flow*. Langmuir. 2004; 20(18): 7444-58.

(36) Taisne L., Walstra P., Cabane B. *Transfer of oil between oil droplets*. Journal of Colloid and Interface Science. 1996; 184(2): 378-90.

(37) Lobo L., Svereika A. *Coalescence during emulsification: 2. Role of small molecule surfactants*. Journal of Colloid and Interface Science. 2003; 261(2): 498-507.

(38) Tcholakova S., Denkov N.D., Lips A. *Comparison of solid particles, globular proteins and surfactants as emulsifiers*. Physical Chemistry Chemical Physics. 2008; 10(12): 1608-27.

(39) Tcholakova S., Denkov N.D., Ivanov I.B., Campbell B. *Coalescence stability of emulsions containing globular milk proteins*. Advances in Colloid and Interface Science. 2006; 123-126: 259-93.

Chapter 4

Formation of Pickering and mixed emulsifier systems stabilised o/w emulsions via Confined Impinging Jets processing

The content of this chapter is currently under review in the Journal of Food and Bioproducts Engineering.

Abstract

This study investigates for the first time the production of 10 and 40 wt.% oil-in-water emulsions stabilised by an array of particles and mixed emulsifier (Tween20-silica) concentrations. CIJs performance was evaluated for a range of hydrodynamic conditions (energy dissipation rates, $\bar{\varepsilon}_{th}$) and multipassing through the CIJs geometry followed by a monitoring of the emulsion storage stability. Overall, it was demonstrated that droplet size reduction was promoted as higher energy levels of $\bar{\varepsilon}_{th}$ were approached, regardless of the formulation. Following emulsion recirculation under fixed jet mass flow rate, the residence time associated with two passes was sufficient to ensure no further changes in terms of both average droplet size ($d_{3,2}$) and span of the droplet size distribution. Only when Tween20 and silica were mixed at low concentrations (0.01 and 0.10 wt.%, respectively), this emulsifier system could not promote any droplet size reduction upon both processing and multipassing. All systems showed excellent stability over 40 days of storage and it was possible to demonstrate that the combination of the emulsifiers aided in prolonging the emulsion stability. In conclusion, this investigation aims to extend the current range of emulsion microstructures that can be produced by CIJs to further enhance its industrial applicability.

Keywords

Pickering Emulsion;

Mixed emulsifier system;

Confined Impinging Jets;

4.1. Introduction

The emulsification performance of high-energy processing techniques (e.g. high-shear mixing, ultrasound treatment and high-pressure homogenisation) in the turbulent regime has been extensively investigated and characterised for a wide range of emulsion formulations (1). In the turbulent regime (provided that there is enough emulsifier to stabilise the formed interfacial area), the final emulsion droplet size and droplet size distribution largely depend on the characteristic time scale of the emulsifier adsorption at the droplet interface (2). Therefore, the selection of the emulsifier represents a crucial choice to ensure an efficient emulsification process (3). Surfactants and nanoparticles (amongst others) represent common examples of emulsifier systems used to aid droplet stabilisation upon processing. Surfactants can usually adsorb at the droplet interface more rapidly than particles (4). What is more, once adsorbed at the interface, surfactants lower the interfacial tension, thus favouring droplet break-up (5). Conversely, although particles are not surface-active, Pickering emulsions have shown better resistance against droplet coalescence, which is realised by the particles' (almost) irreversible adsorption at the interface (6, 7). The slower mechanism of particle adsorption at the interface additionally implies that droplet stabilisation is mainly driven by the capacity of the processing technique to achieve high levels of turbulence (8). These differences also explains why (during processing, under similar levels of turbulence) the emulsion droplet size of systems stabilised by surfactants is usually smaller (9). A possible strategy that could be employed to mitigate the differences in the droplet size between particle- and surfactant-stabilised emulsions is represented by adding a small amount of surface-active species during the processing of Pickering emulsions. It has been shown that by using such mixed emulsifier systems, it may be possible to combine the benefits deriving from the use of both species to produce emulsions

with a smaller droplet size (than that of particle-stabilised systems) and with greater storage stability (than that of surfactant-stabilised systems) (10-12).

Notwithstanding the consent of high-energy manufacturing methods for the high-throughput processing of small droplets, their major limitations are associated with the unavoidable waste of a large part of their energy input as dissipated heat, which makes these techniques energetically inefficient (13, 14). Low-energy approaches, such as membrane or microfluidic emulsification, exploiting the spontaneous formation of droplets as a consequence of detachment from the membrane pore or a microchannel junction, overcome such energy efficiency problems since these do not rely on turbulence (15, 16). However, due to the very absence of turbulence, these techniques are less effective in promoting the transport of slower emulsifiers (such as particles) at the drop interface, often resulting in larger droplet sizes. Furthermore, their development for larger-scale production still faces the major challenge of achieving high throughputs (15, 16).

In contraposition, Confined Impinging Jets (CIJs) have shown the potential of overcoming both of these limitations. In CIJs two (either the pure oil and water phases or two pre-emulsion) jets collide at high velocities within a confined geometry (17). CIJs exploit the energy dissipated upon impingement as the driving force for the turbulent production of emulsions rather than the application of high-levels of shearing, pressure or cavitation (17). Due to the confined mixing volume, droplets experience rather uniform disruptive forces, resulting in the high throughput production of emulsions with tailored microstructural features (e.g. droplet size and droplet size distribution) (18). The energy dissipation rate generated upon jet collision can be theoretically estimated (19) according to:

$$\bar{\varepsilon}_{th} = \frac{2\, Q_{jet}\, \Delta P}{\rho V_{CIJs}} \qquad (4.1)$$

where Q_{jet} is the jet flow rate, ΔP is the pressure at which jet collision takes place, ρ is the density of either the pure phase in each jet or the pre-emulsion, and V_{CIJs} is the volume within the CIJs geometry where jet collision and mixing occur. The eq. 4.1 differs from eq. 3.4 in that the term of the kinetic energy per unit time is neglected because it is several orders of magnitude smaller than the pressure energy per unit time term ($2\, Q_{jet}\, \Delta P$), over the whole range of jet flow rates.

Emulsification using CIJs represents a relatively new area of research and as a consequence the literature on this topic is still somewhat limited. CIJs processing of dilute emulsions (volume fractions < 10 vol.%) has been evaluated for a range of different emulsifiers (Tween20, Span80, Whey Protein, Lecithin or Sodium Dodecyl Sulphate), hydrodynamic conditions (jet flow rates) and residence times (including recirculation through the mixing chamber) (20). It was observed that the smallest droplet size (~2 μm) was achieved approaching the highest jet flow rates, independently from the type of surfactant used. More recently, it has also been shown that CIJs processing allowed the production of dilute emulsions having an average droplet dimension within the nano-size range (~700 nm) but only if coupled with an ultrasound treatment (21). An additional study investigated the use of CIJs for the production of emulsions with dispersed phase content up to 80%, in the surfactant (Tween20)-poor and -rich regime, hydrodynamic conditions as well as residence times (17). In this work, CIJs operation could induce droplet size reduction only when the process took place within the identified optimal processing window (i.e. mass jet flow rate, W_{jet} , > 176 g/min) and pre-emulsions were prepared with an average droplet size above a certain threshold (~10 μm). The CIJs emulsification performance remained almost unaffected upon variation of the dispersed phase mass fraction with all emulsions reaching their lowest droplet size (~ 8μm) when processed under the highest W_{jet},

regardless of the surfactant concentration. Furthermore, recirculation (up to 4 passes) within the CIJs cavity under fixed W_{jet} produced as an effect the narrowing of the emulsions droplet size distribution with minor variations in their average droplet size.

Despite the CIJs potential to assist in the formation of dilute as well as more concentrated emulsions with small droplet sizes at high levels of turbulence and at low-energy inputs, no studies (to the best of the authors' knowledge) have previously reported on the assessment of the CIJs emulsification performance in producing Pickering and mixed-emulsifier (surfactant and particles) stabilised o/w emulsions. Thus, this study reports for the first time on the use of CIJs to process dilute (10 wt.%) as well as semi-concentrated (40 wt.%) emulsions stabilised by either particles or mixed emulsifier systems. The emulsion microstructure was evaluated in terms of final droplet sizes and droplet size distributions resulting from both exposure to a range of CIJs hydrodynamic conditions and multi-passing (recirculation) through a fixed turbulent environment. Emulsion stability was also assessed following a storage period of 40 days.

Overall, the present study aims to extend the current spectrum of emulsion microstructures that can be produced by CIJs, thus building upon the process's lower-energy credentials and capacity to deliver high product throughputs to further enhance its industrial applicability.

4.2. Materials and Methods

4.2.1. Materials

All oil-in-water (o/w) emulsions were prepared by using de-ionised water obtained from a reverse osmosis filtration system as the continuous phase. Commercial sunflower oil (viscosity = 50 cP) was purchased by a local retailer and used as the dispersed phase. Both Polysorbate20, i.e. Tween20, (Hydrophilic Lipophilic Balance, HLB =16.70 and molecular weight=1227.54 g/mol, critical micelle concentration = 0.06 mM) and a 30 wt.% suspension of silica in Water (Ludox HS, surface area 220 m_2/g and density 1.21 g/mL) were supplied by Sigma-Aldrich Company (UK) and used as emulsifiers.

4.2.2. Methods

4.2.2.1. Dispersion and characterisation of silica particles in water

For the preparation of the silica-in-water dispersion, the 30wt.% Ludox solution was added to the continuous phase and their quantity adjusted accordingly to reach the desired particle concentration (0.10 to 5 wt.% of the total emulsion weight, i.e. 500 g). The initial pH of the solution (~10) was then lowered to ~2 using the required quantities of hydrochloric acid (HCl, 1M) and sodium hydroxide (NaOH, 1M). It has been shown that to produce effective stabilisation of o/w emulsions, it is possible to modify the surface character of hydrophilic silica by lowering the pH of the aqueous medium to 2 (22). The silica particle size, particle size distribution and ζ-potential were then characterised at 22°C by using a dynamic light scattering analysis technique, Zetasizer (Malvern Instruments). Each experiment was repeated three times. Figure 4.1 shows the effect of the variation in pH on the above parameters. The particle size remained (practically) unaffected over the entire range of pH. Upon the reduction of the pH from 10 to 2, the particle size distribution became slightly narrower while the zeta potential

strongly decreased from - 45 mV to 0 mV (e.g. isoelectric point), respectively. The steep reduction of the Silica zeta potential is due to the complete protonisation of the Silanol groups on the surface of the particles as the pH is lowered (22).

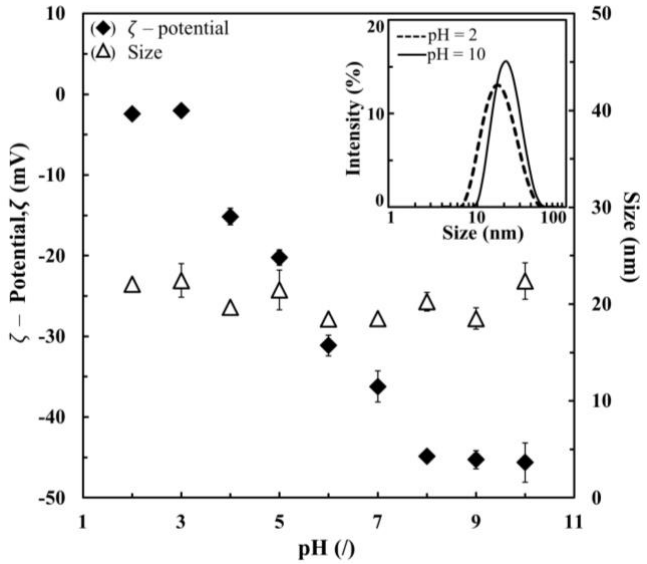

Figure 4.1. Silica particle size (Δ) and ζ-potential (◆) varying as a function of the pH. All data points are mean values (n=3) and error bars are reported as a single standard deviation. Where not visible error bars result smaller than symbols. (Inset Graph) Particle size distributions resulting from the reduction of the pH from 10 (solid line) to 2 (dashed line) of the silica-in-water dispersion.

4.2.2.2. Emulsion preparation

Emulsions were prepared following a two-step procedure, which included: *(i)* high-shear mixing to form the initial coarse pre-emulsion followed by *(ii)* emulsification within the Confined Impinging Jets (CIJs) device.

4.2.2.2.1. Pre-emulsion preparation

A. Preparation of nano-particle stabilised o/w pre-emulsions

The required amount of vegetable oil (10% or 40 % of the total emulsion weight, i.e. 500 g) was added to the silica-in-water dispersion (prepared as described in section 4.2.2.1). Sunflower

oil and the silica-in-water solution were then pre-emulsified by means of a Silverson L5 Series Laboratory High-Shear Mixer, equipped with an emulsor screen of 33 mm in diameter, for 3 min at 2000 RPM.

B. Preparation of mixed emulsifier stabilised o/w pre-emulsions

The required concentration of Tween20 (0.01 or 0.1 wt.% of the total emulsion weight, i.e. 500 g) was dissolved in the silica-in-water dispersion (prepared as described in section 4.2.2.1) by using a magnetic stirrer for 10 min, before the addition of the desired amount of sunflower oil (10% or 40% of the total emulsion weight). The silica-in-water dispersion, Tween20 and the vegetable oil were then pre-emulsified by means of a Silverson L5 Series Laboratory High-Shear Mixer, equipped with an emulsor screen of 33 mm in diameter, for 3 min at 2000 RPM.

4.2.2.2.2. CIJs processing

As the second stage, the pre-emulsions were processed through the CIJs geometry, Figure 4.2 , by means of a single pulse-less micro-pump (external gear pump) with jet mass flow rates varying from 85.50 to 702 g/min. Prior impingement the flow was split into two equal streams by using a Y-junction, whereas after leaving the CIJs chamber, emulsions samples were collected and stored in sample pots.

To study the effect of multipassing, emulsions were processed through the CIJs under fixed inlet mass jet flow rate (352.75 g/min) and were collected in a beaker. This was then transferred back to the feed and the formed emulsion was re-processed up to 4 times. Each experiment was repeated twice.

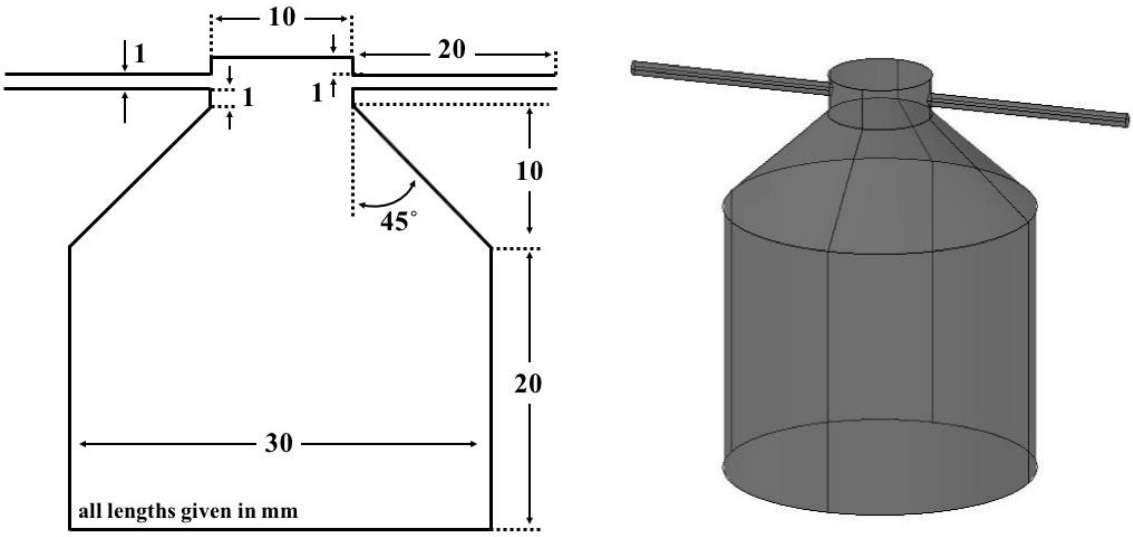

Figure 4.2. Schematic and three-dimensional representation of the CIJs geometry employed in this study; all dimensions are given in millimetres.

4.2.2.3. Droplet size measurements

The measurement of droplet size and droplet size distribution were carried out by using a Mastersizer 2000 (Malvern Instruments). Samples were diluted to 3 vol.% in order to avoid multiple-light scattering. Within the Mastersizer, samples were tested three times at room temperature (22˚C) and an average was calculated. Each experiment was repeated twice.

4.2.2.4. Interfacial tension measurements

The equilibrium interfacial tensions (γ) of the o/w interface both without and with emulsifier systems at varying concentration were measured using a K11-Force Tensiometer (Krüss, GmbH) equipped with a Wilhelmy plate at room temperature (22°C). Table 4.1 shows that the interfacial tension of the plain sunflower oil-water interface resulted equal to 24.95 $\pm$ 0.02 mN/m in excellent agreement with the literature values. Upon variation of the silica concentration from 0.10 to 5 %, the o/w interfacial tension slightly deviated from the plain o/w γ, decreasing from 24.51 $\pm$ 0.03 to 20.41 $\pm$ 0.01, respectively. This minimal reduction may be

addressed to the presence of surface-active contaminants associated with the particle solution (7). With the addition of (0.01 and 0.1 wt.%) Tween20 to (0.10 and 1wt.%) silica, the γ dropped to similar values shown for the interfacial tensions of the o/w interface solely stabilised by Tween20, according with the results observed in the literature.

Table 4.1. Equilibrium interfacial tension, γ, of the emulsifier systems used in this study. [a]Equilibrium interfacial tension of the oil/water system deprived on any emulsifier.

Silica (wt.%)	Tween20 (wt.%)	γ (mN/m)
/[a]		[a]24.95 ± 0.02
0.10		24.51 ± 0.03
1		24.30 ± 0.02
2		22.60 ± 0.02
5		20.41 ± 0.01
	0.01	6.04 ± 0.01
	0.10	5.34 ± 0.02
0.10	0.01	6.60 ± 0.03
1		4.82 ± 0.03
0.10	0.10	4.58 ± 0.02
1		4.13 ± 0.03

4.2.2.5. Stability

Samples were stored in the laboratory at room temperature (22°C) over a period of 40 days to evaluate the long-term emulsion stability. Since creaming occurred in most of the sample analysed in this study, the samples were gently re-dispersed before re-measuring their droplet size and droplet size distribution.

4.3. Results and discussion

4.3.1. o/w emulsions solely stabilised by particles

The effect of varying the silica concentration on the average droplet size ($d_{3,2}$) of both 10 wt.% and 40 wt.% o/w pre-emulsions processed through the CIJs under varying hydrodynamic conditions is presented in Figure 4.3. CIJs hydrodynamic conditions are expressed in terms of the theoretically estimated energy dissipation rate, $\bar{\varepsilon}_{th}$, according to eq. 4.1. Silica concentrations of 0.10, 1, 2 and 5 wt.% were used for the preparation of all pre-emulsions, although systems with a high dispersed phase content (40 wt.%) and low particle concentration (0.10 wt.%) rapidly phase separated following pre-mixing and thus processing through the CIJs was not performed.

The data presented in Figure 4.3.A for the 10 wt.% oil pre-emulsions shows that the droplet sizes for these systems were practically the same for silica concentrations up to 2 wt.%, whereas a small size reduction occurred for pre-emulsions containing 5 wt.% silica. Since the pre-mixing stage conditions during the production of all systems were the same, the pre-emulsion droplet size decrease is most likely associated with an increased particle interfacial adsorption rate facilitated by the higher silica concentration. However, once the dispersed phase fraction was increased to 40 wt.% and thus the interfacial area became larger, the pre-emulsion droplet size was independent of silica concentration (Figure 4.3.B).

The pre-emulsions were then processed through the CIJs device using a range of hydrodynamic conditions. The $d_{3,2}$ variation with the $\bar{\varepsilon}_{th}$ demonstrated a common trend among the different formulations and oil mass fractions (Figure 4.3). At low values of $\bar{\varepsilon}_{th}$ ($< 2\times10^3$ W/kg), the pre-emulsion average droplet size was practically unaffected by the flow conditions within the CIJs chamber. Under these low $\bar{\varepsilon}_{th}$ conditions, all the systems maintained a similar identity to their respective pre-emulsions with variations in droplet size (Figure 4.3.A)

contained within the experimental error. On the other hand, as the $\bar{\varepsilon}_{th}$ increased (highlighted areas in Figure 4.3), the droplet size reduction became more pronounced and all systems reached the lowest droplet size (~10 μm) at the highest value of $\bar{\varepsilon}_{th}$ regardless of particle concentration and oil content. In a recently published study (17), it was demonstrated that the jet collision was compromised at low $\bar{\varepsilon}_{th}$, resulting in relatively poor mixing conditions and ultimately impeding CIJs emulsification capacity (within this energy dissipation rate range) . Contrarily, as higher levels of $\bar{\varepsilon}_{th}$ are approached (i.e. optimal processing conditions), the droplet size of (surfactant-stabilised) emulsions steeply decreased reaching its minimum value (~10μm) at the highest $\bar{\varepsilon}_{th}$.

The span values of all CIJs produced emulsions exhibited the same response with respect to $\bar{\varepsilon}_{th}$, a behaviour which was in fact independent of particle concentration (inset graphs in Figure 4.3). Within the region of deficient operation, the span values remained rather similar to those of the corresponding pre-emulsions, further suggesting that pre-emulsion microstructure remains practically unchanged when processing at such low jet flow rates. However, in the optimal CIJs processing window (highlighted area), all span values exhibit a similar increase; droplet size distributions became progressively broader at higher energy dissipation rates. This is in agreement with the findings observed in the literature focusing on the performance of other emulsification techniques, which also explains why as a common practice recirculation is often required to reach the desired emulsion microstructure (23, 24).

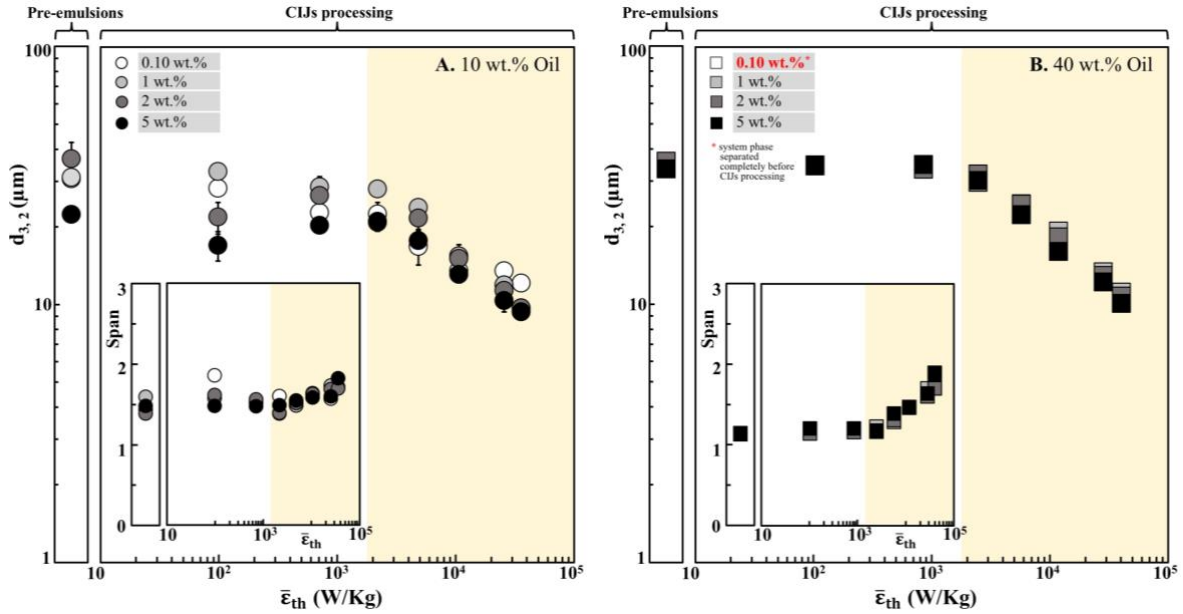

Figure 4.3. Emulsion Sauter diameter ($d_{3,2}$) as a function of the theoretically predicted energy dissipation rate ($\bar{\varepsilon}_{th}$; eq. 4.1) following CIJs processing of pre-emulsions with 10 wt.% (A) and 40 wt.% (B) oil mass fractions in the presence of an array of silica particles, ranging in concentration from 0.10 to 5 wt.%. Also shown (inset graphs), span values as a function of $\bar{\varepsilon}_{th}$. Highlighted areas in both the main and the inset graphs represent optimal CIJs processing conditions. All data points are average values (n=6) and error bars represent one standard deviation. Where not visible error bars are smaller than symbols.

4.3.2. o/w emulsions stabilised by mixed-emulsifier systems

Figure 4.4 shows the effect of $\bar{\varepsilon}_{th}$ on the Sauter diameter ($d_{3,2}$) of 10 wt.% and 40 wt.% o/w emulsions stabilised by surfactant–particle (Tween20-silica) mixed-emulsifier systems. Tween20 concentrations of 0.01 or 0.10 wt.% were combined with either 0.10 or 1 wt.% silica to form 10 wt.% (Figure 4.4.A and C) and 40 wt.% (Figure 4.4.B and D) o/w pre-emulsions which were subsequently processed through the CIJs. Figure 4.4 also includes $d_{3,2}$ versus $\bar{\varepsilon}_{th}$ data for emulsions stabilised solely by the equivalent concentrations (to those in the mixed-emulsifier system) of either the surfactant or particle species alone.

The variation of the $d_{3,2}$ of the 10 wt.% o/w emulsions stabilised by 0.01 wt.% of Tween20 and 0.10 or 1 wt.% of silica with the $\bar{\varepsilon}_{th}$ is presented in Figure 4.4.A. As observed in the previous section, both 0.10 and 1 wt.% particle-stabilised emulsion $d_{3,2}$ retained their pre-emulsion identity at low $\bar{\varepsilon}_{th}$ before being reduced to a minimum value of ~10 μm within the optimal

processing window. Differently, the $d_{3,2}$ of the emulsion solely stabilised by the surfactant (0.01 wt.% of Tween20) was initially subjected to an increase, probably due to a combination of both the CIJs poor mixing efficiency at low $\bar{\varepsilon}_{th}$ and the fact that surfactants provide a less robust interface than particles (25, 26). Nonetheless, under efficient CIJs operation, the $d_{3,2}$ then followed similar trend and values than those showed by Pickering systems. Once surfactant and particles were mixed together at low concentrations (0.01 and 0.10 wt.% respectively), the $d_{3,2}$ exhibited a different dependency with the $\bar{\varepsilon}_{th}$. The Sauter diameter fluctuated around an average value of ~ 40 µm and no deviation from this trend was observed across the entire range of $\bar{\varepsilon}_{th}$. The addition of a surfactant to particle-system (or vice versa) can either enhance or undermine their efficiency as emulsifiers depending on both their type and relative concentration (8, 10, 12). It appears that, once mixed at low concentrations, the particles-surfactant system could not induce an effective stabilisation during CIJs processing regardless of the hydrodynamic conditions. Contrarily, as the particle concentration was increased to 1 wt.%, the Sauter diameter showed an initial increase to then undergo a steep reduction as the CIJs was operated under full capacity, in alignment with the trend observed with the systems stabilised by the single emulsifiers. The results suggest that the increase in the particle concentration induced a more efficient droplet stabilisation during processing thus resulting in the observed trend similar to that of the emulsions stabilised by the sole particles or surfactant.

Analogous trends were observed as the dispersed phase content was increased to 40 wt.%, Figure 4.4.B. The diameter of emulsions stabilised by the sole particles or surfactant decreased at increasing $\bar{\varepsilon}_{th}$ to reach a minimum value (~12 and 18 µm, respectively) as a higher $\bar{\varepsilon}_{th}$ was approached. For the mixed emulsifier systems, the $d_{3,2}$ of the low silica concentration co-stabilised emulsion remained constant at low values of $\bar{\varepsilon}_{th}$. Within the optimal operation region, the Sauter diameter was initially reduced followed by a rapid increase as the processing

conditions became progressively more severe. Overall, despite higher energy dissipation conditions create favourable conditions for droplet size reduction, as this tendency increases (i.e. at further higher $\bar{\varepsilon}_{th}$), the observed raise in the $d_{3,2}$ suggests that the mixed emulsifier system could not efficiently stabilise emulsion droplets (strongly in agreement with the results of Figure 4.4.A), thus very likely resulting in their coalescence (i.e. in the shown $d_{3,2}$ increase).

Differently, at a higher particle concentration, the emulsion Sauter diameter remained fairly constant within the low energy dissipation rate region to then decrease to a minimum value (~20 μm) within the optimal CIJs operating window, following the trend of the emulsions stabilised by the single emulsifiers and similarly to the trend observed in Figure 4.4.A. Overall (with exception of the low particle co-stabilised emulsions), the processing conditions established during CIJs operation were such to minimise the differences in formulation (i.e. type and concentration of emulsifier as well as of the interfacial tension, Table 4.1) among the different systems investigated for both dispersed phase mass fractions.

Any possible variation in the Sauter diameter arising from the use of different emulsifier(s) was minimised once the Tween20 concentration was increased to 0.10 wt.% for both dispersed phase mass fractions, Figure 4.4.C and D. For the 10 wt.% o/w emulsions (Figure 4.4.C) stabilised by mixed emulsifiers, the $d_{3,2}$ did not significantly vary across the different formulations (either stabilised by mixed or sole emulsifier systems). In agreement with the trend observed in Figure 4.3 and Figure 4.4.A-B, the $d_{3,2}$ remained fairly constant before being reduced within the optimal operating window. All the systems showed a similar droplet size reduction as well as a similar smallest droplet size (~ 10 μm) achieved at the highest level of $\bar{\varepsilon}_{th}$.

Once the dispersed phase content was increased to 40 wt.% (Figure 4.4.D), emulsions practically retained their (original pre-emulsion) droplet diameter at low $\bar{\varepsilon}_{th}$, before undergoing

a sharp reduction within the optimal processing window, and reaching a fairly similar $d_{3,2}$ (~10-15 μm) at the highest $\bar{\varepsilon}_{th}$ value, independently on the formulation.

With exception of the low-particle stabilised systems for both oil load contents, overall it appears that the CIJs hydrodynamic conditions, i.e. the energy dissipation rate, are the main parameter affecting the final emulsion droplet size.

The microstructural properties of emulsions stabilised by mixed surfactant-particles systems display an array of behaviour depending on their synergistic interactions, that in turn are affected by the type and relative concentration of emulsifiers as well as on the selected processing method (27). An earlier study demonstrated that the combination of silica and Tween20, at concentrations (3 and 0.10 wt.%, respectively) where each of them gave unstable (50 wt.%) castor o/w emulsions, resulted in stable systems after processing (28). A previous investigation reported the displacement of nano-particles from the oil-water interface by surfactant molecules with the application of shear, when the surfactant was used at concentration above its critical micellar concentration (29). Conversely, in another study the authors showed that the coupling of a non-ionic surfactant (monoolein) with silica nanoparticles during high-shear mixing improved the long-term stability of o/w emulsion through a two-stage synergistic mechanism (8). Overall, it is clear that drawing general conclusions about the stabilisation mechanisms of mixed emulsifier systems is extremely challenging and their behaviour largely depends (amongst other factors) on the specific formulation and processing parameters.

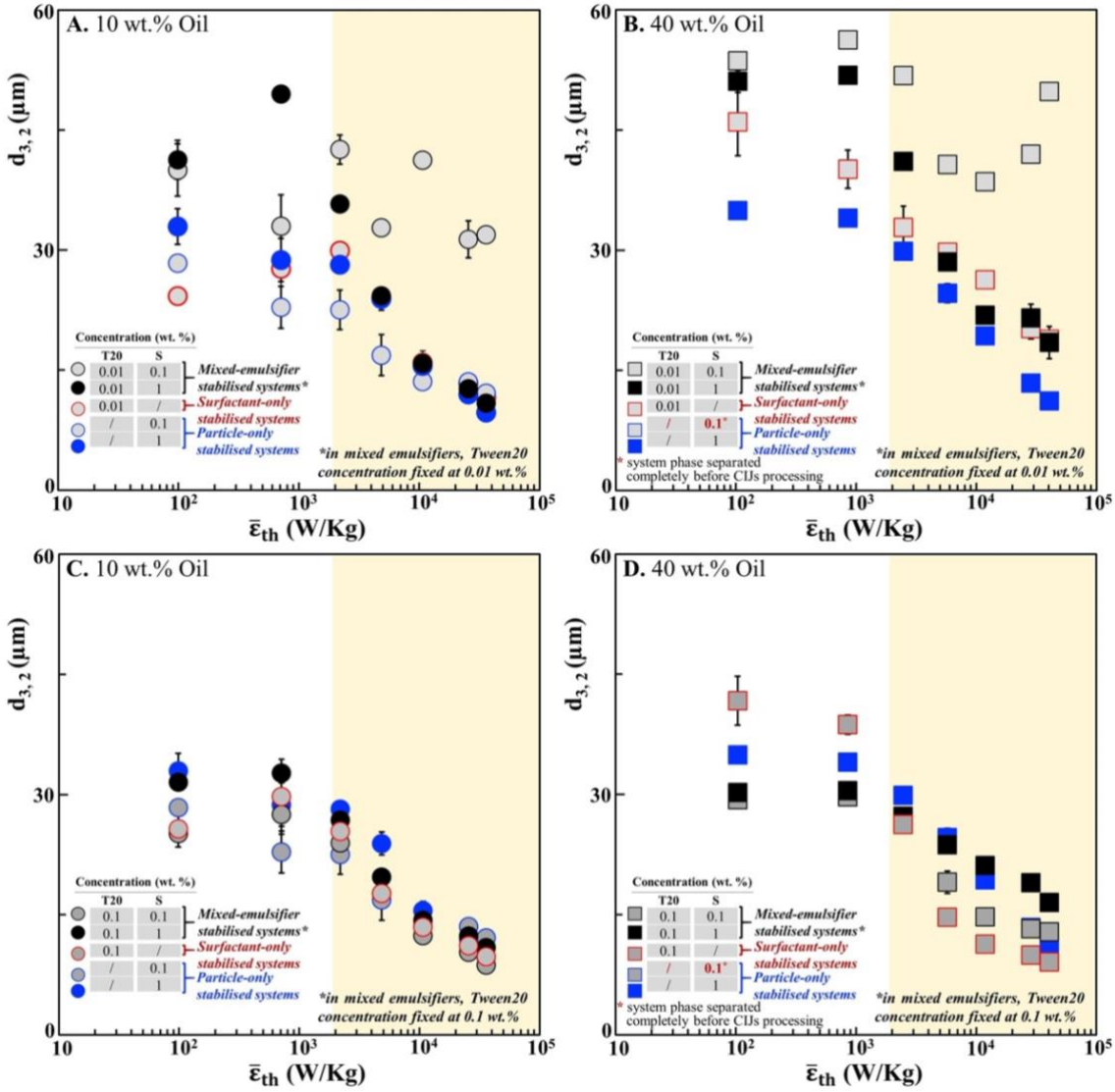

Figure 4.4. Emulsion Sauter diameter ($d_{3,2}$) as a function of the theoretically predicted energy dissipation rate ($\bar{\varepsilon}_{th}$; eq. 4.1) following the CIJs processing of pre-emulsions with 10 wt.% (A and C) and 40 wt.% (B and D) oil mass fractions, in the presence of mixed emulsifier (Tween20 and silica) systems; emulsifier concentrations are given in each figure legend. Also shown are the $d_{3,2}$ versus $\bar{\varepsilon}_{th}$ data for CIJs processed pre-emulsions stabilised solely by either of the two species in the mixed emulsifier systems alone. Highlighted areas represent the range of $\bar{\varepsilon}_{th}$ corresponding to optimal CIJs operation. All data points are mean values (n=6) and error bars are reported as a single standard deviation. Where not visible error bars result smaller than symbols.

4.3.3. Effect of CIJs recirculation

During operation of traditional emulsification techniques (e.g. high-pressure homogeniser, microfluidiser), emulsion droplets experience a wide range of disruptive forces upon a single

pass, possibly resulting in larger average droplet sizes and/or broader droplet size distributions (14). As a consequence, if both smaller droplets and narrower droplet size distributions are required, it is usually necessary to recirculate emulsions through the emulsification apparatus a number of times (24, 30).

The effect of the residence time on the emulsion Sauter diameter ($d_{3,2}$) and the span of the droplet size distribution was explored by the recirculation of all systems through the CIJs device for a total of 4 passes. Multi-passing was conducted under a single jet flow rate of 352.75 g/min corresponding to fixed hydrodynamic conditions with an $\bar{\varepsilon}_{th}$ value of $\sim 5 \times 10^3$ W/kg for both the 10 and 40 wt.% o/w emulsions. The selected jet flow rate is within the range of optimal CIJs operation but at the same time not significantly high as to overshadow any formulation-driven droplet size potential differences.

The change of the 10 wt.% o/w emulsion droplet size and span stabilised by 0.01 wt.% of Tween20 and 0.10 or 1 wt.% of silica as a function of the number of passes through the CIJs is presented in Figure 4.5.A. When both emulsifiers were used at low concentrations (0.01 wt.% Tween20 and 0.10 wt.% silica), the $d_{3,2}$ remained unaffected by the recirculation in the CIJs device. This result confirms, in line with the findings shown in Figure 4.4.A, that this couple of emulsifiers (used at these concentrations) could induce no droplet size reduction, even after spending a prolonged time within the high energy dissipation region of the CIJs.

However, as the silica concentration was increased to 1 wt.% (at fixed 0.01 wt.% of Tween20), the average droplet size reached its minimum value after the second pass with no other changes taking place upon further recirculation, similarly to the emulsions solely stabilised by the two emulsifiers alone. It is also worth mentioning that the span values of the droplet size distributions remained fairly constant as a function of the number of passes, with negligible differences between the different emulsifier systems.

The effect of the recirculation on both the $d_{3,2}$ and the span values of emulsions with a higher oil load (40 wt.%) were also evaluated (Figure 4.5.B). In this case the increase in interfacial area exacerbated the poor stabilisation efficiency of the mixed system with the lowest concentration of emulsifiers (0.01 wt.% Tween20 and 0.10 wt.% silica). In fact, the Sauter diameter increased as a result of recirculation from ~40μm (first pass) to ~60μm (third pass),and remained constant after then. These findings align with the trend observed in Figure 4.4.B. While in that case, the average droplet size increases as a consequence of exposing the emulsion to a progressively increasing $\bar{\varepsilon}_{th}$, equivalently during multi-passing, the $d_{3,2}$ increases as a result of exposing the emulsion for a longer time under fixed $\bar{\varepsilon}_{th}$. For mixed emulsifier systems with a higher particle concentration (1 wt.%), the resulting Sauter diameter did not change after the second pass, with $d_{3,2}$ values being rather close to the ones for emulsions solely stabilised by either of the emulsifiers alone. The span values of the distributions (similarly to the trend shown in Figure 4.5.A) remained practically constant over each pass and were largely similar across the different formulations.

As the Tween20 concentration in the mixed emulsifier system was increased to 0.10 wt.%, differences in the $d_{3,2}$ values for emulsions containing either 10 wt.% or 40 wt.% dispersed phase became negligible (Figure 4.5.C and D, respectively). The minimum droplet size was realised after the second pass while the span values remained constant with increasing residence time within the CIJs turbulent environment, regardless of whether emulsions were stabilised by mixed or sole emulsifier formulations.

Other studies on CIJs reported that the droplet size distributions of emulsions with much lower (to those investigated here) dispersed phase contents (up to a volume fraction of 0.10) was the major parameter affected by recirculation (20). Similarly, other studies evaluating the emulsification capacity of a high-pressure homogeniser or microfluidiser concluded that the

droplet size distribution was the major emulsion microstructural feature affected by the multi-passing (31-33). Recirculation is often necessary in traditional emulsification practice because due to the large volumes where homogenisation takes place, droplets experience largely non-uniform disruptive forces, thus possibly resulting in a larger average droplet diameter and/or broader droplet size distribution. One of the possible advantages of using CIJs lies in its small volume, which allows to most of the droplets to pass through the high-energy dissipation region without bypassing it (19). In the present study, both emulsion droplet size and span remained practically unaffected after the second pass, thus suggesting that the residence time associated with two passes is sufficient to ensure that the generated hydrodynamic conditions are experienced by the entirety of the sample volume under processing. In addition, by looking at the different impact of either (an increasing) $\bar{\varepsilon}_{th}$ or recirculation (at fixed $\bar{\varepsilon}_{th}$) on the $d_{3,2}$ (Figure 4.3 and 4.4), this could also hint that the magnitude of the energy dissipation rate affect the microstructure of the different emulsions more than its duration.

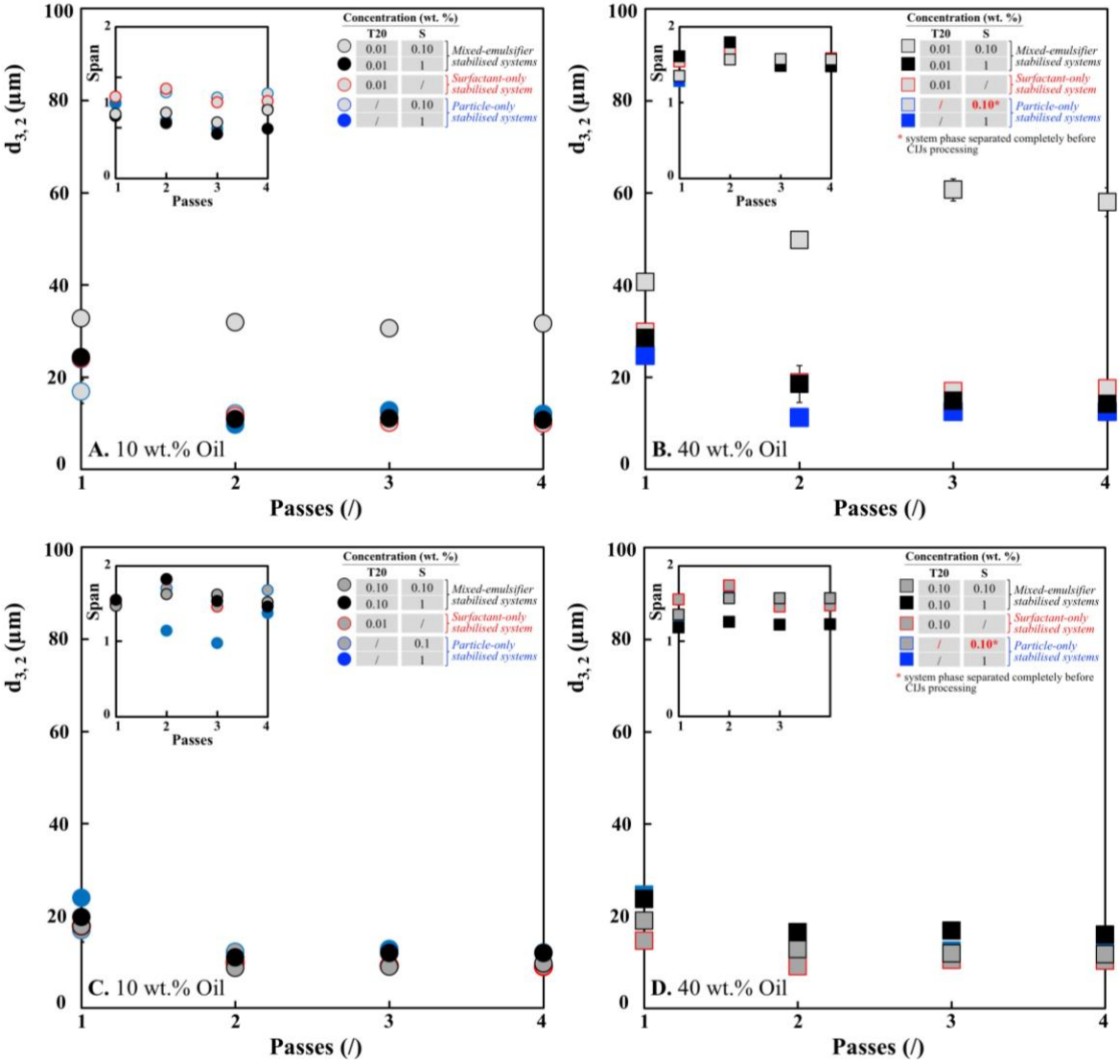

Figure 4.5. Emulsion Sauter Diameter ($d_{3,2}$) and span values (inset graphs) as a function of the number of passes through the CIJs geometry (at a fixed mass jet flow rate of 352.75 g/min corresponding to fixed hydrodynamic conditions with an $\bar{\varepsilon}_{th}$ (eq. 4.1) value of ~5×10^3 W/kg) for both the 10 (A-C) and 40 (B-D) wt.% dispersed phase contents, in the presence of mixed emulsifiers; emulsifier concentrations are given in each figure legend. Also shown are the $d_{3,2}$ versus the number of passes data for CIJ processed pre-emulsions stabilised solely by either of the two species in the mixed emulsifier systems alone. All data points are mean values (n=6) and error bars are reported as a single standard deviation. Where not visible error bars result smaller than symbols.

4.3.4. Long-term emulsion stability

The stability of all emulsions produced after a single pass in the CIJs geometry (at a fixed $\bar{\varepsilon}_{th}$ value of ~$5\times10_3$ W/kg) was monitored at room temperature (22°C) over a storage period of 40 days. Figure 4.6 and Figure 4.7 present the emulsion average diameters ($d_{3,2}$) upon formation in the CIJs device and after 40 days of storage, for systems stabilised by silica alone (Figure 4.6) or by the mixed (Tween20 and silica) emulsifier formulations (Figure 4.7); in each case data for both the 10 wt.% and 40 wt.% dispersed phase contents are given.

The $d_{3,2}$ data of 10 wt.% oil content emulsions stabilised by silica particles alone (Figure 4.6.A) clearly demonstrated the high stability of these systems. Their Sauter diameter, regardless on the concentration of particles used, remained practically unaltered after the 40 days of storage. This is also confirmed by the negligible changes to the droplet size distribution over the same storage period (inset in Figure 4.6.A). Emulsion stability was also maintained for the 40 wt.% dispersed phase content systems (Figure 4.6.B) stabilised by silica at concentrations equal and greater to 1 wt.%. Pre-emulsions containing 0.10 wt.% silica rapidly underwent phase separation prior to CIJs processing and thus have not been included here.

A similar behaviour was also exhibited by the 10 wt.% oil content emulsions stabilised by the mixed emulsifier systems (Figure 4.7.A). Both the Sauter diameters and droplet size distributions for these systems remained unaltered during storage.

As the dispersed phase content was increased to 40 wt.%, emulsion stability was retained for all mixed emulsifier concentrations except for the lowest one; 0.01 wt.% Tween20 and 0.10 wt.% silica (Figure 4.7.B). For these systems, the $d_{3,2}$ increased from ~40 μm (after CIJs processing) to ~60 μm (at the end of the storage period). It should be highlighted that, as previously discussed, the pre-emulsions containing 0.10 wt.% silica phase separated immediately after their preparation, whereas, in our previous work, we showed that although

the emulsions stabilised by only 0.01 wt.% Tween20 remained stable after CIJs processing ($d_{3,2}$ ~ 25µm), these phase separated during the storage period, i.e. 40 days (17). Thus, there is a clear evidence that the combination of the emulsifiers (even at concentrations where each of them on their own do not give a stable emulsion microstructure) aids in prolonging the emulsion stability, although in this case the droplet size was not entirely retained (Figure 4.7.B).

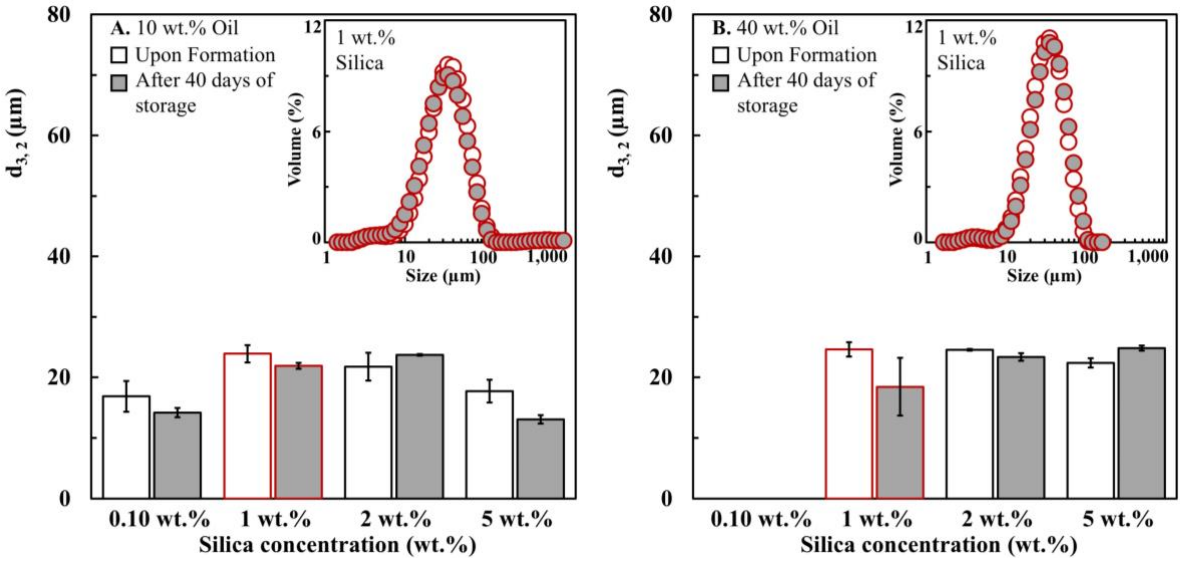

Figure 4.6. Long-term stability of emulsions manufactured following a single pass within the CIJs device (at a fixed jet flow rate of 352.75 g/min, i.e. corresponding to a $\bar{\varepsilon}_{th}$ (eq. 4.1) equal to ~5×10^3 for 10 wt.% (A) and 40 wt.% (B) oil fraction, respectively) as a function of the silica concentration; concentrations are shown in the graph. The open and solid (grey) bars represent the Sauter diameter ($d_{3,2}$) immediately after the CIJs processing and following the 40 days of storage, respectively. All data points are mean values (n=6) and error bars are reported as a single standard deviation. (Inset chart) Droplet size distributions for the corresponding dispersed phase mass fraction stabilised by 1 wt.% of silica, immediately after the CIJs processing (open symbols) and following the 40 days of storage (solid grey symbols).

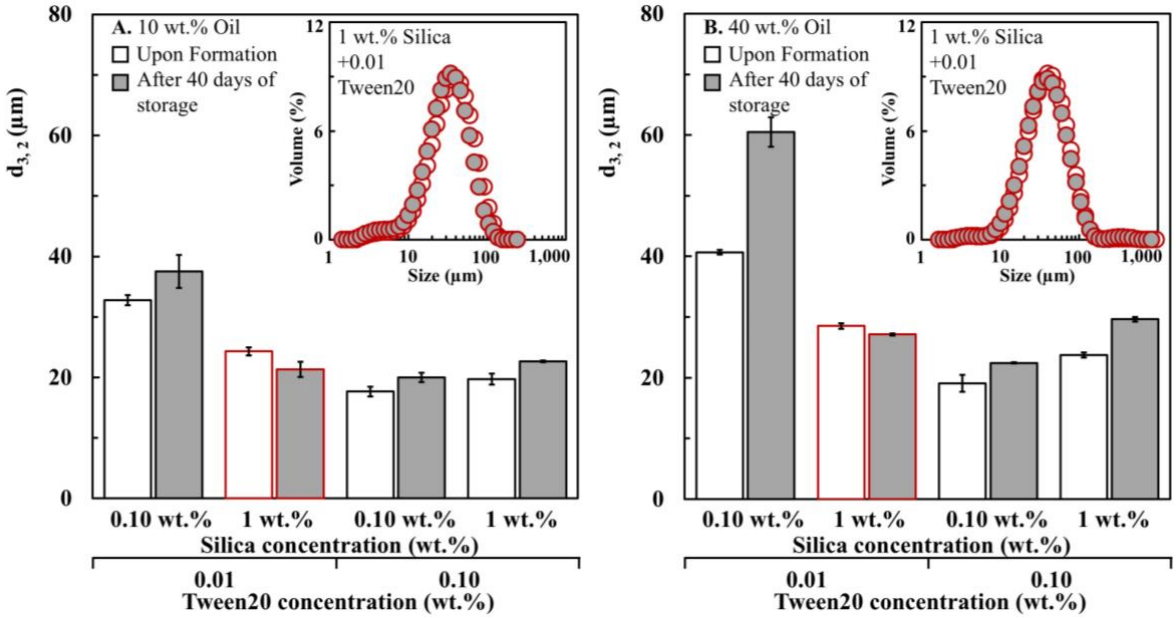

Figure 4.7. Long-term stability of emulsions manufactured following a single pass within the CIJs device (at a fixed jet flow rate of 352.75 g/min, i.e. corresponding to a $\bar{\varepsilon}_{th}$ (eq. 4.1) equal to ~$5\times10_3$ for 10 wt.% (A) and 40 wt.% (B) oil fraction, respectively) stabilised by mixed surfactant-particle emulsifier systems; concentrations are shown in the graph. The open and solid (grey) bars represent the Sauter diameter ($d_{3,2}$) immediately after the CIJs processing and following the 40 days of storage, respectively. All data points are mean values (n=6) and error bars are reported as a single standard deviation. (Inset chart) Droplet size distributions for the corresponding dispersed phase mass fraction stabilised 1 wt.% silica combined with 0.01 (A) and 0.10 (B) wt.% of Tween20, immediately after processing (open symbols) and following the 40 days of storage (solid grey symbols).

4.4. Conclusions

The present study reports for the first time on the preparation of o/w emulsions, stabilised by different concentrations of either Pickering particles alone or mixed emulsifier (surfactant and particles) formulations, using Confined Impinging Jets (CIJs). Systems resulting from the CIJs processing of both dilute (10 wt.%) and semi-concentrated (40 wt.%) pre-emulsions were produced over a range of CIJs hydrodynamic conditions (energy dissipation rates, $\bar{\varepsilon}_{th}$) as well as after multiple passes through the CIJs geometry (recirculation), and their long-term storage stability was assessed.

The average droplet diameter ($d_{3,2}$) of the particle-stabilised systems (for both 10 wt.% and 40 wt.% oil content) was only reduced (from that of their pre-emulsion predecessors) following

processing within the previously determined (17) optimal (in terms of $\bar{\varepsilon}_{th}$) CIJs operation window, reaching the smallest $d_{3,2}$ (~10μm) under fully turbulent conditions, regardless of the particle concentration used. Emulsions stabilised by the mixed (surfactant and particles) emulsifier formulations also followed this trend, with systems at the lowest concentration (0.01 wt.% Tween20 and 0.10 wt.% silica) being the only exception. The latter gave emulsions of either practically unchanged (at a 10 wt.% oil content) or increasing (at a 40 wt.% oil content) $d_{3,2}$ values at CIJs hydrodynamic conditions of higher $\bar{\varepsilon}_{th}$. Multi-passing of these systems through the CIJs geometry (at an intermediate, but still within optimal operation, fixed $\bar{\varepsilon}_{th}$) demonstrated that the original (1_{st} pass) emulsion droplet diameter is only further reduced following a second passage and that subsequent recirculation attempts had only a minimal effect on emulsion microstructure. In contrast to the requirement for multiple passes (at fixed hydrodynamic conditions) in typical emulsification processes in order to achieve the lowest emulsion droplet size possible, CIJs demonstrated that this can be realised at a much earlier processing stage and therefore at a reduced expenditure in terms of energy input. Finally, emulsion stability was shown to be driven by formulation rather than processing aspects. The concentration of the particle or mixed emulsifier stabilising intervention was mainly responsible for ensuring that emulsion stability was maintained over the studied 40 days storage period, while CIJs hydrodynamic conditions and multi-passing primarily control the final droplet size and droplet size distribution.

In conclusion, this study extends the effectiveness of CIJs as an easy-to-operate tool to promote a turbulent emulsification environment and allow for the manufacture of a large array of emulsions (including Pickering emulsions) under a wide range of processing conditions. The potential of CIJs to produce a wide spectrum of emulsion microstructures together with the

process's lower-energy credentials and capacity to deliver high product throughputs, are progressively enhancing its industrial applicability.

List of references

(1) Rayner M. *Scales and Forces in Emulsification*. In: Rayner M., Dejmek P., (eds.). *Engineering Aspects of Food Emulsification and Homogenisation*. 1st ed. Boca Raton: CRC press; 2015. p. 3-32.

(2) McClements D.J., Jafari S.M. *Improving emulsion formation, stability and performance using mixed emulsifiers: A review*. Advances in Colloid and Interface Science. 2018; 251: 55-79.

(3) Donsì F. *Chapter 11 - Applications of Nanoemulsions in Foods*. In: Jafari S.M., McClements D.J., (eds.). *Nanoemulsions*. 1st ed. Oxford: Academic Press; 2018. p. 349-77.

(4) Dickinson E. *Use of nanoparticles and microparticles in the formation and stabilization of food emulsions*. Trends in Food Science & Technology. 2012; 24(1): 4-12.

(5) Kralova I., Sjöblom J. *Surfactants used in food Industry: A review*. Journal of Dispersion Science and Technology. 2009; 30(9): 1363-83.

(6) Chevalier Y., Bolzinger M.-A. *Emulsions stabilized with solid nanoparticles: Pickering emulsions*. Colloids and Surfaces A: Physicochemical and Engineering Aspects. 2013; 439: 23-34.

(7) Binks B.P., Rodrigues J.A., Frith W.J. *Synergistic interaction in emulsions stabilized by a mixture of silica nanoparticles and cationic surfactant*. Langmuir. 2007; 23(7): 3626-36.

(8) Pichot R., Spyropoulos F., Norton I.T. *Mixed-emulsifier stabilised emulsions: Investigation of the effect of monoolein and hydrophilic silica particle mixtures on the stability against coalescence*. Journal of Colloid and Interface Science. 2009; 329(2): 284-91.

(9) Tcholakova S., Denkov N.D., Lips A. *Comparison of solid particles, globular proteins and surfactants as emulsifiers*. Physical Chemistry Chemical Physics. 2008; 10(12): 1608-27.

(10) Nesterenko A., Drelich A., Lu H., Clausse D., Pezron I. *Influence of a mixed particle/surfactant emulsifier system on water-in-oil emulsion stability*. Colloids and Surfaces A: Physicochemical and Engineering Aspects. 2014; 457: 49-57.

(11) Huang Y., Wang R., Wu Y., Gao Z., Dai C. *Study on stabilizing emulsion by mixing nano-silica and cationic surfactants with different chain length*. IOP Conference Series: Earth and Environmental Science. 2019; 218: 012071.

(12) Zafeiri I., Horridge C., Tripodi E., Spyropoulos F. *Emulsions co-stabilised by edible Pickering particles and surfactants: the effect of HLB value*. Colloid and Interface Science Communications. 2017; 17: 5-9.

(13) Jafari S.M., Assadpoor E., He Y., Bhandari B. *Re-coalescence of emulsion droplets during high-energy emulsification*. Food Hydrocolloids. 2008; 22(7): 1191-202.

(14) Lee L., Norton I.T. *Comparing droplet breakup for a high-pressure valve homogeniser and a Microfluidizer for the potential production of food-grade nanoemulsions*. Journal of Food Engineering. 2013; 114(2): 158-63.

(15) Kobayashi I., Mukataka S., Nakajima M. *Effect of slot aspect ratio on droplet formation from silicon straight-through microchannels.* Journal of Colloid and Interface Science. 2004; 279(1): 277-80.

(16) Vladisavljević G.T., Kobayashi I., Nakajima M. *Production of uniform droplets using membrane, microchannel and microfluidic emulsification devices*. Microfluidics and Nanofluidics. 2012; 13(1): 151-78.

(17) Tripodi E., Lazidis A., Norton I.T., Spyropoulos F. *On the production of oil-in-water emulsions with varying dispersed phase content using Confined Impinging Jet Mixers*. Industrial & Engineering Chemistry Research. 2019; 58(32): 14859-72.

(18) Chiou H., Chan H.-K., Prud'homme R.K., Raper J.A. *Evaluation on the use of Confined Liquid Impinging Jets for the synthesis of nanodrug particles*. Drug Development and Industrial Pharmacy. 2008; 34(1): 59-64.

(19) Siddiqui S.W., Zhao Y., Kukukova A., Kresta S.M. *Characteristics of a Confined Impinging Jet Reactor: energy dissipation, homogeneous and heterogeneous reaction products, and effect of unequal flow*. Industrial & Engineering Chemistry Research. 2009; 48(17): 7945-58.

(20) Siddiqui S.W., Norton I.T. *Oil-in-water emulsification using Confined Impinging Jets*. Journal of Colloid and Interface Science. 2012; 377(1): 213-21.

(21) Siddiqui S.W., Wan Mohamad W.A.F., Mohd. Rozi M.F., Norton I.T. *Continuous, high-throughput flash-synthesis of submicron food emulsions using a Confined Impinging Jet Mixer: effect of in situ turbulence, sonication, and small surfactants*. Industrial & Engineering Chemistry Research. 2017; 56(44): 12833-47.

(22) Dickinson E. *Food emulsions and foams: Stabilization by particles*. Current Opinion in Colloid & Interface Science. 2010; 15(1): 40-9.

(23) Walstra P. *Principles of emulsion formation*. Chemical Engineering Science. 1993; 48(2): 333-49.

(24) McClements D.J. *Food Emulsions: Principles, Practices and Techniques*. 3rd ed. Boca Raton: CRC press; 2016.

(25) Aveyard R., Binks B.P., Clint J.H. *Emulsions stabilised solely by colloidal particles*. Advances in Colloid and Interface Science. 2003; 100-102: 503-46.

(26) Binks B.P. *Particles as surfactants-similarities and differences*. Current Opinion in Colloid & Interface Science. 2002; 7(1): 21-41.

(27) Ravera F., Ferrari M., Liggieri L., Loglio G., Santini E., Zanobini A. *Liquid–liquid interfacial properties of mixed nanoparticle–surfactant systems*. Colloids and Surfaces A: Physicochemical and Engineering Aspects. 2008; 323(1): 99-108.

(28) Midmore B.R. *Synergy between silica and polyoxyethylene surfactants in the formation of o/w emulsions*. Colloids and Surfaces A: Physicochemical and Engineering Aspects. 1998; 145(1): 133-43.

(29) Vashisth C., Whitby C.P., Fornasiero D., Ralston J. *Interfacial displacement of nanoparticles by surfactant molecules in emulsions*. Journal of Colloid and Interface Science. 2010; 349(2): 537-43.

(30) Floury J., Desrumaux A., Lardières J. *Effect of high-pressure homogenization on droplet size distributions and rheological properties of model oil-in-water emulsions*. Innovative Food Science & Emerging Technologies. 2000; 1(2): 127-34.

(31) Qian C., McClements D.J. *Formation of nanoemulsions stabilized by model food-grade emulsifiers using high-pressure homogenization: Factors affecting particle size*. Food Hydrocolloids. 2011; 25(5): 1000-8.

(32) Tesch S., Gerhards C., Schubert H. *Stabilization of emulsions by OSA starches*. Journal of Food Engineering. 2002; 54(2): 167-74.

(33) Karbstein H., Schubert H. *Developments in the continuous mechanical production of oil-in-water macro-emulsions*. Chemical Engineering and Processing: Process Intensification. 1995; 34(3): 205-11.

Chapter 5

Comparison of the performance of high- and low-energy methods for the production of emulsions relevant to food

Abstract

This study aims to assess the performance of high- (high-pressure homogeniser, HPH; high-shear mixer, HSM) as well as of low-energy (confined impinging jets, CIJs; rotating membrane, RM) emulsification techniques over a broad range of processing parameters (average energy dissipation rate, $\bar{\varepsilon}_{th}$; flow regime; energy density, Ev; energy efficiency, EF; and residence time, t_{res}) for the production of dilute (10 wt.%) as well as more concentrated (40 wt.%) emulsions, in the presence of either surfactant or nanoparticles acting as the sole emulsifier. It was observed that during HPH, HSM and CIJs processing, emulsions were produced under a turbulent flow regime, contrarily to RM where the flow was laminar. The performance of the HPH was very much dependent on the type of emulsifier used, while all other techniques were practically unaffected by both emulsifier and oil phase content. Overall, the HPH treatment generated the highest $\bar{\varepsilon}_{th}$ and comparable Ev to the HSM. The CIJs operated at intermediate $\bar{\varepsilon}_{th}$ and Ev conditions, while RM exhibited the lowest values for both these parameters. The HPH produced the smallest droplet sizes ($d_{3,2}$) in the presence of surfactant, but could not provide emulsions below a 8 μm diameter when silica was used as the emulsifier. The CIJs and HSM gave emulsions with similar $d_{3,2}$ values, although under significantly different energy inputs. The RM produced emulsions with larger (than all other methods) droplets, but under significantly lower $\bar{\varepsilon}_{th}$ and Ev values. CIJs and the RM were the most energy efficient processes. For all techniques (with the exception of RM where recirculation was not performed), emulsion recirculation (under fixed hydrodynamic conditions) significantly affected droplet size distribution but only marginally reduced $d_{3,2}$. However, increasing the residence time within the emulsification apparatus (via recirculation), strongly decreased the EF of all processing techniques. The CIJs still remained the most energy-efficient method while HPH and HSM processing resulted in lower EFs with

their relative values dependent on the type of emulsifier used. Emulsion generation is an extremely important operation in foods and this study provides a concise but thorough evaluation of the processing principles, advantages and limitations of established (HPH, HSM) and emerging (CIJs and RM) emulsification techniques by comparing their performance over an extensive range of processing and formulation parameters.

5.1. Introduction

A number of emulsification techniques have been developed to produce emulsions within the context of foods. These can be broadly classified according to the level of energy required to homogenise the emulsion components (e.g. continuous and dispersed phases, emulsifier) (1). High-energy methods (e.g. high-shear mixers, high-pressure or ultrasonic homogenisers) are those mostly employed industrially and exploit the application of elevated levels of turbulence or cavitation (caused by shear, pressure, shock-waves or a combination of these) to produce fine emulsion droplets from a wide variety of raw materials (2). Despite their ease of operation, flexibility and high–throughput production, the major drawback of such high-energy techniques is their large energy demand (3). In fact, a substantial part of this energy input is dissipated as heat, which strongly reduces their (energy) efficiency and may result in undesirable temperature increases during manufacturing.

As possible alternatives to this group of techniques, low-energy methods (e.g. membrane or microchannel emulsification) have more recently received great attention. During membrane or microchannel emulsification, droplets are individually formed following their spontaneous detachment from the membrane pore or the microchannel junction, resulting in emulsion microstructures of very narrow droplet size distributions (4-6). Notwithstanding their potentially low energy requirement and the outstanding degree of control over the final emulsion microstructure (if compared to their high–energy counterparts), these methods, in their current configurations, are still characterised by low product throughputs, which makes their large scale implementation troublesome (4-6).

In contraposition to the above categories, Confined Impinging Jets (CIJs) represent an attractive solution possibly addressing some of the limitations associated with both groups of techniques. In CIJs, the collision of two jets within a confined environment (rather than the

application of high levels of shear or pressure) enables the highly–controlled and continuous turbulent production of emulsions at low energy inputs (7).

Given the growing number of emulsification operations, the choice of the most suitable one becomes increasingly complicated. Selection depends on a span of different parameters such as desired product throughput, type and concentration of raw material, required droplet size and droplet size distribution as well as energy expenditure during processing (among others) (1, 8). Viable strategies to compare the performance of different emulsification processes thus become more and more important. At present, such approaches focus on how processing parameters (such as energy dissipation rate, flow regime, energy density and energy efficiency) and formulation characteristics (such as dispersed phase content, and type/concentration of emulsifier) influence aspects of the resulting emulsion microstructure (such as average droplet size and droplet size distribution) (9, 10).

The energy dissipation rate ($\bar{\varepsilon}_{th}$) indicates the energy available per unit time and unit volume for droplet disruption (11). Under laminar flow conditions, the $\bar{\varepsilon}_{th}$ is a function of the continuous phase viscosity and the shear rate (12). In the turbulent regime, where the flow is chaotic, the smallest energy-bearing eddies generate the energy dissipation rate responsible for droplet formation (12). The Kolmogorov theory allows for the estimation of the size of the smallest eddies; also known as Kolmogorov eddy size, λ_k (13, 14). Based on a comparison between the λ_k and the resulting average emulsion droplet size ($d_{3,2}$) obtained upon processing, one can distinguish between Turbulent Inertial (TI) and Turbulent Viscous (TV) flow regime (15). In the former case, emulsion droplets are larger than the Kolmogorov eddy size ($d_{3,2} > \lambda_k$) and the drop diameter does not depend on either the dispersed phase mass fraction or the emulsion viscosity. In the latter case, the droplet size is smaller than the one predicted by the Kolmogorov theory ($d_{3,2} < \lambda_k$). In this flow regime, a smaller $d_{3,2}$ is observed

at higher continuous phase viscosities, thus suggesting that the TV regime usually results more effective (than the TI one) in producing smaller droplets.

The energy density (E_v) represents the energy input per unit time and unit volume (16). The concept of energy density has been extensively utilised in literature to compare emulsification methods (15, 17-19). It has been shown that E_v relates to the emulsion Sauter diameter (when plotted on a double logarithmic scale) through a linear dependency ($E_v \propto d_{3,2}^{-b}$). This relationship, also known as the process function, links an important microstructural parameter ($d_{3,2}$) to an (easy-to-measure) processing feature (E_v) (20). The characteristic slope, b, contains information about both the flow conditions and the type of apparatus used; e.g. b is ~0.35-0.4 and ~0.6 for High-Shear Mixing and High-Pressure Homogenisation, respectively, both under predominantly turbulent inertial flow conditions, and b ~1 for cross flow membrane emulsification under laminar flow regime (9, 20).

The energy efficiency (EF) describes the portion of the total energy input that actually contributes to the formation of the emulsion microstructure (8). The EF is defined as the ratio between the minimum amount of energy theoretically required to form an emulsion (proportional to the interfacial tension and the difference in interfacial area) over E_v.

In addition to processing parameters, the performance of emulsification methods can be evaluated for various formulation aspects, with the dispersed phase content and the type of emulsifier representing the most common parameters for comparison (9, 21). Several studies have evinced that, during processing, higher dispersed phase contents result in larger droplet sizes (22-24). In fact, the presence of a higher oil load can increase the frequency of droplet collisions and thus coalescence, if an inadequate amount of emulsifier is present to cover the newly-formed droplets.

Low-molecular weight surfactants as well as nanoparticles represent two main groups of emulsifiers typically employed in emulsion-based formulations (25). During processing, low-molecular weight surfactants quickly adsorb at the droplet interface facilitating droplet breakage due to their ability to reduce the oil-water interfacial tension (25). On the other hand, following their (almost) irreversible adsorption at the droplet interface (26, 27), nanoparticles form an interfacial layer that is more resistant (compared to surfactants) to coalescence events (26, 28). However, particles are not surface-active and because of their larger dimensions tend to exhibit slower interfacial adsorption kinetics. What is more, particle adsorption is predominantly driven by convection rather than diffusion and therefore their effectiveness as emulsifiers mainly relies on the emulsification method capacity to create processing conditions such as to promote their transport to the droplet interface (29).

The performance of specific emulsification methods has been extensively investigated in the literature for a wide range of formulation parameters and mostly compared based on the concept of the energy input (15, 18, 20, 30-34). Nevertheless, in-depth experimental studies comparing emulsification efficacy across different techniques for a broader spectrum of processing variables seem less available (to the best of the authors knowledge). This study aims to assess the performance of high- (high-pressure homogeniser, high-shear mixer) as well as of low-energy (confined impinging jets, rotating membrane) emulsification techniques over a broad range of processing parameters (average energy dissipation rate, $\bar{\varepsilon}_{th}$; flow regime; energy density, Ev; and energy efficiency, EF) for the production of dilute as well as more concentrated emulsions, in the presence of either surfactant or nanoparticles as the sole emulsifier.

5.2. Materials and methods

5.2.1. Materials

All oil-in-water emulsions were prepared using deionised water (from a reverse osmosis filtration system) as the solvent for the continuous phase and commercially available sunflower oil (viscosity = 50 mPa.s) as the dispersed phase. Both Polysorbate20 (Tween20; HLB = 16.7 and molecular weight = 1227.54 g/mol) and a 30 wt.% suspension of silica in water (Ludox HS; surface area = 220 m_2/g and density = 1.21 kg/L) were kindly provided by Sigma-Aldrich Company (UK) and used as emulsifiers.

5.2.2. Methods

5.2.2.1. Emulsifier dispersion in the continuous phase

For the dispersion of the surfactant in the continuous phase, the required concentration (1 wt.% of the total emulsion mass, 500 g) was dissolved in water and mixed using a magnetic stirrer for 10 min. For the preparation of the silica-in-water dispersion, appropriate amounts of the 30 wt.% Ludox solution were added to water in order to achieve the desired particle concentration (1 wt.% of the total emulsion weight, 500 g). This silica concentration was used for the preparation of all emulsions except those prepared using the rotating membrane, where a concentration of 3 wt.% was used instead. The initial pH of the solution (~10) was then lowered to ~2 using hydrochloric acid (HCl, 1M) and sodium hydroxide (NaOH, 1M). It has been previously shown that lowering the pH of the dispersion to pH 2 suppresses the negative charges exhibited by the Ludox particles at their native pH and allows for the successful Pickering stabilisation of o/w emulsions (26). The average particle size of the dispersion remained constant with a value of about 20 nm across the entire range of pH, as determined from Dynamic Light Scattering (Zetasizer, Malvern).

5.2.2.2. o/w emulsion preparation via different emulsification methods

A. High-pressure homogeniser

For the production of the 10 and 40 wt.% O/W emulsions via the High-Pressure Homogeniser (HPH) the desired amount of sunflower oil (total emulsion weight equal to 500 g) was initially added to the dispersion of water and emulsifier (prepared as described in section 5.2.2.1). The components were then pre-emulsified by means of a Silverson L5 Series Laboratory High-Shear Mixer, equipped with an emulsor screen of 33 mm in diameter, for 4 min at 2000 RPM at room temperature (22 ˚C). Following the pre-treatment, the coarse emulsion was then processed through a High-Pressure Homogeniser (NS1001L PANDA, GEA Niro Soavi, Italy) at a pressure varying between 100 and 800 bar. To study the effect of the residence time, the produced emulsions were recirculated at constant low (100 bar), intermediate (500 bar) and high (800 bar) pressure up to 4 times.

B. High-shear mixer

For the production of the 10 and 40 wt.% o/w emulsions via the High-Shear Mixer (HSM) the desired amount of sunflower oil (total emulsion weight equal to 500 g) was initially added to the dispersion of water and emulsifier (prepared as described in section 5.2.2.1). The components were then emulsified by means of a Silverson L5 Series Laboratory High-Shear Mixer, equipped with an emulsor screen of 33 mm in diameter, for 4 min at a fixed rotational speed (between 3000 and 9000 RPM) at room temperature (22˚C). To study the effect of the residence time, emulsions were mixed at constant low (3000 RPM), intermediate (6000 RPM) and high (9000 RPM) rotational speed for 4, 8,12 and 16 min.

C. Confined Impinging Jets

For the production of the 10 and 40 wt.% o/w emulsions via the Confined Impinging Jets (CIJs) the desired amount of sunflower oil (total emulsion weight equal to 500 g) was initially added to the dispersion of water and emulsifier (prepared as described in section 5.2.2.1). The components were then pre-emulsified by means of a Silverson L5 Series Laboratory High-Shear Mixer, equipped with an emulsor screen of 33 mm in diameter, for 4 min at 2000 RPM at room temperature (22 ˚C). Following the pre-treatment, the coarse emulsion was then processed through the CIJs geometry used in previous studies (35, 36), by means of a single pulse-less micro-pump (external gear pump) with jet mass flow rate varying from 176 to 702 g/min. Prior impingement, the flow was split into two equal streams by using a Y-junction. To study the effect of the residence time, the produced emulsions were recirculated at constant low (176 g/min), intermediate (440 g/min) and high (702 g/min) jet mass flow rate up to 4 times.

D. Rotating Membrane

The experiments were carried out by using a tubular, hydrophilic SPG membrane of 6.1 μm as the mean pore size supplied by SPG Technology Co. Ltd., Miyazaki, Japan. The membrane had diameter and length equal to 10 and 45 mm, respectively, corresponding to an effective surface area of 14.1 cm^2. The membrane wall thickness was approximately 1 mm. The membrane was equipped on a IKA Eurostar digital overhead stirrer and positioned in the processing vessel (with a diameter corresponding to 100 mm) containing the dispersion of water and emulsifier (prepared as described in section 5.2.2.1). The sunflower oil was pushed through the pores at a constant pressure (2 bar) while the membrane rotational speed was varied between 500 and 2000 RPM. The mass of sunflower oil was recorded over time and

the experiment was stopped when the desired amount of dispersed phase corresponding to a concentration of either 10 or 40 wt.% was reached. Emulsion batch sizes varying between 40 and 200 g were produced. The RM experimental setup employed for this study is described more in more detail in earlier publications (37, 38).

E. Note on the evaluation of the effect of the residence time on the formation of emulsion microstructures via the different techniques

While in continuous emulsification techniques (e.g. HPH and CIJs) this can be accomplished by recirculating a number of times the initially produced emulsions through the homogeniser or the impingement chamber, in a batch configuration (such as the HSM employed here) this can be achieved by extending the period over which mixing takes place. While for the former (HPH and CIJs), a recirculation step (n) can be easily defined to correspond to the physical passing of an emulsion through the processing chamber of each device, in the case of the HSM an effective recirculation step can be instead expressed as the ratio of any prolonged mixing/residence time (t_{res}) over a specific 'initial' residence time ($t_{res,o}$); in the present study a $t_{res,o}$ value of 4 minutes was chosen and multiples of this (up to four times) were used as the prolonged t_{res} (8, 12 and 16 min). It is worth noting that the manner by which the effective *n* is defined for HSM processing also applies to HPH and CIJs operation; the residence time (t_{res}) of an emulsion following each recirculation step *n* through the turbulent environment created in the HPH or CIJs, will obviously be $n \times t_{res,o}$, where $t_{res,o}$ the initial (first pass) residence time.

In the RM, the dispersed phase is pushed through the membrane pores into the continuous phase to form the emulsion (also known as direct emulsification) (39, 40). The (eventual) recirculation of the newly created emulsion would not replicate the same processing

conditions experienced during the first step, since an already formed emulsion (and not the pure oil phase) would be forced through the membrane pores. This is conceptually different from the way the recirculation occurs in the other methods. In fact, for the case of both the HPH and the CIJs, an emulsion (either rough or already processed) experiences the same turbulent environment at each pass, whereas in the HSM, the emulsion components are mixed under the same rotational speeds for different time lengths. What is more, in the RM, the (potential) passage of the newly formed emulsion through the pores would not occur under the same conditions as the direct emulsification, due to the formation of a layer of oil droplets on the upstream side of the membrane, which increases the resistance to the passage of droplets. Therefore, the effect of the residence time on the emulsion recirculation was not considered for the RM.

5.2.2.3. Droplet size measurements

The measurement of droplet size and droplet size distribution were carried out by using a Mastersizer 2000 (Malvern Instruments). Samples were diluted to 3 vol.% in order to avoid multiple-light scattering. Samples were tested three times at room temperature (22˚C) and an average was calculated. Each experiment was repeated twice.

5.2.2.4. Interfacial tension measurements

The equilibrium interfacial tensions (γ) of the oil-water interface both without and in the presence of the emulsifiers, Figure 5.1, were measured by using a K11-Force Tensiometer (Krüss, GmbH) equipped with a Wilhelmy plate at room temperature (22˚C) and repeated in triplicates. Upon addition of either 1 wt.% or 3 wt.% of silica as the emulsifier, the interfacial tension remained similar to the one of the plain oil-water system. Differently, the γ decreased

to ~5 mN/m in the presence of 1 wt.% of Tween20. The results are in excellent agreement with the literature values.

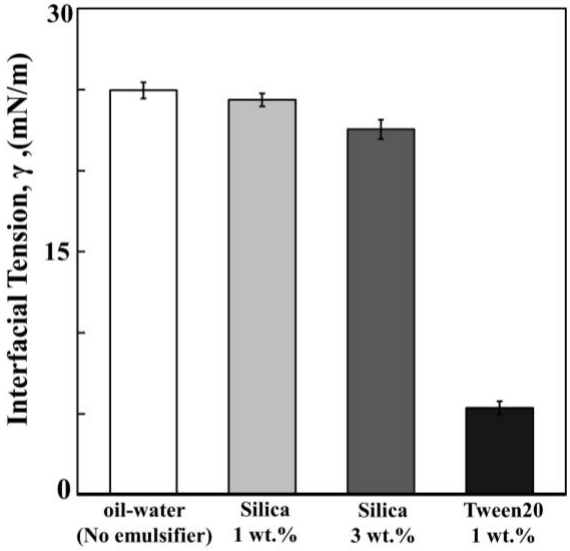

Figure 5.1. Dynamic interfacial tension (γ) data for the plain oil-water interface in the absence of emulsifier and in the presence of 1 wt.% of Tween20, 1 wt.% and 3 wt.% of silica. Each experiment was repeated three times.

5.2.2.5. Theoretical estimation of the average energy dissipation rate in the different emulsification methods

A. High-pressure homogeniser

In a High-Pressure Homogeniser (HPH), the average energy dissipation rate ($\bar{\varepsilon}_{th}^{HPH}$) generated within the apparatus can be theoretically estimated by the energy associated with the homogenisation pressure (P_h) and the emulsion volumetric flow rate (Q) over the HPH volume of the valve (V_{HPH}) where the emulsion experiences the turbulent forces and the fluid density (ρ_{em}) (33, 34):

$$\bar{\varepsilon}_{th}^{HPH} = \frac{P_h Q}{\rho_{em} V_{HPH}} \qquad (5.1)$$

According to the manual provided by the manufacturer for the HPH employed in this investigation the V_{HPH} can be assumed to be equal to $1x10^{-5}$ m^3.

B. High-shear mixer

In a High-Shear Mixer (HSM), the average energy dissipation rate ($\bar{\varepsilon}_{th}^{HSM}$) generated within the apparatus can be theoretically estimated by considering the following relationship (41-43):

$$\bar{\varepsilon}_{th}^{HSM}=K_p\ \rho_c N^3 D^5/m_{em} \qquad (5.2)$$

with ρ_c the continuous phase density, N the revolutions per second and D the impeller diameter, and m the total mass of the emulsified ingredients (500 g for the case investigated here). The constant K_p is termed as the power number and is constant (=2.1, for the emulsor screen employed used in this study) for Reynolds numbers above 10^4 (41-43). The Reynolds number (Re_{HSM}) in a High-Shear Mixer is defined as follows:

$$Re_{HSM}=\frac{\rho_c\ N\ D^2}{\eta_c} \qquad (5.3)$$

with η_c the continuous phase viscosity.

Table 5.2 demonstrates that the $Re_{HSM} > 10^5$ across the entire range of HSM processing conditions employed in this study.

Table 5.2. High-Shear Mixer Reynolds number (Re_{HSM}; eq. 5.3) as a function of the impeller revolutions per minute.

Revolutions per Minute (RPM)	**Re_{HSM}**
3000	$5.45x10^6$
4500	$8.17x10^6$
6000	$1.09x10^7$
7500	$1.36x10^7$
9000	$1.63x10^7$

C. Confined Impinging Jets

In a Confined Impinging Jets (CIJs), the average energy dissipation rate ($\bar{\varepsilon}_{th}^{CIJs}$) generated from the jet collision can be theoretically estimated by the energy associated with the pressure (P_{coll}) at which the two jets collide with a volumetric flow rate (Q_{jet}) within the CIJs mixing chamber volume (V_{CIJs}) (44):

$$\bar{\varepsilon}_{th}^{CIJs} = \frac{2\, Q_{jet}\, P_{coll}}{\rho_c V_{CIJs}} \qquad (5.4)$$

D. Rotating Membrane

For the case of laminar flow the average energy dissipation rate ($\bar{\varepsilon}_{th}^{RM}$) can be theoretically estimated as a function of the continuous phase viscosity, the shear rate ($\dot{\gamma}$) experienced by the droplets and the continuous phase viscosity (η_c) as well as the continuous phase density (ρ_c):

$$\bar{\varepsilon}_{th}^{RM} = \frac{\dot{\gamma}^2\, \eta_c}{\rho_c} \qquad (5.5)$$

In the Rotating Membrane the shear rate generated by the rotation of the membrane can be calculated as follows (38, 45):

$$\dot{\gamma} = \frac{\pi\, R_M N}{15\,(R_V^2 - R_M^2)} \qquad (5.6)$$

with R_V and R_M the radii of the vessel and membrane, respectively, while N represents the revolution per minute of the rotating membrane.

In the RM, assessment of the flow regime can be conducted through the calculation of both the Reynolds number (Re_c) of the continuous phase and the Taylor number (Ta) (38, 45):

$$Re_c = \frac{\omega\, R_M\, \rho_c (R_V - R_M)}{\eta_c} \qquad (5.7)$$

$$Ta = Re_c \sqrt{\frac{2(R_V - R_M)}{(R_V + R_M)}} \qquad (5.8)$$

with ω the angular velocity of the membrane surface.

Figure 5.2 demonstrates that both the Reynolds and Taylor numbers are contained within the boundaries (2100 and 800, respectively) delimiting the regions of laminar flow (46, 47). In the RM, laminar conditions are usually observed for narrow vessel diameters, more viscous continuous phase or low rational speeds (5, 37).

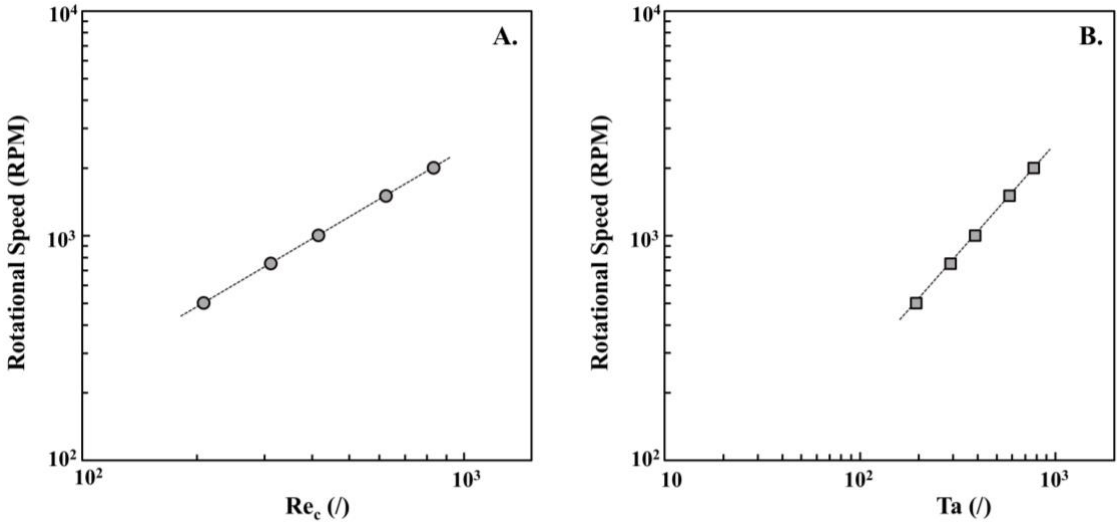

Figure 5.2. Influence of the membrane rotational speed on the (A) continuous phase Reynolds (Re_c; eq. 5.7) and (B) Taylor (Ta; eq. 5.8) numbers. In both figures, the lines only represent a guide for the reader's eye.

5.2.2.6. Theoretical estimation of the Kolmogorov eddy size

From the Kolmogorov theory it is possible to estimate the average size of the smallest eddies (λ_k) contributing to the droplet disruption through the following relationship:

$$\lambda_k = \varepsilon_{th}^{-1/4} \eta_c^{3/4} \rho_c^{-3/4} \qquad (5.9)$$

5.2.2.7. Theoretical estimation of the energy density in the different emulsification methods

A. High-pressure homogeniser

In a High-Pressure Homogeniser (HPH), the energy density (E_V^{HPH}) can be assumed equal to the homogenisation pressure, P_{HPH} (20):

$$E_V^{HPH} = P_{HPH} \quad (5.10)$$

B. High-shear mixer

In a High-Shear Mixer (HSM), the energy density (E_V^{HSM}) can be estimated by considering the time required to mix the components (t_{res}), the average energy dissipation rate generated upon mixing ($\bar{\varepsilon}_{th}^{HSM}$; eq. 5.2) and the continuous phase density (ρ_c) (43):

$$E_V^{HSM} = t_{res}\, \bar{\varepsilon}_{th}^{HSM} \rho_c \quad (5.11)$$

C. Confined Impinging Jets

In a Confined Impinging Jets (CIJs), the energy density (E_V^{CIJs}) can be assumed equal to the pressure at which the jet collision takes place, P_{CIJs} (i.e. the pressure imposed by the gear pump):

$$E_V^{CIJs} = P_{CIJs} \quad (5.12)$$

D. Rotating Membrane

In a Rotating Membrane (RM), the energy density (E_V^{RM}) can be estimated by considering the time required to reach the desired amount of dispersed phase (t_{dp}) in the vessel, the average

energy dissipation rate ($\bar{\varepsilon}_{th}^{RM}$; eq. 5.5) experienced by the droplets as consequence of the membrane rotation and the continuous phase density (ρ_c) (1):

$$E_V^{RM} = t_{dp}\ \bar{\varepsilon}_{th}^{RM} \rho_c \qquad (5.13)$$

E. Comparison of the energy densities resulting from the inclusion of the pre-emulsification stage

Differently from the HSM and RM, where emulsification takes place starting from the pure oil and water phases, both the HPH and the CIJs involve the processing of a pre-emulsion. As explained in section 5.2.2.2, for the preparation of the pre-emulsion, water, oil and emulsifier are roughly emulsified in a high-shear mixer. In principle, the presence of an additional step prior homogenisation may increase the overall energy input. Figure 5.3 confronts the HPH and the CIJs energy density with ($E_v + E_V^{PRE}$) and without (E_v) the inclusion of the energy required for the pre-emulsification stage of both 10 and 40 wt.% o/w emulsions. The results clearly indicates that the energy densities of both techniques remained practically unchanged by the inclusion of the pre-emulsification stage (for both oil dispersed phase contents). For this reason, the values of the single E_v will only be used in the result section 5.3.2, which will compare the performance of the manufacturing techniques based on the concept of E_v.

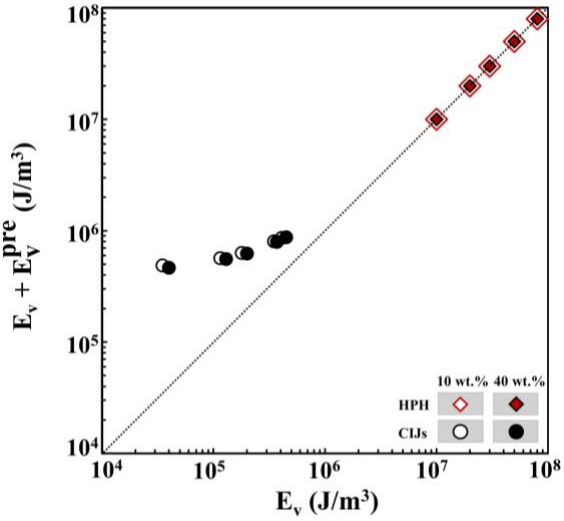

Figure 5.3. Comparison of the energy densities with (E_v + E_V^{PRE}) and without (E_v) the inclusion of the energy required for the pre-emulsification stage of both 10 (empty symbols) and 40 (solid symbols) wt.% o/w emulsions in the case of both the High-Pressure Homogeniser, HPH (diamonds), and the Confined Impinging Jets, CIJs (circles).

5.2.2.8. Theoretical estimation of the energy efficiency in the different emulsification methods

The energy efficiency (EF) of an emulsification method can be computed by comparing the minimum energy (E_{th}) theoretically required to form the emulsion and the energy density of the emulsification apparatus (evaluated as explained in section 5.2.2.7) (8):

$$EF = \frac{E_{th}}{E_v} \qquad (5.14)$$

The E_{th} can be estimated as follows:

$$E_{th} = \gamma \Delta A = \gamma\, 6\, \phi \left(\frac{1}{d_{3,2|AP}} - \frac{1}{d_{3,2|Coarse}} \right) \qquad (5.15)$$

with γ the interfacial tension, ϕ the dispersed phase volumetric fraction, ΔA the difference in interfacial area or the difference in the reciprocal of the Sauter diameters of the emulsions after processing ($d_{3,2|AP}$) and the Sauter diameter of the coarse pre-emulsion ($d_{3,2|Coarse}$). In

cases such as the HSM and the RM, where emulsification starts from two distinct phases, the term $1/d_{3,2|Coarse}$ is assumed equal to zero.

For the estimation of the EF following the exposure of the emulsions to longer residence times, both eq. 5.14 and 5.15 can be modified as follows:

$$EF= \frac{E_{th}}{n\, E_v} \qquad (5.16)$$

$$E_{th}= \gamma\, \Delta A= \gamma\, 6\, \phi\, \left(\frac{1}{d_{3,2|AP}} - \frac{1}{d_{3,2|Coarse}}\right) \qquad (5.17)$$

with *n* representing the recirculation step, while the $d_{3,2|n+1}$ and the $d_{3,2|n}$ the Sauter diameters resulting from recirculation at *n+1* and *n*, respectively.

5.3. Results and discussion

5.3.1. Impact of the energy dissipation rate and flow regime on the emulsion droplet size

Figure 5.4 presents the effect of the theoretically calculated mean energy dissipation rate ($\bar{\varepsilon}_{th}$; section 5.2.2.5.) on the average droplet size ($d_{3,2}$) of both 10 and 40 wt.% (oil content) o/w emulsions formed using either the High–Pressure Homogeniser (HPH), High–Shear Mixer (HSM), Confined Impinging Jets (CIJs) or the Rotating Membrane (RM) device. Emulsions were stabilised by either 1 wt.% Tween20 (Figure 5.4.A) or by 1 wt.% silica (Figure 5.4.B), with the only exception being the particle-stabilised emulsions produced via RM (for both oil contents). In this case, because the systems rapidly phase separated following membrane processing, the concentration of silica particles was increased to 3 wt.%, which enabled the production of stable emulsions.

The data in Figure 5.4.A show the variation of the Sauter diameter with $\bar{\varepsilon}_{th}$ for all surfactant-stabilised o/w emulsions; containing either 10 or 40 wt.% of dispersed phase. The smallest droplet sizes were observed using the HPH, under the largest $\bar{\varepsilon}_{th}$ (10^6-10^8 W/Kg) compared to the other methods. Typical values for the $\bar{\varepsilon}_{th}$ of a HPH are found within the range 10^6-10^{10} W/Kg, depending on the pressure, the HPH geometrical configuration and the properties of the to-be-processed materials (48, 49). The $d_{3,2}$ resulting from the HPH decreased with the homogenisation pressure independently on the oil mass fraction. However, a higher oil load induced the formation of larger droplets.

In comparison to HPH, CIJs and HSM produced larger droplet sizes but at lower levels of energy dissipation rate; $\bar{\varepsilon}_{th}$ values are similar to those found in literature for both techniques (7, 44, 49, 50). In both cases the smallest droplet size was observed at higher rotational speeds (in the HSM) or jet flow rates (in the CIJs). The average droplet sizes of emulsions formed in the high-shear mixer were smaller than those produced in the CIJs, although the $\bar{\varepsilon}_{th}$ levels

reached in the latter were significantly higher. The CIJs is a continuous processing method with notably short residence times (~10^{-3} s) (51). On the contrary, under the batch HSM configuration employed in this study, emulsions were subjected to (although lower compared to the CIJs) $\bar{\varepsilon}_{th}$ over a longer time period (4 min), which may explain the observed differences in the $d_{3,2}$. In addition, a higher dispersed phase content (40 wt.%) did not induce any changes to the Sauter diameter of emulsions obtained from the HSM. In this case, it seems that the final emulsion $d_{3,2}$ is mainly affected by the processing conditions established during operation. In the case of the CIJs, the same increase in dispersed phase resulted in a slightly higher $d_{3,2}$ at low $\bar{\varepsilon}_{th}$ (i.e. lower jet flow rates) with such differences completely disappearing towards the higher range of the applied energy dissipation rates.

The RM generated the largest droplet sizes but at much lower energy dissipation rates compared to all other techniques. The $d_{3,2}$ was slightly reduced at higher membrane rotational speeds and no significant differences in droplet size were observed after increasing the dispersed phase content.

Figure 5.4.B depicts the variation of the $d_{3,2}$ with the $\bar{\varepsilon}_{th}$ for (10 and 40 wt.%) o/w emulsions stabilised by silica nanoparticles produced via the different techniques. If compared to Figure 5.4.A, emulsions produced via the HPH presented a significantly larger Sauter diameter. What is more, the $d_{3,2}$ remained practically constant (~8 and ~11 μm for 10 and 40 wt.% oil contents, respectively) across the entire range of pressures. Not surprisingly, emulsions with an average drop diameter similar or below 1 μm could not be formed, analogously to the case of the Tween20-stabilised emulsions (Figure 5.4.A). In the literature, it has been well accepted that to effectively stabilise emulsion droplets the nanoparticle size must be at least 10 times smaller (52). Although, the silica nanoparticles used in this study had a an average diameter equal to ~20 nm (section 5.2.2.1), there are numerous reports

suggesting that the particulate entities actually involved in the mechanism of droplet stabilisation are particle aggregates of mean diameter 100 nm and above (53, 54). Taking into account this information, it is therefore reasonable to expect the trend observed in Figure 5.4.B. In fact, while the tendency of the HPH is to form small droplets (as observed in Figure 5.4.A for the case of emulsions stabilised by the surfactant), these are probably not sufficiently covered by the nanoparticles (or nanoparticle aggregates) during processing, which may therefore promote re-coalescence events. What is more, particles are not surface-active (Figure 5.1), thus making the droplet size reduction upon processing more challenging if compared to the case of surfactants. In addition, the fact that the $d_{3,2}$ remains constant over the entire pressure range could also imply that the $d_{3,2}$ obtained is the smallest achievable in the HPH used in this study with this emulsifier at the given concentration (for both oil contents).

The Sauter diameter of emulsions obtained through the HSM showed a different trend. For the 10 wt.% o/w emulsions, the $d_{3,2}$ decreased from ~24 μm to ~ 4 μm as the highest rotational speed was approached. For the 40 wt.% the smallest droplet size observed was equal to ~7 μm. In both cases, in the region of high $\bar{\varepsilon}_{th}$, emulsions presented droplet sizes smaller than the ones attained by HPH. The observed difference probably occurred because, even for the case of emulsions stabilised by surfactant (Figure 5.4.A), which presented a lower interfacial tension (Figure 5.1), the $d_{3,2}$ produced by the HSM remained above 1 μm across the entire range of $\bar{\varepsilon}_{th}$, differently from the same case but for the HPH.

The change in the emulsifier did not affect the processing performance of CIJs. While at lower jet flow rates, a higher dispersed phase content resulted in a larger $d_{3,2}$, the smallest droplet size (~15 μm) was observed at higher $\bar{\varepsilon}_{th}$ regardless of the oil load. As previously

discussed, the CIJs produced slightly larger droplet size than the HSM, although over a range of higher $\bar{\varepsilon}_{th}$.

Droplet stabilisation by means of nanoparticles altered the RM performance (compared to Figure 5.4.A). For both oil mass fractions, the resulting $d_{3,2}$ were larger than those obtained from all the other techniques (using the same emulsifier, Figure 5.4.B) and RM in the case of surfactant-stabilised emulsions (Figure 5.4.A). When 10 wt.% o/w emulsions were formed through the rotating membrane, the $d_{3,2}$ decreased to a minimum (~65 μm) at increasing rotational speeds. Differently, for a higher dispersed phase load, the Sauter diameter initially underwent an increase to then be reduced as the rotational speed was progressively incremented. Compared to low-molecular weight surfactants, transport of nanoparticles to the drop interface occurs more slowly (55). In the RM, due to the absence of turbulence (differently to the other methods observed in this study), droplet stabilisation is mainly limited by the capacity of the rotation of the membrane to generate a mixing environment where the nanoparticle convective transport is facilitated. Although this is observed for the 10 wt.% o/w emulsions, as the oil content increased the trend varied. At 40 wt.%, the $d_{3,2}$ increased at low rotational speeds probably because the mild mixing conditions combined with the larger interfacial area could not promote an effective droplet stabilisation. However, at higher rotational speeds, the transport of particles to the interface was very likely assisted, which thus also enabled the (observed) $d_{3,2}$ reduction. It must be noted that, for SPG membranes, the expected average droplet size should result about 3 times larger than the pore size (4-5), which is ~20-30 μm for the particular case of this study. This is in strong disagreement with the results observed in Figure 5.4 for the RM for both emulsifiers. It may be possible that due to the very low levels of turbulence achieved during operation as well as to the small vessel diameter where the dispersed phase was pushed (very likely not allowing

dispersion of the oil droplets far from the rotating membrane), emulsifier adsorption at the interface could not result in a stabilisation such as to hinder the formation of larger emulsion droplets; with this effect being even more exacerbated for the case of emulsions stabilised by nanoparticles (i.e. slow adsorbing emulsifier agents), where even larger $d_{3,2}$ were observed (Figure 5.4.B).

To determine the type of flow regime established during emulsification, the $d_{3,2}$ values of all emulsions (for both oil contents) obtained from the energy-intensive methods (HSM and HPH) and from the CIJs were compared with the theoretically calculated Kolmogorov eddy size, λ_k (Figure 5.4.A-B). Such comparison could not be carried out for systems resulting RM processing, since it was earlier shown (Figure 5.2) that under the current setup and processing conditions a laminar flow regime is expected. In addition, this eventual comparison would not fundamentally be correct, since the mechanism of droplet formation in the RM is not based on the drop fragmentation.

The $d_{3,2}$ of surfactant-stabilised emulsions obtained from the high-pressure treatment showed similar values to the ones of the Kolmogorov eddy size for both oil mass fractions (Figure 5.4.A). From these results, it is difficult to clearly establish the dominant type of flow regime taking place during homogenisation. Due to its widespread use in industry, several works have focused on the HPH emulsification performance. It has been shown that the HPH efficiently operates in the TI-regime when the dispersed phase has a viscosity below 500 mPa.s (33). At higher oil viscosities, viscous turbulent forces were the predominant mechanism driving emulsion formation in the homogeniser cavity (33). Although the majority of existing literature confirms that turbulence (whether viscous or inertial) is the main mechanism causing droplet fragmentation, there are still some studies suggesting that, depending on the processing conditions, cavitation effects may also take place and could have

a significant contribution (56, 57). In particular it was proposed that the intensity of both phenomena probably increases at larger homogenisation pressures (24).

For the HSM, the $d_{3,2}$ of both 10 and 40 w.% o/w emulsions were smaller than the corresponding λ_k (Figure 5.4.A). Based on this, it was possible to conclude that viscous turbulent forces encouraged emulsion formation during high-shear mixing. In literature, a great deal of attention has focused on developing suitable scaling rules based on the existing theory of turbulence. Several works showed that batch HSM emulsification is mostly governed by turbulent mechanisms (except in the case of very viscous material, where the flow regime may be laminar) (58), and both TI or TV flow regimes were observed depending on a large number of processing (e.g. rotational speed, impeller geometry and dimensions) as well as formulation (dispersed phase content, materials viscosity) aspects (42, 49, 59).

For the CIJs the drop size data obtained are larger than the respective λ_k across the entire range of energy dissipation rates, thus indicating that emulsification occurs in the TI regime. Other studies on the use of CIJs to form surfactant-stabilised systems of low dispersed phase content (up to 10 wt.%) also suggest the occurrence of the same type of turbulent conditions (60). In another publication utilising CIJs for emulsification, a transition from a TI to a TV flow regime was observed as the dispersed phase content was progressively increased from 10 to 60 wt.% (7).

Figure 5.4.B compares the $d_{3,2}$ values of silica-stabilised emulsions to the corresponding λ_k value(s). For both the HSM and the CIJs, similar trends to those observed in Figure 5.4.A were shown, while for the HPH the $d_{3,2}$ was significantly larger than the predicted eddy size. In any of these cases, whether a similar behaviour to that seen in Figure 5.4.A was maintained (HSM and CIJs) or not (HPH), it is not possible to infer on the flow regime during emulsification. In principle, although variations in the Sauter diameter could suggest

alterations to the emulsification regime, the differences in $d_{3,2}$ are only observed due to the change of emulsifier type. In particular, one must note that the majority of the theoretical description of emulsification was derived for surfactant-stabilised systems.

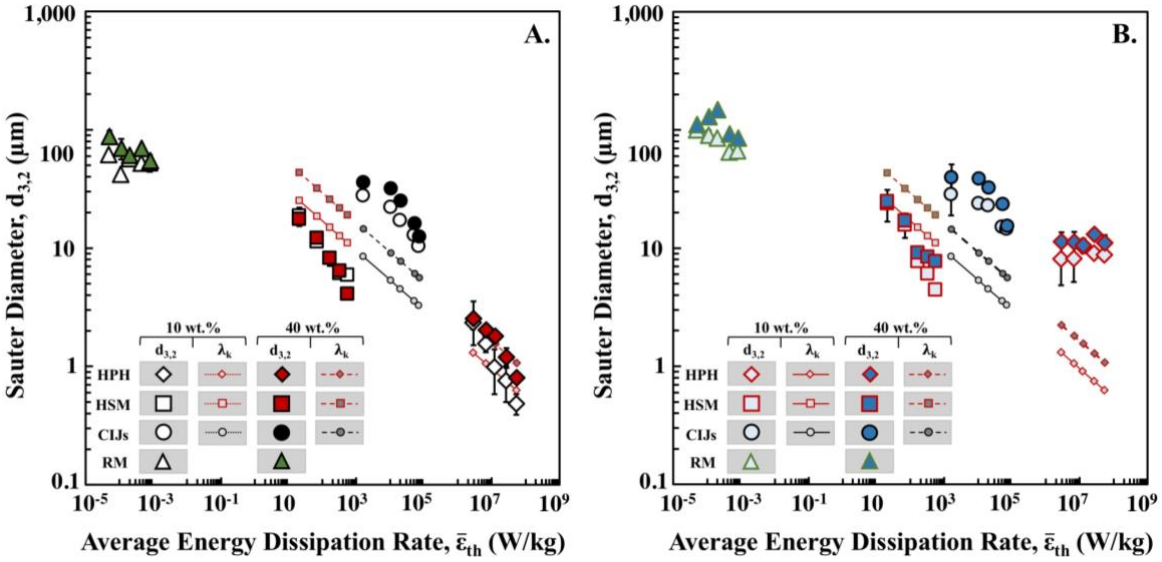

Figure 5.4. Effect of the theoretically estimated energy dissipation rate ($\bar{\varepsilon}_{th}$; calculated as explained in section 5.2.2.5) on the Sauter diameter ($d_{3,2}$) of Tween20- (A) and silica- (B) stabilised 10 and 40 wt.% o/w emulsions produced via High-Pressure Homogeniser (HPH), High-Shear Mixer (HSM), Confined Impinging Jets (CIJs) and Rotating Membrane (RM) treatments. For each turbulence-based processing technique (HPH, HSM and CIJs), the theoretical Kolmogorov eddy size, λ_k; eq. 5.9) is also reported; solid and dotted lines for each λ_k are only shown as a guide. No λ_k is instead shown for the RM which instead operates under laminar flow regime conditions (Figure 5.2). Symbols are reported in each figure's legend. All data points are mean values (n=6) and error bars represent one standard deviation of the mean; where not visible, error bars are smaller than the used symbols.

5.3.2. Impact of the energy density on the emulsion microstructure

5.3.2.1. Impact of the energy density on the emulsion microstructure during processing

Figure 5.5.A-B depicts the Sauter diameter ($d_{3,2}$) of both 10 and 40 wt.% o/w emulsions stabilised by either surfactant (Figure 5.5.A) or nanoparticles (Figure 5.5.B) versus the energy density (E_v) of each emulsification apparatus investigated in this study. The energy density for each setup was calculated following the methodology explained in section 5.2.2.7. For each

data set, the best curve fit is also represented and the value of the exponent, *b*, of the process function ($E_v \propto d_{3,2}^{-b}$) is reported in both figure legends.

In surfactant-stabilised emulsions, the lowest droplet size was obtained with the HPH, Figure 5.5.A. Emulsions produced via the HSM treatment presented a larger $d_{3,2}$ yet within a similar range of E_v ($10^6 – 10^8$ J/m^3). In this respect, the HPH resulted more efficient than the HSM in the production of smaller droplets. Within the HPH cavity, the energy is dissipated in much shorter times (if compared to the HSM), thus causing larger energy dissipation rates (Figure 5.4.A-B), and in turn smaller droplet sizes (11).

Differently, in the HSM a larger portion (if compared to the HPH) of the total energy input is dissipated as a heat and does not contribute to the droplet formation (11). In addition, the droplet size reduction in the HPH showed a steeper dependency with the E_v, if compared to the HSM one, as demonstrated by the characteristic exponents. The values of *b* in the HPH were 0.55 and 0.75 (for 10 and 40 wt.% as the dispersed phase content, respectively) while in the HSM, the exponent assumed values of 0.36 and 0.42. For the HSM treatment, typical *b* values are expected to be close to 0.4, in agreement with our findings (15, 18, 20, 31). For the HPH, *b* usually assumes values close to 0.6, although this parameter may present a slight more flexible variability depending on the HPH valve geometrical characteristics (15, 18, 20, 31).

Emulsification via the CIJs resulted in similar droplet sizes to those observed after the high-shear processing but at significantly lower energy densities ($10^4 – 10^6$ J/m^{3}compared to $10^6 – 10^8$ J/m^3 observed in both the HSM and the HPH). Within this range, the droplet size reduction induced by the CIJs followed a similar trend to the HSM, as demonstrated by the values of the exponent *b*, i.e. 0.38 and 0.42 for 10 and 40 wt.% oil, respectively.

Emulsification via the membrane treatment produced the largest $d_{3,2}$ if compared with the droplet size obtained with all the other methods, yet within a range of E_v (50-5x10^3 J/m^3) considerably lower. For both oil mass fractions, higher membrane rotational speeds did not induce any fast droplet size reduction, as demonstrated by the small values assumed by the characteristic exponent *b* (0.01 and 0.13 for 10 and 40 wt.% as the oil load, respectively). It must also be noted that the E_v required to produce the 40 wt.% o/w emulsions resulted 5 times larger than the energy density needed to generate the more dilute systems. In the literature, it is suggested that although the membrane emulsification operates for energy densities below 10^3-10^6 J/m^3, the exact range strongly rises as larger dispersed phase mass fractions are produced (8, 19). The E_v was found to increase by more than 3 orders of magnitude for the production of highly concentrated emulsions (dispersed phase content up to 80 wt.%) (8, 19). What is more, the extent of the droplet size reduction resulted highly dependent on the type of membrane emulsification apparatus employed. For cross-flow membrane emulsification the $d_{3,2}$ rapidly decreased with the E_v ($b \sim 1$) independently from both the dispersed phase mass fraction and the type and quantity of surfactant (31). Nevertheless, in other works focusing on the performance of the rotating membrane, *b* assumed much smaller values (~ 0.2), more in line with the weaker dependency observed in this study (37, 38).

For the case of emulsions stabilised by nanoparticles, similar trends to those shown in Figure 5.5.A were observed with only exception being the droplet size resulting from the high-pressure homogenisation, Figure 5.5.B. As observed in the previous section, high-pressure processing could not induce an efficient droplet reduction across the entire range of pressures. The $d_{3,2}$ remained rather constant with the HPM energy input as also demonstrated from the low values of the characteristic slope (0.05 and 0.02 for 10 and 40 wt.% as the oil load, respectively).

On the other hand, the HSM performance was not affected by the presence of silica as the emulsifier. The Sauter diameter decreased with the E_v. The $d_{3,2}$ of 10 wt.% o/w emulsions was subjected to a faster reduction (b = 0.55) than the systems containing a higher amount of dispersed phase (b = 0.38).

Emulsions produced through the CIJs presented similar values to those resulting from the HSM. The hydrodynamic conditions established during CIJs operation induced a similar droplet size reduction between the two different oil mass fractions.

Similarly to the results of Figure 5.5.A, the reduction in droplet size of nanoparticle stabilised-emulsions produced through the RM did not significantly vary with the energy density for both dispersed phase contents.

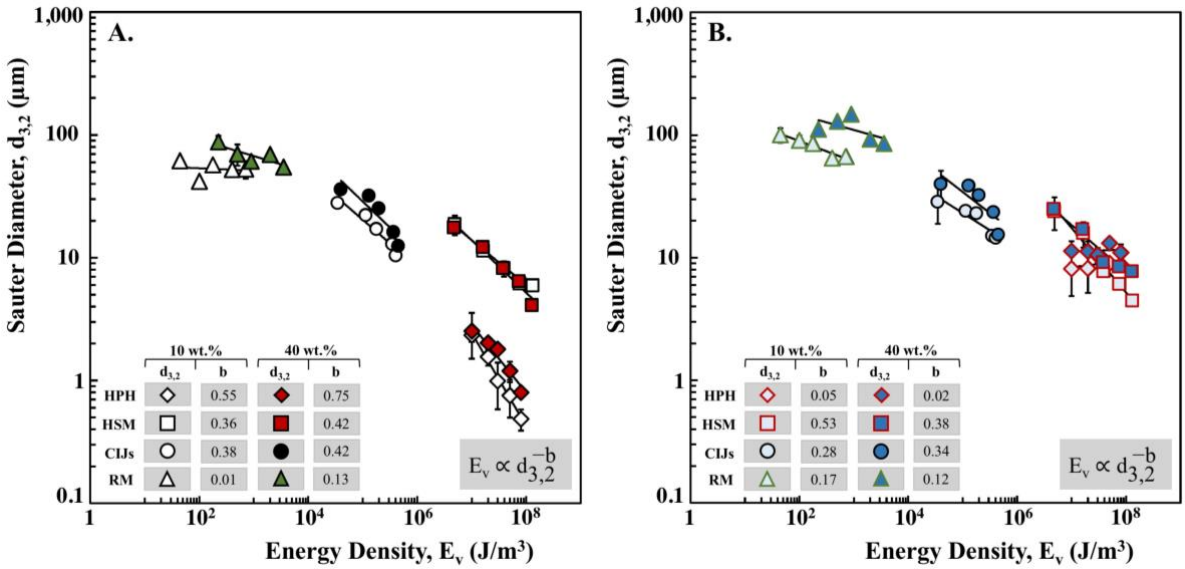

Figure 5.5. Dependency of the Sauter diameter ($d_{3,2}$) of both 10 and 40 wt.% o/w emulsions in the presence of Tween20 (A) and silica (Bw2) on the Energy Density (E_v; calculated as explained in section 5.2.2.7) of High-Pressure Homogeniser (HPH), High-Shear Mixer (HSM), Confined Impinging Jets (CIJs) and Rotating Membrane (RM) treatments. Symbols are reported in each figure's legend. For each data set in both figures, the best fit of the process function ($E_v \sim d_{3,2}^{-b}$) is also shown and the value of the exponent *b* are reported in both figures' legends. All data points are mean values (n=6) and error bars represent one standard deviation of the mean; where not visible, error bars are smaller than the used symbols.

Figure 5.6.A-D present the droplet size distributions (DSDs) of 10 wt.% o/w emulsions stabilised by either surfactant (A-B) or particles (C-D) following their processing at the lowest and highest energy density (Figure 5.5.A) via the four methods compared in this study. The figure also reports the span values ($Span_{Low}$ and $Span_{High}$) corresponding to both processing conditions for each of the techniques. The DSDs at varying E_v for each technique in the case of more concentrated systems (for both emulsifiers) are not shown since these showed similar variations to the dilute systems.

For the case of emulsions processed through the HPH, the data display that, although the average droplet size was greatly reduced, the width of the DSD noticeably increased with the energy density, Figure 5.6.A. In the HPH, broad droplet size distributions are normally expected because emulsions droplets experience largely non-uniform disruptive forces (61). The uneven nature of these forces increases at larger homogenisation pressures, thus resulting in broader DSD (if compared to those obtained at lower pressures), in line with observed results (61). Contrarily, in the presence of silica as the emulsifier, the droplet size remained constant while the droplet size became appreciably narrower, Figure 5.6.B. Although emulsions processed in the HPH experience a wider range of disruptive forces at higher pressures, droplets are however exposed to a more turbulent environment. Since for the case of nanoparticle-stabilised emulsions it resulted clear that the droplet size could not be further reduced with at an increasing pressure (Figure 5.5.B), the more turbulent environment could possibly promote particle adsorption at the droplet interface, thus resulting in the observed narrower DSD.

With the HSM, in the presence of surfactant, the DSD was only shifted towards a lower size, i.e. indicating the observed reduction in the Sauter diameter (Figure 5.5.A), while the span values remained practically unaltered by the increase in the E_v, Figure 5.6.A. On the

other hand, in particle stabilised emulsions, the increase in E_v caused a reduction in droplet size and at the same time a broader DSD, as demonstrated by the span values, Figure 5.6.B. The observed differences may be explained based on the fact that low-molecular weight surfactants assist droplet break-up and stabilisation by quickly adsorbing at the droplet interface and lowering the interfacial tension (Figure 5.1), thus forming similarly wide DSD also under different processing conditions, with a major impact observed on the Sauter diameter. Differently, during the processing of Pickering emulsions, the extent of droplet break-up mainly depends on the effectiveness of the turbulence generated within the emulsification apparatus to promote particle transfer to the drop interface. Furthermore, nanoparticles adsorb at the interface more slowly that surfactants and additionally are not surface active, thus likely resulting in the observed larger span values when emulsions were processed under the highest E_v (if compared to the case of surfactant-stabilised emulsions, Figure 5.6.B).

Similarly, the DSD of emulsions (in the presence of surfactant) produced via the CIJs treatment overall kept their width regardless of the E_v value, Figure 5.6.C. What is more, in case of particle-stabilised emulsions, the increase in E_v generated emulsions with both a smaller average drop diameter and a narrower droplet size distribution (Figure 5.6.D), differently from what observed in the HSM (Figure 5.6.B). A potential advantage of CIJs consists in the possibility to continuously produce emulsions at large throughputs (i.e. short residence times) in a turbulent environment where disruptive forces are more uniform than the high-energy counterparts (7). This can probably explain why a narrower DSD was obtained at larger E_v compared to the same case in the HSM.

Although in the RM the average droplet size was not greatly affected by the increase in the rotational speed (Figure 5.5.A-B), the span of the DSD underwent a considerable reduction

when droplets were stabilised by means of the Tween20, Figure 5.6.C. Under both E_v conditions, the narrowest DSDs were observed among the different techniques. Due to its low-energy mode of operation, RM is characterised by the formation of highly-uniform emulsions, because droplets experience rather similar shear forces that drive their detachment from the membrane pores. Differently from the higher energy counterparts, these forces are uniform even at larger E_v, i.e. more similar droplets can be formed providing that the emulsifier quickly adsorbs at the drop interface (such as the case of a low molecular weight surfactants). In fact, neither the emulsion $d_{3,2}$ nor the span were affected by larger membrane rotational speeds for the case of particle stabilised droplets, Figure 5.6.D. Due to the absence of turbulence in the RM, the transport of particles at the interface resulted more challenging. Firstly, this had an impact on the higher concentration of silica (3 wt.%) used to stabilise the formed emulsion. In fact, by adopting the same quantity of nanoparticles (1 wt.%) to the other techniques, the emulsions formed via the RM immediately phase separated after processing. In addition, despite the higher concentration, the lack of turbulence in the RM could probably not induce efficient transport of particles at the interface such as to cause evident changes in either the $d_{3,2}$ or the span across the whole range of membrane rotational speeds.

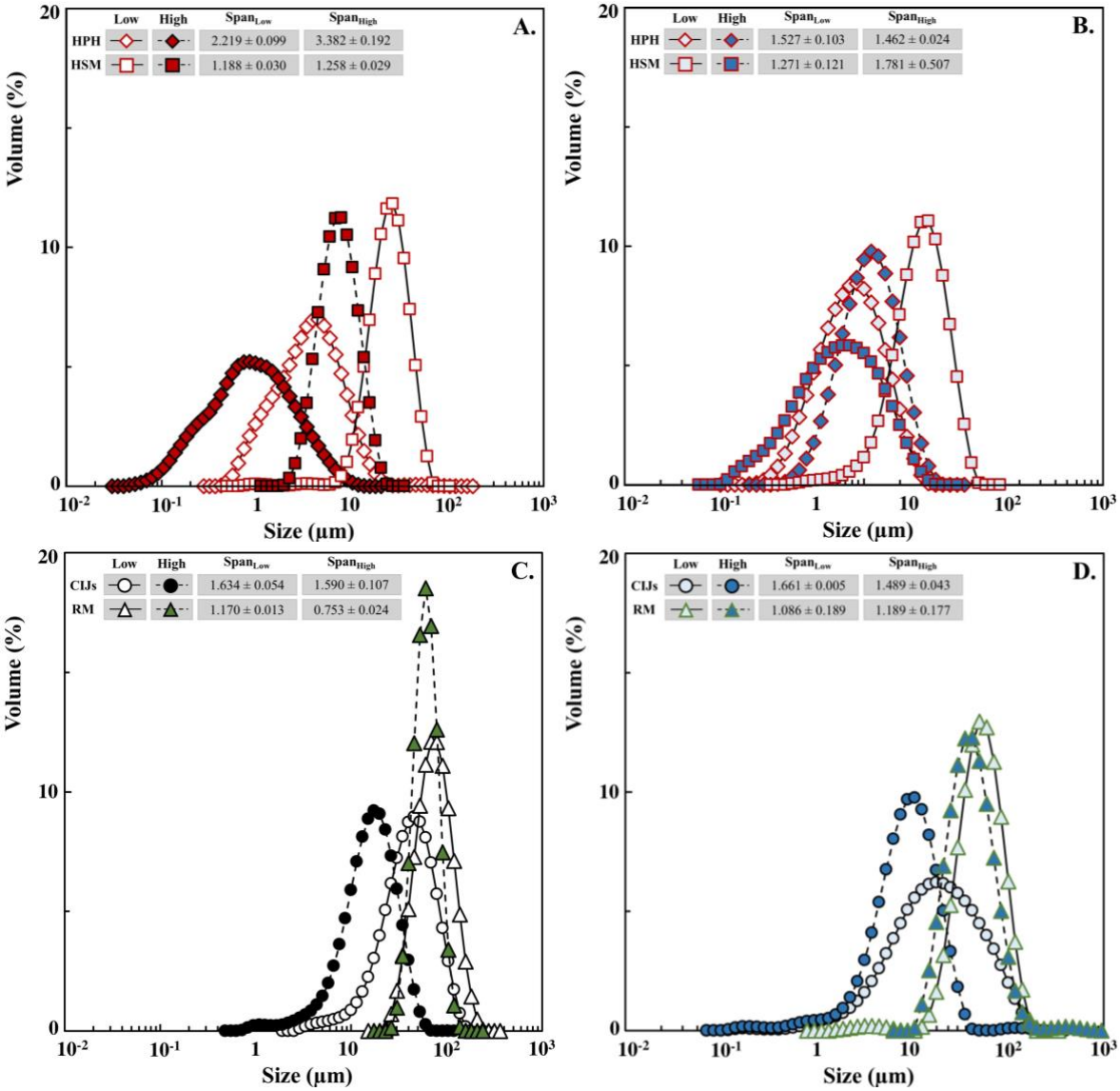

Figure 5.6. Droplet size distributions (DSDs) of 10 wt.% o/w emulsions produced at the lowest and highest E_V (Figure 5.5.A-B) via the High-Pressure Homogeniser, HPH, and the High-Shear Mixer, HSM, in the presence of Tween20 (A) and silica (B) as well as via the Confined Impinging Jets, CIJs, and the Rotating Membrane, RM, in the presence of Tween20 (C) and silica (D). Symbols as well as the span values corresponding to the DSDs obtained at the lowest ($Span_{Low}$) as well as at the highest ($Span_{High}$) E_V are reported in each figure's legend.

5.3.2.2. Impact of the energy density and of the residence time on the emulsion microstructure

In emulsification practice, emulsions are often recirculated through the emulsification apparatus under fixed hydrodynamic conditions to increase the duration that emulsion droplets experience the turbulent field. Provided there is enough emulsifier to stabilise the interfacial created, prolonged exposure may cause a reduction in the average droplet size and/or encourage the refining of the emulsion droplet size distribution (62).

Figure 5.7 shows the effect of extending the recirculation step (n; defined as explained in section 5.2.2.2.E) on the Sauter diameter ($d_{3,2}$) of surfactant- and particle-stabilised o/w emulsions (with a fixed oil content of 10 wt.%) obtained via HPH (A-B), HSM (C-D) and CIJs (E-F) processing under fixed energy density conditions. For each technique, the effect of the residence time was evaluated under three fixed hydrodynamic conditions corresponding to the lowest ($E_{v,l}$), highest ($E_{v,h}$), as well as an intermediate ($E_{v,i}$) energy density value (Figure 5.5.A-B). Details on the selected conditions can be found in section 5.2.2.2. The dependency of the Sauter diameter with respect to the residence time for emulsions of a 40 wt.% oil content showed similar trends (irrespectively of either the emulsification method or type of emulsifier utilised) to the more dilute (10 wt.%) systems, thus only the latter results are reported here.

In the HPH, for surfactant-stabilised emulsions, the $d_{3,2}$ reached its minimum value after the second pass (Figure 5.7.A). The extent of this reduction was larger as the homogenisation pressure was increased. The observed reduction in $d_{3,2}$ after the second (and up to the fourth) pass was fairly modest independently of the pressure applied during recirculation. No variations in droplet size were observed when silica-stabilised emulsions were recirculated through the HPH and regardless of the pressure used (Figure 5.7.B). This is in line with the

earlier findings in the present study (see Figure 5.5.B), where the $d_{3,2}$ of the particle-stabilised emulsions was shown not to be affected by HPH processing at increasing E_v values (after a single pass through the device).

For HSM processing, recirculation (in this case, the extension of the initial mixing/residence time, $t_{res,1}$ = 4 min, progressively to 16 min) did not induce appreciable variations in the $d_{3,2}$ values of emulsions stabilised by either Tween20 (Figure 5.5.C) or silica (Figure 5.5.D); regardless of the rotational speed used.

In the case of CIJs, negligible changes in the Sauter diameter (for emulsions stabilised by either of the two emulsifiers) were observed when recirculation took place at the lowest E_v (i.e. at the lowest mass jet flow rate); see Figure 5.5.E. However, when multipassing was carried out under the more intense (fixed) hydrodynamic conditions (higher E_v), $d_{3,2}$ initially decreased after the second pass through the device but then remained constant upon further recirculation.

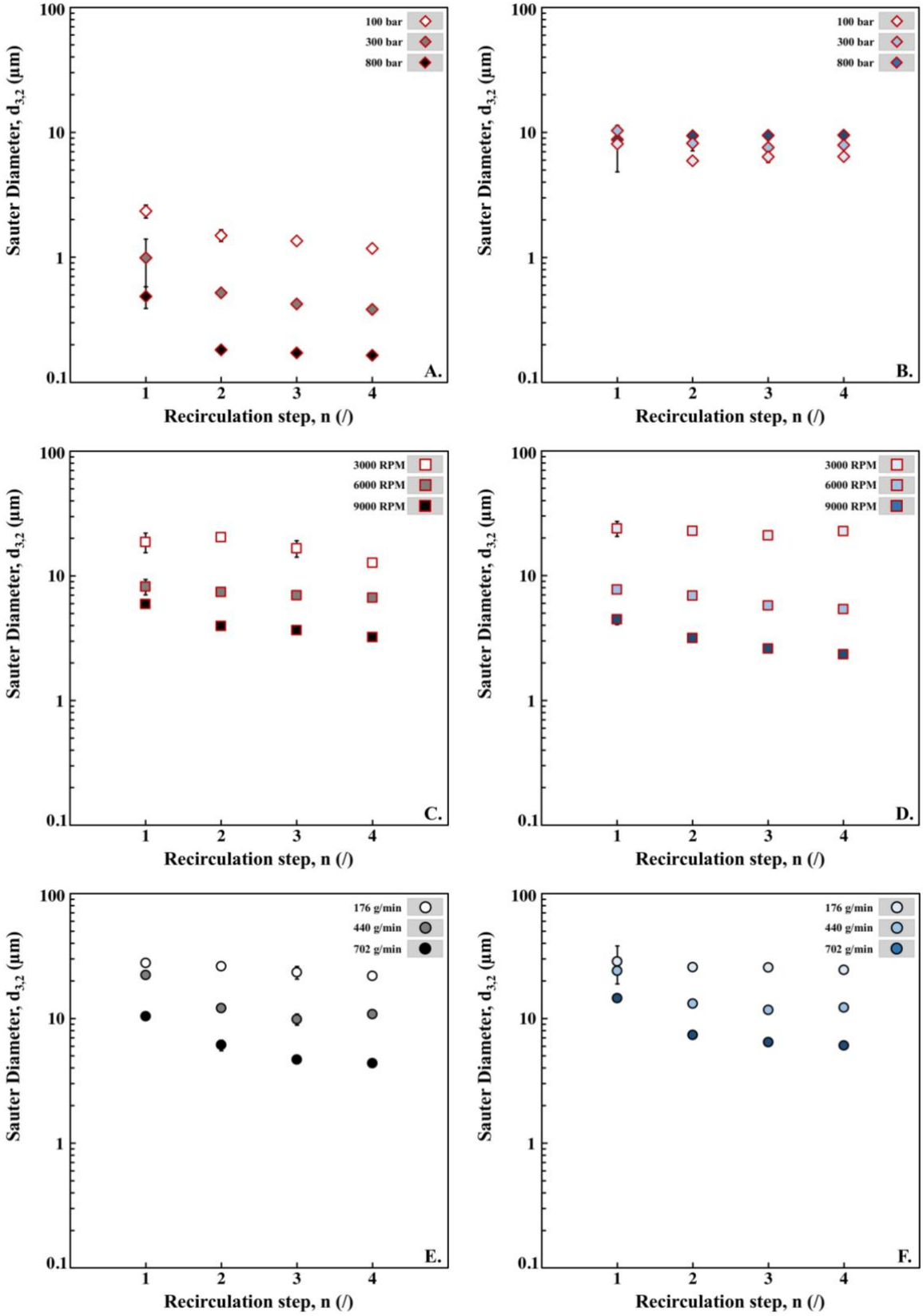

Figure 5.7. Variation of the Sauter diameter ($d_{3,2}$) as a function the recirculation step (n; defined as explained in section 5.2.2.2.E) of 10 wt.% o/w emulsions in the presence of 1 wt.% of either Tween20 or silica processed via the High-Pressure Homogeniser, HPH (A-B), the

High-Shear Mixer, HSM (C-D) and the Confined Impinging Jets, CIJs (E-F) under fixed low, intermediated and high E_v conditions. Symbols are reported in each figure's legend. All data points are mean values (n=6) and error bars represent one standard deviation of the mean; where not visible, error bars are smaller than the used symbols.

Figure 5.8 depicts the effect of the recirculation step (n; defined as explained in section 5.2.2.2.E) on the droplet size distributions (DSDs) of surfactant- and nanoparticle-stabilised 10 wt.% o/w emulsions obtained via the HPH (A-B), HSM (C-D) and the CIJs (E-F) under fixed energy density conditions. For each technique, the effect of the residence time on the DSD is shown for the lowest and highest E_v (Figure 5.5.A-B). The change of the DSDs with *n* evaluated under (fixed) intermediate E_v is not shown to improve the readability of the figures. The variation of the DSDs of 40 wt.% oil emulsions with respect to *n* showed similar trends (regardless of both the technique and the emulsifier adopted) to the more dilute (10 wt.%) ones, thus only the latter results are reported here.

In the HPH, the increase in the *n* on the DSD of surfactant-stabilised o/w emulsions caused a reduction of the width of the distributions for both hydrodynamic conditions, Figure 5.8.A. The span values decreased from 2.338 and 3.382 (after a single pass) to 1.543 and 2.194 (after the fourth pass) for 100 and 800 bar, respectively. One can further notice that the span values resulting from processing at a higher homogenisation pressure (800 bar) were higher than the those showed at a lower pressure (100 bar). This in line with the fact that in the HPH, the turbulent conditions become increasingly less-uniform as the pressure is increased (57, 62, 63). When emulsions were stabilised by particles, although (as also observed in Figure 5.7.B) neither the higher pressure nor the increase in the residence time (or a combination of both factors) caused any variation in the $d_{3,2}$. Recirculation at the lowest pressure (100 bar) did not produce appreciable change in the DSD characteristics, while under the highest E_v (i.e. corresponding to 800 bar), a narrower DSD was observed from the first (span value equal to

1.462) to the fourth pass (span value equal to 1.203). The results suggest that although the processing conditions established within the high-pressure apparatus could not induce any reduction in $d_{3,2}$, upon recirculation under the highest homogenisation pressure (800 bar), the emulsion microstructure was greatly refined.

For the emulsification in the HSM, the DSD of emulsions in the presence of surfactant as the emulsifier remained practically unchanged (both in terms of span and $d_{3,2}$) with the *n* under the lowest E_v (3000 RPM), Figure 5.7.C. Differently, when emulsions were exposed to higher hydrodynamic conditions (e.g. 9000 RPM), a four times larger *n* only caused a minor reduction in the emulsion Sauter diameter but it was accompanied by an increase in the width of the distribution. The span value increased as a consequence of the formation of a large portion of droplets with a diameter below 1 μm (not observed for a single t_{res}). For particle-stabilised emulsions, a slightly narrower DSD was observed as a consequence of extending the residence time in the high-shear environment during emulsification under the lowest E_v, Figure 5.7.D. However, a larger *n* at a fixed high E_v induced a dramatic rise in the width of the DSD. The span increased from 1.781 (at a single t_{res}) to 3.963 (at four times the t_{res}). Although the extended residence time promotes the formation of smaller droplets (as observed in Figure 5.7.C for the case of surfactant-stabilised systems), the presence of silica as the emulsifier hampers this tendency. Therefore, whereas a part of the initial DSD is subjected to this reduction driven by the prolonged t_{res}, another portion of droplets cannot be further reduced resulting in a DSD with a broader width.

For the CIJs processing, recirculation of surfactant-stabilised emulsions at the lowest jet mass flow rate produced a narrower width together with a smaller $d_{3,2}$ from the first to the fourth pass, Figure 5.7.E. On the other hand, when multipassing was conducted under the highest value of jet mass flow rate, a longer t_{res} in the CIJs emulsification environment only

caused a reduction in droplet size with marginal changes in the width of the DSD. For emulsions stabilised by nanoparticles, the span of the DSD was reduced (from 1.661 to 1.207 corresponding to the first and fourth pass, respectively) upon multipassing under the lowest E_v with negligible changes in the $d_{3,2}$, Figure 5.7.F. Contrarily, at a higher jet mass flow rate, the width of the DSD increased from 1.775 (first pass) to 2.164 (fourth pass) while, at the same time, this was accompanied by a decrease the Sauter diameter. According to the data of Figure 5.7.D for silica-stabilised emulsions processed via the HSM, the presence of particles as the emulsifier limits the tendency of reducing the majority of the DSD to smaller particles when the systems are exposed to the highest hydrodynamic conditions for a longer t_{res}. As a consequence, despite the diameter of a portion of droplets decreases, another with a larger $d_{3,2}$ seems to remain unaffected by the prolonged exposure to the turbulent environment thus resulting in the broader DSD. One should also highlight that this effect is observed to a minor extent in the CIJs (if compared to the HSM) probably because the high-shear treatment allowed the production of smaller droplets than the CIJs under the highest E_v.

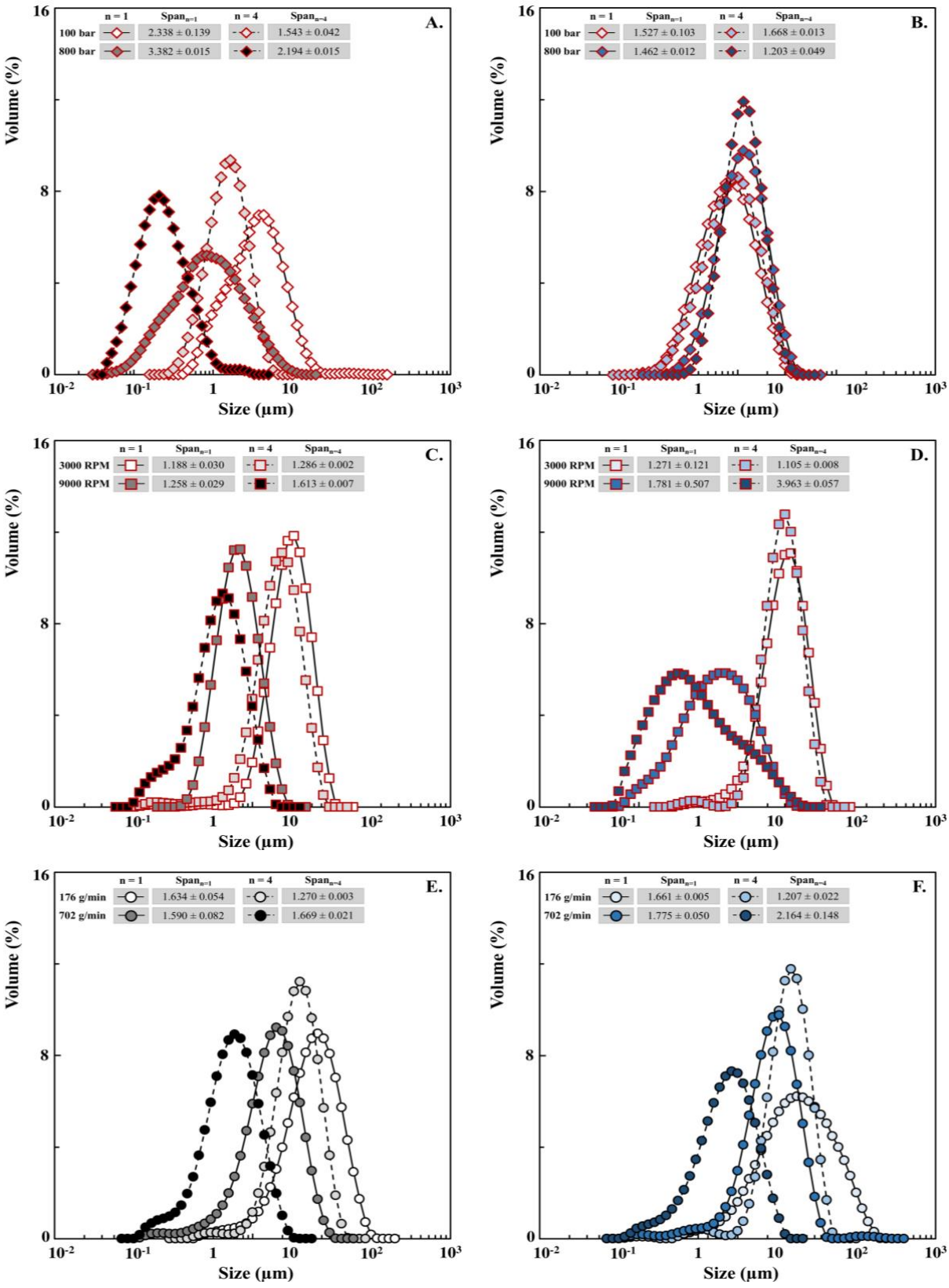
A.
n = 1 Span$_{n=1}$ n = 4 Span$_{n=4}$
100 bar 2.338 ± 0.139 1.543 ± 0.042
800 bar 3.382 ± 0.015 2.194 ± 0.015
B.
n = 1 Span$_{n=1}$ n = 4 Span$_{n=4}$
100 bar 1.527 ± 0.103 1.668 ± 0.013
800 bar 1.462 ± 0.012 1.203 ± 0.049
C.
n = 1 Span$_{n=1}$ n = 4 Span$_{n=4}$
3000 RPM 1.188 ± 0.030 1.286 ± 0.002
9000 RPM 1.258 ± 0.029 1.613 ± 0.007
D.
n = 1 Span$_{n=1}$ n = 4 Span$_{n=4}$
3000 RPM 1.271 ± 0.121 1.105 ± 0.008
9000 RPM 1.781 ± 0.507 3.963 ± 0.057
E.
n = 1 Span$_{n=1}$ n = 4 Span$_{n=4}$
176 g/min 1.634 ± 0.054 1.270 ± 0.003
702 g/min 1.590 ± 0.082 1.669 ± 0.021
F.
n = 1 Span$_{n=1}$ n = 4 Span$_{n=4}$
176 g/min 1.661 ± 0.005 1.207 ± 0.022
702 g/min 1.775 ± 0.050 2.164 ± 0.148
Volume (%)
Size (µm)

Figure 5.8. Droplet size distributions (DSDs) of 10 wt.% o/w emulsions in the presence of 1wt.% of either Tween20 or silica produced via the High-Pressure Homogeniser, HPH (A-B), the High-Shear Mixer, HSM (C-D) for a single (n=1) and a four times larger (n=4) recirculation step (defined as explained in section 5.2.2.2.E), under the lowest and highest E_V (from Figure 5.5.A-B). Symbols as well as the span values corresponding to the DSDs obtained under both recirculation steps ($Span_{n=1}$ and $Span_{n=4}$) are reported in each figure's legend.

5.3.3. Impact of the energy density and residence time on the energy efficiency

The energy efficiency (EF) of an emulsification technique can be estimated from a comparison between the theoretically required energy to form an emulsion and its total energy input (section 5.2.2.8). Despite their ability in producing small droplets, high-energy manufacturing methods are inherently characterised by low values of EF (below 0.1%) (21). This is because, during processing, the turbulence generated in the emulsification apparatus must give rise to local disruptive pressure gradients able to overcome the (typically very high) Laplace pressure gradients ($\approx \gamma/d^2$) providing resistance of droplets to break-up (1). On the other hand, in emulsification methods characterised by a low energy approach (leveraging the spontaneous droplet formation), EF values are significantly higher (above 1%) (21). However, one of the major challenge limiting their large-scale implementation is associated with the difficulties to find suitable configurations delivering high – throughput processing (21). Based on this, it results clear that characterisation of the energy efficiency of emulsification methods represents an additional vector which can be used to compare the emulsification performance among different setups.

Figure 5.9.A-B show the variation of the Energy efficiency (EF) with the Energy Density (E_V) of each emulsification apparatus investigated in this study for the manufacturing of both 10 and 40 wt.% o/w emulsions stabilised by either surfactant (Figure 5.9.A) or nanoparticles (Figure 5.9.B).

Overall, Figure 5.9.A-B show that in all methods the EF decreased as a higher energy amount was input into the system, i.e. as smaller droplets were formed (Figure 5.5.A-B). The extent of this decrease resulted strictly dependent on the type of manufacturing technique.

For surfactant-stabilised systems, the production via the HSM gave the lowest values of EF (Figure 5.9.A), $4x10^{-4}$ % to $3.5x10^{-3}$ % and $1.4x10^{-3}$ % to $2.5x10^{-2}$ % for 10 and 40 wt.% respectively. The EF decreased with the E_v more rapidly if compared to the HPH for both oil contents. In addition, for the processing of emulsions with equal dispersed phase content, the EFs from the HPH resulted higher than the HSM of an order of magnitude.

Compared to both methods, although the CIJs presented a similar EF-E_v relationship to the HSM, CIJs manufacturing gave rise to higher energy efficiencies, ranging from $8.0x\ 10^{-2}$ to $3.3x\ 10^{-1}$ % and from $2.2x\ 10^{-1}$ to $8.7x\ 10^{-1}$ % for 10 and 40 wt.% as the dispersed phase mass fraction, respectively. From a comparison between the methods based on turbulence as the main mechanism of droplet disruption, CIJs processing showed the potential of producing similar droplets to the HSM (Figure 5.5.A) but with significantly higher EFs (more than two orders of magnitude). Compared to both methods, the HPH processing resulted in intermediate EFs to produce the smallest droplet sizes (Figure 5.5.A).

The differences in EF among these systems can be explained based on the concept of the residence time. In fact, despite the E_v of HPH and HSM were rather similar (Figure 5.5.A), in the HSM energy is dissipated over a time (4 min) significantly longer than the HPH's ($\sim10^{-3}$s) (64). Differently, CIJs gives even higher EF than both methods due to the combination of very short residence times and a lower E_v (Figure 5.5.A).

Compared to the three methods, the EFs from the RM showed the highest values, well above 1%. Nevertheless, the EF rapidly decreased with the E_v (for both oil mass fractions) despite the minimal effect of the processing conditions on the Sauter diameter (Figure 5.5.A).

It should also be highlighted that while for the turbulent processing techniques (HPH, HSM and CIJs) the EF increased with the dispersed phase content, the opposite trend was observed for the RM, i.e. the EF decreased for the production of more concentrated systems. This difference is likely due to the fact that in the RM to produce more concentrated systems the dispersed phase must be pushed through the pores of the rotating membrane (at a fixed pressure) for a time longer than the one required to form the more dilute ones. As a consequence of this, a higher energy input is required for the production of concentrated emulsions, thus resulting in lower EF. Differently in all the other methods, emulsions are processed at a fixed energy input regardless of the oil content and the EF of such methods is usually improved by processing emulsions with a higher dispersed phase mass fraction (eq. 5.15) (11, 65). The manufacturing of more concentrated systems is usually characterised by less friction losses thus a larger portion of the overall energy input contributes to the droplet formation (11, 65). Emulsion can be diluted afterwards to reach the desire concentration (11, 65).

Similar trends were overall observed for the variation of the EF with the E_v during the processing of 10 and 40 wt.% o/w emulsions stabilised by nanoparticles, Figure 5.9.B.

The EF decreased with the E_v for all the techniques investigated. Turbulence-based methods became more energy efficient during the production of more concentrated emulsions while the RM energy efficiency decreased during the production of emulsions with a higher dispersed phase content.

However, two main differences should be highlighted with respect to Figure 5.9.A. Firstly, both the HSM and the HPH show similar EFs for both oil mass fractions. This result was expected since similar $d_{3,2}$ were produced over a similar range of E_v (Figure 5.5.B). Secondly, for all methods, the manufacturing of nanoparticle-stabilised systems resulted in higher EF

values if compared to the corresponding case where droplets were stabilised by the surfactant (Figure 5.9.A), due to a higher value of interfacial tensions (Figure 5.1), which in turns increases the theoretically energy required to form the emulsion (eq. 5.15).

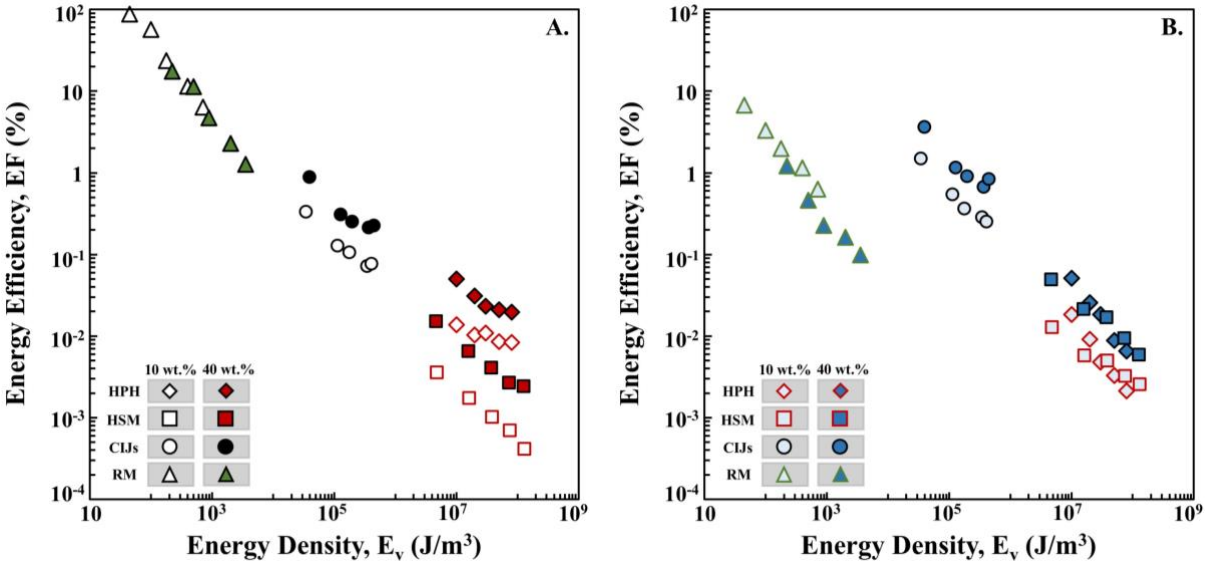

Figure 5.9. Variation of the Energy Efficiency (EF; eq. 5.14) with the Energy Density (calculated as explained in section 5.2.2.7) for the processing of 10 and 40 wt.% o/w emulsions via the High-Pressure Homogeniser (HSP), the High-Shear Mixer (HSM), the Confined Impinging Jets (CIJs) and the Rotating Membrane (RM) in the presence of Tween20 (A) and silica (B). Symbols are reported in each figure's legend.

As observed in the previous section (Figure 5.7 and 5.8), the exposure of emulsions to longer residence times within a specific emulsification apparatus may have beneficial effects on the final product microstructure (e.g. reduction in the average droplet size and/or narrowing of the droplet size distribution). However, this strategy also inherently carries a possible drawback represented by the potential lowering of the overall methods' energy efficiency. Therefore very often, a trade-off between the desired product properties and the processing efficiency must be found.

Figure 5.10.A-B depicts the variation of the energy efficiency (EF) as a consequence of processing for an extended residence time (expressed as the recirculation step, *n*) under the

highest energy density value (from Figure 5.5.A-B) of the 10 wt.% o/w emulsions in the presence of both Tween20 (Figure 5.10.A) and silica (Figure 5.10.B) as the emulsifiers. The data representing the change of EF with *n* deriving from the extended processing of *(i)* the 10 wt.% o/w emulsions under lower E_v values and *(ii)* the 40 wt.% emulsions under any E_v, are not reported since these showed similar trends to those observed in Figure 5.10.A-B.

For both the surfactant (Figure 5.10.A) and the particle (Figure 5.10.B) stabilised emulsions, it was observed that the EF strongly diminished as the systems were exposed to the turbulent environment for longer residence times. In both cases, the biggest reduction was observed after n=2, whereas the EF underwent smaller variations above it for each of the techniques. Through exposing the emulsions to longer residence times, the EF decreased over 2-4 orders of magnitude depending on the processing technique.

For the case of surfactant-stabilised systems (Figure 5.10.A), the CIJs showed the largest EFs ($\sim 10^{-1}$%, at n=1, to $\sim 10^{-4}$% at n=4). In contrast, emulsification via the HSM gave the smallest EF values ($\sim 10^{-7}$% at n=4) while the high-pressure treatment presented intermediate EFs ($\sim 10^{-7}$% at n=4).

For emulsion re-processing in the presence of particles (Figure 5.10.B), CIJs again presented the largest EFs (with values similar to those showed in Figure 5.10.A), while the HPH demonstrated to be the least energy-efficient processing method ($\sim 10^{-8}$% at n=4). In this case, intermediate EF values were observed after emulsion re-processing through the HSM.

Compared to both the HSM and HPH, the CIJs represents the most efficient method clearly due to the significantly lower energy input required for emulsification (Figure 5.5). For the HSM and the HPH, which instead operated over a similar range of energy input, their performance varied depending on the emulsifier used. When Tween20 was used as the emulsifier (and under the highest E_v), the emulsion $d_{3,2}$ obtained from the HPH as a result of

the recirculation were significantly smaller than those obtained via the HSM (Figure 5.7.A and Figure 5.7.C for the HPH and the HSM, respectively). As a result of this difference, the high-pressure treatment resulted more efficient because larger interfacial areas were obtained under a similar energy input (eq. 5.17). On the other hand, in the case of nanoparticle-stabilised emulsions, the HSM processing caused smaller droplet sizes than the HPH (Figure 5.7.B and Figure 5.7.D for the HPH and the HSM, respectively), therefore resulting in higher EF values.

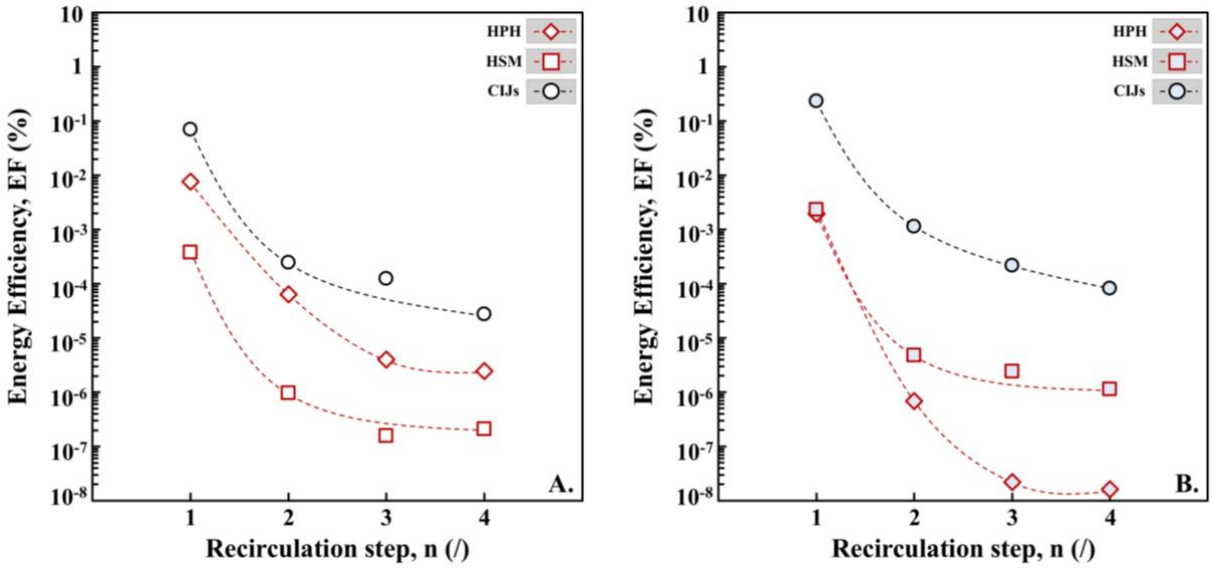

Figure 5.10. Variation of the Energy Efficiency (EF; eq. 5.17) as a function of the recirculation step, *n* (defined as explained in section 5.2.2.2.E), for the processing of 10 wt.% o/w emulsions via the High-Pressure Homogeniser (HSP), the High-Shear Mixer (HSM) and the Confined Impinging Jets (CIJs) in the presence of Tween20 (A) and silica (B). Symbols are reported in each figure's legend.

5.4. Conclusions

Both high- and low-energy methods can be used to produce emulsions and their choice depends on a wide range of different factors such as the desired product throughput, the type and concentration of raw materials, the required droplet size and droplet size distribution as

well as the energy expenditure during processing (among others). This study aims to compare the emulsification performance of high- (high-pressure homogeniser, HPH, and high-shear mixer, HSM) and low-energy (confined impinging jets, CIJS, and rotating membrane, RM) for a number of processing (flow regime, average energy dissipation rate, $\bar{\varepsilon}_{th}$, energy density, E_v, energy efficiency, EF, residence time, t_{res}) as well as formulation (dispersed phase load, type of emulsifier) parameters by assessing their impact on the emulsion microstructure (average droplet size, $d_{3,2}$, and droplet size distribution, DSD).

It was shown that while the RM operated under laminar flow regime, emulsion manufacturing via all the other methods took place in turbulent regime. In the presence of surfactant as the emulsifier, the smallest $d_{3,2}$ was achieved through the high-pressure treatment, which also showed the highest values of $\bar{\varepsilon}_{th}$. Although both the HSM and the CIJs showed comparable $d_{3,2}$ (yet higher than the HPH) over the entire range of operating conditions used, the CIJs operation generated $\bar{\varepsilon}_{th}$ significantly higher. Compared to the three methods, the RM produced the largest $d_{3,2}$ at the lowest $\bar{\varepsilon}_{th}$, probably due to both the low energy approach and the laminar flow conditions. When silica was instead used as the emulsifier, the trends remained overall unchanged, with the only exception being represented by the HPH where its operation could not induce a droplet size reduction below 8μm.

Independently on both the oil mass fraction and the emulsifier used, it was also observed as HPH and HSM functioned over a similar range of high energy inputs, while CIJs and RM guaranteed emulsification to take place to intermediate and rather low E_v, respectively, over the whole range of processing conditions. Upon processing, the surfactant stabilised emulsions resulting from the high-pressure treatment had the highest polydispersity (with the span values increasing as the homogenisation pressure was increased) compared to all the other methods. Intermediate values were shown by both the HSM and CIJs while the

narrowest DSDs were achieved during the membrane operation. During processing of emulsions stabilised by nanoparticles, the differences in polydispersity resulted less evident among the different methods. In addition, due to the large energy expenditure, the HSM and HPH showed the lowest values of EFs during operation, while on the other side, due to the lower energy input, CIJs and RM the highest ones. Interestingly, for the methods whose mode of operation was based on turbulence as the main mechanism of droplet break-up, the EF increased for the production of more concentrated systems, while for the RM this was not the case. In fact, the EF decreased when 40 wt.% oil in water emulsions were produced (if compared to the 10 wt.% ones) because of the longer time required to push the dispersed phase through the membrane pores.

Through the exposure of emulsions to longer the residence times within the emulsification apparatus under fixed hydrodynamic conditions in the turbulence-based techniques (this was not performed for the RM), the DSD was the major microstructural parameter affected with minor changes observed in terms of $d_{3,2}$. Overall, the span of the DSD decreased as emulsions spent longer times in the turbulent environment generated during emulsification. However on the other side, longer residence times strongly reduced the EF of all methods, with this reduction being dependent on the type of apparatus. CIJs showed the highest EF (regardless of the emulsifier used) if compared to both HSM and HPH. The EF of the latter two methods varied depending on the emulsifier employed during emulsification. In the case of surfactant-stabilised emulsions, the lowest EF was observed in the HSM, due to the longer times required for emulsification. Contrarily in the presence of particles, the lowest EF was showed during HPH operation, mainly because despite the recirculation, the droplet size could not be further reduced.

In conclusion, this study aims to offer a comprehensive comparison of established as well as emerging emulsification techniques by highlighting their main principles, advantages and limitations, through experimentally assessing their emulsification performance for a wide range of processing as well as formulation parameters.

List of References

(1) McClements D.J. *Food Emulsions: Principles, Practices and Techniques*. 3rd ed. Boca Raton: CRC press; 2016.

(2) Donsì F. *Chapter 11 - Applications of Nanoemulsions in Foods*. In: Jafari S.M., McClements D.J., (eds.). *Nanoemulsions*. 1st ed. Oxford: Academic Press; 2018. p. 349-77.

(3) Charcosset C. *2 - Preparation of nanomaterials for food applications using membrane emulsification and membrane mixing*. In: Grumezescu A.M., (ed.). *Emulsions*. Oxford: Academic Press; 2016. p. 37-69.

(4) Spyropoulos F., Hancocks R.D., Norton I.T. *Food-grade emulsions prepared by membrane emulsification techniques*. Procedia Food Science. 2011;1:920-6.

(5) Vladisavljević G.T., Kobayashi I., Nakajima M. *Production of uniform droplets using membrane, microchannel and microfluidic emulsification devices*. Microfluidics and Nanofluidics. 2012; 13(1): 151-78.

(6) Hancocks R.D., Spyropoulos F., Norton I.T. *Comparisons between membranes for use in cross flow membrane emulsification*. Journal of Food Engineering. 2013; 116(2): 382-9.

(7) Tripodi E., Lazidis A., Norton I.T., Spyropoulos F. *On the production of oil-in-water emulsions with varying dispersed phase content using Confined Impinging Jet Mixers*. Industrial & Engineering Chemistry Research. 2019; 58(32): 14859-72.

(8) Rayner M. *Scales and Forces in Emulsification*. In: Rayner M., Dejmek P., (eds.). *Engineering Aspects of Food Emulsification and Homogenisation*. 1st ed. Boca Raton: CRC press; 2015. p. 3-32.

(9) Jafari S.M., Assadpoor E., He Y., Bhandari B. *Re-coalescence of emulsion droplets during high-energy emulsification*. Food Hydrocolloids. 2008;22(7):1191-202.

(10) Tontul I., Topuz A. *Chapter 13 - Microencapsulation of Plant Oils Rich in Alpha-Linolenic Acid: Effect of Processing Parameters*. In: Sagis L.M.C., (ed.). *Microencapsulation and Microspheres for Food Applications*. Oxford: Academic Press; 2015. p. 253-69.

(11) Walstra P. *Principles of emulsion formation*. Chemical Engineering Science. 1993; 48(2): 333-49.

(12) Walstra P. *Physical Chemistry of Foods*. New York: Dekker M; 2003.

(13) Kolmogorov A.N. *Drop breakage in turbulent flow*. Comptes rendus de l'Académie des Sciences. 1949; 66: 825-30..

(14) Hinze J.O. *Fundamentals of the hydrodynamic mechanism of splitting in dispersion processes*. AIChE Journal. 1955; 1(3): 289-95.

(15) Stang M., Schuchmann H., Schubert H. *Emulsification in High-Pressure Homogenizers*. Engineering in Life Sciences. 2001; 1(4): 151-7.

(16) Jafari S.M., He Y., Bhandari B. *Production of sub-micron emulsions by ultrasound and microfluidization techniques*. Journal of Food Engineering. 2007; 82(4): 478-88.

(17) Stang M., Karbstein H., Schubert H. *Adsorption kinetics of emulsifiers at oil—water interfaces and their effect on mechanical emulsification*. Chemical Engineering and Processing: Process Intensification. 1994; 33(5): 307-11.

(18) Karbstein H., Schubert H. *Developments in the continuous mechanical production of oil-in-water macro-emulsions*. Chemical Engineering and Processing: Process Intensification. 1995; 34(3): 205-11.

(19) Joscelyne S.M., Trägårdh G. *Membrane emulsification-a literature review*. Journal of Membrane Science. 2000; 169(1): 107-17.

(20) Schubert H., Ax K., Behrend O. *Product engineering of dispersed systems*. Trends in Food Science & Technology. 2003; 14(1): 9-16.

(21) Santana R.C., Perrechil F.A., Cunha R.L. *High- and low-energy emulsifications for food applications: a focus on process parameters*. Food Engineering Reviews. 2013; 5(2): 107-22.

(22) Walstra P., Smulders P.E.A. *Emulsion Formation*. In: Bink B.P. (ed.). *Modern Aspects of Emulsion Science*: Cambridge: The Royal Society of Chemistry; 1998. p. 56-99.

(23) Floury J., Desrumaux A., Lardières J. *Effect of high-pressure homogenization on droplet size distributions and rheological properties of model oil-in-water emulsions*. Innovative Food Science & Emerging Technologies. 2000; 1(2): 127-34.

(24) Floury J., Legrand J., Desrumaux A. *Analysis of a new type of high pressure homogeniser. Part B. study of droplet break-up and recoalescence phenomena*. Chemical Engineering Science. 2004; 59(6): 1285-94.

(25) Binks B.P. *Particles as surfactants-similarities and differences*. Current Opinion in Colloid & Interface Science. 2002; 7(1): 21-41.

(26) Dickinson E. *Food emulsions and foams: Stabilization by particles*. Current Opinion in Colloid & Interface Science. 2010; 15(1): 40-9.

(27) Dickinson E. *Exploring the frontiers of colloidal behaviour where polymers and particles meet*. Food Hydrocolloids. 2016; 52: 497-509.

(28) Duffus L.J., Norton J.E., Smith P., Norton I.T., Spyropoulos F. *A comparative study on the capacity of a range of food-grade particles to form stable o/w and w/o Pickering emulsions*. Journal of Colloid and Interface Science. 2016; 473: 9-21.

(29) Pichot R., Spyropoulos F., Norton I.T. *Mixed-emulsifier stabilised emulsions: Investigation of the effect of monoolein and hydrophilic silica particle mixtures on the stability against coalescence*. Journal of Colloid and Interface Science. 2009; 329(2): 284-91.

(30) Behrend O., Ax K., Schubert H. *Influence of continuous phase viscosity on emulsification by ultrasound*. Ultrasonics Sonochemistry. 2000; 7(2): 77-85.

(31) Schubert H., Engel R. *Product and Formulation Engineering of Emulsions*. Chemical Engineering Research and Design. 2004; 82(9): 1137-43.

(32) Tcholakova S., Lesov I., Golemanov K., Denkov N.D., Judat S., Engel R., et al. *Efficient emulsification of viscous oils at high drop volume fraction*. Langmuir. 2011; 27(24): 14783-96.

(33) Vankova N., Tcholakova S., Denkov N.D., Ivanov I.B., Vulchev V.D., Danner T. *Emulsification in turbulent flow: 1. Mean and maximum drop diameters in inertial and viscous regimes*. Journal of Colloid and Interface Science. 2007; 312(2): 363-80.

(34) Vankova N., Tcholakova S., Denkov N.D., Vulchev V.D., Danner T. *Emulsification in turbulent flow: 2. Breakage rate constants*. Journal of Colloid and Interface Science. 2007; 313(2): 612-29.

(35) Siddiqui S.W., Norton I.T. *Oil-in-water emulsification using Confined Impinging Jets*. Journal of Colloid and Interface Science. 2012; 377(1): 213-21.

(36) Siddiqui S.W. *The effect of oils, low molecular weight emulsifiers and hydrodynamics on oil-in-water emulsification in Confined Impinging Jet Mixer*. Colloids and Surfaces A: Physicochemical and Engineering Aspects. 2014; 443: 8-18.

(37) Lloyd D.M., Norton I.T., Spyropoulos F. *Processing effects during rotating membrane emulsification*. Journal of Membrane Science. 2014; 466: 8-17.

(38) Lloyd D.M., Norton I.T., Spyropoulos F. *Process optimisation of rotating membrane emulsification through the study of surfactant dispersions*. Journal of Food Engineering. 2015; 166: 316-24.

(39) Santos J., Vladisavljević G.T., Holdich R.G., Dragosavac M.M., Muñoz J. *Controlled production of eco-friendly emulsions using direct and premix membrane emulsification*. Chemical Engineering Research and Design. 2015; 98: 59-69.

(40) Vladisavljević G.T., Shimizu M., Nakashima T. *Preparation of monodisperse multiple emulsions at high production rates by multi-stage premix membrane emulsification*. Journal of Membrane Science. 2004; 244(1): 97-106.

(41) Pacek A.W., Man C.C., Nienow A.W. *On the Sauter mean diameter and size distributions in turbulent liquid/liquid dispersions in a stirred vessel*. Chemical Engineering Science. 1998; 53(11): 2005-11.

(42) Calabrese R.V., Francis M.K., Mishra V.P., Phongikaroon S. *Chapter 19 - Measurement and Analysis of Drop Size in a Batch Rotor-Stator Mixer*. In: van den Akker H.E.A., Derksen J.J (eds.). *10th European Conference on Mixing*. Amsterdam: Elsevier Science; 2000. p. 149-56.

(43) Pacek A.W., Ding P., Utomo A.T. *Effect of energy density, pH and temperature on de-aggregation in nano-particles/water suspensions in high shear mixer*. Powder Technology. 2007; 173(3): 203-10.

(44) Siddiqui S.W., Zhao Y., Kukukova A., Kresta S.M. *Characteristics of a Confined Impinging Jet Reactor: energy dissipation, homogeneous and heterogeneous reaction products, and effect of unequal flow*. Industrial & Engineering Chemistry Research. 2009; 48(17): 7945-58.

(45) Vladisavljević G.T., Williams R.A. *Manufacture of large uniform droplets using rotating membrane emulsification*. Journal of Colloid and Interface Science. 2006; 299(1): 396-402.

(46) Schadler V., Windhab E.J. *Continuous membrane emulsification by using a membrane system with controlled pore distance*. Desalination. 2006; 189(1): 130-5.

(47) Aryanti N., Williams R.A. *Analysis of rotating membrane emulsification performance for oil droplet production based on the Taylor vortices approach*. Particulate Science and Technology. 2018; 36(8): 913-9.

(48) Håkansson A., Trägårdh C., Bergenståhl B. *Dynamic simulation of emulsion formation in a high pressure homogenizer*. Chemical Engineering Science. 2009; 64(12): 2915-25.

(49) Zhang J., Xu S., Li W. *High shear mixers: A review of typical applications and studies on power draw, flow pattern, energy dissipation and transfer properties*. Chemical Engineering and Processing: Process Intensification. 2012; 57-58: 25-41.

(50) Hall S., Pacek A.W., Kowalski A.J., Cooke M., Rothman D. *The effect of scale and interfacial tension on liquid–liquid dispersion in in-line Silverson rotor–stator mixers*. Chemical Engineering Research and Design. 2013; 91(11): 2156-68.

(51) Johnson B.K., Prud'homme R.K. *Chemical processing and micromixing in confined impinging jets*. AIChE Journal. 2003; 49(9): 2264-82.

(52) Berton-Carabin C.C., Schroën K. *Pickering emulsions for food applications: background, trends, and challenges*. Annual Review of Food Science and Technology. 2015; 6(1): 263-97.

(53) Hunter T.N., Pugh R.J., Franks G.V., Jameson G.J. *The role of particles in stabilising foams and emulsions*. Advances in Colloid and Interface Science. 2008; 137(2): 57-81.

(54) Leal-Calderon F., Schmitt V. *Solid-stabilized emulsions*. Current Opinion in Colloid & Interface Science. 2008; 13(4): 217-27.

(55) Zafeiri I., Horridge C., Tripodi E., Spyropoulos F. *Emulsions co-stabilised by edible Pickering particles and surfactants: the effect of HLB value*. Colloid and Interface Science Communications. 2017; 17: 5-9.

(56) Håkansson A., Fuchs L., Innings F., Revstedt J., Bergenståhl B., Trägårdh C. *Visual observations and acoustic measurements of cavitation in an experimental model of a high-pressure homogenizer*. Journal of Food Engineering. 2010; 100(3): 504-13.

(57) Håkansson A. Droplet breakup in high-pressure homogenizers. In: Rayner M., Dejmek P., (eds.). *Engineering Aspects of Food Emulsification and Homogenisation*. 1st ed. Boca Raton: CRC press; 2015. p. 125-48.

(58) Kiss N., Brenn G., Pucher H., Wieser J., Scheler S., Jennewein H., et al. *Formation of O/W emulsions by static mixers for pharmaceutical applications*. Chemical Engineering Science. 2011; 66(21): 5084-94.

(59) Hall S., Cooke M., El-Hamouz A., Kowalski A.J. *Droplet break-up by in-line Silverson rotor–stator mixer.* Chemical Engineering Science. 2011; 66(10): 2068-79.

(60) Siddiqui S.W., Wan Mohamad W.A.F., Mohd. Rozi M.F., Norton I.T. *Continuous, high-throughput flash-synthesis of submicron food emulsions using a Confined Impinging Jet Mixer: effect of in situ turbulence, sonication, and small surfactants*. Industrial & Engineering Chemistry Research. 2017; 56(44): 12833-47.

(61) Schultz S., Wagner G., Urban K., Ulrich J. *High-Pressure Homogenization as a Process for Emulsion Formation*. Chemical Engineering & Technology. 2004; 27(4): 361-8.

(62) Qian C., McClements D.J. *Formation of nanoemulsions stabilized by model food-grade emulsifiers using high-pressure homogenization: Factors affecting particle size*. Food Hydrocolloids. 2011; 25(5): 1000-8.

(63) Lambrich U., Schubert H. *Emulsification using microporous systems*. Journal of Membrane Science. 2005; 257(1): 76-84.

(64) Perrier-Cornet J.M., Marie P., Gervais P. *Comparison of emulsification efficiency of protein-stabilized oil-in-water emulsions using jet, high pressure and colloid mill homogenization*. Journal of Food Engineering. 2005; 66(2): 211-7.

(65) Walstra P. *Formation of Emulsions*. In: Becher P., (ed.). *Encyclopedia of emulsion technology: Basic theory*. New York: Marcel Dekker; 1985. p. 60-100.

Chapter 6

Conclusions and future research directions

6.1 Conclusions

This study overall demonstrated the potential of Confined Impinging Jets as a viable route for the continuous, turbulent yet low-energy processing of emulsion-based structures by extending its application to a wide span of diverse formulations. An overview of the conclusions drawn from each result chapter of this study are summarised and collected in the current section.

Confined Impinging Jets could be adopted as an effective tool to produce o/w emulsions with a dispersed phase content up to 80 wt.% in both the surfactant-poor and -rich regime.

This result chapter focused on the assessment of the CIJs capacity and emulsification performance for the production of dilute as well as highly concentrated emulsions (dispersed phase content up to 80 wt.%) in both the surfactant-poor and -rich regime under varying hydrodynamic conditions.

From both an experimental and computational evaluation, the optimal CIJs operation was realised when *(i)* the inlet jet mass flow rate, Wjet, > 176 g/min and at the same time *(ii)* the pre-emulsion $d_{3,2}$ was higher than the d_{max} evaluated under fixed W_{jet}. From CFD data, at values of the jet mass flow rate below 176 g/min, the CIJs operation resulted compromised, i.e. no jet collision was observed. It was suggested that the new geometrical setup was potentially responsible for the inappropriate functioning at low jet flow rates. In fact, the CIJs cavity was devised with a longer jet-to-jet distance and a larger outlet diameter (than the one used in other studies) to overcome the backpressure developed during the emulsification of more concentrated systems. Experimentally, the CIJs emulsification capacity additionally resulted very much dependent on the original droplet size of the to-be-processed pre-emulsion. From a comparison of the pre-emulsion $d_{3,2}$ with the d_{max}, the data showed that the reduction in $d_{3,2}$

following the CIJs processing under varying jet flow rate was only realised when pre-emulsions presented a $d_{3,2}$ larger than the d_{max} corresponding to the hydrodynamic conditions produced by the used W_{jet} (provided that the mass jet flow rate was high enough to encourage successful jet impingement).

It was also reported from an experimental standpoint on the assessment of the CIJs emulsification performance for the processing of o/w emulsions with a wide range of oil contents, in the surfactant-poor and surfactant-rich regime, at different operational conditions and residence times.

Overall, the pre-emulsion $d_{3,2}$ decreased as the W_{jet} increased (within the determined optimal range of operation) independently on the dispersed phase mass fraction. Under the strongest hydrodynamic conditions, all systems showed a similar mean droplet size and polydispersity. It was also observed, based on a comparison with the theoretically calculated Kolmogorov eddy size, a transition from a turbulent inertial (TI) to turbulent viscous (TV) regime of emulsification taking place by increasing the oil mass fraction from 40 to 60 wt.%. Differently, it was proposed as the emulsion droplet size reduction for highly concentrated systems (80 wt.%) was instead due to the predominant hydrodynamic interactions between neighbouring droplets rather than to turbulence effects.

The increase of the residence time (e.g. multipassing) under fixed hydrodynamic conditions primarily caused a reduction of the span of the droplet size distribution of the processed emulsions with minor effects on the average emulsion droplet size.

Furthermore, the experimental data demonstrated that the ability of CIJs processing to reduce the emulsion $d_{3,2}$ was strongly dependent on the surfactant availability (e.g. surfactant concentration to the oil content). The $d_{3,2}$ of formulations with low surfactant availability (e.g. surfactant-poor regime) was majorly driven by surfactant concentration and oil content (e.g.

formulation aspects) rather than the energy dissipation rate generated by jet collisions (e.g. processing aspects) as in the case of formulations with high surfactant availability (e.g. surfactant-rich regime).

Although, most of the systems overall showed a good stability upon storage regardless of their formulation, to establish a clear correlation between the surfactant availability and the long-term storage stability resulted a rather complex operation.

The CIJs resulted a flexible processing method, which could successfully handle a wide spectrum of emulsion microstructures, including those formed in the presence of nanoparticles and mixed surfactant-nanoparticles systems as emulsifiers.

This result chapter focused on the evaluation of the CIJs processing performance of dilute as well as semi-concentrated (dispersed phase content up to 40 wt.%) o/w emulsions stabilised by a broad array of both nanoparticles and mixed surfactant-nanoparticles concentrations.

For both 10 and 40 w.% emulsions processed under varying CIJs hydrodynamic conditions in the presence of different silica concentrations, the average droplet diameter remained unaffected by the CIJs processing at low energy dissipation rates (or equivalently low W_{jet}). In fact, within the region of compromised jet impingement, both the pre-emulsion average droplet size and the size distribution were both practically unaltered by the flow conditions. On the other hand, within the previously identified optimal processing window, the reduction in the pre-emulsion Sauter diameter became more and more pronounced as the mass jet flow rate was increased. All systems reached the lowest droplet size (~ 10 μm) at the highest value of W_{jet}, regardless of the formulation.

Differently, when mixed emulsifier systems were used, it was proposed that the CIJs emulsification performance resulted strongly dependent on the relative quantity of Tween20

and Silica. In particular, when surfactant and particles were used at low concentrations (0.01 and 0.1 wt.%, respectively), although emulsion formation upon CIJs processing was possible, these systems could not very likely provide an efficient droplet stabilisation during a single pass as well as during recirculation in the CIJs cavity. During the single processing of 10 wt.% o/w emulsions, the $d_{3,2}$ fluctuated with the energy dissipation rate and no a clear trend could be established. During the single pass of more concentrated systems (40 wt.%), the Sauter diameter was subjected to a steep increase as the processing conditions became more severe, confirming the poor stabilisation mechanism offered by the emulsifier system (at the given concentration) observed with the more dilute emulsions. Upon recirculation, the $d_{3,2}$ of 10 wt.% emulsions remained constant, while it became progressively larger with the number of passes as the oil content was increased to 40 wt.%. Differently at higher either particles or surfactant concentrations, the resulting emulsion droplet size and droplet size distribution due to CIJs processing and recirculation were similar to the emulsion were the sole particle or surfactants were used. For all these cases, upon processing the smallest droplet size was achieved when the highest turbulence was approached, while, upon recirculation, no further variation of both the Sauter diameter and the width of the drop size distribution were observed after the second pass through the CIJs geometry.

Finally, all emulsions showed an excellent stability upon long-term storage over a period of 40 days independently on both the dispersed phase load and emulsifier system used. Interestingly it was observed a clear evidence that the combination of the emulsifiers (even at concentrations where each of them on their own did not give a stable emulsion microstructure) aided in prolonging the emulsion stability.

The CIJs represented an effective viable, energy-sustainable alternative to already-established low- and high-energy manufacturing techniques.

In this result chapter, the CIJs emulsification performance was compared against that of established low-energy (rotating membrane, RM) as well as high-energy (high pressure homogeniser, HPH, and high-shear mixer, HSM) food manufacturing tools for a range of processing parameters (average energy dissipation rate, flow regime, energy density and energy efficiency) for the production of dilute as well as semi-concentrated emulsions in the presence of either surfactant or nanoparticles acting as the sole emulsifiers.

It was demonstrated that while the RM operated under laminar flow regime, emulsion manufacturing via all the other methods took place in turbulent regime. As established from a comparison of the emulsion $d_{3,2}$ with the theoretically estimated Kolmogorov eddy size, in the presence of surfactant as the emulsifier, the HSM and the CIJs operated under a turbulent viscous and inertial regime, respectively. Differently, for the HPH, it resulted difficult to establish the dominant type of flow regime due to the close relation between the average drop diameter and the Kolmogorov eddy size. When silica was used as the emulsifier, although variations in the Sauter diameter could suggest alterations to the emulsification regime, it was proposed that the differences in $d_{3,2}$ were not caused by a modification of the flow regime but only by the presence of a different emulsifier.

In the presence of surfactant, the smallest $d_{3,2}$ was achieved through the high-pressure treatment, which also showed the highest values of energy dissipation rate $\bar{\varepsilon}_{th}$. Although both the HSM and the CIJs showed comparable $d_{3,2}$ (yet larger than those resulting from the HPH) over the entire range of operating conditions used, the CIJs operation generated $\bar{\varepsilon}_{th}$ significantly higher. Compared to the three methods, the RM produced the largest $d_{3,2}$ at the lowest $\bar{\varepsilon}_{th}$, probably due to both the low energy approach and the laminar flow conditions. When Silica

was instead used as the emulsifier, the trends remained overall unchanged, with the only exception being represented by the HPH where its operation could not induce a droplet size reduction below 8μm.

Independently on both the oil mass fraction and the emulsifier used, it was demonstrated that both the HPH and the HSM functioned over a similar range of high energy inputs, while CIJs and RM guaranteed emulsification to take place to intermediate and rather low Ev, respectively, over the whole range of processing conditions. Upon processing, the surfactant stabilised emulsions resulting from the high-pressure treatment had the highest polydispersity (with the span values increasing as the homogenisation pressure was increased) compared to all the other methods. Differently, while the emulsions resulting from both the HSM and CIJs showed intermediate span values, the narrowest DSDs were achieved during the membrane operation, according to the expectations. During processing of emulsions stabilised by nanoparticles, the differences in polydispersity resulted less evident among the different methods.

The HSM and HPH showed the lowest values of EFs during operation, while on the other side, due to the significantly lower energy inputs, the emulsion manufacturing through both the CIJs and RM resulted in the highest EFs. Interestingly, for the methods whose mode of operation was based on turbulence as the main mechanism of droplet break-up, the EF increased at higher oil loads, while for the RM this was not the case. In fact, the EF decreased when 40 wt.% oil in water emulsions were produced (if compared to the 10 wt.% ones) due to the longer time required to push the dispersed phase through the membrane pores.

Through the exposure of emulsions to longer residence times within the emulsification apparatus under fixed hydrodynamic conditions in the turbulence-based techniques (this was not performed for the RM), the DSD was the major microstructural parameter affected with minor changes observed in terms of $d_{3,2}$. Overall, the span of the DSD decreased as emulsions

spent longer times in the turbulent environment generated during emulsification. However on the other side, longer residence times strongly reduced the EF of all methods, with this reduction being dependent on the type of apparatus. CIJs showed the highest EF (regardless of the emulsifier used) if compared to both HSM and HPH. The EF of the latter two methods varied depending on the emulsifier employed during emulsification. In the case of surfactant-stabilised emulsions, the lowest EF was observed in the HSM, due to the longer times required for emulsification. Contrarily in the presence of particles, the lowest EF was showed during HPH operation, mainly because despite the recirculation, the droplet size could not be further reduced.

6.2 Future research directions

Whilst the study presented in this thesis has come to an end, it has also uncovered a number of areas that would be of high scientific interest to be further addressed. Some of these points may either have been initially explored and have not been included as part of this study due to time constriction or have not been addressed at all during the course of the PhD period. Some of the identified points for recommended future research directions are summarised as follows:

Experimental visualisation and understanding of the emulsification flow regime established during CIJs operation and cross comparison with CFD data.

The accurate flow characterisation by means of Particle Image Velocimetry (PIV) could be crucial for the fully understanding and optimisation of CIJs used as an effective tool for emulsion production. However, due to the optical inaccessibility of emulsions, it is suggested that by matching the refractive indexes of the two phases, the precise velocity fields, local

values of the energy dissipation rates as well as its distribution (both axially and radially) across the mixing chamber could be evaluated.

What is more, the experimental data could be cross-linked to a more in-depth multiphase computational characterisation of the CIJs processing. The assessment of the average droplet size and droplet size distribution resulting from CIJs processing could be evaluated by means of a discrete model coupled to population balance equations.

The combination of both aspects could lead to rapid optimisation and prototyping of new CIJs configurations to then undertake eventual scale-up activities.

Scale-up activities of CIJs as a potential large scale emulsification manufacturing technique.

Despite the large CIJs production capacity even at experimental scale, the undertaking of scale-up activities may be desirable to demonstrate the effectiveness and (perhaps) the limitations of this technique for further increases in its production throughputs. These should aim to demonstrate that this method could be employed to mass-produce emulsion based products having the same exact microstructural features as the resulting from the original small scale experiments. One of the most important parameters to consider should be the optimal geometrical characteristics of the mixing chamber. As demonstrated in the course of this study, despite the energy dissipation conditions within the CIJs cavity are inhomogeneous, its small dimensions guarantee that the majority of processed pre-emulsion flow through the high energy dissipation region thus resulting in emulsions having rather uniform properties if compared to other emulsification techniques. What is more, the CIJs geometrical features indirectly affects the key characteristic time scale for emulsification. Any modification in the CIJs volume chamber as well as in the jet diameter would affect, on one side, the residence time in the CIJs

turbulent environment, and on the other, the jet flow rate, i.e. the energy dissipation rate. In turn, variations in energy dissipation rate may have an influence on the eddy life time, droplet deformation time, emulsifier transfer time at the interface, droplet contact time, the drainage time between two interacting droplets, amongst others. Due to the multitude of mechanisms taking place at the same time during emulsification, any scale-up activity aiming to increase the CIJs throughputs should specifically account for these aspects to avoid compromising on the quality of operation.

Expanding the CIJs capability towards the production of more complex microstructures. During the course of the PhD studies, it was preliminary explored the possibility to expand the CIJs capability towards the manufacturing of more complex microstructures, with double emulsions and fluid gels representing two cases. However, both investigations could not be included as a part of this thesis mostly due to time limitations.

For double emulsions, in addition to stability challenges, one of the major limitations in their preparation concerns the second step of emulsification during which an already formed emulsion is again emulsified to form either a w/o/w or o/w/o double emulsion. Typically, one of the requirement of the second step is to execute emulsification without affecting the microstructure of the already-formed emulsion. This could usually be achieved either through low-energy manufacturing methods (e.g. membrane or microchannel emulsification) or upon high-shear mixing at low rotational speeds, by gradually adding the additional components to the primary emulsion. In either cases, it results evident that the large-throughput production is compromised. In this context, the CIJs can be used as the low energy route coming into play during the second step of emulsification, when an already formed emulsion can be forced to impinge against the additional phase in order to form tailored double emulsion based

microstructures. Similarly to the work conducted in this study for the case of simple emulsions, the effect of both processing and formulation parameters on the double emulsion microstructure quality could be assessed.

For the case of fluid gels, their tailored production could also be implemented by exploiting the high-level of shear generated during the CIJs operation (comparable to the ones currently observed in pin-stirrers). Fluid gels can be formed in the CIJs due to the presence of a sufficiently energetic flow field that stops the polymer solution to undergo aggregation by shearing and causes the formation of microparticles. For instance, in the case of alginates, it is well known that the production of microparticles occurs over the milliseconds to seconds time scale, which is comparable to the characteristic residence time occurring during CIJs operation, which is in the order of magnitude of the milliseconds. In the current configuration, CIJs would allow the impingement of an ionic and a biopolymer solution. Alternatively, one may also think to execute some geometrical variations in the CIJs chamber, such as the addition of a third inlet. For instance, this would allow the low flow rate injection of an ionic solution from the top of the chamber towards the stagnation zone where the collision of two biopolymer solutions takes place.